Energy

GEOTHERMAL

DOE/ID/12148-T1
(DE84011204)

INVESTIGATIONS OF WATER–ROCK INTERACTION IN GEOTHERMAL SYSTEMS OF JAPAN AND TAIWAN

Final Report

By
J. G. Liou
Renald N. Guillemette

March 1984

Work Performed Under Contract No. FC07-80ID12148

Southern Illinois University
Carbondale, Illinois

Technical Information Center
Office of Scientific and Technical Information
United States Department of Energy

DISCLAIMER

DISCLAIMER

This report has been reproduced directly from the best available copy.

Available from the National Technical Information Service, U. S. Department of Commerce, Springfield, Virginia 22161.

Price: Printed Copy A14
Microfiche A01

Codes are used for pricing all publications. The code is determined by the number of pages in the publication. Information pertaining to the pricing codes can be found in the current issues of the following publications, which are generally available in most libraries: *Energy Research Abstracts (ERA); Government Reports Announcements* and Index (*GRA* and I); *Scientific and Technical Abstract Reports (STAR);* and publication NTIS-PR-360 available from NTIS at the above address.

DOE/ID/12148-T1
(DE84011204)
Distribution Category UC-66

Final Report

Investigations of Water-Rock Interaction in Geothermal Systems of Japan and Taiwan

by

Principal Investigator: Prof. J.G. Liou

Associate Investigator: Renald N. Guillemette*

Department of Geology
Stanford University
Stanford, CA 94305

Supervisor: Dr. Susan M. Prestwich
Advanced Technology Branch
Energy and Technology Division
Department of Energy
Idaho Falls, Idaho 83401

* present address: Dept. of Geology, Southern Illinois University
Carbondale, IL 62901

March 1984

TABLE OF CONTENTS

INTRODUCTION

Japan and Taiwan provide excellent examples of active geothermal systems in island arc terrains in which geology and tectonic features are well understood. Development of geothermal power has been greatly emphasized in these countries because it is potentially a major energy resource in active volcanic areas. Exploration of geothermal energy in Japan and Taiwan began in the early sixties. Intensive geological-geochemical-geophysical studies of thermal waters and core samples in many Japanese geothermal systems have been completed. Many power plants have been installed. One purpose of this contract is to get more into the literature data and information concerning the geothermal systems and to conduct systematic study of drill hole core samples in classical island arc such as Japan. The knowledge deduced from the classical island arc can apply to the exploration of geothermal energy in the northwestern United States where the tectonic and petrologic settings are similar to those of Japan. With this idea in mind, the DOE sponsored the present project (1) to investigate systematic petrological study of drill hole core samples in selected geothermal areas in both Japan and Taiwan, and (2) to compile available references for geothermal research in Taiwan (Appendix A) and in Hakune (Appendix B) and Onikobe, Japan.

Our basic premise of this project is that the changing composition and temperature of geothermal fluids as a function of time will be recorded by the paragenesis, compositions and isotopic properties of the associated mineral assemblages, and that the latter can be used to reconstruct the evolution of a geothermal system. During the funding period of September 30th, 1982 to November 15th, 1983 with a total budget of $96,717 we have conducted detailed mineralogical-petrological-geochemical investigations of drill hole core samples from Onikobe, Japan. The results are described in detail as Memoir No. 3, Hydroscience & Geotechnology Lab, Saitama University, published in 1983. This memoir is reproduced as Section IV in this report and describes geological, geochemical, petrological and hydrological characteristics of a classic geothermal system in Japan. Further interpretations of petrological and geochemical data of drill hole core samples from the Onikobe system are included in an in-press manuscript entitled "Compositions and Parageneses of Secondary Minerals in the Onikobe geothermal system, Japan" as Section V in this report. This paper was also presented at the International Water-Rock Interaction Symposium at Misasa Japan. The extended abstract is reproduced here as Section VI.

During the grant period, we have also investigated drill hole core samples from Hakone (in Japan) and from the Tatun geothermal area (in Taiwan). We selected these two other systems to compare with that of the Onikobe system because they are recognized as classic examples of a geothermal system in island arc and because geological-geochemical-geophysical information is available to us. However, because of limited time and budget, we are not able to study them in as much detail as those in the Onikobe. A preliminary and short description on the Tatun geothermal system is included in Section VII of this report.

As described in detail for the Onikobe geothermal system, hydrous Ca-Al silicates such as laumontite, yugawaralite, wairakite, prehnite and epidote are common in addition to clay minerals. Their appearance in the geothermal system is a function not only is temperature (depth), but also composition of rocks and their interacting fluids. In order to understand their paragenesis and composition, systematic studies of their stabilities were also completed under the support of this contract. The results have been published respectively in the American Mineralogist for the laumontite-yugawaralite-wairakite relations as Section II and in the Journal of Petrology for the prehnite-epidote equilibria as Section III of this report.

Under the auspices of the DOE support, one Ph.D. thesis entitled "Geochemical and experimental investigations of andesite-water interactions and their relationship to Island-arc geothermal system" by Renald N. Guillemette was completed in August, 1983 and many other projects were initiated. We thank the DOE-SC07-80ID-12145 for gracious support and we particularly appreciate Drs. Susan M. Prestwich, Kent Hastings, and Dennis L. Nielson of the DOE for their encouragement and guidence.

American Mineralogist, Volume 67, pages 937–943, 1982

Experimental investigation of yugawaralite–wairakite equilibrium

YISHAN ZENG[1] AND J. G. LIOU

Department of Geology
Stanford University
Stanford, California 94305

Abstract

Yugawaralite ($CaAl_2Si_6O_{16}\cdot 4H_2O$) occurs most commonly in active geothermal areas and is associated with other zeolites including laumontite and wairakite. The stability field of yugawaralite was experimentally investigated using conventional hydrothermal apparatus over a *P–T* range of 200–350° C and 0.25–2 kbar and run duration of 14 to 61 days. The reversal experiments indicate that the *P–T* curve of the reaction yugawaralite = wairakite + $2SiO_2$ + $2H_2O$ passes through 225±5° C at 0.25 kbar, 223±5° C at 0.5 kbar, 238±5° C at 1 kbar and 245±5° C at 2 kbar P_{fluid}. The thermodynamic parameters of yugawaralite were calculated: ΔS_f = −2175.46±12.01 J/mol-K, $\Delta G°_f$ = −8387.69±4.01 kJ/mol, ΔH_f = −9036.19±4.01 kJ/mol. The equilibrium curve, yugawaralite = laumontite + $2SiO_2$, was estimated by employing the thermodynamic data and the calculated slope of 31.3 bars/° C. Present and previous experiments define an invariant point where yugawaralite, wairakite and laumontite are stable. The invariant point was located at 234° C and 550 bars in experimental conditions where $P_{H_2O} = P_{total}$. In geothermal systems where P_{H_2O} is about 1/3 P_{total}, the occurrence of yugawaralite is restricted to depths not much greater than 0.5 km. This result is consistent with its limited occurrence in active geothermal areas.

Introduction

Yugawaralite ($CaAl_2Si_6O_{16}\cdot 4H_2O$) was first described by Sakurai and Hayashi from vein fillings near the Yugawara Hot Spring, Japan in 1952. This calcium zeolite has since been reported to occur often with other zeolites, including laumontite and wairakite as euhedral crystals filling cavities and veins in geothermal areas and as microcrystals in low-grade metamorphosed volcanic rocks. Yugawaralite of the first case includes the type locality; Heinabergsjokell, Iceland (see Barrer and Marshall, 1965); Onikobe (Seki and Okumura, 1968) and Shimoda, Japan (Sameshima, 1969); Chena Hot Springs areas, Alaska (Eberlein *et al.*, 1971); Osilo, Sardinia, Italy (Pongiluppi, 1977); Bombay, India (Wise, 1978) and Yellowstone National Park (Bargar and Beeson, 1981; Bargar *et al.*, 1981). These occurrences suggest that yugawaralite is formed at low pressures and temperatures and is related to geothermal activity. Yugawaralites from the Tanzawa Mountains (Seki *et al.*, 1969a) are believed to be the product of low-grade metamorphism, with an extremely high geothermal gradient.

P–T stability relations of some calcium zeolites including laumontite, wairakite, and stilbite in the system $CaAl_2Si_2O_8$–SiO_2–H_2O have been investigated (Liou, 1970 and 1971a, b); however the stability of yugawaralite and its relationship to those of other calcium zeolites has not been experimentally determined. Seki (1969) and Harada (1969) have suggested that the stability field of yugawaralite is intermediate between the stabilities of laumontite and wairakite with regard to temperature.

The purposes of the present study are (1) to experimentally determine the univariant equilibrium curve of the reaction yugawaralite = wairakite + $2SiO_2$ + $2H_2O$; (2) to calculate the thermodynamic parameters of yugawaralite; (3) to outline the *P–T* stability relationships among yugawaralite, wairakite and laumontite, and (4) to correlate the experimental results with paragenesis of Ca-zeolites in geothermal systems. Chemographic relations of laumontite, yugawaralite, wairakite, quartz and some other calcium zeolites are plotted in the system $CaAl_2Si_2O_8$–SiO_2–H_2O in Figure 1.

[1]Permanent address: Department of Geology, Beijing University, Beijing, China.

0003–004X/82/0910–0937$02.00

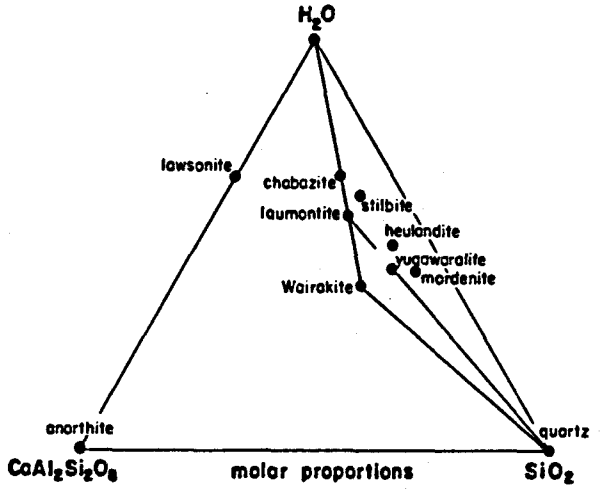

Fig. 1. Chemographic relations of some calcium zeolites and related minerals in the ternary system $CaAl_2Si_2O_8$–SiO_2–H_2O.

Experimental methods

Conventional cold seal hydrothermal apparatus was used in the present study; details of the experimental procedure are described by Liou (1971a). The starting materials include wairakite from Onikobe, yugawaralite from Yugawara, and laumontite from the Tanzawa Mountains, Japan. The compositions, optical and X-ray properties, and abbreviations of these zeolites are listed in Table 1. To ensure their purity, all of these minerals and quartz were ground and examined by X-ray diffraction. The charges for each experiment consisted of mixtures of yugawaralite as reactant and wairakite + quartz (with molar ratio of Wr/Qz[2] = 1/2) as products in subequal weight proportions and excess H_2O. Other charges had mixtures of laumontite and yugawaralite + wairakite + quartz in the weight ratio 1:2 with the ratios among yugawaralite, wairakite and quartz the same as above.

The charges were run from 30 to 61 days at temperatures ranging from 200° C to 350° C, and pressures from 250 bars to 2000 bars. The recorded temperatures are thought to be accurate to ±5° C and the pressures indicated by the gauges to be ±30 bars. All the charges were examined by microscope, X-ray diffraction and a scanning electron microscope with X-ray energy dispersive system.

Use of the above mineral mixtures as starting materials in the experiments avoided nucleation problems and enhanced the growth of seeded materials in their fields of stability. Phase relations were deduced by observing which assemblage grew at the expense of the other. The direction of reaction was established by comparing the relative intensities of main X-ray diffraction peaks (which were measured by area-ratio) of reactants and products before and after the experiment. When the mixture of yugawaralite + wairakite + quartz was used in the experiments, three intensity ratios, $Yu_{(140)}/Wr_{(400)}$, $Yu_{(111)}/Wr_{(211)}$, and $Yu_{(002)}/Wr_{(332)}$, were used. For the mixtures of laumontite + yugawaralite + wairakite + quartz, the intensities of only four peaks, $Lm_{(110)}$ and $Lm_{(002)}$, $Yu_{(111)}$ and $Wr_{(211)}$, were measured because the other X-ray diffraction peaks overlapped substantially.

Newton (1966) demonstrated that, where the extent of reaction is not large, the direction of reaction cannot be positively recognized by comparison of X-ray diffractometer charts. This difficulty was encountered in some experiments which are close to the equilibrium temperatures. In the present study, many runs with durations of 60 days and under closely similar P_{fluid}–T conditions were made and the results showed consistent reaction direction. Each isobaric equilibrium temperature for the reaction $Yu = Wr + Qz + H_2O$ was determined by at least 4 runs within a 50° C temperature interval.

In order to obtain reproducible intensity ratios of diffraction peaks, samples for the X-ray mounts were prepared according to the same procedure and 2 to 5 X-ray diffraction patterns of each charge were taken under identical conditions (Cu$K\alpha$ radiation, 35 kV accelerating potential, 16 mA emission current, ¼° 2θ/min scanning speed, 30 in./hr chart speed, intensity amplifier 1×10^2 and time constant 4). The areas of diffraction peaks were accurately measured by using a compensating polar planimeter. All run products were also examined by using a scanning electron microscope (SEM/EDAX) to detect the growth and dissolution of phases in order to verify the results obtained by X-ray diffraction.

Experimental results

The experimental results from a total of 35 runs using the mixture of yugawaralite + wairakite + quartz as starting material are listed in Table 2 and shown in Figure 2. The growth of wairakite at the expense of yugawaralite was readily detected for those experiments at temperatures greater than 250° C because 20–50% conversion occurred. However, the phase equilibration at temperatures lower than 250° C, especially P–T conditions close to

Table 1. Chemical compositions, optical and X-ray properties of natural wairakite, laumontite and yugawaralite used as starting materials

	Wairakite (Wr)*	Laumontite (Lm)**	Yugawaralite (Yu)***
SiO_2	54.91	50.99	59.29
TiO_2	0.01	0.02	tr.
Al_2O_3	22.75	21.87	17.43
Fe_2O_3	0.64	0.09	0.05
FeO	0.64	0.11	0.25
MnO	0.01	0.02	none
MgO	0.23	tr.	0.11
CaO	11.69	12.00	9.90
Na_2O	0.60	0.38	0.26
K_2O	0.31	0.10	tr.
H_2O^+	8.23	14.02	12.85
H_2O^-	0.19	0.29	0.10
Total	100.01	99.89	100.24
α	1.498±0.002	1.506±0.002	1.493
β		1.512±0.002	1.499
γ	1.502±0.002	1.516±0.002	1.501
a_o	13.85	14.737±0.004	6.73
b_o	13.66	13.006±0.002	13.95
c_o	13.56	7.550±0.003	10.03
β	90°20'	111.97±0.02	111°30'

*After Liou (1970)
**After Liou (1971a)
***After Seki and Okumura (1966)

[2]Abbreviations: Wr—wairakite; Qz—quartz; Yu—yugawaralite; Lm—laumontite.

Table 2. Experimental results for the reaction: yugawaralite (Yu) = wairakite (Wr) + $2SiO_2$ + $2H_2O$

Run No.	Temperature °C	Duration days	Direction of reaction
	P_{H_2O} = 500 bars		
43	210	61	Yu ← Wr
39	220	30	Yu ← Wr
72	222	60	Yu ← Wr
50	230	60	Yu ← Wr
66	235	60	Yu → Wr
71	244	60	Yu → Wr
32	255	28	Yu → Wr
33	275	28	Yu → Wr
20	294	21	Yu → Wr
13	325	21	Yu → Wr
	P_{H_2O} = 1000 bars		
17	217	28	Yu ← Wr
74	222	60	Yu ← Wr
51	224	61	Yu ← Wr
73	228	60	Yu ← Wr
36	234	30	Yu ← Wr
61	235	60	Yu ⇄ Wr
45	241	31	Yu ⇄ Wr
62	246	60	Yu → Wr
35	250	30	Yu → Wr
23	256	28	Yu → Wr
18	275	28	Yu → Wr
15	300	28	Yu → Wr
21	325	14	Yu → Wr
	P_{H_2O} = 2000 bars		
52	221	59	Yu ← Wr
22	236	32	Yu ← Wr
42	238	32	Yu ← Wr
63	240	60	Yu ← Wr
65	250	58	Yu → Wr
64	260	60	Yu → Wr
19	264	30	Yu → Wr
37	274	30	Yu → Wr
38	287	31	Yu → Wr
14	301	28	Yu → Wr
16	333	28	Yu → Wr
7	348	31	Yu → Wr

equilibrium, is extremely difficult to detect because of the sluggishness of the reaction. Only about 5–20% change took place even in experiments of 2 months duration. In the present study many experiments under closely similar temperature conditions were made and examination of dissolution and growth of wairakite by using SEM was found to be very useful for determining reaction direction. In the reaction products from runs within the wairakite field (Fig. 2), especially at pressures higher than 1000 bars, freshly grown, well formed wairakite crystals with trapezohedron-cubic faces were found. In the products run within the yugawaralite field, poorly crystallized yugawaralite and subrounded wairakite

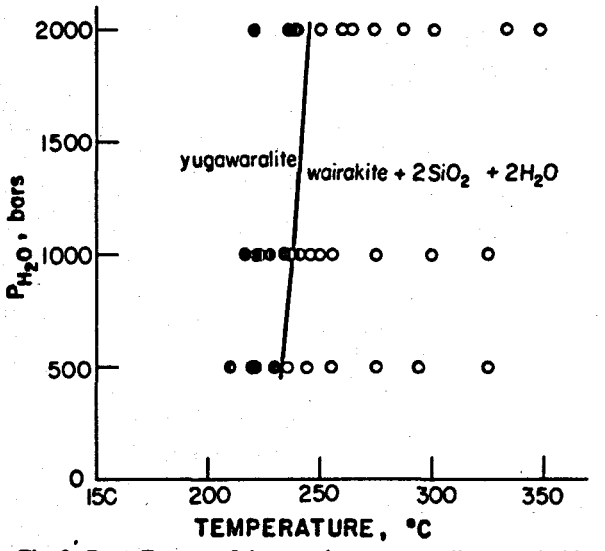

Fig. 2. P_{fluid}–T curve of the reaction yugawaralite = wairakite + $2SiO_2$ + $2H_2O$, experimentally determined by using the mixture of yugawaralite + wairakite + quartz (run data listed in Table 1).

occurred. No new phases were detected by either X-ray diffraction or SEM observation.

A combination of the criteria of intensity ratios of X-ray peaks and SEM observations was used to locate the equilibrium curve of the reaction as

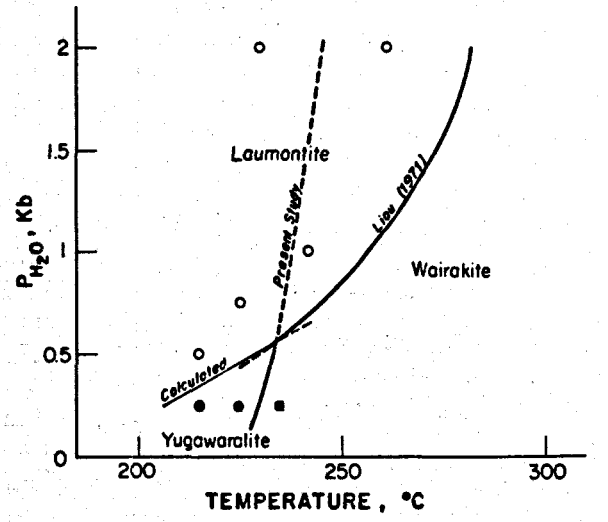

Fig. 3. P_{fluid}–T stability diagram for yugawaralite, laumontite, and wairakite in the presence of excess quartz and fluid. Open circles (laumontite), solid circles (yugawaralite) and solid squares (wairakite) show the strongest tendency of growth among the three zeolites in the four-mineral mixture experiments. The equilibrium P–T curve of the reaction yugawaralite = wairakite + $2SiO_2$ + $2H_2O$ is from the present experimental determination. The equilibrium dehydration curve of laumontite is from Liou (1971a); the P–T curve of the reaction, yugawaralite = laumontite + $2SiO_2$ is calculated.

passing through 233±5° C at 500 bars, 238±5° C at 1000 bars and 245±5° C at 2000 bars. The steep slope of the *P–T* curve suggests that the reaction is relatively insensitive to pressure in the range 0.5–2.0 kbar.

Integrating the present results with a previous study on laumontite–wairakite equilibrium in the $CaAl_2Si_2O_8$–SiO_2–H_2O system by Liou (1971a), the portion of the present wairakite–yugawaralite curve above 500 bars is metastable in the field of laumontite. Apparently, the three Ca-zeolites, yugawaralite, wairakite and laumontite have identical CaAl formula contents; hence, in the system with excess SiO_2 and H_2O, they define an invariant point. The intersection of the two experimentally determined univariant curves for reactions Yu = Wr + $2SiO_2$ + $2H_2O$ and Lm = Wr + $2H_2O$ locate the invariant point at about 234° C and 550 bars. Radiating from the invariant point is another reaction, Yu = Lm + $2SiO_2$. The phase relationships shown in Figure 3 are also consistent with those proposed by Harada (1969).

In order to experimentally outline the invariant relationship, seven experiments with mixtures of laumontite + yugawaralite + wairakite + quartz were carried out. The data are listed in Table 3 and are plotted in Figure 3. Based on the reconnaissance experiments and results described in the previous sections, it was concluded that yugawaralite is stable at lower temperatures relative to wairakite and at lower pressures relative to laumontite. The stability field of yugawaralite is bounded by the reaction Yu = Wr + Qz + H_2O at high temperature and by the reaction Yu = Lm + Qz at high pressure.

Discussion

Calculation of thermodynamic data for yugawaralite

The thermodynamic parameters of yugawaralite were calculated from the experimentally determined reversed *P–T* brackets using the method of Fisher and Zen (1971) and Zen (1972). All data used in the calculations are listed in Table 4.

Table 3. Experimental results with the mixture of laumontite (Lm), yugawaralite (Yu), wairakite (Wr) and quartz (Qz)

Run No.	Temp. °C	P_{H_2O} bars	Duration days	Changes in Run Products Lm/Yu	Wr/Lm	Yu/Wr	Tendency of mineral crystallization
84	230	2000	31	+	−	+	Lm > Yu > Wr
83	261	2000	31	+	−	−	Lm > Wr > Yu
86	242	1000	30	+	−	−	Lm > Wr > Yu
85	225	750	30	+	−	+	Lm > Yu > Wr
88	215	500	30	+	−	+	Lm > Yu > Wr
87	225	250	30	−	±	+	Yu > Wr > Lm
91	235	250	30	−	+	±	Wr > Yu > Lm

For the reaction, Yu = Wr + Qz + H_2O, the *P–T* brackets are: (1) 233±5° C, 500 bars; (2) 238±5° C, 1000 bars; (3) 245±5° C, 2000 bars. The combination of points 1, 3 and 2, 3 were used in the calculation. The calculated thermodynamic parameters of yugawaralite are:

$$\Delta S^\circ_{f(298,1)} = -2175.46\pm12.01 \text{ J/mol-K},$$

$$\Delta G^\circ_{f(298,1)} = -8387.69\pm4.01 \text{ kJ/mol};$$

$$\Delta H^\circ_{f(298,1)} = -9036.19\pm4.01 \text{ kJ/mol}.$$

Estimation of the P–T curve of the reaction yugawaralite = laumontite + $2SiO_2$

Using the data listed in Table 4, the slope of the equilibrium curve for Yu = Lm + $2SiO_2$ was estimated according to the Clapeyron equation. The calculated slope is 31.3 bars/° C, assuming that variation of volume and entropy changes with temperature for the solid–solid reaction is negligible. From the intersection of these experimentally determined univariant lines for Lm = Wr + $2H_2O$ and Yu = Wr + 2Qz + $2H_2O$, the *P–T* line for the solid–solid reaction Yu = Lm + 2Qz was drawn according to the calculated slope. The result is shown in Figure 3. The calculated phase relations among yugawaralite, wairakite and laumontite in the presence of excess quartz and fluid are consistent with the reconnaissance experiments using the three Ca-zeolites as starting materials described in the previous section. Figure 3 indicates that yugawaralite is restricted in its stability to temperatures lower than 233° C and pressures lower than 550 bars (about 1.5 km in depth) at the experimental conditions of $P_{H_2O} = P_{total}$.

It should be pointed out that the equilibrium Yu = Lm + 2Qz is a solid–solid reaction, hence its *P–T* locations are independent of fluid composition and of P_{H_2O}/P_{total}. In contrast, the two experimentally determined dehydration reactions shown in Figure 3 are very sensitive to variation in P_{H_2O}/P_{total} ratio. The P_{fluid}/P_{total} ratio in geothermal systems has been suggested to be about 0.3 (Coombs *et al.*, 1959). The phase relationships among the three Ca-zeolites under such conditions of $P_{H_2O} = 0.3\ P_{total}$ were estimated using their calculated thermodynamic parameters and are shown in Figure 4. The invariant point shifts toward lower temperatures and lower pressures along the *P–T* line of Yu = Lm

Table 4. Thermodynamic parameters of some Ca-zeolites and quartz

Mineral	Laumontite	Wairakite	Quartz	Yugawaralite
Formula	$CaAl_2Si_4O_{12}\cdot 4H_2O$	$CaAl_2Si_4O_{12}\cdot 2H_2O$	SiO_2	$CaAl_2Si_6O_{16}\cdot 4H_2O$
ΔG°_f (kJ/mol)	-6685.22	-6185.45	-856.65	-8387.69
ΔH°_f (kJ/mol)	-7237.11	-6612.01	-911.08	-9036.19
ΔS^*_f (J/mol·K)	-1851.05	-1430.69	-182.58	-2175.46
V° (J/bar·mol)	20.7638	18.6951	2.2697	26.6033
Source	Helgeson et al. (1978)	Helgeson et al. (1978)	Helgeson et al. (1978)	present study

*Calculated from ΔG°_f and ΔH°_f

+ Qz with decreasing P_{H_2O}/P_{total} ratio. At the P_{H_2O} = 0.3 P_{total}, the invariant point is estimated to be about 172° C and 230 bars P_{total}. Apparently, in geothermal systems where the fluid phase contains abundant other components in addition to H_2O, and where P_{fluid}/P_{total} ratios may be approximately 0.3, yugawaralite stability would be considerably restricted to smaller P–T fields and to lower temperatures.

Geological applications

The experimental results, which have located the stability field of yugawaralite at low temperatures and pressures, are consistent with its occurrences in geothermal fields and low-grade metamorphic terrains. Seki and Okumura (1968) described yugawaralite from the Onikobe geothermal area at depths between those corresponding to the laumontite zone (110.00–139.00 m) and the wairakite zone (deeper than 141.20 m) and at 110° C. The yugawaralite is associated with laumontite, wairakite, quartz, pyrite and chloritic minerals in an altered dacite tuff. The results of temperature measurements in drill holes at Yellowstone National Park (Bargar and Beeson, 1981; Bargar *et al.*, 1981) indicate that yugawaralite in drill hole Y-2 is restricted to a narrow zone of 149–152.2 m at temperatures of about 200° C whereas in drill hole Y-3, it is formed in a zone of about 73 m in depth and 170° C. These direct temperature measurements in both Yellowstone and Onikobe geothermal systems are plotted in Figure 4 and are compatible with the present data.

As shown in Figure 4, the paragenetic depth sequence of Ca-zeolites in a geothermal system is highly dependent on imposed thermal gradient, P_{H_2O}/P_{total} ratio and other factors including solution compositions (*e.g.*, Giggenbach, 1981). In a geothermal system with relatively high geothermal gradient and high P_{H_2O}/P_{total} ratio, yugawaralite may be stable and the depth sequence could be mordenite→laumontite→yugawaralite→wairakite. On the other hand, in the regions with lower geothermal gradient and lower P_{H_2O}/P_{total} ratio, yugawaralite is not stable and zonation of Ca-zeolite could be mor-

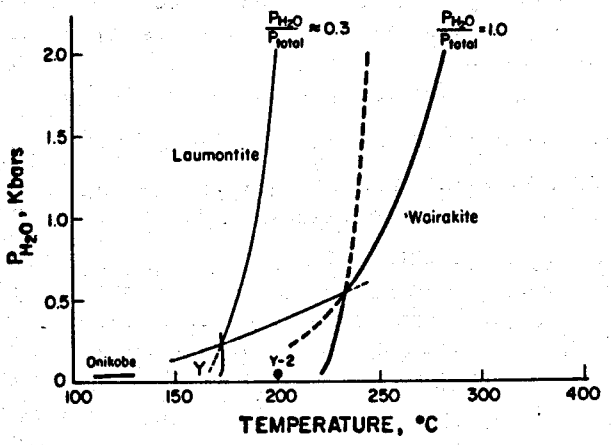

Fig. 4. P_{fluid}–T diagram showing the stability relations among yugawaralite (Y), laumontite, and wairakite in the presence of excess quartz and fluid at P_{H_2O}/P_{Total} = 1.0 and 0.3. The recorded temperatures and depths for yugawaralite occurrences in Onikobe (Seki *et al.*, 1969) and in Y-2 hole of Yellowstone (Bargar and Beeson, 1981) geothermal systems are also plotted for comparison.

denite→laumontite→wairakite. Because many geologic, solution and hydrologic conditions may control both P_{H_2O}/P_{total} ratio and geothermal gradient, different depth zonations of Ca-zeolite may occur even in a single geothermal system. Such variations have been recorded in the Onikobe geothermal area by Seki *et al.*, (1969b).

The yugawaralite in Alaska occurs about 14 miles from Chena Hot Springs and was suggested to have been deposited under conditions of low fluid pressure of 150–350 bars and temperature ranges of 200° to 300° C (Eberlein *et al.*, 1971). Although there is no past or present thermal spring activity at the yugawaralite locality, the yugawaralite is associated with stellerite, stilbite and laumontite. The suggested temperatures may be 100° C too high in the light of the presently determined stability of yugawaralite and that of stilbite (Liou, 1971b).

The occurrence of yugawaralite in the thermally metamorphosed aureoles of the Tanzawa Mountains (Seki *et al.*, 1969a) merits comment. The geothermal gradient for the hydrothermal formation of stilbite, laumontite and wairakite has been suggested to be high (Seki *et al.*, 1969a). Both wairakite and yugawaralite occur together with chlorite + prehnite + pumpellyite in some metamorphosed basaltic and andesitic rocks. Within these rocks the assemblages yugawaralite–chlorite–quartz, yugawaralite–laumontite–calcite–quartz, and yugawaralite–wairakite–calcite have been recorded in veins, cavities or druses. The close association of these three calcium zeolites together with quartz–chlorite suggests that they may have crystallized at *P–T* conditions very close to those of the invariant point. On the other hand, these zeolites may have formed at different times, and hence under different *P–T* conditions. Moreover, wairakites from the Tanzawa Mountains contain substantial amounts of Na (>1 wt.%) (Seki and Oki, 1969), hence, Na-bearing wairakite and yugawaralite may be stable within the yugawaralite field.

The present results provide a very restricted *P–T* stability field for yugawaralite which accounts for its restricted occurrence only at depths shallower than 500 m in geothermal systems. The presence of yugawaralite in hydrothermally altered rocks can potentially be used as a geobarometer.

Acknowledgments

This study was conducted during the senior author's 2-year advanced training at Stanford University, supported by the government of the PRC. The experimental study was supported by NSF grant EAR 79-09138 and DOE FC07-80ID-12148. We wish to thank Drs. R. C. Newton, Y. Seki and Mary Keskinen for discussion and review of the manuscript.

References

Bargar, K. E. and Beeson, M. H. (1981) Hydrothermal alteration in research drill hole Y-2, Lower Geyser Basin, Yellowstone National Park, Wyoming. American Mineralogist, 66, 473–490.

Bargar, K. E., Beeson, M. H. and Keith, T. E. C. (1981) Zeolites in Yellowstone National Park. Mineralogical Record, 12, 29–38.

Barrer, R. M. and Marshall, D. J. (1965) Synthetic zeolites related to ferrierite and yugawaralite. American Mineralogist, 50, 484–489.

Coombs, D. S., Ellis, A. J., Fyfe, W. S. and Taylor, A. M. (1959) The zeolite facies, with comments on the interpretation of hydrothermal syntheses. Geochimica et Cosmochimica Acta, 17, 53–107.

Eberlein, G. D., Erd, R. C., Weber, R. and Beatty, L. B. (1971) New occurrence of yugawaralite from the Chena Hot Springs Area, Alaska. American Mineralogist, 56, 1699–1717.

Fisher, J. R. and Zen, E-an (1971) Thermochemical calculations from hydrothermal phase equilibrium data and the free energy of H_2O. American Journal of Science, 270, 297–314.

Giggenbach, W. F. (1981) Geothermal mineral equilibria. Geochimica et Cosmochimica Acta, 45, 393–410.

Harada, K. (1969) Further data on the natural association of Ca-zeolites. Journal of the Geological Society of Japan, 75, 629–630.

Helgeson, H. C., Delany, J. M., Nesbitt, H. W. and Bird, D. K. (1978) Summary and critique of the thermodynamic properties of rock-forming minerals. American Journal of Science, 278-A, 1–229.

Liou, J. G. (1970) Synthesis and stablity relations of wairakite $CaAl_2Si_4O_{12}{\cdot}2H_2O$. Contributions to Mineralogy and Petrology, 27, 259–282.

Liou, J. G. (1971a) *P–T* stabilities of laumontite, wairakite, lawsonite, and related minerals in the system $CaAl_2Si_2O_8$–SiO_2–H_2O. Journal of Petrology, 12, 379–411.

Liou, J. G. (1971b) Stilbite–laumontite equilibrium. Contributions to Mineralogy and Petrology, 31, 171–177.

Newton, R. C. (1966) Some calc-silicate equilibrium relations. American Journal of Science, 264, 204–222.

Pongiluppi, D. (1977) A new occurrence of yugawaralite at Osilo, Sardinia. Canadian Mineralogist, 15, 113–114.

Sakurai, K. and Hayashi, A. (1952) Yugawaralite, a new zeolite. Scientific Report, Yokohama National University, Sec. II, no. 1, 69–77.

Sameshima, T. (1969) Yugawaralite from Shimoda, Shizuoka Pref., central Japan. Earth Science (Journal of the Japanese Association of Amateur Mineralogists), 71–78.

Seki, Y. (1969) Facies series in low-grade metamorphism. Journal of the Geological Society of Japan, 75, 255–266.

Seki, Y., and Haramura, H. (1966) On chemical composition of yugawaralite (in Japanese with English Abstract). Journal of the Japanese Association of Mineralogists, Petrologists, and Economic Geology, 56, 107–111.

Seki, Y., and Okumura, K. (1968) Yugawaralite from Onikobe active geothermal area, northeast Japan. Journal of the Japanese Association of Mineralogists, Petrologists, and Economic Geology, 60, 27–33.

Seki, Y., Oki, Y., Matsuda, T., Mikami, K. and Okumura, K. (1969) Metamorphism in the Tanzawa Mountains, central Japan (II). Journal of the Japanese Association of Mineralogists, Petrologists, and Economic Geology, 61, 50–75.

Seki, Y., Onuki, H., Okumura, K., and Takashima, I. (1969) Zeolite distribution in Katayama geothermal area, Onikobe, Japan. Japanese Journal of Geology and Geography, 40, 63–79.

Wise, W. S. (1978) Yugawaralite from Bombay, India. Mineralogical Record, 5, 296.

Zen, E-an (1972) Gibbs free energy, enthalpy and entropy of ten rock-forming minerals: calculations, discrepancies, implications. American Mineralogist, 57, 524–553.

Manuscript received, January 5, 1982;
accepted for publication, May 3, 1982.

Prehnite – Epidote Equilibria and their Petrologic Applications

by J. G. LIOU, HYUNG SHIK KIM*, AND SHIGENORI MARUYAMA†

Department of Geology, Stanford University, Stanford, California 94305

(*Received 8 November 1982; in revised form 4 March 1983*)

ABSTRACT

The stability relations of prehnite and epidote were experimentally determined for the bulk composition of $Ca_2Al_2FeSi_3O_{12}(OH)$ + excess H_2O using conventional hydrothermal apparatus and solid oxygen buffer techniques. Three starting materials were used: (I) mixtures of natural prehnite and hematite, (II) mixtures of synthetic epidote and natural prehnite + hematite in subequal proportion; and (III) reground run products. Over a range of f_{O_2}, epidote was readily synthesized from starting material (I) at 500–550 °C, 5–8 kb P_{fluid}, run duration of 7 to 45 days, and prehnite grew at the expense of its high-T epidote assemblage at temperatures below 350 °C, 2–8 kb, run duration of 20 to 50 days. Grandite garnet was in some cases detected, especially in the synthetic run products at lower f_{O_2} values and at higher temperature in longer experiments.

Microprobe analyses indicate that the $Fe^{3+}/(Fe^{3+} + Al)$ ratios of synthetic epidotes and prehnites vary as a function of f_{O_2} and temperature. Both epidote and prehnite are most iron-rich at 325 °C and 2 kb, 353 °C and 5 kb and 373 °C and 8 kb and f_{O_2} of the HM buffer; they become more aluminous with decreasing f_{O_2} and with increasing temperature. Such change in composition is consistent with their variations in cell dimensions.

The phase relations of prehnite and epidote are defined by continuous reactions where a transition zone between the garnet-in reaction and the prehnite-out reaction occurs at 325–343 °C, 2 kb, 353–375 °C, 5 kb and 373–395 °C, 8 kb P_{fluid} and f_{O_2} of the HM buffer. The minimum stability for the garnet-bearing assemblages is defined by the garnet-in reaction, and the maximum stability for the prehnite-bearing assemblages by the prehnite-out reaction. Sliding equilibria involving phases with continuous change in composition apparently are common for low-grade metamorphism. The present results combined with previously determined relations for prehnite, zoisite, and epidote delineate a petrogenetic grid which is consistent with parageneses and variation in Fe/Al ratios of coexisting prehnite and epidote in metabasites of the prehnite–pumpellyite and pumpellyite–actinolite facies and in altered rocks from many geothermal systems.

INTRODUCTION

Epidote and prehnite are common in various low-grade metamorphic rocks and in hydrothermal assemblages from active geothermal systems. They may occur together as common prehnite–pumpellyite facies assemblages with chlorite + albite + quartz, or they may appear separately as secondary phases after plagioclase or as hydrothermal minerals in veins and amygdules in metavolcanic rocks. Both epidote and prehnite are characterized by compositional variations within octahedral sites in the basic formulas $Ca_2(Al,Fe)_3Si_3O_{12}(OH)$ for epidote and $Ca_2(Al,Fe)(AlSi_3)O_{10}(OH)_2$ for prehnite. Solid solutions for both series are not complete. Minerals of the epidote and prehnite groups are rarely found with greater than 40 and 20 per cent replacement, respectively, of aluminum by ferric iron. The most common extremes are usually cited as approximately 33 per cent of the pistacite end-member for epidote and about 5 per cent of the Fe end-member for prehnite. The effects of temperature, fluid pressure and oxygen fugacity on the stability and composition of epidote and prehnite minerals have been experimentally determined as well as deduced from natural

Present Address: * Department of Geology, College of Sciences, Korea University, Seoul, Korea. † Department of Earth Sciences, Toyama University, Toyama 930, Japan.

[Journal of Petrology, Vol. 24, Part 4, pp. 321–342, 1983]

parageneses (e.g. Miyashiro & Seki, 1958; Holdaway, 1972; Liou, 1971, 1973; Bird *et al.*, in press). However, the stability relations and partitioning of Fe^{+3} and Al between prehnite and epidote and the effect of temperature and oxygen fugacity on prehnite composition have not been investigated.

The stability relations between prehnite and epidote are defined by a continuous reaction within a transition zone where both compositions and proportions of reacting phases vary continuously with P–T–f_{O_2} space. Such sliding equilibria are very common in low-grade metamorphism and have been studied by many authors (Seki, 1971; Coombs *et al.*, 1977; Nakajima *et al.*, 1977; Frost, 1980). The purposes of the present study are (1) to delineate experimentally the phase relations between prehnite, epidote and garnet for a 33 per cent pistacite bulk composition; (2) to construct temperature-compositional relationships for prehnite–epidote systems; and (3) to illustrate the significance of sliding equilibria in low-grade metamorphism. All these will contribute toward a better understanding of the quantitative effects of solid solutions on low-grade metamorphic minerals.

EXPERIMENTAL METHOD

Synthesis and stability relations of prehnite and epidote were studied by employing conventional hydrothermal apparatus and procedures as described in other papers (Schiffman & Liou, 1980; Apted & Liou, 1983). Argon was used as the pressure medium for experiments above 2 kb and H_2O for those at 2 kb. The pressure fluctuations were within ± 1 per cent at all pressures, and temperature within ± 5 °C for runs at 2 kb and ± 10 °C for the 5–8 kb experiments.

Three kinds of starting materials were used for the experiments: (I) a mixture of natural prehnite and hematite in the stoichiometric proportions of $Ca_2Al_2FeSi_3O_{12}(OH)$, which is equivalent to an epidote composition of Ps 33. However, as the natural prehnite contains 0·88 wt. per cent Fe_2O_3 and 27·13 wt. per cent of CaO (see Table 4), the composition of the starting material is slightly off the epidote composition of Ps 33; (II) mixtures of synthetic epidote and natural prehnite + hematite in subequal proportions; and (III) reground run products. Mixture I was used to synthesize epidote in runs of 7 to 45 days duration whereas mixtures II and III were used for reversal experiments of 15 to 50 days to detect the reaction direction.

Experimental run products were routinely examined with the petrographic microscope. Phase assemblages were determined using X-ray powder patterns and stability relations deduced by observing which assemblage grew at the expense of the other. The direction of reaction was established by comparison of X-ray intensities of the high- and low-temperature assemblages.

An ARL electron microprobe was used for the quantitative analysis of experimentally grown prehnites and epidotes which were more than 5 microns in diameter. Normal operating conditions were 15 kV accelerating potential, 0·02 microamperes sample current and 10 seconds counting time. Three detectors were used for analyses of three elements simultaneously at a single spot. X-ray counts for Fe, Si, Al were recorded first, followed by Fe, Ca, Al in order to check for consistent Fe and Al contents for the synthetic epidotes and prehnites. Two kaersutite crystals were used as standards.

The unit cell parameters of the synthetic epidote and prehnite were measured by using silicon (a = 5·430 Å at 25 °C) as an internal standard and a Norelco X-ray diffractometer employing Ni-filtered CuK_α radiation. Two oscillations were scanned (1°/4 min.) and 6–10 peaks were used for least squares refinement by the computer program of Appleman *et al.* (1972).

The abbreviations for the solid phases and oxygen buffer assemblages described in this

paper are listed in Table 1. The compositions of the starting material I, epidote, prehnite, grandite and other related phases in the system Fe_2O_x–Al_2O_3–CaO with excess quartz and H_2O are plotted in Fig. 1. The heavy lines represent solid solution compositions for epidote ranging from Ps 0 to 33, prehnite with $Fe^{3+}/(Fe^{3+} + Al)$ ratio of 0·0 to 0·25 and grandite

TABLE 1

Abbreviations and compositions of phases and oxygen buffer assemblages

Ep = Epidote, $Ca_2Al_{3-x}Fe_xSi_3O_{12}(OH)$, where $x < 1{\cdot}05$
Zo = Zoisite, $Ca_2Al_3Si_3O_{12}(OH)$
Pr = Prehnite, $Ca_2Al_{1-x}Fe_xAlSi_3O_{10}(OH)_2$, where $x < 0{\cdot}5$
Gd = Grandite, $Ca_3(Fe, Al)_2Si_3O_{12}$
Gr = Grossular, $Ca_3Al_2Si_3O_{12}$

And = Andradite, $Ca_3Fe_2Si_3O_{12}$
Gt = Garnet, $Ca_3(Al,Fe)_2Si_3O_{12}$
An = Anorthite, $CaAl_2Si_2O_8$
Mt = Magnetite, $FeFe_2O_4$
Ht = Hematite, Fe_2O_3
Qz = Quartz, SiO_2

HM = Hematite–Magnetite Buffer, Fe_2O_3–Fe_3O_4
NNO = Nickel–Nickel Oxide Buffer, Ni–NiO
QMF = Quartz + Magnetite + Fayalite Buffer, SiO_2–Fe_3O_4 + Fe_2SiO_4
IM = Iron–Magnetite Buffer, Fe–Fe_3O_4

IW = Iron–Wustite Buffer, Fe–FeO
MW = Magnetite–Wustite Buffer, Fe_3O_4–FeO
F = Fluid

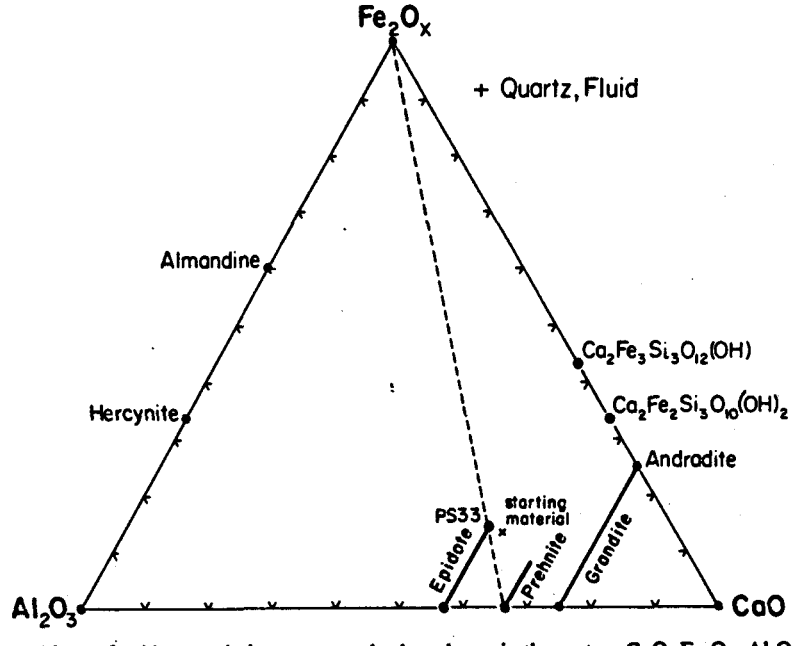

FIG. 1. Compositions of epidote, prehnite, garnet and other phases in the system CaO–Fe_2O_x–Al_2O_3–SiO_2–H_2O with excess quartz and fluid as mole proportions. Thick solid lines represent solid solution of epidote, prehnite and garnet. $Ca_2Fe_3Si_3O_{12}(OH)$ and $Ca_2Fe_2Si_3O_{10}(OH)_2$ are ideal Fe-end members of epidote and prehnite, respectively. X is the composition of starting materials for the present study.

from grossular to andradite. Epidote of Ps 33 lies on the join between hematite and prehnite, suggesting a simple reaction: epidote (Ps 33) + H_2O = prehnite + hematite. However, as will be discussed later in this paper, the reaction relationship is not that straightforward. Instead, the reaction passes through a transition zone in which both the compositions and the proportions of prehnite and epidote vary continuously with changing temperature and oxygen fugacity.

DESCRIPTION OF SYNTHETIC PHASES

Epidote

Epidote was readily synthesized from starting material I at 500–550 °C using various oxygen buffers, 5 to 8 kb P_{fluid}, and run durations of 7 to 45 days. However, at 2 kb, because of nucleation difficulties and slow reaction rates, synthesis of epidote was not successful. At given T and f_{O_2} conditions, higher pressure, probably at least 3 kb, may be necessary for the successful synthesis of epidote as a single phase. This result was consistent with the synthesis of high purity epidote-group minerals only at P_{fluid} greater than 5 kb (Liou, 1973).

All synthetic run products contained over 90 per cent epidote with minor amounts of prehnite and hematite, and the additional phases garnet and quartz in some experiments. The synthetic epidotes crystallized as 3–10 micron granules or as euhedral tabular forms of 15 microns length (especially for those formed at high temperature and high pressure). The crystals are pale to greenish yellow in color with weak or no pleochroism.

Selected microprobe analyses of the synthetic epidotes are presented in Table 2. Synthetic epidotes are regarded as $Ca_2Al_{3-x}Fe_xSi_3O_{12}(OH)$ where x is less than 1·05. For several run products, 5–7 analyses were completed for each charge; the range of Fe_2O_3 and the most representative composition of epidote are listed in the table. For other products (e.g. Run #32,38), only 1–2 analyses were possible; hence, only the representative composition is

TABLE 2

Electron microprobe analyses of epidotes formed at various f_{O_2}–T–P_{fluid} conditions

	Run no. 15 (HM, 513 °C, 8 kb, 358 hrs)	*Run no. 41 (HM, 499 °C, 2 kb, 789 hrs)*	*Run no. 47 (NNO, 552 °C, 8 kb, 258 hrs)*	*Run no. 42 (NNO, 502 °C, 2 kb, 789 hrs)*	*Run no. 38 (QMF, 376 °C, 2 kb, 725 hrs)*	*Run no. 49 (QMF, 414 °C, 5 kb, 482 hrs)*
SiO_2	36·36	36·80	36·65	37·03	37·84	37·00
CaO	23·41	23·07	23·51	22·78	23·71	24·10
Al_2O_3	21·96	20·17	24·38	23·84	24·97	24·22
Fe_2O_3*	16·95	17·63	13·83	14·36	13·07	12·81
Subtotal	98·68	97·67	98·37	98·01	98·59	98·13
			Number of cations based on 25 oxygens			
Si	5·83	5·99	5·83	5·96	5·91	5·92
Al	4·15	3·85	4·59	4·48	4·60	4·57
Fe^{+3}	2·05	2·16	1·66	1·72	1·54	1·47
Ca	4·02	4·02	4·02	3·89	3·97	4·13
Ps	33	35	27	31	25	25
Range of Fe_2O_3	17·23–15·56	18·01–16·97	14·96–11·76			14·25–11·07

* Total Fe as Fe_2O_3.

shown. The $Fe^{3+}/(Fe^{3+} + Al)$ ratio of the epidote decreases as f_{O_2} decreases in agreement with the observations of Holdaway (1972) and Liou (1973).

The unit cell parameters of the synthetic epidotes are given in Table 3; also listed are the experimental run conditions and angular displacement for $2\theta(020)_{Ep}-2\theta(111)_{Si}$ using CuK_α radiation. The range of the unit cell dimensions is $a(\pm 0{\cdot}009) = 8{\cdot}921$–$8{\cdot}842$ Å; $b(\pm 0{\cdot}004) = 5{\cdot}667$–$5{\cdot}618$ Å; $c(\pm 0{\cdot}012) = 10{\cdot}199$–$10{\cdot}110$ Å; $\beta(\pm 0{\cdot}052°) = 115{\cdot}770°$–$115{\cdot}296°$ and cell volume $(\pm 0{\cdot}65) = 463{\cdot}75$–$457{\cdot}47$ Å^3. For comparison, the unit cell parameters of some natural epidotes are also shown in Table 3. The cell parameters increase with increasing oxygen fugacity and with decreasing temperature; this variation is attributed to the increase of Fe^{3+} substitution for Al.

Prehnite

Prehnite was crystallized from its high-temperature equivalents at 300 °C using various oxygen buffers, 2 to 8 kb P_{fluid}, and run durations of 20 to 50 days. The prehnite appears as distinct euhedral crystals—stubby orthorhombic prisms about 2–10 microns in size. Prismatic crystals show parallel extinction with positive elongation and rather high birefringence.

Synthetic prehnites are generally regarded to be $Ca_2Al_{1-x}Fe_x(AlSi_3)O_{10}(OH)_2$ where x is less than 0·5 according to the present work and also to the results of Surdam (1969) and

TABLE 3

Unit cell dimensions and angular separations of the diffraction peaks (020_{Ep}–111_{Si}) for some synthetic and natural epidotes

Run no.	Buffer	P_{fluid} (bars)	Temp. (°C)	Duration (hours)	a, Å ±0·009	b, Å ±0·004	c, Å ±0·012	β(°) ±0·052	V, Å^3 ±0·65	$\Delta 2\theta CuK_\alpha$(°) ±0·012
15	HM	8000	513	358	8·907	5·642	10·189	115·490	462·19	3·240
59–6	HM	8000	386	954	8·917	5·652	10·180	115·330	463·73	3·244
39	HM	5000	388	1152	8·910	5·646	10·199	115·365	463·63	3·170
17	HM	5000	349	670	8·900	5·648	10·180	115·360	463·75	3·175
41	HM	2000	499	789	8·891	5·667	10·178	115·320	463·57	3·167
47	NNO	8000	552	258	8·897	5·659	10·168	115·311	462·76	3·171
55	NNO	5000	428	501	8·908	5·648	10·179	115·353	462·80	3·167
52	NNO	5000	499	1005	8·921	5·637	10·179	115·388	462·44	3·227
42	NNO	2000	502	789	8·903	5·639	10·168	115·328	461·40	3·339
48	NNO	2000	422	524	8·901	5·645	10·187	115·459	462·12	3·260
54	NNO	2000	389	735	8·914	5·658	10·177	115·333	463·92	3·272
46	QMF	8000	552	258	8·900	5·618	10·189	115·296	460·39	3·185
59–5	QMF	8000	412	889	8·891	5·658	10·165	115·353	462·10	3·192
49	QMF	5000	414	482	8·894	5·648	10·167	115·415	461·30	3·208
58	QMF	5000	402	998	8·894	5·638	10·173	115·406	460·73	3·162
38	QMF	2000	376	715	8·894	5·630	10·169	115·362	460·10	3·185
43	QMF	2000	503	789	8·889	5·627	10·162	115·311	459·49	3·333
53	QMF	2000	389	735	8·889	5·644	10·157	115·459	460·10	3·222
59	QMF	2000	363	981	8·911	5·646	10·168	115·465	461·87	3·122
51	IM	5000	499	1005	8·842	5·663	10·110	115·534	456·78	3·093
59–2	IM	5000	550	616	8·884	5·639	10·140	115·770	457·47	3·212
Natural epidote[1]					8·904	5·649	10·173	115·403	462·10	3·204
Natural epidote[2]					8·907	5·660	10·180	115·400	463·60	3·146
Natural epidote[3]					8·899	5·639	10·166	115·383	460·90	3·269

[1] from San Isido, Baja California, with composition $Ca_{1.99}Fe^{3+}_{0.01}Al_{1.94}Fe_{0.99}Si_3O_{12}(OH)$ (Myer, 1965).
[2] from Westfield, Massachusetts, with composition $Ca_{1.99}Fe^{3+}_{0.03}Al_{1.94}Fe_{1.04}Si_3O_{12}(OH)$ (Liou, 1973).
[3] from Gaspe, Quebec with composition $Ca_{1.94}Fe^{3+}_{0.05}Na_{0.05}Al_{2.08}Fe_{0.83}Mg_{0.07}Si_3O_{12}(OH)$ (Myer, 1966).

Coombs *et al.* (1977). Microprobe analyses of four synthetic and one natural prehnites are listed in Table 4, which gives the range of Fe_2O_3 and the most representative composition for each charge together with its experimental conditions. As with epidote, the $Fe^{3+}/(Fe^{3+} + Al)$ ratio in the octahedral site for the synthetic prehnite varies as a function of oxygen fugacity.

TABLE 4

Electron microprobe analyses of prehnites formed at various f_{O_2}–T–P_{fluid} conditions and natural prehnite

	Run no. 21 (HM, 300 °C, 2 kb, 986 hrs)	*Run no. 59–7 (NNO, 401 °C, 8 kb, 676 hrs)*	*Run no. 52 (NNO, 499 °C, 5 kb, 1005 hrs)*	*Run no. 59–5 (QMF, 412 °C, 8 kb, 889 hrs)*	*Run no. 43 (QMF, 503 °C, 2 kb, 789 hrs)*	*Run no. 38 (QMF, 376 °C, 2 kb, 725 hrs)*	*Natural* prehnite (starting material)*
SiO_2	43·20	43·00	42·94	43·45	42·05	43·85	42·50
CaO	25·78	26·39	25·91	26·39	27·12	25·99	27·13
Al_2O_3	20·36	20·35	25·02	20·90	23·87	21·01	24·29
Fe_2O_3 (total Fe)	4·91	4·53	0·92	3·92	1·23	3·70	0·88
Subtotal	94·45	94·27	94·79	94·66	94·27	94·55	94·80
	Number of cations based on 11 oxygens						
Si	3·05	3·04	2·97	3·05	2·95	3·07	2·96
Al^{IV}	0·95	0·96	1·03	0·95	1·05	0·93	1·04
Al^{VI}	0·75	0·74	1·01	0·78	0·94	0·81	0·95
Fe^{+3}	0·26	0·24	0·05	0·21	0·06	0·20	0·05
Ca	1·95	2·00	1·92	1·99	2·04	1·95	2·02
$Fe^{+3}/Al^{VI} + Fe^{+3}$	0·26	0·24	0·05	0·21	0·06	0·20	0·05
$Fe^{3+}/(Al + Fe^{3+})$	0·13	0·12	0·02	0·11	0·03	0·10	0·02
Range of Fe_2O_3	3·08–5·91	3·69–4·85	0·75–1·17	2·69–4·51	0·90–1·51		

* Natural prehnite from Prospect, New South Wales.

TABLE 5

Unit cell dimensions of prehnites formed at various f_{O_2}–T–P_{fluid} conditions and natural prehnites

Run no.	*Buffer*	*P_{fluid} (bars)*	*Temp. (°C)*	*Duration (hours)*	*a, Å ±0·003*	*b, Å ±0·03*	*c, Å ±0·03*	*V, Å³ ±0·3*
59–6	HM	8000	386	954	4·637	5·477	18·403	467·39
21–1	HM	5000	377	689	4·652	5·488	18·447	470·96
41	HM	2000	499	789	4·648	5·485	18·411	469·39
21	HM	2000	300	986	4·655	5·492	18·498	492·91
47	NNO	8000	552	258	4·639	5·457	18·439	466·75
34	NNO	5000	350	785	4·645	5·471	18·396	467·49
54	NNO	2000	389	735	4·622	5·524	18·362	468·80
59–1	NNO	2000	369	836	4·642	5·481	18·454	469·52
46	QMF	8000	552	258	4·634	5·489	18·429	468·63
59–5	QMF	8000	412	889	4·630	5·452	18·428	465·17
58	QMF	5000	402	998	4·645	5·488	18·432	469·87
59	QMF	2000	363	981	4·643	5·492	18·473	471·05
38	QMF	2000	376	715	4·644	5·490	18·452	470·44
*Natural Prehnite					4·642	5·473	18·421	470·00

* Natural prehnite from Prospect, New South Wales (same as Table 4).

Because regrinding the prehnites in run products for reversal experiments markedly reduced the grain size, the prehnites in reversal experiments are not coarse enough for microprobe analyses. Therefore, the few prehnite analyses listed in the table are not sufficient to detect the relationship between temperature and the $Fe^{3+}/(Fe^{3+} + Al)^{VI}$ ratio.

The unit cell parameters of synthetic prehnites together with those of the natural prehnite used for the starting material are shown in Table 5; also listed are the experimental run conditions. A considerable range in unit cell dimensions of the synthetic prehnites was found; they are $a(+0{\cdot}003)$ = 4·655–4·622 Å, $b(+0{\cdot}03)$ = 5·524–5·452 Å, $c(\pm 0{\cdot}03)$ = 18·498–18·362 Å and cell volume $(\pm 0{\cdot}3)$ = 472·91–465·17 Å^3. The cell edges or volumes correlate systematically with the experimental conditions: as for epidotes, they increase with increasing oxygen fugacity and with decreasing temperature. The increase in unit cell size for the synthetic prehnite is attributed to an increase in iron content (Deer *et al.*, 1962; Surdam, 1969).

Iron Oxides

Iron oxides occur as minor phases (e.g. less than 5 volume per cent) in all synthetic and reversal run products. Their presence was detected by optical and X-ray diffraction methods. Hematite crystallized together with magnetite in the experiments at the f_{O_2} defined by the HM buffer whereas magnetite crystallized as the only iron oxide at f_{O_2} defined by the NNO and QMF buffers.

The unit cell dimensions of synthetic and natural magnetites are listed in Table 6. The range of a axes is 8·402–8·397 Å at f_{O_2} defined by the HM buffer, 8·402–8·378 Å at the NNO buffer, 8·397–8·384 Å at the QMF buffer and 8·390–8·381 Å at the IM buffer. As suggested by the data, the cell parameters of synthetic magnetite decrease slightly and

TABLE 6

Unit cell dimensions of synthetic and natural magnetites

Run no.	*Buffer*	P_{fluid} *(bars)*	*Temp. (°C)*	*Duration (hours)*	a, Å ±0·002	V, Å^3 ±0·5
59–6	HM	8000	386	954	8·397	592·07
41	HM	2000	499	789	8·402	593·05
47	NNO	8000	552	258	8·378	588·02
52	NNO	5000	499	1005	8·393	591·30
34	NNO	5000	350	785	8·402	593·05
42	NNO	2000	502	789	8·398	592·22
48	NNO	2000	422	524	8·399	592·46
46	QMF	8000	552	258	8·384	589·32
49	QMF	5000	414	482	8·393	591·23
58	QMF	5000	402	998	8·391	590·81
38	QMF	2000	399	715	8·394	591·43
43	QMF	2000	503	789	8·390	590·59
53	QMF	2000	389	735	8·393	591·30
59	QMF	2000	363	981	8·397	592·03
51	IM	5000	499	1005	8·391	590·59
59–2	IM	5000	550	616	8·380	588·59
Natural magnetite					8·379	588·27
Synthetic magnetite					8·396	591·86

Natural magnetite: From Lovers Pit, Minevilk, New York, (Newhouse & Glass, 1936).

Synthetic magnetite: National Bureau of Standard, Monograph 25, Section 5, 31 (1967).

systematically with decreasing f_{O_2} or with increasing temperature along the buffer curves at constant P_{fluid}. From the data of Turnock & Eugster (1958), such a variation is mainly attributed to the substitution of Al for Fe^{3+} at the higher temperature and more reducing environments.

Garnet

Garnet was detected by X-ray diffraction as a minor phase (less than 5 per cent in volume) in some run products of synthesis and reversal experiments. The measurement of garnet cell dimensions was not attempted because its X-ray reflections are weak and overlap with those of major phases such as epidote, prehnite and magnetite. Microprobe analyses of garnet were not possible due to the fine grain size (less than 2 microns in diameter) and the small amount present. However, Liou (1973) has noted that with decreasing f_{O_2}, the grossular component in synthetic grandite garnet increases, as reflected by the systematically decreasing value of the cell edge and refractive index (N_D). His results support the suggestion that the $Fe^{3+}/(Fe^{3+} + Al)$ ratio of grandite varies as a function of f_{O_2} and temperature.

EXPERIMENTAL RESULTS*

Run data

The synthesis run data indicate that the high-temperature assemblages consisted of epidote, garnet, hematite and magnetite with small amounts of prehnite at the f_{O_2} defined by the HM buffer. However, in lower f_{O_2} experiments, phases such as epidote, garnet, quartz and magnetite with a minor prehnite were encountered. Charges with greater than 80 per cent epidotes were synthesized at temperatures of 500–550 °C, and at various f_{O_2} values.

Fifteen reversal runs were first performed in a narrow temperature range of 300–425 °C with various f_{O_2} buffers and 2 kb P_{fluid} in order to determine the equilibrium temperature and the continuous nature of the equilibrium relation between prehnite and epidote. Twenty-seven reversal runs at $P_{fluid} = 5$ and 8 KB were later completed to determine the effect of P_{fluid} on the isobaric f_{O_2}–T relations. The reversal experiments at 2 kb P_{fluid} required durations of 30 to 50 days, whereas at 5–8 kb P_{fluid} the reaction was readily reversed in 20 to 35 days. Epidote and magnetite were detected as stable phases in all run products. However, prehnite was present only in lower f_{O_2} and in lower temperature runs, and garnet in higher f_{O_2}–higher temperature runs. Both garnet and prehnite, together with epidote and magnetite, occur only in the P–T field of a transition zone shown in Figs. 2–4.

The experimental results on the prehnite–epidote stability are plotted on conventional isobaric log f_{O_2}–T diagrams of Figs. 2 and 3. The maximum stability limit of epidote (Liou, 1973) is shown for comparison. Both Liou's and the present experiments have identical bulk starting compositions.

As shown in Figs. 2–3, epidote has a wide stability field over the temperature range of 300–550 °C, 2–8 kb P_{fluid} and at various f_{O_2} values. The present results have delineated two reactions; for simplicity, we use the phrase *garnet-in reaction* to define the minimum stability for the garnet-bearing assemblages and the *prehnite-out reaction* for the maximum stability of the prehnite-bearing assemblages for the given bulk composition. A transition zone occurs between these two assemblages where the three phases epidote, prehnite and garnet are stable. It should be noted that the compositions of these phases vary with the P_{fluid}–T–f_{O_2} conditions and they are therefore designated with solid solution (s.s.) as a subscript.

* The experimental run tables are available from the senior author.

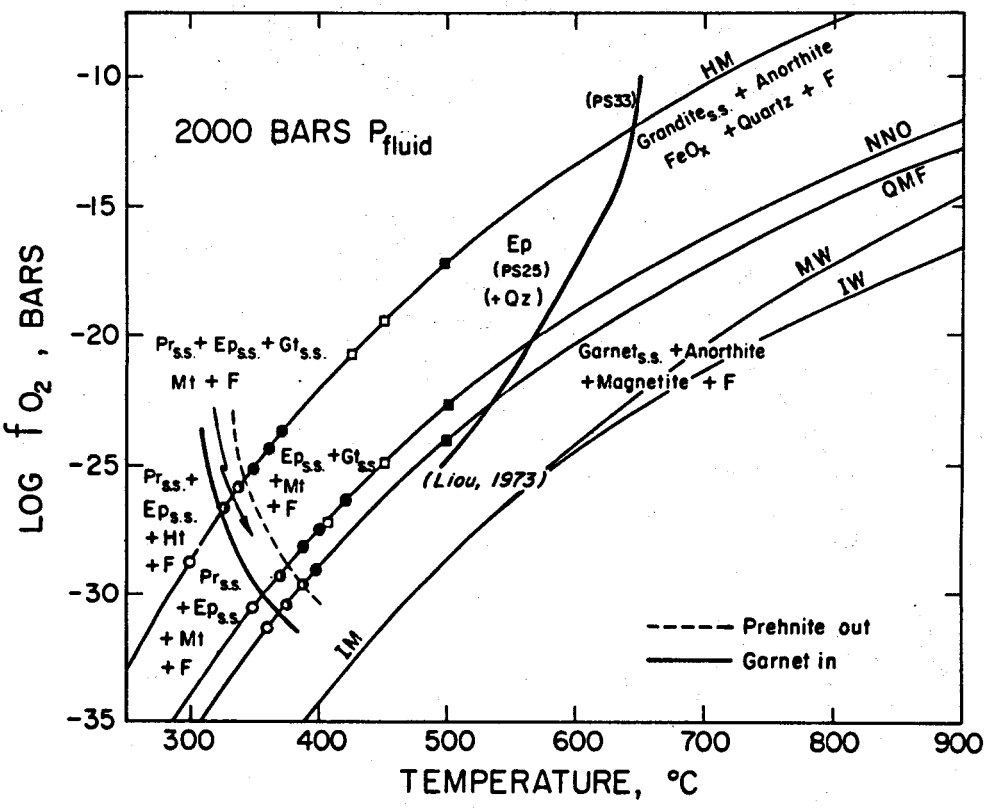

FIG. 2. Log f_{O_2}–T diagram for the garnet-in and prehnite-out reactions at 2000 bars P_{fluid}. High and low temperature assemblages are shown. Circles are for reversal experiments and squares are for synthesis runs. Solid circles: assemblage epidote$_{s.s.}$ + garnet$_{s.s.}$ is stable. Open circles: assemblage prehnite$_{s.s.}$ + epidote$_{s.s.}$ is stable. Half circles: assemblage epidote$_{s.s.}$ + prehnite$_{s.s.}$ + garnet$_{s.s.}$ is stable. Solid squares: successful growth of high-T assemblage. Open squares: unsuccessful synthesis runs. The previously determined curve for the maximum stability of epidote from Liou (1973) is also shown for comparison. The oxygen buffer curves of Huebner (1971) are corrected for pressure.

Garnet-in reaction

The garnet-in reaction is defined by a discontinuous reaction: prehnite$_{s.s}$ + iron oxide + O_2 = epidote$_{s.s.}$ + grandite$_{s.s}$ + fluid. Depending on the oxygen fugacity, the iron oxide is either hematite–magnetite or magnetite. The univariant line for the garnet-in reaction was located on the basis of reversal of the reaction. In the products run at temperatures above the univariant line, garnet appears and magnetite and prehnite decrease. The reaction is shown as a solid line in Figs. 2–4. The garnet-in reaction line crosses the HM buffer curve at 325 ± 5 °C, 2 kb, 353 ± 10 °C, 5 kb, 373 ± 10 °C, 8 kb, the NNO buffer curve at 356 ± 5 °C, 2 kb, 385 ± 10 °C, 5 kb, 405 ± 10 °C, 8 kb and the QMF buffer curve at 369 ± 5 °C, 2 kb, 395 ± 10 °C, 5 kb and 412 ± 10 °C, 8 kb P_{fluid}. The equilibrium temperature for the garnet-in reaction at f_{O_2} defined by the HM buffer is about 40–45 °C lower than those of the NNO and QMF buffers.

As discussed in the previous sections, with successively increasing temperature and decreasing f_{O_2}, both epidote and prehnite become progressively more aluminum-rich and coexisting garnet moves toward the grossular end-member; concomitantly, the $Fe^{+2}Al_2O_4$ component of magnetite increases. At temperatures ranging from 325 °C to 405 °C, 2 kb

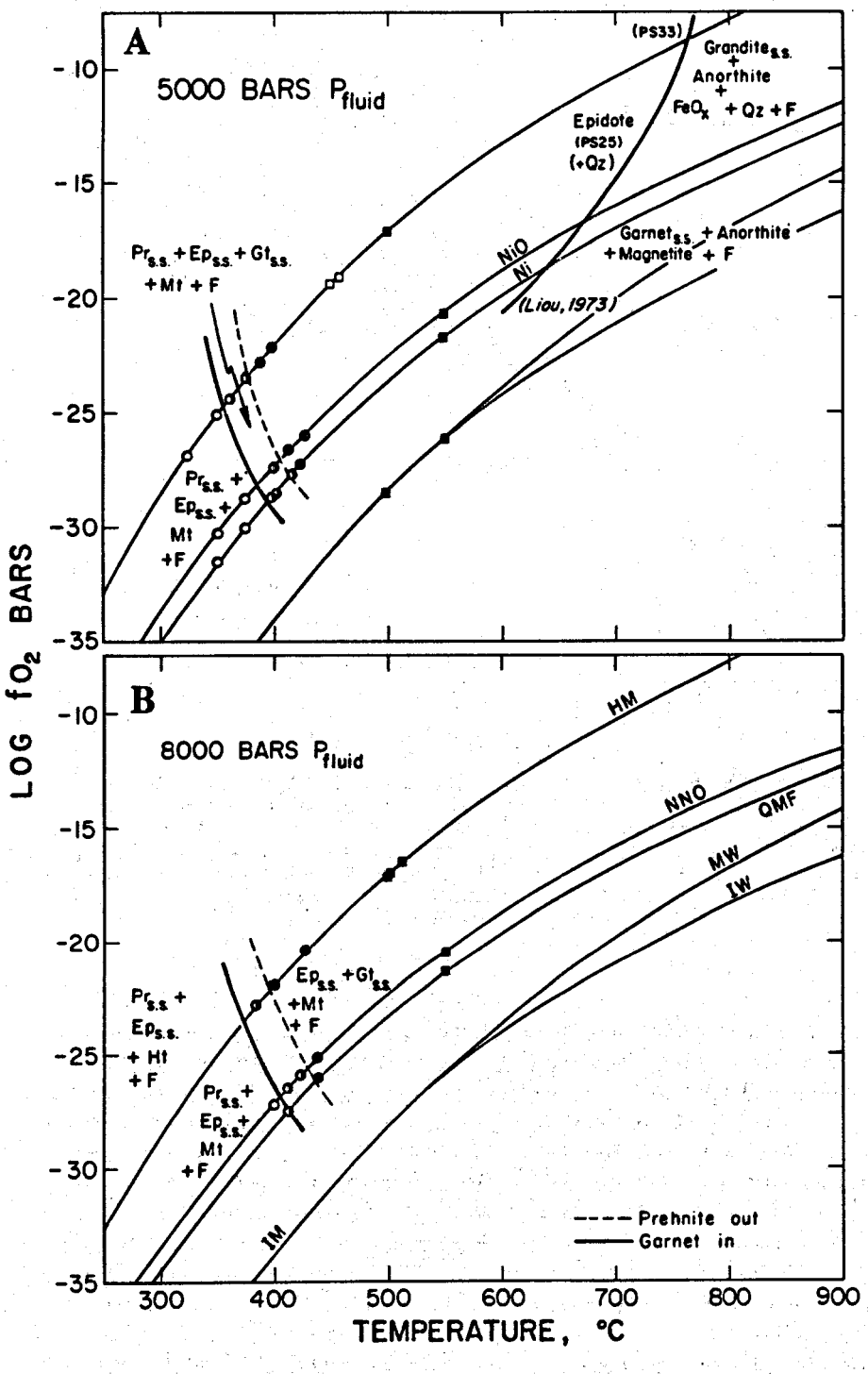

FIG. 3. Log f_{O_2}–T diagram for the garnet-in and prehnite-out reactions at 5000 (A) and 8000 (B) bars P_{fluid} (symbols are same as Fig. 2).

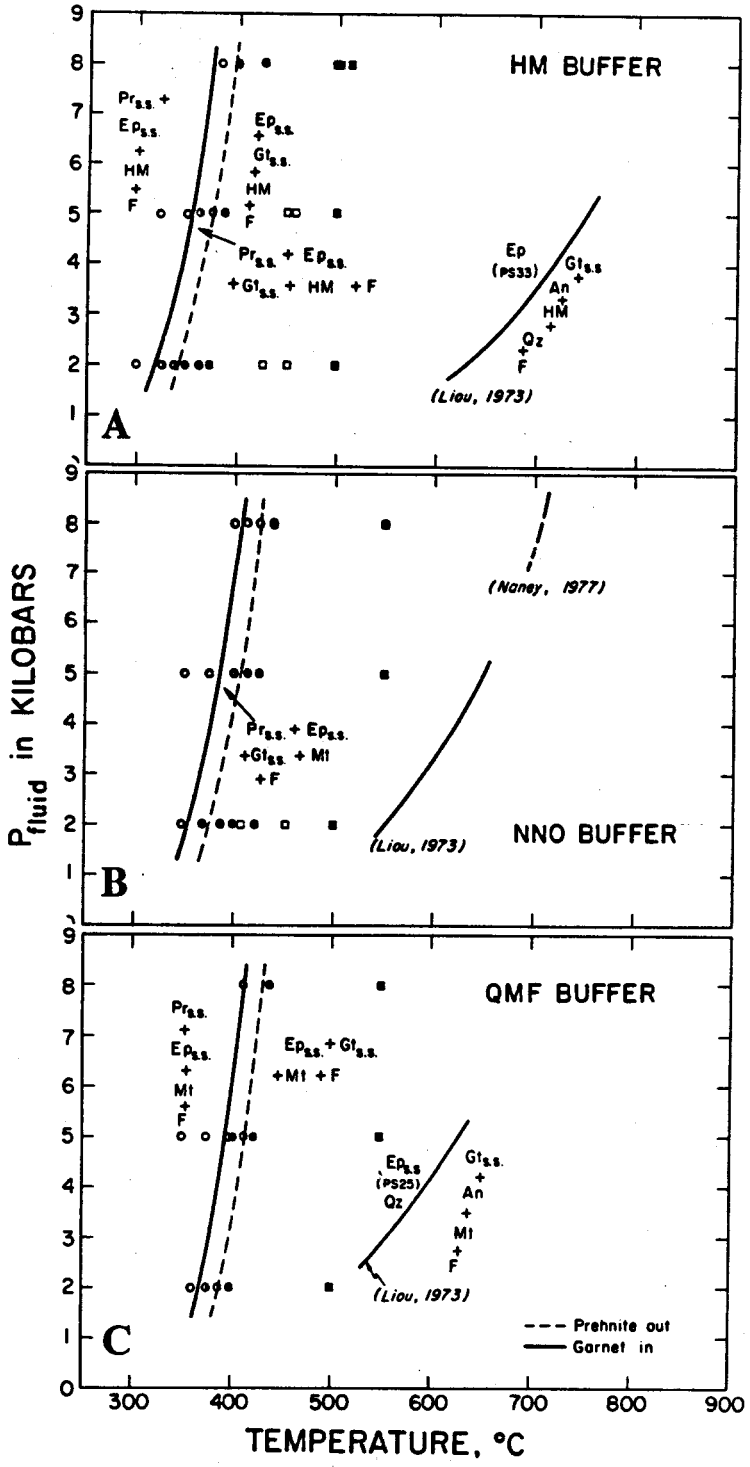

FIG. 4. P_{fluid}–T diagram for the garnet-in and prehnite-out reactions at the f_{O_2} of the HM (A), NNO (B), and QMF (C) buffers. The previously determined curves for the maximum stability of epidote from Liou (1973) and from Naney (1977) are shown for comparison (symbols are same as Fig. 2).

P_{fluid} and f_{O_2} defined by the HM buffer, the coexisting epidote and prehnite have their maximum Fe^{3+} contents at the conditions defined by the garnet-in reaction, with the epidote containing higher Fe^{+3} than the coexisting prehnite.

Prehnite-out reaction

The prehnite-out reaction is defined by the continuous reaction: prehnite$_{s.s.}$ + iron oxide = epidote$_{s.s.}$ + garnet$_{s.s.}$ + fluid. The reaction is expressed by a dashed line in both $\log f_{O_2}$–T and P_{fluid}–T diagrams. Laboratory experiments on the epidote and prehnite minerals have proven difficult. Because of extremely sluggish reaction at low temperatures and especially at low pressures, several methods and types of experimental evidence were necessary to delineate the equilibrium temperature of the prehnite-out reaction. To ensure accurate delineation of this equilibrium, three kinds of starting materials were used: (1) for the starting material II, mixtures of synthetic epidote + natural prehnite + hematite, the amount of epidote increases and the amount of prehnite decreases as the equilibrium boundary of the reaction is approached; (2) for the starting material III, using the run products at temperatures above the prehnite-out reaction, the charge shows a slight increase of prehnite and a decrease of epidote at temperatures below the reaction line, and (3) the metastable prehnites found in the run products at temperatures above the prehnite-out reaction are much more aluminous (Table 4).

Following the above procedures, the equilibrium temperature for the prehnite-out reaction was determined. The prehnite-out reaction crosses the HM buffer curve at 343 ± 5 °C, 2 kb, 375 ± 10 °C, 5 kb, and 395 ± 10 °C, 8 kb, the NNO buffer curve at 377 ± 5 °C, 2 kb, 407 ± 10 °C, 5 kb, and 430 ± 10 °C, 8 kb and the QMF buffer curve at 388 ± 5 °C, 2 kb, 416 ± 10 °C, 5 kb and 435 ± 10 °C, 8 kb P_{fluid}. Apparently, at f_{O_2} values defined by the HM buffer, the upper stability limit of prehnite is about 35 and 45 °C lower than that in the NNO and QMF buffers, respectively.

As shown in Figs. 2–4, the garnet-in and prehnite-out lines are almost parallel; the epidote$_{s.s.}$ + garnet$_{s.s.}$ + magnetite assemblage is stable at high f_{O_2} and temperature, and the prehnite$_{s.s.}$ + magnetite + epidote$_{s.s.}$ assemblage is stable at low f_{O_2} and temperature. In a narrow f_{O_2}–T region, prehnite$_{s.s.}$ + garnet$_{s.s.}$ are stable along with epidote and iron oxide for the bulk composition.

The P_{fluid}–T relations for the garnet-in and prehnite-out reactions together with the maximum stability of epidote (Liou, 1973; Naney, 1977) are shown in Fig. 4. The garnet-in and prehnite-out lines have P_{fluid}–T slopes of about 1 kb/9 °C. The steep slope of the univariant lines suggests that the reactions are not sensitive to variation in P_{fluid}, which is quite different from the upper stability limit of epidote. Such a difference is mainly due to the smaller amounts and smaller volume of H_2O and/or larger ΔS involved in the prehnite–epidote reactions compared to the high-temperature dehydration of epidote described by Liou (1973). The transition zone has a temperature range of about 20 °C at 2 kb, 22 °C at 5 kb and 25 °C at 8 kb P_{fluid}.

PREHNITE–EPIDOTE EQUILIBRIA

The garnet-in and prehnite-out reactions should be considered in the system CaO–FeO–Fe_2O_3–Al_2O_3–SiO_2–H_2O. Fig. 5 shows the phase relations of prehnite, epidote, garnet and hematite as a function of temperature in the pseudo-ternary system CaO–Fe_2O_3–Al_2O_3 with excess quartz and fluid at 2 kb P_{fluid} and f_{O_2} defined by the HM buffer; X gives the starting composition for the present experiments. Four isobaric–isothermal sections are drawn for increasing temperature to show the compositional relations among garnet,

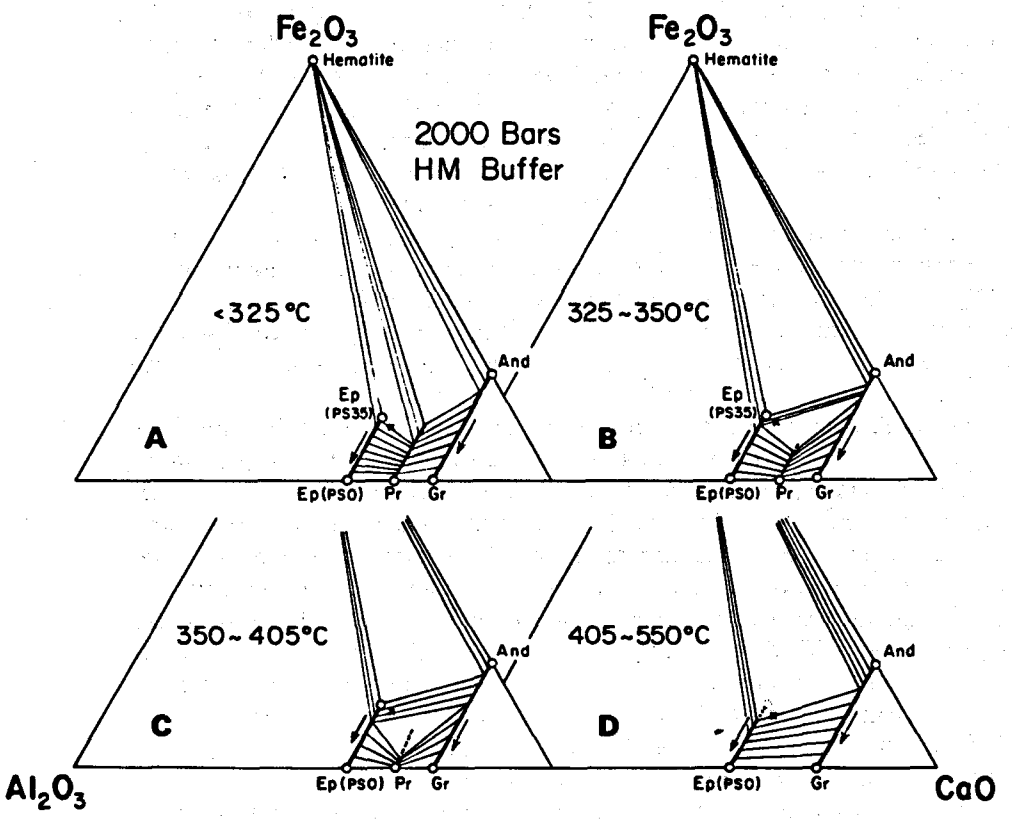

FIG. 5. Phase relations of prehnite, epidote, garnet and hematite as a function of temperature in the system CaO-Fe_2O_3–Al_2O_3–SiO_2–H_2O with excess quartz, and fluid at 2000 bars P_{fluid} and f_{O_2} of the HM buffer. Positions of tie lines are qualitative. X is the starting composition for the present study and arrows indicate the shift of composition with increasing temperature.

epidote, prehnite and hematite for both three-phase and two-phase assemblages. These diagrams were constructed based on the present and previous experimental results and deduced from natural parageneses and mineral compositions.

Phase relations for the pseudo-ternary system CaO–Fe_2O_3–Al_2O_3 at temperatures below 325 °C are shown in Fig. 5A. Grandite garnets are assumed to have complete solid solution whereas both epidote and prehnite have limited extensions of solid solution. The 3-phase assemblages prehnite$_{s.s.}$ + epidote$_{s.s.}$ + HM and prehnite$_{s.s.}$ + HM ± grandite are stable at this P–T–f_{O_2} condition. Fe-epidote cannot coexist with andradite garnet. At 325 °C, a discontinuous reaction, prehnite$_{s.s.}$ + HM = epidote$_{s.s.}$ + grandite$_{s.s.}$ + quartz + H_2O, occurs. This reaction is equivalent to the garnet-in reaction of the present study.

At temperatures between 325 °C and 350 °C, the phase relations for the system are shown in Fig. 5B. Two 3-phase assemblages epidote$_{s.s.}$ + prehnite$_{s.s.}$ + garnet$_{s.s.}$, and epidote$_{s.s.}$ + grandite + hematite and tie lines for 2-phase assemblages are indicated. At any given temperature, the compositions of epidote, prehnite and garnet of the 3-phase assemblages are fixed. With increasing temperature and at the f_{O_2} of the HM buffer, epidote$_{s.s.}$, prehnite$_{s.s.}$ and garnet$_{s.s.}$ become more aluminous and the 3-phase region shifts toward the Al_2O_3–CaO join as indicated by arrows. For the bulk composition of the present study, the 3-phase assemblage prehnite + epidote + grandite garnet is stable.

The phase relations at temperatures between 350° and 405 °C are similar to those at 325° to 350 °C except that the two-phase region of epidote$_{s.s.}$ + grandite becomes wider and those of epidote$_{s.s.}$ + prehnite$_{s.s.}$ and prehnite$_{s.s.}$ + grandite become much restricted with increasing temperature. For the bulk composition of the present study, prehnite becomes unstable and a two phase region of epidote$_{s.s.}$ + grandite occurs instead of the 3-phase assemblage epidote$_{s.s.}$ + prehnite$_{s.s.}$ + grandite. The continuous prehnite-out reaction for the bulk composition of the present study can be written as prehnite$_{s.s.}$ = epidote$_{s.s.}$ + grandite + quartz + fluid.

The phase relations at temperatures above 405 °C, 2 kb P_{fluid} and the f_{O_2} values defined by the HM buffer curve are shown in Fig. 5D. Prehnite is no longer stable and the only 3-phase field is epidote$_{s.s.}$ + grandite + hematite. With increasing temperature, both grandite and epidote increase their Al_2O_3 content as shown by arrows. At the temperature range of 405° to 550 °C, another continuous reaction of epidote$_{s.s.}$ + HM = garnet$_{s.s.}$ + quartz + fluid occurs.

The phase relationships shown in Fig. 5 led to the following conclusions: (1) within the temperature range of 325–550 °C, grandite solid solution may remain complete in the system in the presence of excess quartz, whereas the extents of solid solution for epidote and prehnite become restricted with increasing temperature; (2) tie lines for 2-phase and 3-phase regions show the equilibrium compositions for coexisting phases. These data are deduced from the present experiments, from the available analyses of natural coexisting phases (e.g. Coombs *et al.*, 1977) and from thermodynamic calculations (e.g. Bird & Helgeson, 1981); and (3) the discontinuous reaction at 352 °C represents a crossing of tie-lines and the continuous reaction at 350 °C relates to the shift of the 3-phase field to a 2-phase region for the starting composition of the present experiment. These two reactions are equivalent respectively to the garnet-in and prehnite-out reactions determined by the present study.

The compositional variations and assemblages of minerals shown in Fig. 5 as a function of temperature allow *T–X* relations of phase assemblages to be constructed. This was done under the assumption that epidote, prehnite and garnet solid solutions in the binary systems behave ideally without formation of any intermediate compounds. Fig. 6 is a schematic *T–X* projection of phase relations along the $Ca_2Al_2Si_3O_{10}(OH)_2$–Fe_2O_3 join at 2 kb P_{fluid} and f_{O_2} of the HM buffer. Solid lines are deduced from present and previous experimental data and dashed lines are inferred relations. At temperatures below 325 °C, the 3-phase assemblages prehnite$_{s.s.}$ + hematite + andradite and prehnite$_{s.s.}$ + hematite + epidote$_{s.s.}$ are stable. The 2-phase assemblage prehnite$_{s.s.}$ + epidote$_{s.s.}$ is restricted to Ca-rich compositions and may be stable up to 405 °C. At this temperature, Al-prehnite breaks down to clinozoisite + grossular + quartz + H_2O (Liou, 1971). The discontinuous reaction occurs at 325 °C and the continuous one at about 343 °C for the bulk composition of the present study. These two reactions respectively define the low- and high-temperature compositional lines for the transition zone assemblage $Pr_{s.s.}$ + $Ep_{s.s.}$ + $Gt_{s.s.}$. With increasing temperature, these 3 phases become more aluminous. The partitioning of Al–Fe^{+3} between these phases is such that prehnite is more aluminous than coexisting epidote and garnet, and garnet is the most iron-rich phase (Bird *et al.*, in press). It should also be pointed out that the composition of Al-epidote is much more sensitive to temperature change than that of Fe-epidote whereas the opposite relation holds for prehnite.

Phase relations at higher temperatures in the pseudo-binary system appear to be complicated and cannot be constructed with certainty. An interpretative relation is drawn in Fig. 6; it was deduced from (a) the calculated reaction for the breakdown of clinozoisite (Ps =0) to anorthite + grossular + fluid at about 590 °C, 2 kb P_{fluid} (Holdaway, 1972); (b) relations between zoisite and clinozoisite delineated by Enami & Banno (1980) from natural parageneses; (c) the stability of Fe-epidote (Ps 33) up to 600–670 °C at 2 kb depending on

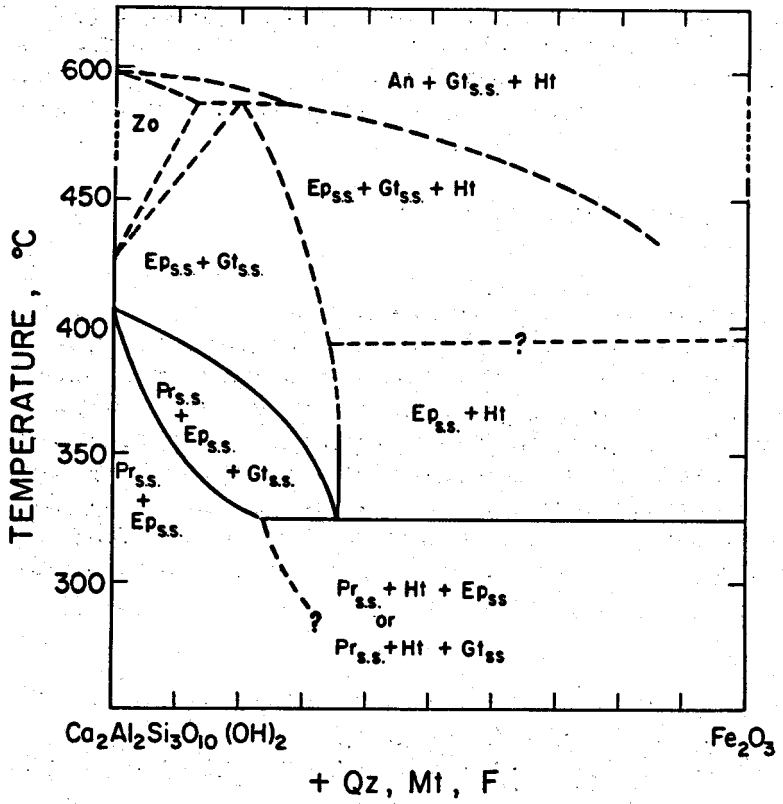

FIG. 6. T–X diagram for the system Fe_2O_3–$Ca_2Al_2Si_3O_{10}(OH)_2$ with excess quartz, magnetite and fluid showing the relations among prehnite, epidote, garnet and hematite at 2000 bars P_{fluid} and f_{O_2} of the HM buffer. The system is pseudo-binary only in the P_{fluid}–T regions where garnet solid solutions form.

the f_{O_2}; and (d) a transition loop with garnet as the higher-temperature phase as suggested by Al-Fe^{+3} partitioning between epidote and garnet (Kitamura, 1975).

Construction of the T–$X_{Fe^{3+}}$ relations and discussion of both continuous and discontinuous reactions can be best illustrated by using Thompson's approach (1976); the results are shown in Fig. 7. For the system discussed in this paper and the f_{O_2} above the HM buffer, five continuous reactions (Ga), (Qz), (Hm), (Pr) and (Ep) and one discontinuous reaction are schematically shown in the P–T diagram of Fig. 7. At constant $P = P_1$ (=2 kb), T–$X_{Fe^{3+}}$ relations of prehnite, epidote and garnet shown in the figure illustrate the following features:

(1) Both continuous and discontinuous reactions are easily recognized in this diagram. For the starting composition of the present system, the continuous reaction is prehnite$_{s.s.}$ = garnet$_{s.s.}$ + epidote$_{s.s.}$ + quartz + fluid. With increasing temperature, these 3 Ca–Al silicates increase their Al content. At the Al-end member, prehnite breaks down to grossular + zoisite + quartz + H_2O at 405 °C and 2 kb P_{fluid} (Liou, 1971). On the other hand, the discontinuous reaction is defined by prehnite$_{s.s.}$ + hematite = epidote$_{s.s.}$ + garnet$_{s.s.}$ + quartz + H_2O. Epidote has maximum Fe^{3+} content at the discontinuous reaction.

(2) In the presence of epidote, prehnite reaches its maximum Fe^{3+} content at the temperature defined by the discontinuous reaction. However, at lower temperatures, prehnite composition is highly dependent on the mineral assemblage. If prehnite coexists with garnet (or presumably another Ca–Al phase) and hematite, it may have higher $X_{Fe^{3+}}$ than the

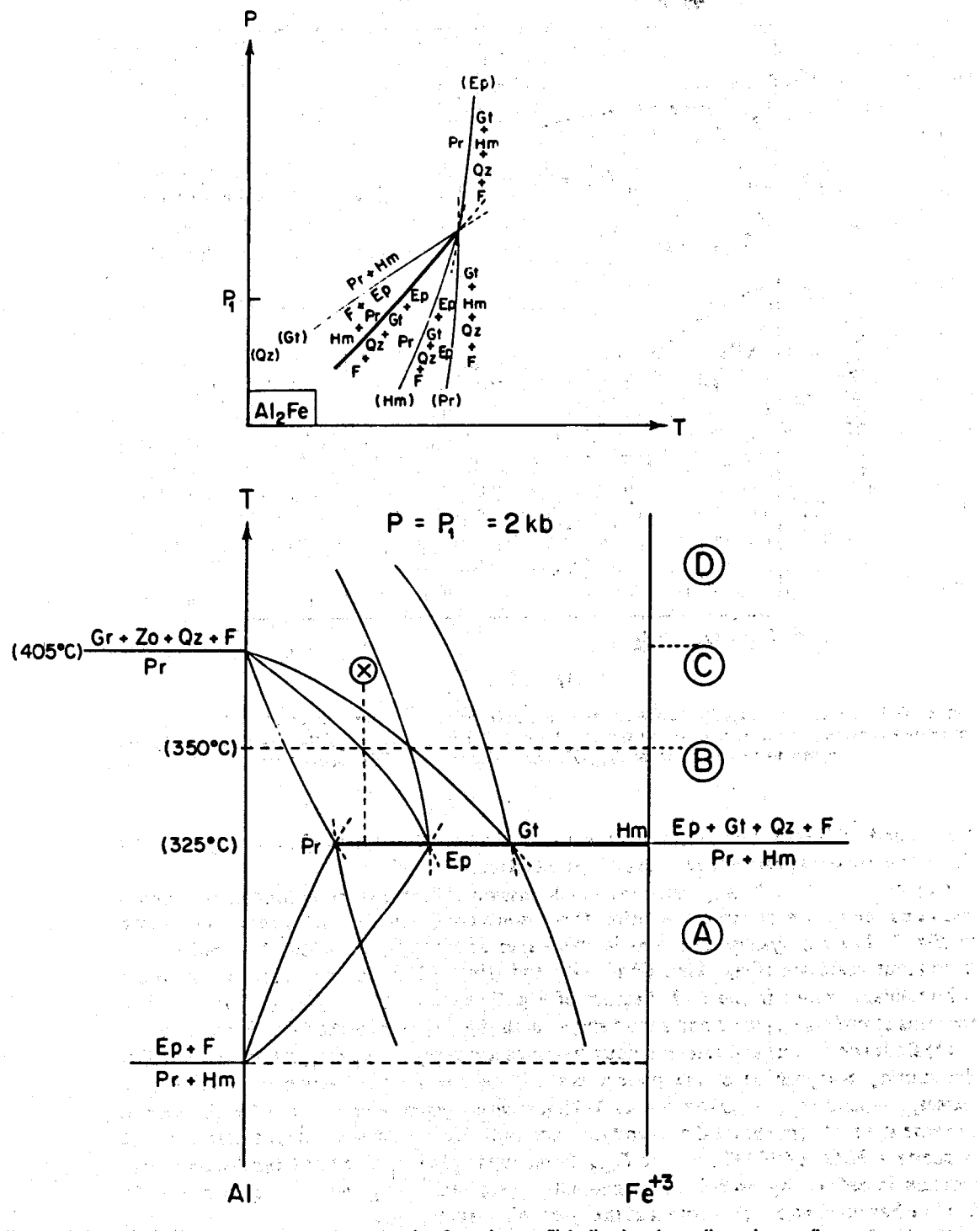

FIG. 7. Schematic P–T and T–X_{Fe-Al} diagrams showing 5 continuous (light lines) and one discontinuous (heavy line) reactions relating prehnite, epidote, garnet, iron oxide, quartz and fluid in system CaO–Fe_2O_x–Al_2O_3–SiO_2–H_2O–O following the procedure of Alan Thompson (1976). Mineral compositions and assemblages shown in Fig. 5A, B, C and D are indicated. X is the starting composition for the present study. Temperatures shown on the diagram are from the present data and Liou (1971).

prehnite coexisting with epidote–hematite–quartz. The temperature–compositional relationship is qualitatively shown in Fig. 7. More systematic compilations of compositions for these Ca–Al silicates are necessary.

(3) Phase relations for the pseudo-ternary system $CaO–Al_2O_3–Fe_2O_3$ as a function of temperature shown in Fig. 5 are schematically designated as A, B, C, and D in Fig. 7. The $T–X_{Fe^{+3}}$ relationship of Fig. 7 provides a quantitative estimate of the Fe^{+3}–Al distribution coefficient among coexisting Ca–Al silicates. It is apparent from Figs. 5–7 that the partitionings are highly dependent on mineral assemblage.

The previous discussions are for phase relations at the f_{O_2} values defined by the HM buffer. At lower f_{O_2} conditions, magnetite is stable in most geologic conditions, and phase equilibria and mineral compositions are significantly different. Fig. 8 is a tetrahedron showing the phase relations of prehnite, epidote, garnet, and iron oxides as a function of f_{O_2} in the system $CaO–FeO–Fe_2O_3–Al_2O_3–SiO_2–H_2O$ in the presence of excess quartz and fluid at a given P_{fluid}. Compositional shifts for magnetite, epidote, prehnite and grandite with decreasing f_{O_2} are shown by arrows. Hence mineral assemblage at various f_{O_2} values could be similar while mineral compositions could be different. For instance, at the f_{O_2} defined by the HM buffer, assemblages hematite + magnetite (b) together with either epidote (c) + prehnite (d) or epidote (c) + andradite (e) or prehnite (d) ± andradite (e) are possibly stable in certain $P–T$ ranges. At the lower f_{O_2} conditions defined by the NNO and QFM buffers, the assemblage magnetite (b′) + epidote (c′) + prehnite (d′) + grandite (e′) is stable. Therefore, at f_{O_2} conditions lower than those of the HM buffer, the phase relations shown in Fig. 6 should be modified.

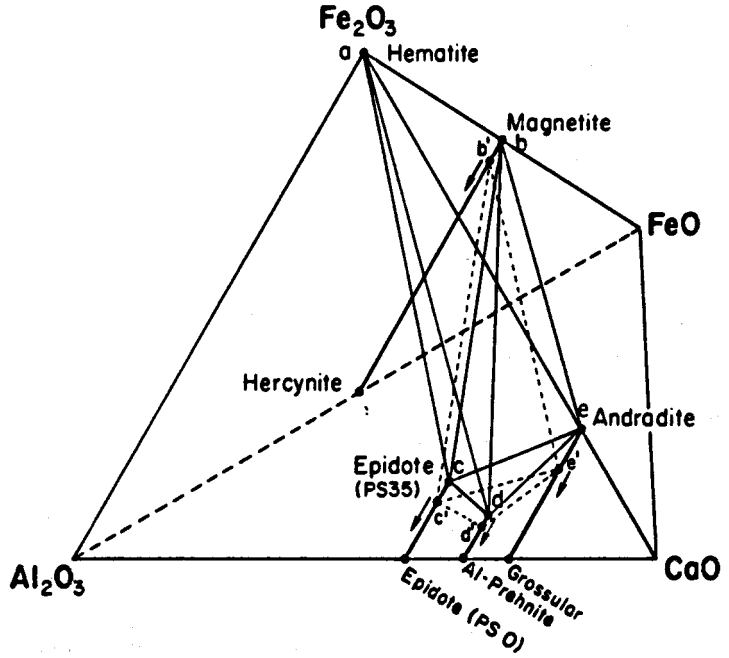

FIG. 8. Tetrahedral projection showing phase relations of prehnite, epidote, garnet, hematite and magnetite as a function of f_{O_2} in the system $CaO–FeO–Fe_2O_3–Al_2O_3$ with excess SiO_2 and H_2O at a particular but unspecified P_{fluid}. Tetrahedrons abcd, abde and bcde are for the systems controlled by the HM buffer. Tetrahedron b′c′d′e′ is for the NNO, QMF and IM buffer systems.

DISCUSSION AND PETROLOGIC APPLICATIONS

Epidote–clinozoisite minerals have a wide stability field and have been recorded in rocks ranging from zeolite facies to magmatic conditions (e.g. Zen & Hammerstrom, 1982) whereas prehnite is widespread in subgreenschist facies rocks at low pressures. However, the assemblage epidote + prehnite ± garnet (+ chlorite + albite + quartz) has not been extensively described due to its restricted P–T–f_{O_2} stability field as demonstrated in the present study. The only documented occurrence of epidote + prehnite + garnet is from spilitized basalt of the prehnite–pumpellyite facies in Gladstone Peak, southern New Zealand (Coombs *et al.*, 1977). This assemblage was inferred to have been recrystallized at 2–3 kb P_{fluid} and 300–400 °C; the $X_{Fe^{+3}}$ content is determined to be 0·53 for garnet, 0·33 for epidote and 0·05 for prehnite. In rocks of increasing grade, these phases become systematically enriched in Al content. Partial assemblages (epidote + prehnite, prehnite + garnet, epidote + garnet) are rather common; the reported occurrences, their $X_{Fe^{+3}}$ contents and estimated P–T conditions are summarized in Table 7. These data, deduced from natural parageneses, are consistent with the present experimental results and the phase relationships shown in Figs. 5–7.

Compositional variations of prehnite and epidote

The extent of solid solution in prehnite defined by the two end-members $Ca_2Al_2Si_3O_{10}(OH)_2$ and $Ca_2Fe^{+3}AlSi_3O_{10}(OH)_2$ has been extensively discussed by previous investigators. The Fe^{+3}-end-member prehnite has not been synthesized nor reported in nature. Hashimoto (1964) suggested that most prehnites have $X_{Fe^{+3}}$ less than 10 per cent although some may extend to 20 per cent. A maximum $X_{Fe^{+3}}$ of 24 per cent and 28 per cent for prehnite solid solution has been reported by Surdam (1969) and Zolotukhin *et al.* (1965), respectively. However, Matsueda (1975) suggested that a compositional gap occurs between 8 and 13 per cent and that the maximum substitution of Fe^{+3} for Al may be up to 10 wt per cent Fe_2O_3 ($X_{Fe^{+3}}$ = 22 per cent). If this gap does exist, then the phase relations between prehnite and epidote described in the previous sections need to be significantly modified. In order to test this hypothesis, microprobe analysed compositions of natural prehnites from zeolite and

TABLE 7

Parageneses, compositions, suggested P–T conditions and distribution coefficients of co-existing Ca–Al silicates from some low-grade metamorphic rocks

Mineral assemblages	X_{Fe}^{Pr}	X_{Fe}^{Ep}	X_{Fe}^{Gt}	*Suggested P–T conditions*	$K_D^{Al-Fe^{3+}}_{Pr-Ep}$	$K_D^{Al-Fe^{3+}}_{Ga-Ep}$	*References*
Pr + Gt + Ch + C_c + Qz	0·24		0·99	2–3 kb, 300–400 °C			Coombs *et al.*, 1977
Pr + Gt + Act + Ch + Qz		0·23	0·67	2–3 kb, 300–400 °C		0·2	Coombs *et al.*, 1977
Pr + Ep + Gt + Pm + Act + Qz	0·05	0·33	0·53	2–3 kb, 300–400 °C			Coombs *et al.*, 1977
Ep + Gt + Ch + Opaque		0·32	0·64	1 kb, 400 °C		0·3	Kitamura, 1975
Ep + Gt + Cpx + C_c		0·24	0·53	1 kb, 470 °C		0·3	Perchuk & Aranovich, 1979
Pr + Ep + Qz	0·19	0·26		Prehnite–pump. facies	1·5		Houghton, 1982
Pr + Ep + Pm + Ch + Ab	0·11	0·27		Prehnite–pump. facies	3·0		Zen, 1974
Ep + Pr + Qz	0·18	0·24		0·4 kb, 320 ·C	3·9		Bird *et al.*, in press
Ep + Pr + Qz	0·18	0·24		0·5 kb, 334 °C	2·9		Bird *et al.*, in press
Pr + Ep + Ch + K_f + Cpx	0·03	0·23		0·5 kb 250–350 °C	9·6		Cavarreta *et al.*, 1980
Pr + Ep + Act	0·03	0·25		Greenschist facies	10·8		Evarts & Schiffman, 1983
Pr + Ep + Mt + Qz	0·10	0·25		2 kb, 376 °C	3·0		The present study

$K_D^{Al-Fe^{3+}}_{Pr-Ep}$: Partition coefficient between prehnite and epidote; $K_D^{Al-Fe^{3+}}_{Gt-Ep}$: Partition coefficient between garnet and epidote.

Ch = chlorite, C_c = calcite, Act = actinolite, Cpx = clinopyroxene, Pm = pumpellyite K_f = K-feldspar

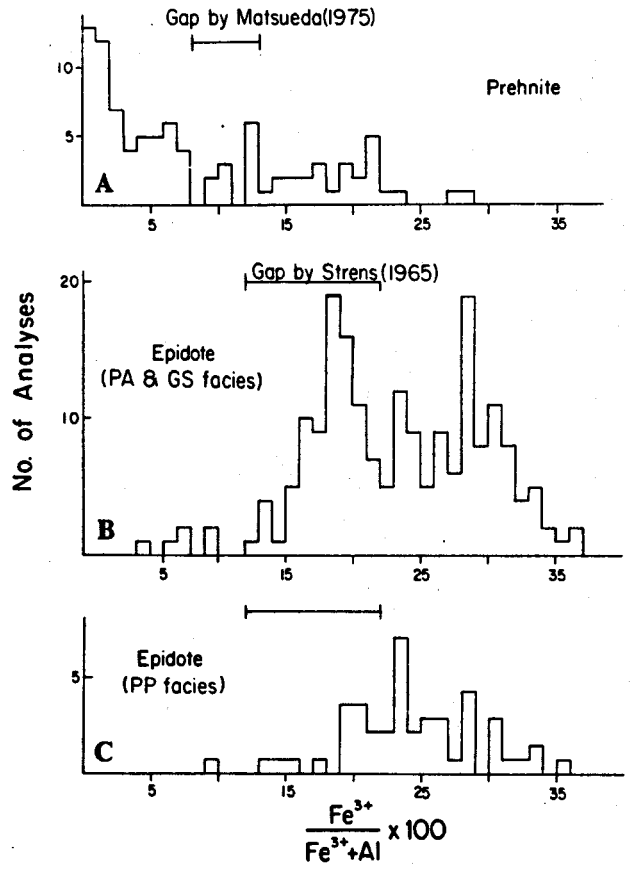

FIG. 9. Histograms showing compositional variations of analyzed prehnite and epidote in low-grade metamorphic rocks together with the proposed compositional gap for prehnite by Matsueda (1975) and for epidote by Strens (1965). A. Data for prehnite are from Surdam (1969), Zen (1974), Coombs *et al.* (1970), Houghton (1982) and Evarts & Schiffman (1983). B. Epidotes for the pumpellyite–actinolite and greenschist facies rocks are from Brown (1967), Toriumi (1972), Coombs *et al.* (1976), and Nakajima *et al.* (1977). C. Epidotes for the prehnite–pumpellyite facies rocks are from Kuniyoshi & Liou (1976), Kawachi (1975), Keith *et al.* (1968), Mehegan *et al.* (1982), Houghton (1982), Smith *et al.* (1982) and Evarts & Schiffman (1983).

prehnite–pumpellyite facies rocks (Surdam, 1969; Coombs *et al.*, 1977; Mehegan *et al.*, 1982; Evarts & Schiffman, 1983; Bird *et al.*, in press) are plotted in Fig. 9A. The results indicate that no compositional discontinuity in the range of 8 to 13 mole per cent exists and that prehnite may contain up to $X_{Fe^{3+}} = 0{\cdot}30$.

The existence of a miscibility gap between Ps 12 and 22 within the epidote series was suggested by Strens (1965). This gap was subsequently reported for natural epidotes from greenschist to garnet amphibolite facies metamorphic rocks (Holdaway, 1965; Hietanen, 1974; Raith, 1976). Available compositions of epidotes from rocks of prehnite–pumpellyite, pumpellyite–actinolite and greenschist facies are plotted in Fig. 9B, C; the data cover the suggested miscibility gap of Strens (1965). Brown (1967) found no gap in epidotes from greenschist facies rocks from part of eastern Otago. Toriumi (1972) confirmed the complete continuity of epidote compositions in the range of Ps 8 to Ps 35 at the pumpellyite–actinolite grade in the Sanbagawa belt, Japan. From these data and from the fact that no direct experimental evidence for such a solvus has been obtained within the range of temperature in

which epidote occurs in nature, it is concluded that epidote solid solution is continuous at least in the range of Ps 10 to Ps 33 (also see Bird *et al.*, in press).

It is known that complete solid solution exists in the grandite garnet system. The linear relationship between physical properties and chemical composition was reported by Liou (1973). Perchuk & Aranovich (1979) also studied the thermodynamics of andradite–grossularite solid solutions from exchange-mineral equilibria with Al and Fe^{+3} aqueous chloride solutions (aq). Their experiments demonstrate complete solid solution between andradite and grossular.

It is concluded that $Fe^{+3}/(Fe^{+3} + Al)$ ratios in prehnite, epidote, garnet and magnetite vary as functions of temperature, P_{fluid} and f_{O_2}. With decreasing temperature and more oxidizing conditions, prehnite, epidote, garnet and magnetite are enriched in Fe^{+3}. The P_{fluid}–T–f_{O_2} relationships shown in Figs. 5–7 are consistent with the compositional variations deduced from natural occurrences and thermodynamic studies.

Sliding equilibria among prehnite, epidote and garnet

The present study indicates that continuous reaction relations exist among prehnite, epidote and garnet as a function of temperature. Field observations are in good agreement with our results, and prehnite is always lower in $X_{Fe^{+3}}$ than coexisting epidote. Seven examples are shown in Table 7. Prehnite ($X_{Fe^{+3}} = 0{\cdot}11$) coexists with epidote of $X_{Fe^{+3}} = 0{\cdot}27$ in a prehnite–pumpellyite facies metabasite, Johnstown (Zen, 1974). In the Larderello-Travale geothermal field, Italy, prehnite of $X_{Fe^{+3}} = 0{\cdot}03$ was found to be stable with epidote of $X_{Fe^{+3}} = 0{\cdot}23$ (Cavarreta *et al.*, 1980). In the Del Puerto ophiolite of Southern California, coexisting prehnite ($X_{Fe^{+3}} = 0{\cdot}08$) and epidote ($X_{Fe^{+3}} = 0{\cdot}25$) are described (Evarts & Schiffman, 1983). These data together with the present results were used to calculate partition coefficients for these minerals. The results are listed in Table 7. As shown in the table, the K_D increases with increasing temperature. Similarly, the Fe–Al distribution coefficient between epidote and garnet has been determined for natural assemblages by Kitamura (1975) and thermodynamically calculated by Perchuk & Aranovich (1979) and Bird & Helgeson (1981). We used their data to draw tie lines for compositions of coexisting epidote and garnet in Figs. 5–7.

It should be pointed out that prehnite with $X_{Fe^{+3}} = 0{\cdot}43$ has been reported by Surdam (1969) and Evarts & Schiffman (1983). According to Fig. 7, such iron-rich prehnite cannot possibly coexist with epidote. One possible explanation is that prehnite enriched its Fe_2O_3 content with decreasing temperature below the temperature of the discontinuous garnet-in reaction. At such low-temperature conditions, prehnite is stable with either laumontite or pumpellyite.

Sliding equilibria involving phases with continuous compositional change are common for low-grade metamorphic reactions. One example of the epidote–pumpellyite sliding equilibrium at pumpellyite–actinolite facies conditions has been illustrated by Nakajima *et al.* (1977) and Schiffman & Liou (1983). Under P–T conditions between those of the maximum stability of Mg-pumpellyite and the minimum stability of Fe-epidote, both pumpellyite and epidote can coexist, with their relationship defined by a continuous reaction similar to the one described in this paper. The partitioning of Fe^{+3} between pumpellyite and epidote in this P–T region is highly dependent on temperature and bulk rock composition. With increasing temperature, the coexisting pumpellyite and epidote decrease their $Fe^{+3}/(Fe^{+3} + Al)$ ratios. At constant temperature, Fe^{+3} may preferentially concentrate in the epidote. The epidote–prehnite relationship described in this paper is similar to that of epidote–pumpellyite.

Most low-grade metabasites consist of two or three Ca–Al hydrosilicates together with albite, white mica, chlorite, quartz, sphene and hematite and/or magnetite. Phase relations

and chemistry of the coexisting Ca–Al silicates are needed in order to use sliding equilibria such as the one described in the present study for the determination of temperature and pressure of metamorphism. Compositions and parageneses of minerals in common low-grade metamorphic basalts can then be shown in a series of Ca–Al–Fe^{+3} plots and T–X diagrams. Figs. 5 and 7 show examples of phase relations and compositions among prehnite, epidote, grandite and iron oxides at four different P–T conditions. The complexity of their relations means that careful examination of natural assemblages and analyses of compositions of coexisting phases are necessary. With such paragenetic diagrams, both continuous and discontinuous reactions can be delineated for progressive metamorphic sequences of basaltic rocks in low, intermediate, and high-pressure series. Hence, P–T conditions of low-grade metamorphism can be more precisely determined.

ACKNOWLEDGEMENTS

The experimental investigations were carried out using the facilities of the Tuttle-Jahns Laboratory for Experimental Petrology at Stanford University. We thank Ron Frost for the suggestion of using Alan Thompson's (1976) projection. This paper was critically reviewed and materially improved by Drs. W. G. Ernst, E-An Zen, B. R. Frost, Mary Keskinen, and Peter Schiffman. Kim was supported by the Ministry of Education, Korea, in his one-year study as a research associate at Stanford. This research was conducted under funding provided by NSF grant EAR 79-09138 and DOE agreement No. DE-FC07-80ID-12148. We thank the above named individuals and institutions for their help and support.

REFERENCES

Appleman, D. E., Evans, H., & Hardwerker, D., 1972. JOB 9214. Indexing and least-squares refinement of powder diffraction data. *U.S. Geol. Surv. Computer Contribution No.* **20**.

Apted, M. J., & Liou, J. G., 1983. Phase relations among greenschist, epidote amphibolite and amphibolite in a basaltic system. *Am. J. Sci., Orville Vol.*

Bird, D. K., & Helgeson, H. C., 1981. Chemical interaction of aqueous solutions with epidote-feldspar mineral assemblages in geological systems. II. Equilibrium constraints in metamorphic/geothermal processes. *Am. J. Sci.* **281**, 576–614.

—— Schiffman, P., Elders, W. A., & Williams, A. E., in press, Calc-silicate mineralization in the Cerro Prieto geothermal field, Baja California, Mexico compared with other active geothermal systems. *Econ. Geol.*

Brown, E. H., 1967. The greenschist facies in part of eastern Otago, New Zealand. *Contr. Miner. Petrol.* **14**, 259–92.

Cavarretta, G., Granelli, G., & Puxeddu, M., 1980. New data on hydrothermal metamorphism in the Larderello-Travale geothermal field. *Proc. 3rd Int. Symp. on Water–Rock Interactions, Edmonton, Canada*, 112–14.

Coombs, D. S., Horodyski, R. J., & Naylor, R. S., 1970. Occurrence of prehnite-pumpellyite facies metamorphism in northern Maine. *Am. J. Sci.* **268**, 142–56.

—— Nakamura, Y., & Vuagnat, M., 1976. Pumpellyite-actinolite facies schists of the Taveyanne formation near Loeche, Valais, Switzerland. *J. Petrology.* **17**, 440–71.

—— Kawachi, Y., Houghton, B. F., Hyden, G., Pringle, I. J., & William, J. G., 1977. Andradite and andradite-grossular solid solutions in very low-grade regionally metamorphosed rocks in Southern New Zealand. *Contr. Miner. Petrol.* **63**, 229–46.

Deer, W. A., Howie, R. A. Zussmann, J., 1962. *Rock-forming minerals.* Vols. 1 and 3. John Wiley & Sons Inc., N.Y.

Enami, M., & Banno, S., 1980. Zoisite–clinozoisite relations in low- to medium-grade high pressure metamorphic rocks and their implications, *Miner. Mag.* **43**, 1005–13.

Evarts, R. C. & Schiffman, P., 1983. Submarine hydrothermal metamorphism of the Del Puerto ophiolite, California. *Am. J. Sci.* **283**, 289–340.

Frost, B. R., 1980. Observations on the boundary between zeolite facies and prehnite-pumpellyite facies. *Contr. Miner. Petrol.* **73**, 365–73.

Hashimoto, M., 1964. The chemistry and optics of prehnite. *J. geol. Soc. Japan*, **70**, 180–3.

—— 1966. On the prehnite-pumpellyite metagraywacke facies. *Ibid.* **72**, 253–65.

Hietanen, A., 1974. Amphibole pairs, epidote minerals, chlorite and plagioclase in metamorphic rocks, northern Sierra Nevada, California. *Am. Miner.* **59**, 22–40.

Holdaway, M. J., 1965. Basic regional metamorphic rocks in part of the Klamath Mountains, northern California. *Ibid.* **50**, 953–77.

—— 1967. Stability of epidote. *Trans. Am. geophys. Un.* **48**, 225.

—— 1972. Thermal stability of Al–Fe epidote as a function of f_{O_2} and Fe content. *Contr. Miner. Petrol.* **37**, 304–40.

Houghton, B. F., 1982. Low-grade metamorphism of the Takitima Group, western Southland, New Zealand. *N. S. J. Geol. Geophys.* **25**, 1–19.

Huebner, J. S., 1971. Buffering techniques for hydrostatic systems at elevated pressures. In: Ulmer, G. C. (ed). *Research techniques for high pressure and high temperature.* Springer-Verlag, N.Y., 123–76.

Kawachi, Y., 1975. Pumpellyite-actinolite and contiguous facies metamorphism in part of upper Wakatipu district, South Island, New Zealand. *N.Z. Geol. Geophys.* **18**, 401–41.

Keith, T. E. C., Muffler, L. J. P., & Cremer, M., 1968. Hydrothermal epidote formed in the Salton Sea geothermal system, California. *Am. Miner.* **53**, 1635–44.

Kitamura, K., 1975. Al–Fe partitioning between garnet and epidote from the contact metasomatic copper deposits of the Chichibu mine, Japan. *Econ. Geol.* **70**, 725–38.

Kuniyoshi, S. & Liou, J. G., 1976. Burial metamorphism of the Karmutsen volcanic rocks, Northeastern Vancouver Island, British Columbia. *Am. J. Sci.* **276**, 1096–1119.

Liou, J. G., 1971. Synthesis and stability relations of prehnite, $Ca_2Al_2Si_3O_{10}(OH)_2$. *Am. Miner.* **56**, 507–31.

—— 1973. Synthesis and stability relations of epidote, $Ca_2Al_2FeSi_3O_{12}(OH)$. *J. Petrology*, **14**, 381–413.

Matseuda, H., 1975. Iron-rich prehnite from the skarn of Sampo mine, Okayama Prefecture, Japan. *Sci. Rept. Geol., Kyushu Univ.* **12**, 91–100.

Mehegan, J. M., Robinson, P. T., & Delaney, J. R., 1982. Secondary mineralization and hydrothermal alteration in the Reydarfjordur drill core, eastern Iceland. *J. geophys. Res.* **87**, 6511–24.

Miyashiro, A., & Seki, Y., 1958. Enlargement of the composition field to epidote and piemontite with rising temperature. *Am. J. Sci.* **256**, 423–30.

Myer, G. H., 1965. X-ray determinative curve for epidote. *Am. J. Sci.* **263**, 78–86.

—— 1966. New data on zoisite and epidote. *Ibid.* **264**, 364–85.

Nakajima, T., Banno, S., & Suzuki, T., 1977. Reaction leading to the disappearance of pumpellyite in low-grade metamorphic rocks of the Sanbagawa metamorphic belt in Central Shikuku, Japan. *J. Petrology*, **18**, 263–84.

Naney, M. T., 1977. Phase equilibria and crystallization in iron and magnesian-bearing granitic systems. *Ph.D thesis, Stanford University.*

Newhouse, W. H., & Glass, J. P., 1936. Some physical properties of certain iron oxides. *Econ. Geol.* **31**, 699–711.

Perchuk, L. L., & Aranovich, L. Ya., 1979. Thermodynamics of minerals of variable composition: andradite-grossularite and pistacite-clinozoisite solid solution. *Phys. Chem. Minerals*, **5**, 1–14.

Raith, M., 1976. The Al–Fe (III) epidote miscibility gap in a metamorphic profile through the Perinee Series of the Tauern Window, Austria. *Contr. Miner. Petrol.* **57**, 99–117.

Schiffman, P., & Liou, J. G., 1980. Synthesis and stability relations of Mg–Al pumpellyite, $Ca_4Al_5MgSi_6O_{21}(OH)_7$. *J. Petrology*, **21**, 441–74.

—— 1983. Synthesis of Fe-pumpellyite and its stability relations with epidote. *J. Metamorphic Geol.*

Seki, Y., 1971. Wairakite–analcime solid solution as an indicator of water pressure in low-grade metamorphism. *J. Geol. Soc. Japan*, **77**, 667–74.

Smith, R. E., Perdrix, J. L., & Parks, T. C., 1982. Burial metamorphism in the Hamersley Basin, Western Australia. *J. Petrology*, **23**, 75–102.

Strens, R. G. J., 1965. Stability relations of the Al–Fe epidotes. *Miner. Mag.* **35**, 464–75.

Surdam, R. C., 1969. Electron microprobe study of prehnite and pumpellyite from the Karmutsen Group, Vancouver Island, British Columbia. *Am. Miner.* **54**, 256–66.

Thompson, A. B., 1976. Mineral reactions in pelitic rocks: I. Prediction of *P–T–X* (Fe–Mg) phase relations. *Am. J. Sci.* **276**, 401–24.

Toriumi, M., 1972. Microprobe study of zoned epidote in the Sanbagawa metamorphic rocks from the Kanto mountains. *J. geol. Soc. Japan*, **78**, 545–48.

Turnock, N. C., & Eugster, H. P., 1958. Magnetite-hercynite relations. *Yb. Carnegie Instn. Washington*, **57**, 209.

Zen, E-An, 1974. Prehnite- and pumpellyite-bearing mineral assemblages, west side of the Appalachian metamorphic belt, Pennsylvania to Newfoundland. *J. Petrology*, **15**, 197–242.

—— & Hammerstrom, 1982. Magmatic epidote: host rocks, mineral compositions and significance. *Abstr. Progr. geol. Soc. Am.* **14**, 652.

Zolotukhin, V. V., Vasipyev, R., & Zyuzin, N. I., 1965. Iron-rich modification of prehnite and a new diagram for prehnites. *Dokl. Akad. Nauk USSR*, **164**, 1390–3.

Investigation of Geothermal Systems in Japan I. Onikobe Geothermal Area

by Y. Seki, J. G. Liou, R. Guillemette,
H. Sakai , Y. Oki, T. Hirano
and H. Onuki

Hydroscience and Geotechnology
Leboratory, Saitama University
Memoir No. 3

July, 1983

Investigation of Geothermal Systems in Japan I. Onikobe Geothermal Area

by Y. Seki[1], J. G. Liou[2], R. Guillemette[2], H. Sakai[3], Y. Oki,[4], T. Hirano[4] and H. Onuki[5]

(1) Hydroscience and Geotechnology Laboratory, Saitama University, Urawa, 338, Japan
(2) Department of Geology, Stanford University, Stanford, California, 94305, U. S. A.
(3) Institute for Thermal Spring Research, Okayama University, Misasa, Tottori, 682-02, Japan
(4) Kanagawa Hot Spring Research Institute, 250−03, Japan
(5) Department of Earth Sciences, Hirosaki Universi ty, Hirosaki, 036, Japan

ABSTRACT

Continuous exploration and development for geothermal power in active volcanic areas such as Japanese Islands have provided excellent opportunity to investigate water-rock interactions in geothermal systems. Our basic premise is that the changing composition and temperature of geothermal fluids as a function of time is recorded by the parageneses, compositions and isotopic properties of the associated mineral assemblages, and that the latter can be used to reconstruct the evolution of a geothermal system. Hence, detailed mineralogical-petrological-geochemical investigation of drill hole core samples is necessary to fully understand the complex effects of rock-water interactions in geothermal systems.

The Onikobe geothermal area is selected for detailed study as part of the U.S.-Japan cooperative project in 1978-1983 because in Onikobe which has been recognized as a classic example of a geothermal system in Japan, many pilot, exploratory and producing wells ranging from 200 to 1300 meters in depth have been drilled and geological-geochemical-geophysical information and nearly complete drill hole core samples are available. Mineralogical and petrological examinations of two drill holes with depth to 350 m (Nos. 123 and 124) and one down to 1155 m (No. 127) were completed; parageneses and compositions of secondary minerals were identified and analyzed. Few selected samples were investigated by SEM and isotopic mass spectrometer. These newly collected chemistries together with available water chemistries and petrological-mineralogical data of other drill hole cores from the Onikobe geothermal area were used to outline the effects of geothermal waters and other controls on the alterations of the enclosing rocks.

The Onikobe caldera is on the eastern edge of the Green Tuff basin in north central Honshu and has an oval-shaped depression about 10 Km in diameter. The Miocene Green tuffs together with younger caldera deposits unconformably

overlie the basement complex of Paleozoic pelitic schists and Cretaceous granodiorite. The caldera formations are Plio-Pleistocene age and consist of both marine and non-marine volcanogenic tuffs and lavas of andesitic to dacitic composition. After the deposition of the caldera sediments and lavas, a dacitic lava dome of 0.35 m.y. BP was intruded into the southern part of the Onikobe basin. Associated with the intrusion were the normal faulting and hydrothermal alterations. The magmatic activity related to the dome formation is believed to be the major heat source for the present-day geothermal activity and associated hydrothermal manifestations in the Onikobe area.

Because of intense hydrothermal alterations, no fault has been positively identified on the surface by geomorphological and geological data. However, occurrence of subsurface faults has been inferred from seismological and electric survey; these subsurface faults may have controlled the three Onikobe geothermal belts which have been delineated from deep drilling of over fifty production and pilot bore-holes.

Thermal waters from the Onikobe geothermal area have been analyzed; they belong to the Na-Cl or Na-Ca-Cl type. They may have evolved from contamination of dissociated HCO_3 and magmatic NaCl-rich solution with meteoric water. However, our new δS^{34} isotopic and geochemical data suggest that a considerable amount of fossil seawater from Miocene Green Tuff in the basement of the Onikobe Quaternary volcano must have supplied some deep wells. Acidic thermal waters with high SO_4 and low Cl contents apparently are confined to shallow depths. This conclusion was supported by the widespread occurrence of calcite in deep drill-hole samples and by drilling of a new production hole at 1255 m with a remarkable amount of alkaline (pH = 8.3~8.5) high-T thermal waters.

In spite of the pervasive hydrothermal alteration, four rock types were identified among those drill hole core samples: andesitic tuff and lava, and dacitic tuff and lava. The andesitic rocks contain mainly augite $\pm$ hypersthene $\pm$ hornblende as major mafic minerals and the dacitic rocks are characterized by

the presence of hornblende and quartz phenocrysts, plagioclase of lower An content and higher contents of glassy matrix or groundmass. Both pyroclastic and lava rocks are highly vesicular and abundant secondary minerals occur in vesicles. Fifteen less altered core samples were analyzed by a wet chemical method; the results indicate that the compositions of the altered rocks vary significantly from their unaltered equivalents. Significant leaching of SiO_2, MgO, $Na_2O + K_2O$, addition of H_2O and S and oxidation of FeO must have occurred during the hydrothermal alteration and such chemical alteration varies from specimen to specimen. Nevertheless, these rocks may belong to Kuno's hypersthene series and may have chemical characteristics of the calc-alkaline series.

The minerals produced by the hydrothermal alteration depend on geologic position, composition of host rock and chemical composition of the fluids. Near the surface, particularly in fumarolic areas, where vigorous boiling occurs and mixing with atmospheric oxygen is possible, the rocks altered to soft siliceous material containing clays, opaline silica, alunite, sulfur and pyrite. At deeper levels, the mineral assemblages are different and zonal distribution of secondary minerals with depth was determined. Secondary minerals in the bore-hole cores occur as (a) precipitation in vesicles and along fractures, (b) replacement of plagioclase and mafic phenocrysts, and (c) replacement of groundmass or volcanic glass.

Clay minerals are the most common phase in the bore-hole cores and consist of smectite, alkaline smectite, chlorite/smectite interstratified minerals, chlorite and illite. They show systematic variations with depth and temperature, correlatable with Ca-zeolites and other minerals. Their characteristic X-ray basal spacings under dry condition and after glycol treatments and morphological features by SEM were described. The chlorite/smectite interstratified phases are variable in composition and contain mainly SiO_2 (28-33 wt%), minor amounts of MnO (0.06-2.0 wt%) and CaO (0.1 to 2.2 wt%), and negligible amounts of K_2O and Na_2O. The Ca content

of the interstratified phase decreases with increasing depth, in accordance with the lower proportion of interlayered smectite observed in the X-ray diffraction results. The chlorites are restricted to deep-hole cores and have a much more restricted range of chemical compositions with much lower CaO and SiO_2 than the chlorite/smectite phase.

Illitic clay minerals are relatively rare compared to chlorite/smectite phases due to low K_2O contents of original rocks. The illitic clay minerals, judging from their X-ray diffraction patterns and limited microprobe compositions, belong to the illite and illite/smectite interstratified minerals. Continuous variations occur in this series; with increasing depth, the smectite component decreases and illite becomes the major K-bearing phase for deep drill hole core samples.

Zeolite minerals are well developed in the core samples and some are exceptionally abundant. Such common zeolites include mordenite, laumontite, yugawaralite and wairakite and their depth distributions were determined. Minor zeolites identified in the core samples include clinoptilolite, dachiardite, chabazite, thomsonite and natrolite. Laumontite is typically found at depths greater than 50 m and shallower than 400 m and yugawaralite at the lower end of the laumontite zone. The analyzed laumontite and yugawaralite have nearly stoichiometric composition with very minor amounts of Fe_2O_3, Na_2O and K_2O. Wairakite is the most abundant zeolite mineral and occurs in most wells at depths greater than 100 m. Many wairakites were analyzed and have considerable ranges of compositions with less than 0.2 wt% Fe_2O_3 as total Fe and 0.1 wt% K_2O. Main variations are defined by 2 end-members "wairakite" and "analcime". All analyzed wairakites range from Wr_{100} to Wr_{76} and no analcime-rich composition was found. There appears to be no correlation between composition of wairakite and depth of its occurrence, nor any pattern between composition and mode of occurrence.

Other Ca-Al silicates include minor prehnite and epidote. The analyzed prehnites span a considerable range of $Fe^{+3}/(Fe^{+3} + Al)$ ratio; the most

iron-rich prehnites contain 6-8 wt% Fe_2O_3 and appear to be stable with epidote + wairakite + quartz + chloritic clay. The veined prehnites are much lower in Fe content and are stable with wairakite ± calcite + quartz. The analyzed epidotes range in pistacite content from 19 to 37 and most analyses are around Ps 29 to 33. The compositional range of epidote is very compatible with those from other geothermal area (e.g., Cerro Prieto). The analyses of epidote and prehnite suggest that no immiscibility gap exists for these phases.

Silica minerals are ubiquitous and include both cristobalite and quartz. Cristobalite is restricted to shallow depths whereas secondary quartz is present in every core samples. Kaolinite is one of the most common phases at the surface of fumarolic areas. However, in drill hole core samples, both kaolinite and pyrophyllite are very minor. Calcite is another common phase which occurs as one of the last phases in paragenetic sequence. All analyzed carbonate grains are calcite in composition with only a few percent Fe, Mg and Mn. Other secondary minerals include albite, ubiquitous pyrite and halite. The $\delta^{34}S$ value of pyrite suggested that fossil seawater within Miocene sediments may have contributed sufficient sulfur for pyrite crystallization at depth.

The zonal distribution of clay and zeolite minerals can be simplified as follows: With increasing depth, the following patterns are: alkaline smectite or smectite ⟶ chlorite/smectite interstratified mineral ⟶ chlorite for clay minerals and mordenite ⟶ laumontite ⟶ yugawaralite ⟶ wairakite for zeolites. We consistently found the general associations that alkaline smectite and smectite occur with mordenite, chlorite/smectite interstratified phase with laumontite, and chlorite with wairakite. Such zonal patterns are correlatable with other geothermal areas in Japan, Iceland, New Zealand and the U.S.

Chemographic relations of common Ca-Al hydrosilicates (Ca-zeolites, epidote and prehnite) together with quartz, carbonate and chlorite/smectite were delineated in a simplified system $CaO-Fe_2O_3-Al_2O_3-(FeO + MgO)-SiO_2$

— H_2O -CO_2. Compositions of prehnite and epidote are plotted in a ternary diagram CaO-Al_2O_3-Fe_2O_3 and tie lines for the coexisting phases in the 2-phase assemblages (wairakite + epidote and wairakite + prehnite) and the 3-phase assemblages (epidote + prehnite + wairakite and wairakite + prehnite + calcite) are drawn. The deduced phase relationships at T of 100-170°C and depth of 200-350 m yield five 3-phase assemblages which have been recorded in other geothermal areas and in low-grade metabasalts. Three conclusions are made from such chemographic relations: (1) Both prehnite and epidote are restricted to Fe-rich composition at low temperatures and become Al-rich with increasing temperature, (2) the Al-end member of both prehnite and epidote are not stable under the physico-chemical conditions of the Onikobe geothermal system, and (3) the Fe-Al partioning between epidote and prehnite suggests that the epidote always contains higher Fe than the coexisting prehnite. Such conclusions are consistent with those data deduced from hydrothermal experiments, thermodynamic calculations and natural observations.

Zonal distributions of minerals and phase relationships observed in the Onikobe geothermal area are controlled by a complex interplay of many factors. Relevant experimentally determined stabilities of Ca-zeolites, clay minerals, epidote and prehnite were used to illustrate the paragenetic depth (temperature) sequence. The effects of other variables including (a) solution chemistry, (b) bulk rock chemistry, (c) rock permeability, (d) local pressure, (e) P_{H_2O}/P_{total}, (f) solid solutions in secondary minerals, (g) CO_2 content and (h) kinetics are briefly discussed. Because of these effects, the apparent observed temperature ranges over which minerals are found in the Onikobe area are generally broader than those expected from the experimental studies.

In order to explain the origin of acid-chlorite solution in the Onikobe geothermal area, a possible fault-hydrologic model was proposed. The origin of this acid fluid could be explained either by a deep-seated magmatic HCl source or by the contamination of neutral chloride waters with a small amount of

near-surface derived acid-sulfate water. The latter could be due to steeply-dipping recharge faults or to corrosion of the well casing. The acid sulfate explanation is favored because of the relative volcanic inactivity of the area and the general hydrologic patterns observed in the Onikobe region.

In summary, the distribuion of secondary phases with depth in the Onikobe geothermal area is primarily controlled by changes in temperature. Depth-dependent zonation patterns are observed for the zeolites, clay minerals and several other secondary phases. The comprehensive and cooperative study of the drill core samples from the Onikobe geothermal area have addressed questions which are necessary for our better understanding of the evolution of a geothermal system. The similarities and differences in mineral parágenesis and interactive modes for water-rock interactions in this and other geothermal systems should be compared and are the subjects of our continuous investigations.

INTRODUCTION

Japan and Taiwan provide excellent examples of active geothermal systems in geologic terrains which are well understood. Development of geothermal power has been greatly emphasized in these countries because it is potentially a major energy resource in active volcanic areas. Exploration for geothermal energy in Japan and Taiwan began in the early sixties, and many exploratory holes have been drilled up to 2000 m in depth. Drill hole cores have been sampled, thermal waters have been analyzed chemically and isotopically, and many other geological data (e.g., temperature gradient, flow rate, permeability) and geophysical data have been collected. A 25 MW geothermal power plant was successfully installed at Onikobe in 1975.

This project on rock-water interaction in geothermal systems was initiated under a U.S.- Japan Project. Since April 1, 1978, the NSF and JSPS have sponsored a joint U.S.-Japan project on coordinated studies of rock-water interactions in geothermal systems utilizing experimental and field approaches. At Stanford, we have studied the interaction of andesitic-basaltic rocks with seawater and meteoric waters from 200°C to 400°C in order to determine the kinetic and equilibrium modes of interaction of rocks with solutions chemically, isotopically and mineralogically. In Japan and Taiwan, the properties of drill hole core samples and the field aspects of rock-water interactions in the Onikobe, Hakone and Tatun geothermal areas were investigated. The field studies include petrological-mineralogical-geochemical examinations of drill-hole core samples and their correlation with the chemical and isotopic properties of thermal waters. The collective specific aims were, and are: (1) to determine the mineralogical, chemical and isotopic characteristics of the hydrothermally altered rocks in these geothermal areas, (2) to deduce the sequence of chemical, mineralogical and geological events that have affected the mineral assemblages of the altered rocks, and (3) to determine the kinetics and equilibrium reactions attending the alteration. The

conclusions and problems posed by the field data are to be correlated with and interpreted by the experimental data, to better our understanding of the genetic processes in geothermal systems.

Our common goal is to study rock-water interactions of Japanese geothermal systems in the hope that some general statements will be possible that apply to processes in this classic island arc. We hope that generalizations applicable to island arcs elsewhere will eventuate. There are many geothermal fields in Japan and some of them have already installed geothermal power plants. However, the project has focused only on a restricted number of areas, in view of time and personnel limitations. We have taken the Onikobe and Hakone areas in Japan and the Tatun in Taiwan as on-going subjects. These geothermal areas were selected for detailed investigation because they are recognized as classic examples and because geological-geochemical-geophysical information and a nearly complete set of drill hole core samples are available. All three of these geothermal areas are in volcanic areas and are largely andesitic, but they differ from one another in the varieties of andesitic and other rocks present, and they differ somewhat in water types; hence, secondary mineral assemblages and mineral parageneses are somewhat different. The similarities and differences among the three geothermal areas could yield some principles relating to water-rock interactions in geothermal systems which might not be apparent from the investigation of a single system.

This report describes the results of our detailed investigations of drill-hole core and thermal water samples from the Onikobe geothermal area. Similar reports will be prepared for the Hakone and Tatun geothermal systems.

THE ONIKOBE GEOTHERMAL AREA

LOCATION AND BACKGROUND

The Onikobe geothermal area is located in the northwestern corner of Miyagi Prefecture, northern Honshu and lies within the Kurikoma - Quasi National Park

(Figure 1).

When the energy crisis became apparent in the early sixties, the Electric Power Developing Co., Inc. carried out exploratory surveys of many geothermal areas in Japan. It was concluded that of all the areas investigated, the Onikobe basin showed the greatest potential for geothermal power generation. In the period from 1962 to 1972, basic exploratory surveys were conducted and many pilot holes were drilled in order to collect samples, to measure subsurface temperatures and compositions of thermal waters and to investigate subsurface structures. As a result of the surveys, the company concluded that the

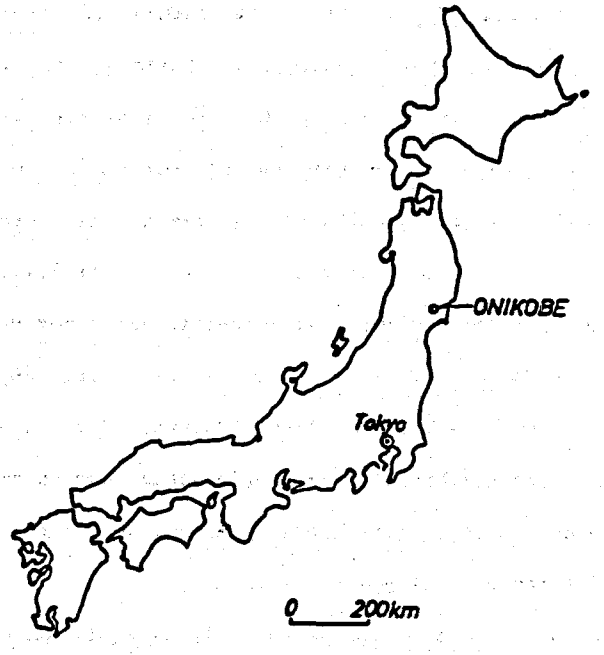

Figure 1. Location of the Onikobe area, Japan.

geothermal steam was sufficiently abundant and of high enough temperature to generate electricity. Hence, the company started constructing a power plant in April of 1973 and it was completed in the spring of 1975. This 25 MW facility has been one of the proto-type geothermal power plants in Japan.

Moreover, the Onikobe geothermal steam is mostly produced from as shallow as 300 meters in depth and this area is characterized by the surface manifestations of the geothermal field. The surrounding areas are covered by natural forest and

the geothermal steam is re-injected into the deep portion of the basin. The installation of the geothermal power plant has preserved the natural beauty of the national park, and therefore the Onikobe geothermal system has been highly publicized.

ACKNOWLEDGEMENT

This report presents research accomplished during the tenure of a United States-Japan scientific cooperative project, supported by NSF 77-23173, DOE-SC07-80ID-12145 and JSPS (Grant 4-R039). Facilities at Stanford University, Saitama University, the Hot Spring Research Institute of Hakone and Institute for Thermal Spring Research, Japan provided bases for the laboratory and analytical studies. Our investigations benefited at all stages from the association with many geologists and civil engineers, particularly Dr. T. Hitosugi, of the Electric Power Development Co., Japan (EPDC). EPDC provided core specimens and many thermal water samples and allowed us to use much of their geological and technological information.

We thank the above mentioned institutions and their personnel and the individuals for their support, comments and advice. J.G. Liou is grateful to the John Simon Guggenheim Memorial Foundation for gracious and unencumbered support during 1978-1979.

PROCEDURES OF THE PROJECT AND METHODS OF INVESTIGATION

Many pilot, exploratory and producing wells ranging from 200 to 1300 meters in depth have been drilled in the Onikobe geothermal area since 1963 by the Electric Development Company Ltd. The sites of drill holes studied are plotted in Figure 2; their columnar stratigraphic sections and temperature distributions are shown in Figures 3, 4, 5 and 6 (these features will be described in detail in later sections). More information on these drill holes is listed in Table 1.

Some preliminary data for drill hole GO-2, GO-5, GO-7 and GO-8 have been published (Seki, Onuki et al., 1969). Many other core samples were examined and

these include core materials from P-5, P-7, P-8, P-10, GO-7, GO-8 and GO-11. These previously accumulated data together with our new observations on recently collected samples from new hole # 123, #124 and #127 will be described in this report. The general procedure of the project and method of investigation are described below.

Plan of the Project

Selection of the Onikobe and Hakone geothermal areas for the cooperative research targets was made in 1977, since their basic geology and hydrologic-geochemical information of their thermal waters are available and both Seki and Oki have been working on these geothermal areas for a number of years. The Tatun geothermal system was added to our project for comparison with the Japanese systems because of its potential economic importance. The group (in part or as a whole) met several times during the 1976-78 period to discuss and define the basic role of each investigator. A set of interesting scientific questions was drawn up, and alternative target areas in Japan and Taiwan were proposed.

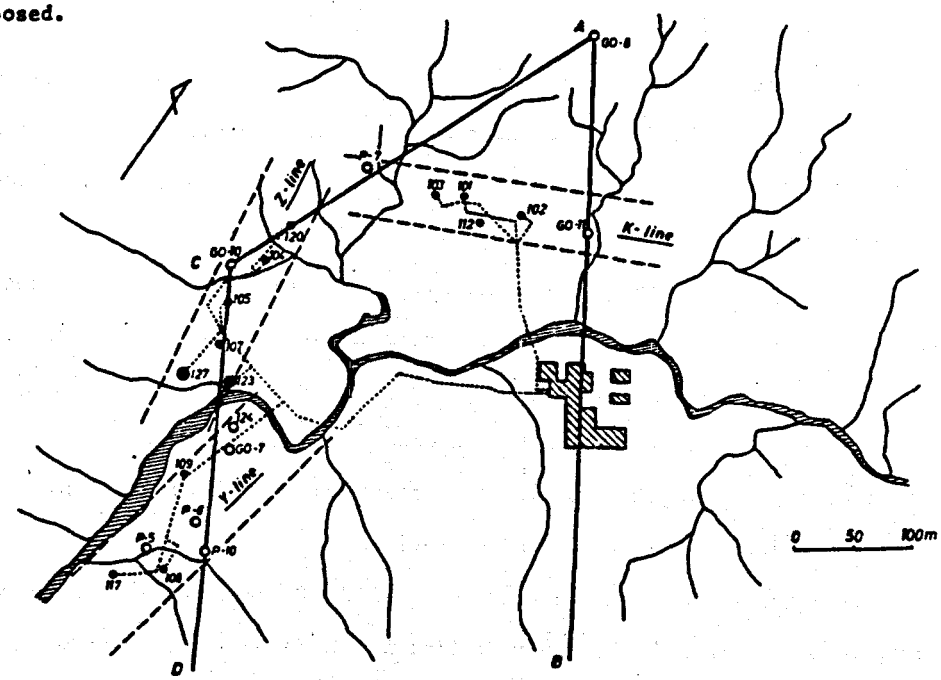

Figure 2. Distribution of bore holes in the Onikobe geothermal area, Japan. Open circles: Bore-holes described in this report. Black dots within Open circle: Production wells (e.g., #123 and #127).

Table 1. Depth from land surface and date of drilling completion of bore-holes plotted in Figure 2.

Number	Depth (m)	Date
GO-7	500.0	1966, Nov.
GO-8	1000.0	1969, June
GO-10	1352.0	1970, Oct.
GO-11	1300.0	1972, Feb.
P-5	75.5	1971, Jan.
P-7	250.0	1971, Apr.
P-8	250.0	1973, July
P-10	203.0	1973, Aug.
101	233.0	1970, Oct.
102	301.0	1971, Sept.
103	228.0	1971, Sept.
104	366.0	1971, Dec.
105	375.0	1972, July
107	362.0	1972, Sept.
108	244.0	1974, Feb.
109	243.0	1973, Jan.
112	320.0	1973, June
117	170.0	1975, May
120	383.0	1976, Apr.
123	351.0	1977, Feb.
124	351.0	1978, Apr.
127	1155.0	1980, July

Field Study and Sample Collection

The group met in Japan during the summer of 1978 and visited many geothermal areas there. At the Onikobe caldera, the power plant was visited and rock types, geologic structures and flowing springs were examined. Two drill hole cores with depths down to 350 m (Nos. 123 and 124) and one down to 1300 m (GO-11) were selected for detailed petrologic-geothermal studies (see Figure 2 for location). Their stratigraphic relations and temperature gradients have been constructed by Seki. Core samples were collected at every 10 to 20 m and were separated into three portions: one to Seki and Oki for petrographic and clay mineral identification, one to Sakai for isotopic study, and one to Stanford for petrographic, microprobe and SEM investigations.

In september 1980, Ray Guillemette visited the Onikobe geothermal areas and collected core samples from a newly drilled No.127 (see Figure 2 for location). This hole was drilled under the recommendation of Seki and Oki based on our petrological-geochemical data, and this has been the best producing well in the

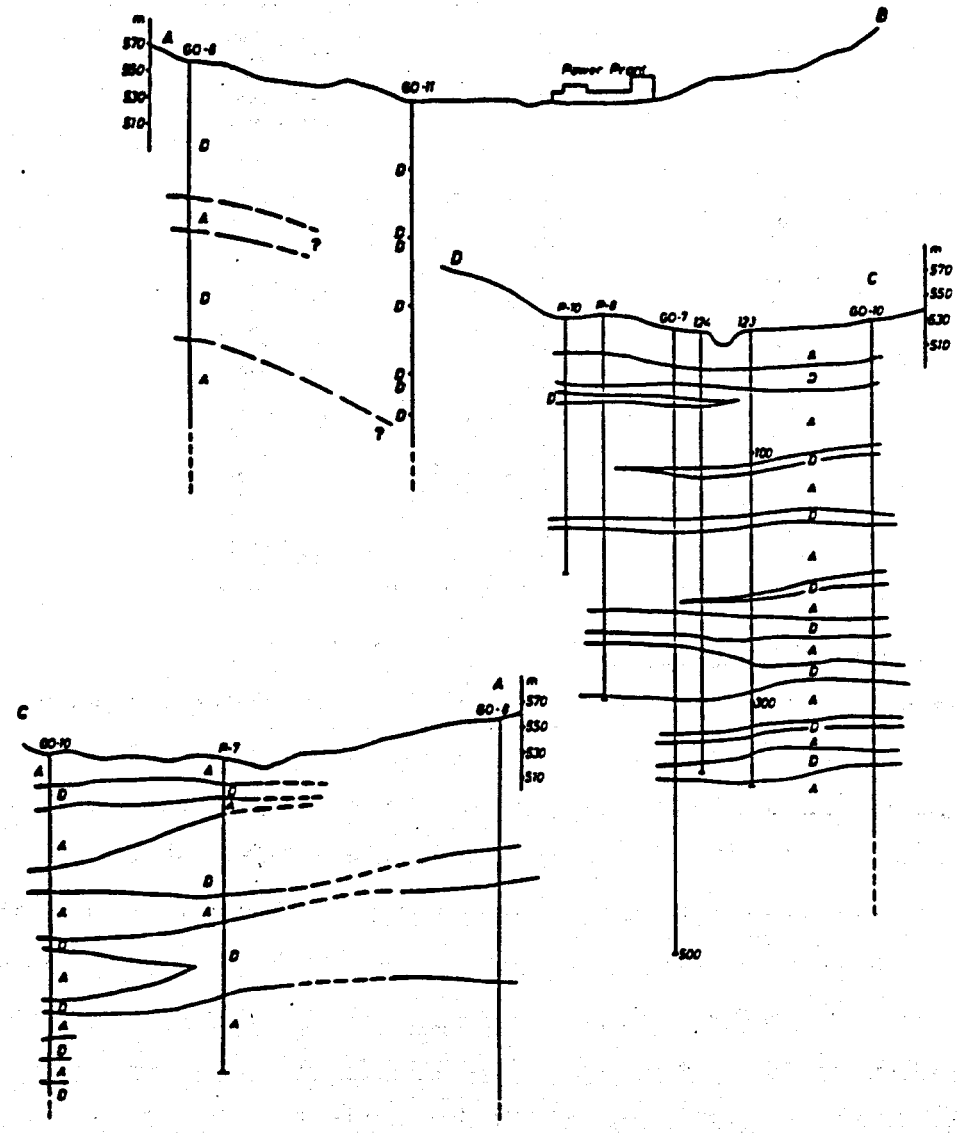

Figure 3. Geologic cross sections along A-B, A-C, and C-D of Figure 2 for the Onikobe geothermal area, Japan. A: Volcanic rocks of andesitic compositions. D: Volcanic rocks of dacitic compositions.

area.

Petrographic Study

During September 1978 to July 1980, we studied the thin sections of drill-hole core samples. Minerals identified include Ca-zeolites (mordenite, stilbite, epistilbite, heulandite, yugawaralite, laumontite and wairakite), analcime, prehnite, epidote, albite, K-feldspar, gypsum, anhydrite, alunite, carbonate, kaolinite, illite, smectite-chlorite clay minerals, pyrite, magnetite, hematite and others. Their paragenetic sequence and depth zonal distribution were delineated.

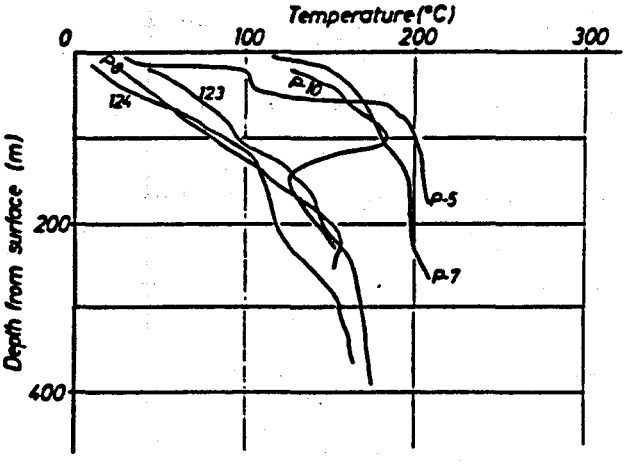

Figure 4. Geothermal gradients for bore-holes, P-5, P-7, P-8, P-10, # 123, and # 124, in the Onikobe geothermal area, Japan.

X-ray Diffraction and SEM Study

By using X-ray diffraction together with Differential Thermal Analyses (DTA), we have identified 4 types of smectite-chlorite clays in these geothermal areas. Systematic study of these clay minerals by Scanning Electron Microscopy (SEM) was undertaken at Stanford in order to determine (1) morphology and crystallinity of the 4 types of clay minerals; (2) textural relationships and paragenesis among the clay minerals and other silicates and (3) compositions of these fine-grained clay minerals. These data are significant for our interpretation of rock-water interactions in geothermal systems, as these clay minerals are ubiquitous and abundant in most drill-hole core samples.

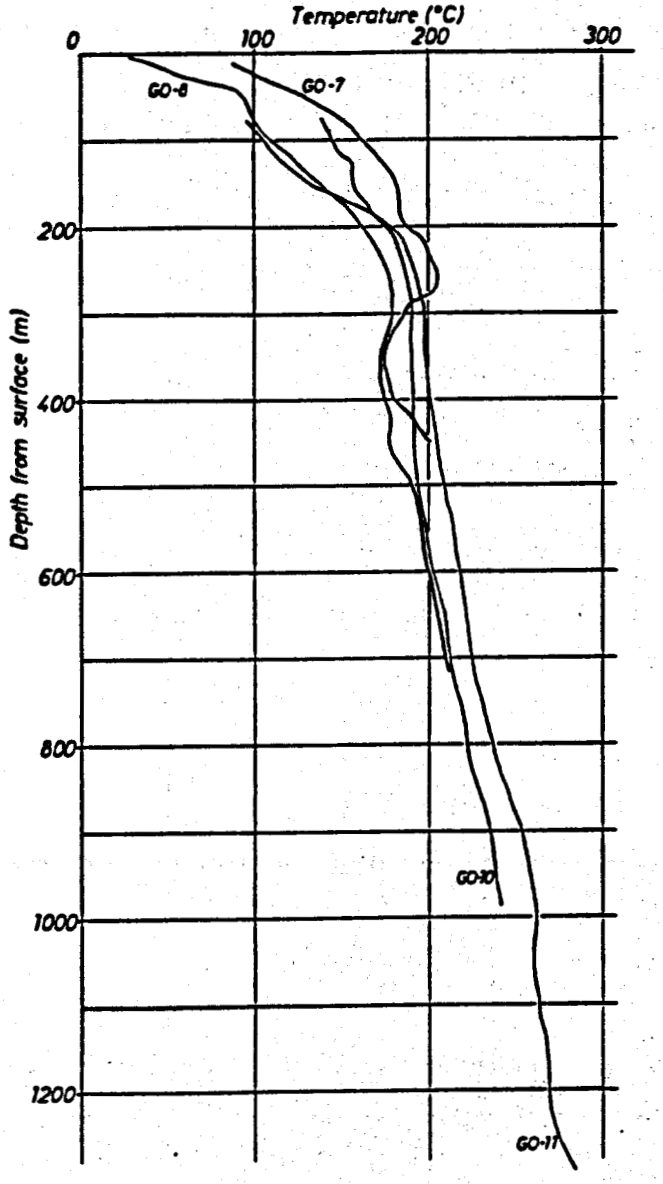

Figure 5. Geothermal gradients for bore-holes GO-7, GO-8, GO-10 and GO-11, in the Onikobe geothermal area, Japan.

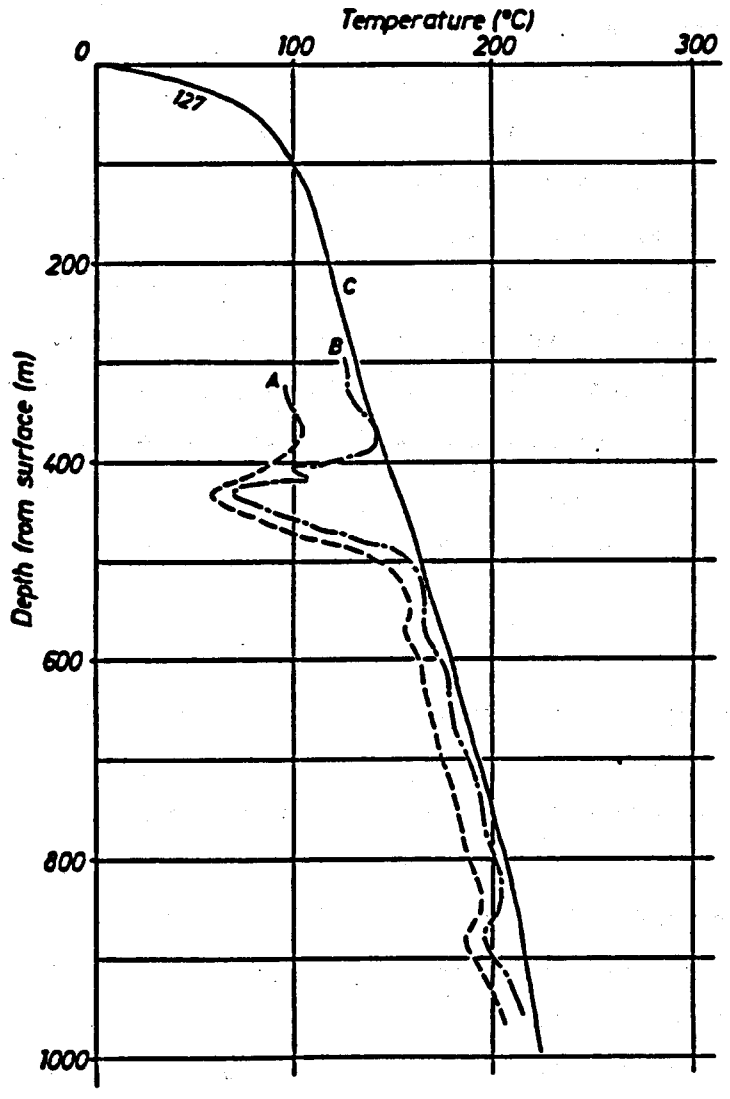

Figure 6. Geothermal gradients for bore hole #127, the Onikobe geothermal area, Japan.
A: 51 hours after the stop of cooling water supply.
B: 99 hours after the stop of cooling water supply.
C: 596 hours after the stop of cooling water supply.

Microprobe Analyses

Microprobe analyses of silicates, clay and carbonate minerals were done at Stanford. It is well known that most Ca-zeolites have extensive compositional variations. For example, wairakite ($CaAl_2Si_4O_{12} \cdot 2H_2O$) and analcime ($Na_2AL_2Si_4O_{12} \cdot 2H_2O$) form a nearly complete solid solution (e.g., Seki and Oki, 1969), yet only the end-member stabilities have been determined (Liou, 1970, 1971a). Therefore, depending on the Ca-Na substitution, wairakite minerals may form at temperatures much lower than those experimentally determined. Both epidote and prehnite from geothermal areas may contain substantial amounts of ferric iron; a previous experimental study by Liou (1973) and studies on natural paragenesis by Seki (1972) and Liou (1979) suggest that Fe-rich epidote may form at very low temperatures in a very oxidized environment. Therefore, compositions of those Ca-Al silicates are important in deciphering the physico-chemical conditions of their formation.

Polished thin sections were prepared for most drill hole core smaples and each section was carefully examined. Individual mineral grains selected for probe analysis were sketched and photographed before being coated with carbon in preparation for microprobe analysis. Microprobe analyses of carbonate and clay minerals require highly polished carbon-coated surfaces. Slight imperfections caused by cleavage, fracture and impurities can significantly affect the analytical results. Moreover, carbonate, clay and zeolite minerals are readily damaged by high electron-beam currents of the small beam diameters used during the microprobe analysis (e.g., Macqueen and Ghent, 1970; Bickle and Powell, 1977; Matsumoto, 1978; Liou, 1979). Therefore, special precautions were necessary to ensure that the data were reliable.

Isotope Studies

Concurrent with the mineralogical-petrological and compositional investigations, stable sulfur isotope studies were made on selective thermal water samples and pyrites in drill core specimens by Sakai in his laboratory.

The data was utilized to establish the source and nature of the hydrothermal fluids.

In conclusion, this report intends to address the following questions which are necessary for our better understanding of the evolution of a geothermal system. This, in turn, will aid in future exploration and assessment of geothermal potential for other areas.

1. The paragenetic sequence of formation of secondary minerals in the Onikobe geothermal area and metamorphic reactions related to their formation.
2. The physico-chemical conditions of their genesis deduced from phase equilibria and their comparison with recorded temperatures, depth, pH and analyzed solution compositions.
3. The spatial patterns of hydrothermal alterations and their relation to the flow of hydrothermal solutions.
4. The source of the hydrothermal fluids responsible for the alteration.
5. The effective water-rock ratio in the geothermal system.
6. The attainment of chemical and isotopic equilibrium in the coexisting minerals.
7. The change of isotopic and fluid compositions and temperature of geothermal fluids as a function of time as recorded in the changes of mineral assemblages in these geothermal areas.

PREVIOUS STUDIES

Solid Materials

The hydrothermal alteration of volcanogenic rocks at the surface of fumarolic areas within the Onikobe caldera basin has been briefly described (e.g., Nakamura, 1959a,b; Nakamura et al., 1961; Hitosugi, 1969; Yamada, 1975; Yamada et al., 1978). Three intensely altered areas around many thermal springs have

been located: (1) Arayu-Katayama area; (2) Ogama-Megama area; and (3) Miyazawa-Fukiage area (e.g., see Figure 7). The areal distribution of secondary minerals including cristobalite, opaline silica, sulfur, limonite, Fe-sulfide, kaolinite, halloysite, alunite and smectite has been delineated by Yamada et al. (1978). Minor zeolites such as mordenite and heulandite have been identified in some of these surface altered volcanic rocks. However, whether these zeolites are the products of the recent hydrothermal alteration or the earlier burial metamorphism is not certain.

The Arayu-Katayama area occupies about 6 km^2 and the original rocks are mainly andesitic-dacitic lavas and their pyroclastic deposits. Hydrothermally altered rocks are colorless and consist of an inner silicified zone and an outer argillized zone around some thermal springs. Some of the zonal distributions are obscure. The silicified rocks contain α-cristobalite, quartz and tridymite as main secondary phases whereas the argillized rocks contain kaolinite, smectite and alunite in addition to the silica phases. Siliceous sinter, sulfur and limonite are actively precipitating from some thermal springs and sulfur crystals are sublimating from fumaroles. Both sulfur and silica veins are abundant.

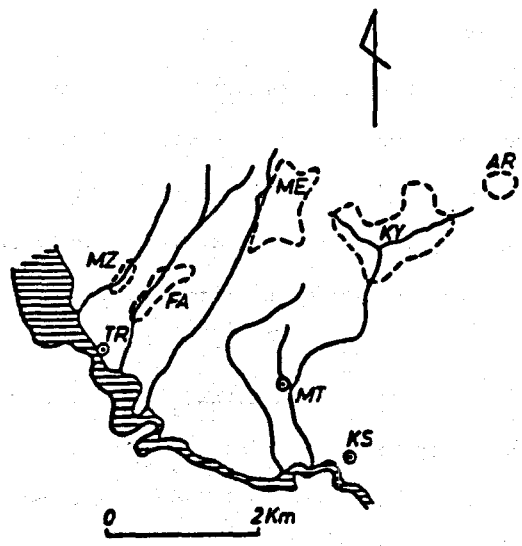

Figure 7. Schematic map showing the localities of fumarolic and hot-spring areas in the Onikobe Caldera, Japan. KY: Katayama; AR: Arayu; ME: Megama; KS: Kanisawa; MT: Mitaki; FA: Fukiage; MZ: Miyazawa; TR: Todoroki.

The Ogama-Megama area covers about 0.5 km^2 and consists of altered massive siltstone with amorphous silica as the major secondary mineral. Surrounding the silica deposit occurs an alunite-kaolinite-opal zone. Around the Miyazawa-Fukiage area, the original white tuffs have been silicified and argillized and a small amount of siliceous sinter is presently precipitating from thermal springs.

The hydrothermal alteration of the deep bore-hole cores of the Onikobe geothermal area has been studied by Seki, Onuki et al. (1969). One hundred and forty core samples from drill holes GO-2, 5, 7, and 8 have been examined by petrographic microscope and by X-ray diffractometer. The zonal distribution of zeolite and clay minerals from the surface to 701.5 m in depth has been determined based on reconnaissance petrographic examination of deep bore hole materials. With increasing depth and temperature, a non-zeolite zone, mordenite zone, laumontite zone and wairakite zone and a variation of clay minerals from smectite to chlorite through chlorite/smectite interstratified clay minerals occur. Yugawaralite has also been found between the laumontite and wairakite zones (Seki & Okumura, 1968). The core materials from bore hore GO-8 at depths of 552.5 and 598.1 m contain wairakite, quartz and pyrite, according to Seki, Onuki et al. (1969). However, the core materials from GO-10 at depths of 1200 m and 1243 m contain quartz, chlorite and mixed-layer clay minerals, together with quartz and kaolinite respectively, but no zeolite. The detailed study of the core samples has not yet been done and it will be carried out in the present study. Nevertheless, the zonal variation of alteration minerals with depth roughly corresponds to the changes of chemical composition of thermal waters in this area.

It is apparent from the above review that except for the reconnaissance study of some drill hole cores by Seki, Onuki et al. (1969), detailed mineral parageneses with respect to depth and their correlation with chemical compositions of the geothermal fluids have not been investigated.

Thermal Waters

Chemical compositions of fumarolic gases and of hot-spring and high-temperature geothermal waters from the Onikobe geothermal area have been collected and examined by a number of investigators (e.g., Tani et al., 1968). Their results will be compared with our data in a later section. The fumarolic gases (at T = 100°C , according to Nakamura et al. 1959) consist of 99.8 vol % H_2O and 0.2 % gas whereas H_2O (about 32-59 %) and CO_2 (35-60 %) are dominant gas components. The high-temperature waters, according to recent studies by Ozawa and Nagashima (1975), Nakamura et al. (1977) and Ozawa et al., (1980), have been thought to be primarily originated from acid HCl - rich fluid formed by volcanic emanation and these acidic waters become neutral or alkaline by interaction with volcanic rocks during their ascent to the surface.

GEOLOGY AND GEOLOGIC SETTING OF THE ONIKOBE CALDERA

The Japanese island arc has experienced repeated volcanism, both terrestrial and submarine. Intensive volcanism that has continued since the early Miocene is believed to be intimately connected with the generation of fumaroles and hot springs, development of high geothermal gradients, evolution of the Green Tuff tectonic belt, and intensive alteration of rocks at the surface and at depth in numerous existing geothermal areas, including Onikobe and the surrounding region.

The zonal distribution of Quaternary volcanic rocks has been revealed by the classic studies of Kuno (1966, 1968b), Katsui et al. (1974); Ishihara (1974), and Miyashiro (1974). They are (successively from the Pacific ocean side of Japan toward the west) (a) an outer volcanic zone with tholeiite and calc-alkaline rocks containing relatively low K_2O and Na_2O, (b) an inner zone of tholeiitic and calc-alkaline rocks with higher K_2O and Na_2O contents, (c) and a westernmost zone characterized by tholeiitic, calc-alkaline and alkali rocks.

The Miocene Green Tuff basin of Japan extends from Hokkaido through Honshu to pass under the sea just east of Mt. Fuji and Izu-Bonin Island and to northern

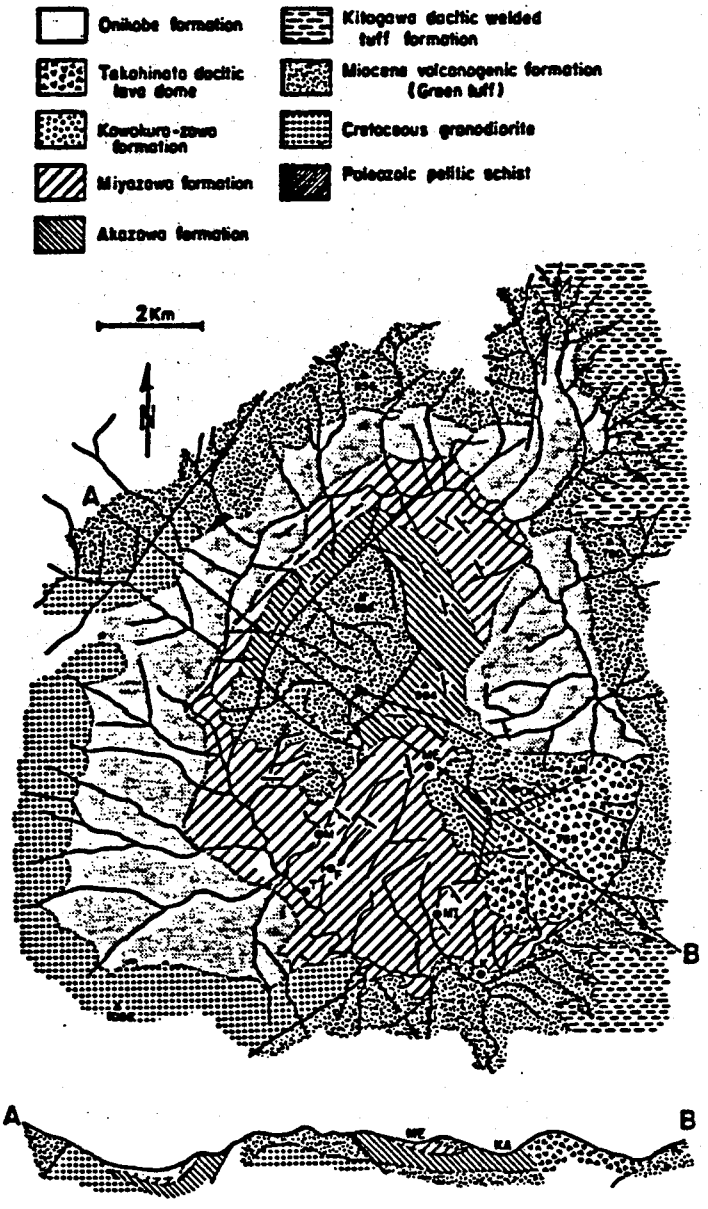

Figure 8. Geologic map and cross section of the Onikobe Caldera, Japan (modified after Yamada et al., 1978). KA: Katayama fumarolic area; OK: Okuno-in fumarolic area; AR: Arayu fumarolic area; ME: Megama fumarolic area; MI: Mitaki Spa; K: Kanisawa Spa; T: Todoroki Spa; F: Fukiage Spa; M: Miyazawa Spa.

Kyushu. The basin has been the site of steady volcanism since the Miocene, and the accompanying thermal and hydrothermal effects are recorded in diverse altered and metamorphosed rocks. The basin contains mainly thick volcaniclastic marine rocks, mostly coarse breccias, and tuff ejected from undersea volcanoes. Intrusive activity during sedimentation emplaced dikes and plugs; some rhyolite masses reached the sea floor, with widespread alteration and mineralization. On burial, the suite of materials was metamorphosed and hydrothermally altered to propylite assemblages. Quaternary volcanism has injected heat, which is being dissipated in part by circulating water systems. In places in the basin the rocks have been subjected to multiple alteration processes.

Table 2. The lithostratigraphic Units of the Onikobe Calders, Japan

Geologic Unit	Thickness (in meters)	Age (in Years before the present)
Onikobe Formation	100	23,380 ± 890* 24,970 ± 1210*
Takahimata Dacite Dome	Unknown	0.3 million**
Kawakurazawa Formation	100	
Miyazawa Formation	300	1.5 million**
Akazawa Formation	500	1.8 Million**
Kitagawa Dacite Welded Tuff Formation	100	2.2-2.4 Million**
Green Tuff Formation	7500	Early-late Miocene
Granodiorite and Schist	Unknown	Palaeozoic

*C^{14} dating; **Fission track dating (both from Yamada et al., 1978)

Stratigraphy

The Onikobe caldera, the site of a geothermal power station, is on the east edge of the Green Tuff basin in north central Honshu. Physiographically, the caldera is characterized by an oval-shaped depression about 10 km in mean diameter. The stratigraphy, structure, and geologic history of this caldera basin have been described by Katayama and Umezawa (1958), Kuno (1952, 1953), Katsui (1955), Nakamura (1959, a, b), Matsuno and Nishimura (1965), Hitosugi and Yoneya (1972), Yamada (1972 a, b, 1973, 1975), and Yamada et al. (1978). The distribution of the lithologic units is shown in Figure 8 and their stratigraphic relations are schematically presented in Table 2. Brief descriptions of these units are as follow:

A. Paleozoic Pelitic Schists and Cretaceous Granodiorite:

Pelitic schist and granodiorite constitute the basement complex of the Onikobe caldera and they unconformably underlie the Miocene Green tuffs and younger formations. The schistose pelitic rocks crop out only along the exposures of National Highway 108 and at the mouth of Suginomori Creek. The schists consist of muscovite + albite + quartz + chlorite; some of them contain graphite. The pelitic rocks were locally intruded by the biotite-hornblende granodiorite of probable late Cretaceous age. The granodiorite is extensively exposed in the western and southern borders of the Onikobe caldera and also sporadically outcrops within uplifted blocks of the Green Tuff formation in the caldera basin. Dikes of rhyolite, dacite, and andesite are intruded into the granodiorite masses and these dikes are probably related to Miocene volcanic activity. The granodiorite was found at the bottom of a deep (1300 m) bore hole (CO-11) drilled by the Japan Electric Development Corporation (Hitosugi, 1970).

B. Miocene Volcanogenic Formation (Green Tuffs):

The Miocene volcanogenic sediments in this area unconformably cover the above noted basement rocks. The Miocene formation consists of lava, agglomerate, tuff breccia and tuff of andesitic and dacitic compositions, intercalated with thin bedded sandstone and shale. The volcanogenic sediments have suffered intense

burial and hydrothermal alteration and the rocks have been replaced by a propylitic assemblage of sodic plagioclase, chlorite clay, illite, quartz, calcite and leucoxene with or without epidote.

The Green Tuff formation is widely distributed in the areas surrounding the Onikobe caldera basin and it also occurs as an uplifted block within the basin. This fact indicates that the Green Tuff formation must form, at least partly, the basement above which Plio-Pleistocene volcanic rocks were accumulated. Hitosugi and Yoneya (1972) concluded that the depth interval between 760 m and 1300 m of bore hole GO-11 drilled at the Onikobe geothermal area is composed of the Miocene Green Tuff formation. However, careful examination of many drill hole core samples from this and other bore holes in the present study can not conclusively confirm the occurrence of the Green Tuffs at the depths noted above. This is because almost all cores from this and other bore holes have suffered severe alteration due to the present geothermal activity and it is difficult to clearly differentiate the Miocene Green tuff from the Plio-Pleistocene volcanic rocks.

C. Pliocene-Pleistocene volcanic and sedimentary rocks:

The Pliocene-Pleistocene rocks were deposited subaerially or in lacustrine envrionments. Geologically they can be divided into six formations, as follows:

(1) Kitagawa dacitic welded tuff formation: This welded tuff formation of about 100 m thickness unconformably overlies the Green Tuff formation and is exposed only outside of the Onikobe caldera basin. The petrological and chemical characteristics of this welded tuff, the product of nuee ardente type volcanic activity, are quite similar to those of a pumice flow and welded tuff formation widely distributed in the surrounding area of the Towada volcano caldera which is located to the north of the Onikobe area (Katsui, 1955). Fission track ages of this welded tuff formation are 2.2, 2.3 and 2.4 my BP (Yamada et al., 1978).

(2) Akazawa Formation: This is the lowest portion of the non-marine basin deposits of the Onikobe caldera and has a thickness of about 500 m. Probably, the circular caldera, the diameter of which is about 10 km, was formed before the

deposition of this Akazawa formation.

This formation is chiefly composed of conglomerate, andesitic and dacitic tuff breccia, and lava flow intercalated with thin beds of siltstone. Pebbles which are considered to have been derived from the above-noted Kitagawa dacitic welded tuff formation were found at the basal part of the Akazawa formation. The fission track age of the andesitic agglomerate of this formation is 1.8 my BP (Yamada et al., 1978).

(3) Miyazawa Formation: This non-marine volcanogenic formation is composed of hornblende dacitic lava flow, tuff breccia and pumice flow breccia with some thin siltstone and conglomerate beds. The thickness of this formation is estimated to be about 300 m. The fission track age of dacitic lava of this formation is 1.5 my BP (Yamada et al., 1978).

(4) Kawakurazawa Formation: This non-marine formation of 100 m thickness unconformably covers the Miyazawa formation. Rocks composing this formation are andesitic lava, tuff breccia and tuff with some insertions of mud-flow deposits. During the deposition of the Kawakurazawa formation a 3 by 4 km basement block was uplifted in the northwestern part of this Onikobe caldera basin.

(5) Takahinata dacite dome: This lava dome forms the oval shaped mountain of Takahinata-yama at the eastern part of the Onikobe caldera basin. Matsuno and Nishimura (1965) and Yamada (1972a, 1972b, 1973, 1975) have considered the lava dome to have been formed after the deposition of the Onikobe formation which is described below. However, absolute age determinations by the fission track method indicate that the Takahinata dacite lava dome was erupted about 0.35 my BP (Yamada et al., 1978), making it much older than the C^{14} dated Onikobe formation. The Takahinata dacite must be unconformably covered by the Onikobe formation as has been noted by Tani et al. (1968).

The Arayu fumarolic area is located within this dacite dome. Other active geothermal areas such as Katayama, Okuno-in and Megama are distributed near the western boundary of the Takahinata dacite dome (for localities, see Figure 7 and 8). The magmatic activity related to the formation of this dome is believed to

be the major heat source for the present day geothermal activity and associated hydrothermal manifestations in the Onikobe caldera basin area. Geomorphological evidence clearly indicate that many fumarolic explosive craters in the Katayama-Arayu area occur at the western and north western flanks of dome-shaped Takahinata volcano (Nakamura, 1959b; Matsuno and Nishimura, 1965). It must be noted that Ozaki and Kanno (1977) have shown the areal distributions of low-resistivity stream flows and high heat discharge on the western side of the Takahinata dacite dome. They showed the north and southwestward stream flows of meteoric groundwater which was heated and contaminated by the volcanic activity related to the Takahinata dacite dome.

(6) Onikobe formation: This non-marine formation of about 100 m thick is composed of conglomerate and siltstone. No volcanic strata such as lava flow and agglomerate are intercalated, but clastic materials derived from surrounding Miocene and Pliocene-Pleistocene volcanic rocks are common. The accumulation of this formation occurred about 24000 years ago based on the C^{14} method (Yamada et al., 1978).

Development of the Onikobe Basin

The geologic development of the Onikobe basin has been considered to be a Krakatau type caldera (Kuno, 1953), a volcano-tectonic depression (Katayama and Umezawa, 1958; Matsuno and Nishimura, 1965) or a resurgent cauldron (Yamada, 1972a). Such differences of opinion appear to be due to the abrupt facies changes and the structural complexity of the lacustrine and volcanogenic deposits (basin deposits) and the lack of concrete correlation data among various lithologic units within the basin and those strata elsewhere. These problems are due partly to the heavy vegetation covering the entire area and partly to the intense hydrothermal alteration of many lithologic units. Nevertheless, the model proposed by Yamada (1972b) is modified and described below.

The Onikobe basin may have formed after the deposition of the Kitagawa welded tuff which occurs both in and outside the basin. The basin deposits, unconformably overlaying the welded tuff, are divided into the Akazawa, Miyazawa,

Kawakurazawa and Onikobe formations in ascending order. Prior to the deposition of the Onikobe non-marine deposits, the Takahinata dacite dome was intruded in the southern part of the basin. A nearly rhomb-shaped block (the Zanno-Mori block) 3 x 4 km in dimension, which consists of the Green Tuff and granodiorite, is exposed in the northwestern part of the caldera. The block is primarily bounded by normal faults and the basin Miyazawa deposits are steeply dipping away from the block. Such relations suggest the block was uplifted after the deposition of the Miyazawa formation. The geological constraints described above suggest that the sequence for the formation of the Onikobe basin can be summarized as follows:

(1) Pre-caldera deposition of the Kitagawa dacitic welded tuff, which unconformably overlies the Green Tuff and grandiorite(2.3 -2.4 M.Y.B.P)

(2) Regional block faulting and formation of a caldera by collapse or subsidence.

(3) Deposition of the non-marine Akazawa (1.8 M.Y.) and Miyazawa formations within the caldera basin.

(4) Uplift of the Zanno-Mori basement block and deposition of the Kawakurazawa formation.

(5) Extrusion of the Takahinata dacite lava (0.35 m.y.) and intense hydrothermal alteration.

(6) Deposition of the non-marine Onikobe formation about 23000-25000 years ago.

Geologic Structure and Fracture Systems

Because of difficulties in traversing the area, the dense vegetation cover, and the intense hydrothermal alteration, the detailed geologic structures of the Onikobe basin have not been worked out. Based on aerial photography, ground surveys and subsurface drilling, some regional structures have been suggested (e.g., Matsuno and Nishimura, 1965; Yamada, 1972a,b).

The Onikobe basin is characterized by a circular depression bounded by a series of ring faults and by a structural dome whose axis is NW-SE inside the basin. Many high-angle normal faults have been suggested to have formed during

the development of the Onikobe basin. Some of these faults were active again later and the Zanno-Mori block of basement rocks was uplifted in the northwestern part of the caldera. Around the Zanno-Mori block where the strata dip steeply, many minor faults are observed.

In general, within the Onikobe basin, minor faults, clastic dikes and joints are well developed and they sporadically occur in the uncomformably overlying younger basin deposits. Minor faults of northwest-southeast direction are cut by those of northeast-southwest direction. Many conjugate systems of fractures and clastic dikes in the southeastern area of the Onikobe basin have been studied in detail by Yamada (1972a,b); in this region the exposure is better and the rocks are less altered. The results of his study indicate that the southeastern part of the caldera has undergone lateral extension. Some fractures and clastic dikes are concentrated along a narrow shear zone extending probably to the foundation of the caldera. The hydrothermal system of the Onikobe caldera is controlled mainly by such fracture systems.

In the Katayama geothermal area of Onikobe, in which geothermal activity is most widely observed and many bore-holes for geothermal power plant have been drilled, no fault could clearly be identified by geomorphological or air-photo geological data. The occurrence of subsurface faults has been inferred from seismological and electric survey data by Hitosugi (1976). Matsuno, and Nishimura (1965) and Nakano (1981) have recently suggested a series of NW-SE trending major faults occuring at depth. These faults may provide channels for high-temperature geothermal water to flow in this area. However, these faults have not been confirmed by geologic surveys and deep drilling. Our studies of many deep drill hole core samples from the Katayama area revealed no lithological or structural features such as slickensides, fault striations or brecciations to substantiate the occurrence of such large faults at depth.

Within the Katayama area, three strong geothermal belts were delineated from drilling of over fifty production and pilot bore holes. These belts may be closely related to those subsurface faults inferred from the geophysical data

mentioned above. These belts are shown in Figure 2 and are respectively called K-line, Y-line and Z-line by the Japanese Electric Development Company. The production wells #101, 102, 103 and 112 are on the K-line, # 108, 109, and 117 are on the Y-line and # 104, 105 and 127 are on the Z-line. Future production wells will be drilled along these three lines which apparently have enough fracture spaces for large flows of high-temperature thermal waters at depth.

CHEMICAL CHARACTERISTICS OF THERMAL WATERS AND STEAMS

Chemical Compositions of Thermal Waters and Steams

Compositions of thermal water from the the Onikobe geothermal area are listed in Table 3 and are plotted in the Cl- CO_2 - SO_4 diagram of Figure 9 and the Na-Ca-Mg diagram of Figure 10. It is apparent from these plots that the thermal water obtained through most bore-holes belongs to the Na-Cl or Na-Ca-Cl type. Thermal water from bore-holes GO-2, GO-3 and GO-5, however, is of other types characterized by higher contents of HCO_3 and/or SO_4.

Chemical compositions of steam associated with thermal water from some bore-holes in this geothermal area are listed in Table 4. Most of the steam consists of less than 2 wt% gas except the one from GO-3. The gases are composed mainly of CO_2 (56-73 wt%) and H_2S (20-40 wt%) with minor amounts of H_2, N_2 and CH_4. The wt% of CO_2 in total gas forming the steam from bore-holes GO-3 and GO-4 are higher than those gases from other bore holes through which the Na-Cl type thermal water is obtained.

The relationships between the Cl content and the contents of other components such as Na, K, Ca, Mg, SO_4 and HCO_3 in the thermal water obtained through deep bore-holes in the Onikobe geothermal area are shown in Figure 11. Na, K, Ca and Mg generally increase with an increase in Cl. SO_4, however, seems to decrease or to remain constant with the increase in Cl content. The HCO_3 contents of some thermal water with very low Cl content are extremely high. It should be mentioned that meteoric water (rain water) contains no Na, K, Ca, Mg,

Table 3. Chemical compositions of thermal waters from deep bore holes in the Onikobe geothermal area, Japan.

	1	2	3	4	5	6	7	8	9	10	11	12	13
	GO-2 (436 m)	GO-3 (319 m)	GO-3	GO-3	GO-3	GO-3	GO-4 (393 m)	GO-5 (300 m)	GO-6 (190 m)	GO-7 (500 m)	GO-7	GO-7	GO-7
K^+	0.68	0.11	0.01	2.35	0.14	4.50	0.01	0.30	0.01	0.85	1.02	19.44	24.04
Na^+	5.71	4.37	0.15	48.28	11.09	18.75	0.07	31.14	0.06	2.94	7.26	187.04	213.14
Ca^{2+}	7.18	0.05	0.15	0.32	0.15		0.08	3.16	0.10	2.60	2.22	50.90	24.30
Mg^{2+}	2.97	0.02	0.01	0.06			0.03	0.34	0.01	0.00	0.00	0.49	
Fe^{2+}		0.05	0.00	0.09			0.00		0.01	0.01			
Al^{3+}		0.04	0.01	0.07			0.00		0.01	0.01			
subtotal	16.54	4.64	0.33	51.17	11.38	23.25	0.20	34.94	0.20	6.76	10.50	257.87	261.48
meq subtotal	26.69	4.84	0.51	91.80	11.53	23.25	0.33	38.44	0.35	9.05	12.72	309.27	285.78
Cl^-	0.10	0.03	0.18	0.48	5.75	12.98	0.05	0.10	0.03	9.15	16.53	302.09	372.32
Br^-													
I^-													
SO_4^{2-}	7.18	0.70	0.01	7.18	1.25	2.97	0.06	7.57	0.00	0.01	0.05	0.64	0.78
HCO_3^-	14.00	1.30	0.30	17.80	1.06		0.47	23.03	0.26	0.35	2.02	0.62	1.54
CO_3^{2-}		0.70		7.90									
subtotal	21.28	2.73	0.49	33.36	8.06	15.95	0.58	30.70	0.29	9.51	18.60	303.35	374.64
meq subtotal	28.46	4.13	0.49	48.45	9.31	18.91	0.64	38.28	0.30	9.52	18.65	303.98	375.42
H_4SiO_4		0.37	0.02				0.05		0.02	0.03			
H_3BO_3			0.04	4.15			0.22		0.11	2.53			
CO_2													
H_2S		0.30	9.15	13.68					0.96	0.07			
TOTAL	37.82	7.74	10.03	102.36	19.44	39.20	1.05	65.64	1.58	18.55	29.1	561.2	636.12
Na/K	8.36	39.75	14.80	20.52	77.57	4.17	7.4	104.9	7.63	3.45	7.10	9.62	8.87
Mg/Ca	0.41	0.45	0.05	0.18			0.43	0.11	0.08	0.001	0.00	0.01	
Cl/SO_4	0.01	0.04	17.50	0.07	4.61	4.37	0.85	0.01	6.25	1144.	318.	476.	477.
Temp. (°C)						240°							
pH	6.90	9.1	4.3	9.5	7.6	8.9	5.1	7.2	4.8	7.4	6.60	6.70	7.2
Ionic Strength	0.0449	0.006	0.001	0.066	0.012	0.0241	0.0007	0.0494	0.0005	0.0119	0.0180	0.3586	0.3557
Reference	Seki et al,1969	JEDC Rep. 1966	Hitosugi 1969	Hitosugi 1969	Yamada 1975	Ozawa & Nagashima 1975	Seki et al, 1969	Yamada 1975	Hitosugi 1969	Hitosugi 1969	JEDC Rep. 1970	Ozawa & Nagash. 1975	Ozawa & Nagash. 1975

Table 3. Chemical compositions of thermal waters from deep bore holes in the Oaikobe geothermal area, Japan. (Continued)

	14	15	16	17	18	19	20	21	22	23	24	25	26
(mmol)	GO-8 (700 m)	GO-8	GO-8	GO-10 (1000 m)	GO-10	GO-10	GO-10	GO-11 (1300 m)	GO-11	GO-11	#101 (233 m)	#103 (228 m)	#103
K^+	2.87	7.42	28.34	13.72	12.89	14.07	18.88	20.72	21.74	25.07		0.04	
Na^+	30.36	52.94	10.35	76.21	77.86	95.70	104.39	135.71	149.20	184.87	80.47	0.17	78.30
Ca^{2+}	4.32	5.24	10.20	15.33	10.18	17.02	21.01	36.43	31.79	23.70	10.50	0.00	9.61
Mg^{2+}	4.61	0.64	2.72	4.08	5.64	5.18	5.60	11.11	17.61	22.75	5.43	0.00	3.13
Fe^{2+}													
Al^{3+}													
subtotal	42.16	66.24	51.61	109.34	106.57	131.97	149.88	203.97	220.34	256.39	96.40	0.21	90.94
meq subtotal	51.09	72.12	64.53	128.76	122.38	154.17	176.48	251.50	269.73	302.86	112.34	0.21	103.76
Cl^-	44.82	56.70	77.92	136.38	149.10	163.88	186.88	269.94	304.07	326.86	107.18	0.09	94.49
Br^-													
I^-													
SO_4^{2-}	0.73	2.54	0.73	0.48	0.57	0.32	0.66	2.09	1.30	1.87	0.85	0.08	0.71
HCO_3^-	0.90		0.30	0.00									
CO_3^{2-}													
subtotal	46.45	59.24	78.95	136.86	149.67	164.20	187.54	272.03	305.37	328.73	108.03	0.17	95.20
meq subtotal	47.18	61.78	79.68	137.34	150.25	164.53	188.19	274.13	306.67	330.60	108.89	0.25	95.91
H_4SiO_4												0.01	
H_3BO_3													
CO_2													
H_2S													
TOTAL	88.60	125.5	130.56	246.2	256.24	296.2	337.4	476.0	525.71	585.1	204.4	0.39	186.23
Na/K	10.60	7.14	0.37	5.55	6.04	6.80	5.53	6.55	6.86	7.38		4.02	
Mg/Ca	1.07	0.12	0.27	0.27	0.55	0.30	0.27	0.30	0.55	0.96	0.52		0.33
Cl/SO_4	61.48	22.32	107.	284.	260.	507.00	285.00	129.00	234.00	174.00	126.00	1.19	133.5
Temp. (°C)	98°	200°		99°			240°		300°				
pH	6.9	8.0	7.0		3.30	2.9	3.8	2.6	2.90	2.5	4.00	4.6	4.10
Ionic Strength	0.0388	0.075	0.0858	0.1529	0.1527	0.1819	0.2096	0.3124	0.3389	0.3561	0.1274	0.0003	0.1133
Reference	JEDC Report 1970	Yamada, 1975	Ozawa et al., 1980	Yamada, 1975	JEDC Report 1970	Ozawa & Nagash. 1975	Ozawa & Nagash. 1975	JEDC Report 1969	Ozawa & Nagash. 1975	Ozawa & Nagash. 1975	Ozawa & Nagash. 1975	JEDC Report 1971	Ozawa & Nagash. 1975

Table 3. Chemical compositions of thermal waters from deep bore holes in the Onikobe geothermal area, Japan. (Continued)

	27	28	29	30	31	32	33	34
	#105 (375 m)	#111 (320 m)	#123 (351 m)	#127 (1000 m)	K-line (a)	Y-line (b)	Z-line (c)	Z-line (d)
K^+		5.73	0.00	5.65	6.83	3.15	13.17	11.84
Na^+	122.67	39.60	0.01	41.48	56.63	33.58	70.34	83.99
Ca^{2+}	58.06	7.22	0.06	1.28	8.75	3.68	18.79	20.02
Mg^{2+}	36.21	1.12	0.00	0.01	1.81	0.01	2.49	3.24
Fe^{2+}		0.78		0.01	1.02	0.01	3.44	4.26
Al^{3+}					0.00			0.00
subtotal	216.94	54.45	0.07	48.43	75.04	40.43	108.23	123.35
meq subtotal	311.20	63.57	0.13	49.73	86.60	44.11	132.95	150.87
Cl^-	253.29	59.92	0.56	48.87	85.30	36.44	144.59	149.89
Br^-								0.01
I^-								
SO_4^{2-}	0.38	1.32	0.14	0.05	0.93	3.35	0.45	0.18
HCO_3^-		0.10		0.08		0.48		
CO_3^{2-}								
subtotal	253.67	61.34	0.70	49.00	86.23	40.27	145.04	150.07
meq subtotal	254.04	62.66	0.84	49.05	87.16	43.62	145.49	150.24
H_4SiO_4					7.61	4.25		9.43
H_3BO_3								
CO_2								
H_2S								
TOTAL	470.61	115.79	0.77	97.43	168.9	80.71	253.27	282.85
Na/K		6.91		7.34	8.29	10.67	5.34	7.09
Mg/Ca	0.62	0.16		0.01	0.21	0.001	0.133	0.16
Cl/SO_4	675.45	45.39	4.00	977.	91.9	10.87	321.	852.
Temp. (°C)					92°	89°	98°	92°
pH	3.2	4.34	2.61	4.75	4.1	8.2	3.34	3.3
Ionic Strength	0.3773	0.0736	0.0007	0.0507	0.099	0.051	0.1644	0.178
Reference	Ozawa & Nagash. 1975	This Paper	This Paper	This Paper	This Paper	This Paper	This Paper	

(a) Mixed thermal water of K-line (#101, 102, 103)
(b) Mixed thermal water of Y-line (#108, 109, 117)
(c) Mixed thermal water of Z-line (#104, 105, 107, 120, 127)
(d) Mixed thermal water of Z-line.

SO_4, HCO_3 and Cl; therefore, it should be plotted near the origins of the diagrams in Figure 11.

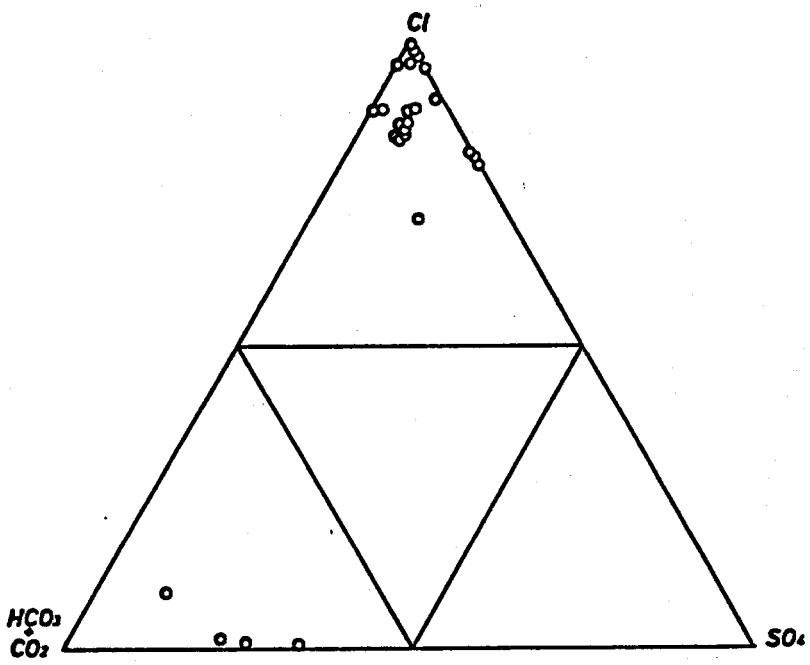

Figure 9. $Cl - \Sigma CO_2(HCO_2 + CO_2) - SO_4$ diagram of thermal waters from bore holes of the Onikobe geothermal area (thermal waters condensed from steam are not included).

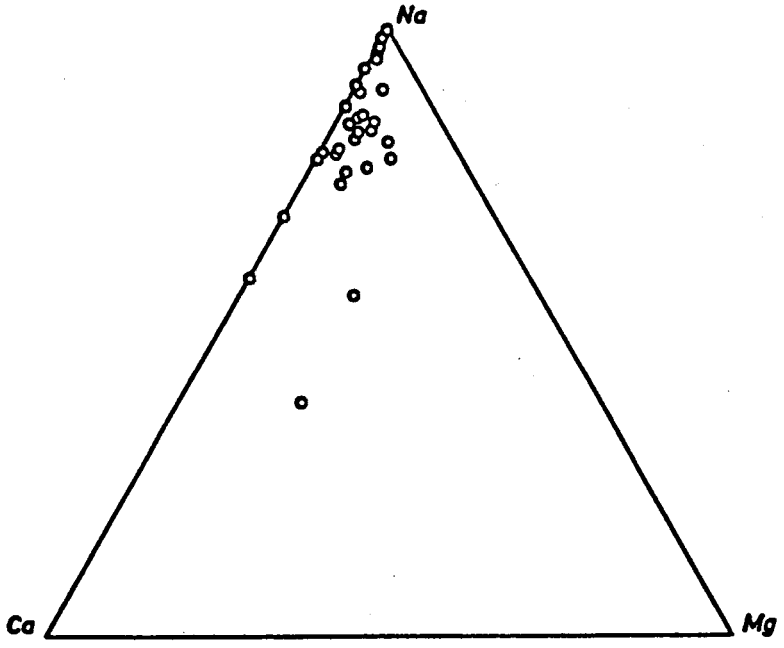

Figure 10. Na-Ca-Mg diagram of thermal waters from bore holes of the Onikobe geothermal area, (thermal waters condensed from steam for power plant are not included).

Table 5 lists chemical compositions of thermal water emitted at hot springs surrounding the Onikobe geothermal area. This thermal water is also of the Na-Cl type, except for the Na-Cl-HCO_3 type of Kanizawa hot spring and the Na-Ca-Cl-SO_4 type of Megama fumarolic area. Figure 12 shows the relationships between the Cl content and the contents of other components in this hot spring thermal water; their relationships are very similar to those of deep bore-hole thermal water of the Onikobe geothermal area shown in Figure 11. However, the hot spring water has a very restricted chemical composition.

Hydrology

On the basis of detailed hydrological examination of rain and snow precipitation, stream flow and discharge rate of geothermal water, Ozaki and Kanno (1977) and Ozaki (1981) have determined that thermal water in the Onikobe geothermal area and its surrounding hot spring areas principally originate from meteoric water permeated to depth from the surface (Figures 13 and 14). The flow directions of meteoric groundwater are shown as arrows in Figure 13; the NW-SE trend observed is similar to that of the present drainages of the Katayama area. Chemical compositions of rain water and river water collected at the surface of the Onikobe geothermal area and its surrounding areas are shown in Table 6.

Deep thermal water and surficial hot spring water of the Onikobe geothermal area may have evolved in the following way:

(1) Precipitation permeated into the ground.

(2) The HCO_3 content of the groundwater may have been somewhat increased by the decomposition of surficial organic material and by the dissociation of organic matter within the siltstone of the Akazawa formation.

(3) NaCl-rich hot solution from depth, probably from Miocene volcanogenic marine sediments forming the basement of Onikobe caldera, was mixed with groundwater (1) and (2) to form Na-Cl type and Na-Cl-HCO_3 type thermal water, respectively.

(4) Some of the HCO_3-rich thermal water may have been formed by the mixing of CO_2-rich volcanic gas with the groundwater (1) or (2).

(5) SO_4-rich thermal water was formed by the mixing of SO_4 (or H_2S)-rich

Table 4. Chemical compositions of steam forming fluids in deep wells of Onikobe geothermal area, Japan (Ozawa and Nagashima, 1975).

Well number*	H_2O %	Gas %	Composition of gas H_2S	CO_2	R	Composition of R H2	N2	CH_4
GO-3	96.0	4.0	20	73	7	69	18	13
GO-4	99.6	0.4	24	68	8	81	11	8
GO-7	99.4	0.6	30	60	10	85	14	1
GO-8	99.0	1.0	29	66	5	20	76	4
GO-10	99.7	0.3	40	56	4	13	77	n.d.
GO-11	98,99	2-1	37	57	6	n.d.	n.d.	n.d.
101	99.0	1.0	30	62	8	84	14	2
103	99.6	0.4	29	63	8	81	16	3
105	99.6	0.4	33	60	7	45	51	4

*Chemical compositions of thermal waters associated with these are shown in Table 3.

volcanic gas or solution from depth with groundwater (1) or (2). SO_4-rich deep thermal water occurs only in a relatively confined narrow area near the Takahinata dacite mass, which is believed to be a major heat source for the Onikobe geothermal area. The narrow area may indicate the presence of fissures or faults through which SO_4 (or H_2S)-rich gas or solution can easily rise.

Hg and As Contents of Thermal Water

Thermal water collected from deep bore-holes of the Onikobe geothermal area are chemically characterized by high Hg contents (Koga and Noda, 1975). Hg and As contents of volcanic rocks strongly altered by fumarolic activity at the land surface of this geothermal area are also high (Tables 7 and 8). A close genetic relationship between Hg deposits and geothermal activity has been reported by White (1965). Koga and Noda (1975) postulated that the high Hg contents of the thermal water and of the surficially altered rocks in the Onikobe geothermal area may indicate a high potential for geothermal resources in this area. They have proposed that a detailed Hg content investigation of the thermal water, fumarolic gases and exposed volcanic rocks would be one of the most useful geochemical methods for the exploration of the Onikobe geothermal

Table 5. Chemical compositions of thermal waters in hot spring areas surrounding the Onikobe geothermal area, Japan.

	1 Fukiage	2 Fukiage	3 Yumoto, Fukiage	4 GS-3 Bore Hole Fukiage*	5 GS-3 Bore Hole Fukiage**	6 Kamisawa	7 Kamisawa	8 Hegesna	9 Hegesna	10 Hitaki	11 Miyasawa	12 Miyasawa	13 Todoroki
K^+	0.46	0.38	0.50	0.53	0.67	0.58	0.32	2.07	3.68	1.67	0.48	0.45	0.58
Na^+	12.58	11.71	13.48	15.91	19.65	9.86	9.03	15.88	26.25	17.39	9.99	11.60	9.86
Ca^{++}	0.50	0.40	0.51	0.63	0.69	0.34	4.12	1.13	2.97	2.75	0.43	0.85	0.38
Mg^{2+}	0.00	0.07	0.00	0.06	0.07	0.06	0.00	0.84	2.18	0.00	0.05	0.00	0.06
Fe^{2+}		0.00		0.01	0.01	0.01		0.04			0.01		0.01
Al^{3+}		0.23		0.12	0.14	0.13		0.31		0.09	0.36		0.13
subtotal	13.54	12.79	14.49	17.26	21.23	10.98	13.47	20.27	35.08	22.10	11.32	12.90	11.02
meq subtotal	14.04	13.73	15.00	18.20	22.28	11.71	17.58	22.92	40.23	25.03	12.54	13.75	11.71
Cl^-	10.97	11.20	12.19	13.48	15.89	5.22	5.78	18.55	29.73	22.26	10.38	10.49	10.10
Br^-	0.01	0.01		0.01	0.01		0.01	0.02	0.03	0.02	0.01	0.01	
I^-		0.00		0.00	0.00			0.00	6.50		0.00		
SO_4^{--}	0.85	0.78	0.95	0.81	1.10	3.12	3.48	4.24		0.32	0.69	0.78	0.63
HCO_3^-	1.00	0.32	1.19	0.50	0.20	8.36	8.40			2.40	0.98	1.00	1.20
CO_3^{--}	0.20	0.55	0.02	0.40	0.60								
subtotal	13.03	12.85	14.35	15.20	17.79	16.70	17.67	22.81	36.26	25.00	12.05	12.28	11.93
meq subtotal	14.09	14.20	15.32	16.41	19.49	19.82	21.15	27.05	42.77	25.31	12.75	13.05	12.57
H_4SiO_4		2.58	2.75	3.50	4.03	1.67	2.51	4.26		3.20	2.09	2.36	4.58
H_3BO_3	0.53			0.38	0.44		0.38		1.98	1.13		0.94	
CO_2						4.43	4.39			0.68	0.28	0.20	0.21
H_2S	0.01	0.04							0.00		0.05		0.00
TOTAL	27.11	28.28	31.59	36.34	43.49	33.78	38.41	47.34	73.32	52.10	25.73	28.67	27.74
Na/K	27.34	30.88	26.75	30.02	29.33	17.14	28.49	7.66	7.13	10.55	20.90	25.77	17.14
Mg/Ca	0.00	0.17	0.00	0.10	0.10	0.16	0.00	0.74	0.73	0.00	0.12	0.00	0.16
Cl/SO_4	12.85	14.29	12.87	16.64	14.44	1.67	1.66	4.37	4.57	70.43	15.04	13.50	15.94
Temp. (°C)	99°	100°	99.2°	100°	100°	60°	56.8°	98°	97°	54.5°	100°	98.5°	87°
pH	8.4	8.4	8.4	8.40	8.5	6.2	6.4	2.4	2.4	6.8	7.4	7.2	7.4
Ionic Strength	0.0156	0.0165	0.0166	0.0196	0.0238	0.0197	0.027	0.0322	0.0532	0.0285	0.0149	0.0150	0.0136
Reference	Nakamura 1959b	Nakamura 1959b	This Paper	Nakamura et al, 1961	Nakamura et al, 1961	Nakamura 1959b	Nakamura 1959b	Nakamura 1959b	Nakamura 1959a	Nakamura 1959a	Nakamura 1959a	Nakamura 1959b	Nakamura 1959a

* one hour after drilling
** 24 hours after drilling

Table 6. Chemical compositions of rain water and river water in the Onikobe geothermal area and surrounding area.

	1 Rain water, Fukiage Aug., 1980	2 Rain water, Katayama Aug., 1978	3 River water Fukiage
K^+	0.163	0.01	
Na^+	2.33	0.18	
Ca_2^+	0.07	0.16	0.04
Mg_2^+	0.04	0.03	0.02
Fe_3^+			0.01
Al^{3+}			0.12
subtotal	2.603	0.38	0.19
meq subtotal	2.70	0.57	0.49
Cl^-	1.81	0.14	0.85
Br^-			
I^-			
SO_4^{2-}	0.03	0.24	0.11
HCO_3^-	0.30		0.36
CO_3^{2-}			
subtotal	2.14	0.38	1.32
meq subtotal	2.48	0.62	1.43
H_4SiO_4		0.00,	0.38
H_3BO_3			
CO_2			
H_2S			
TOTAL		0.76	
Na/K	14.56	19.89	
Mg/Ca	0.57	0.18	0.43
Cl/SO$_4$	21.84	0.61	7.73
Temp. (°C)	12°		
pH	6.49	3.7	6.60
Ionic Strength	0.0026	0.001	0.0015
Reference	This Paper	This Paper	Nakamura 1959

Table 7. Hg contents (ppm) in steam condensates and in altered rocks exposed at the surfaces of Onikobe, Matsukawa, and Otake geothermal areas, Japan (Koga and Noda, 1975).

	Hg contents (ppm)		As contents (ppm)
	Steam Condensates	Altered rocks	
Onikobe	0.153 - 0.411	16.0 - 22.5 (Av. 19.5)	17.9 - 69.4 (Av. 35.4)
Matsukawa	0.049 - 0.061	0.9 - 1.7 (Av. 1.2)	6.1 - 26.7 (Av. 13.4)
Otake	0.0032 - 0.0285	19.9 - 57.9 (Av. 37.9)	1.2 - 22.4 (Av. 10.4)

Table 8. Hg and As contents (ppm) in altered rocks exposed at the surface of the Onikobe, Matsukawa and Otake geothermal areas, Japan (Koga and Noda, 1975).

	Hg	As
Onikobe	16.0-22.5 (Av. 19.5)	17.9-69.4 (Av. 35.4)
Matsukawa	0.9- 1.7 (Av. 1.2	6.1-26.7 (Av. 13.4
Otake	19.9-57.9 (Av. 37.9)	1.2-22.4 (Av. 10.4)

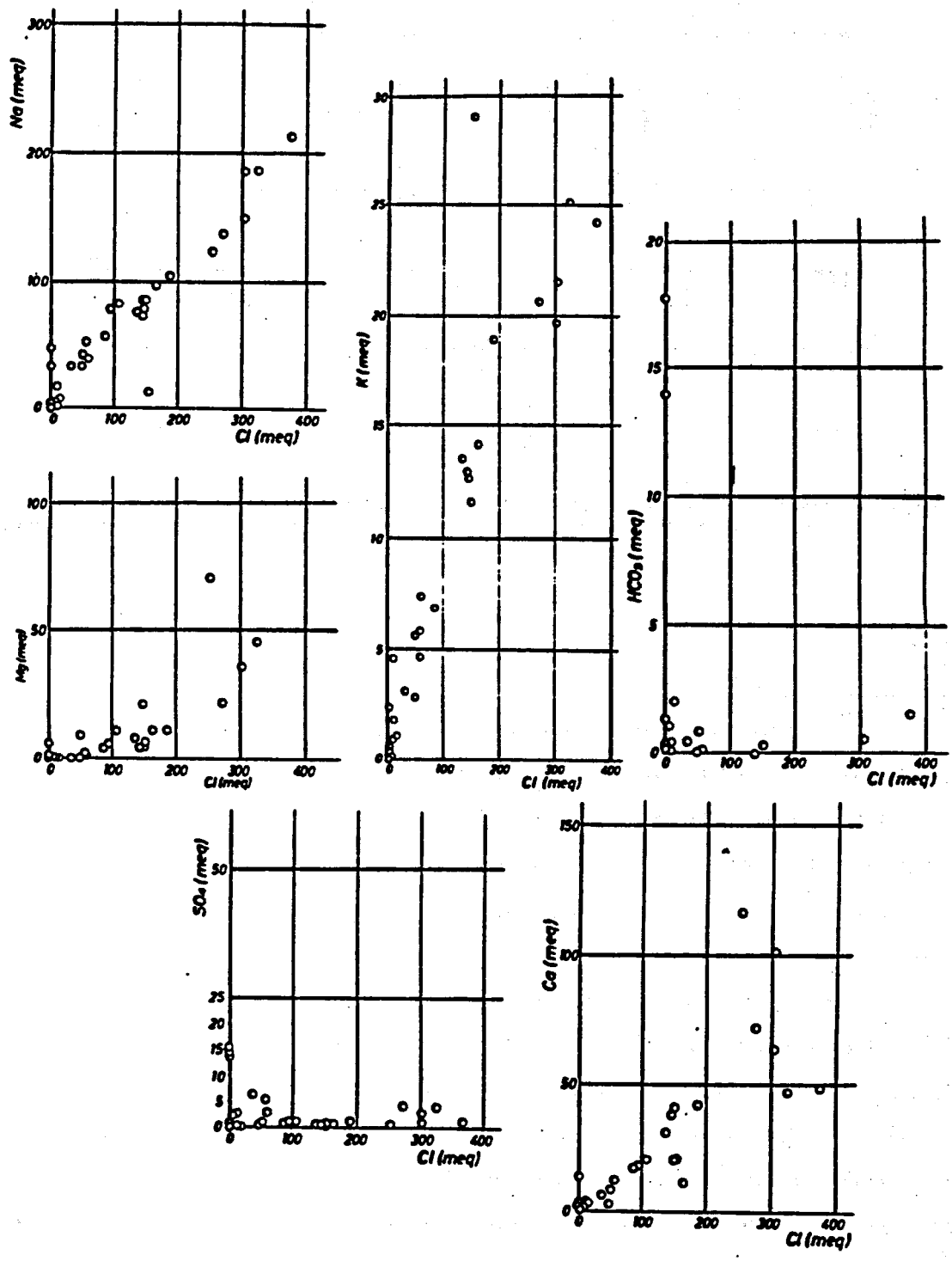

Figure 11. Na-Cl, K-Cl, Ca-Cl, Mg-Cl, SO_4-Cl and HCO_3-Cl diagrams of thermal waters from bore holes in the Onikobe geothermal area, Japan.

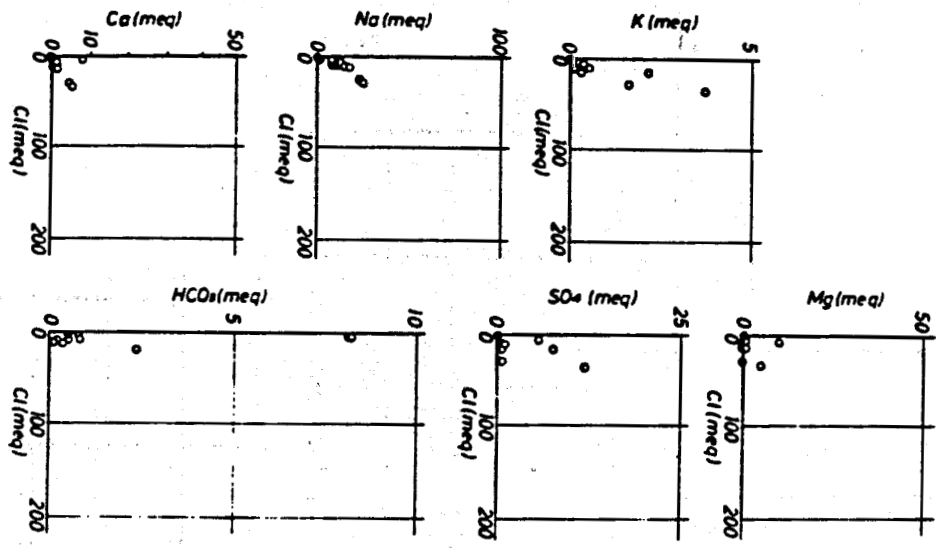

Figure 12. Na-Cl, K-Cl, Ca-Cl, Mg-Cl, SO_4-Cl and HCO_3-Cl diagrams of thermal waters in hot spring areas surrounding the Onikobe geothermal area, Japan.

area.

S Isotope of Thermal Water

The $\delta^{34}S$ values of thermal waters discharged from drill-holes of the Onikobe geothermal area are shown in Table 9. The Y-line, K-line and Z-line waters are mixtures of thermal waters discharged from some wells distributed in the Y-line area, K-line area and Z-line area (see Figure 2), respectively.

The $\delta^{34}S$ values of waters of #102, #111, #124 and Y-line (#108, #112, #117) are about +3.90 which is close to the average value of thermal waters originated mostly from meteoric water. However, thermal waters of the K-line and Z-line have extremely high $\delta^{34}S$ values of +19.90 which is near the $\delta^{34}S$ value of seawater sulfates. The Cl contents of K-line and Z-line thermal waters are over two or three times of the Cl content of Y-line thermal water. The isotope and geochemical data suggest that a considerable amount of fossil seawater from Miocene volcanogenic sediments in the basement of Onikobe Quaternary volcano must have supplied into some deep wells of the Onikobe geothermal area.

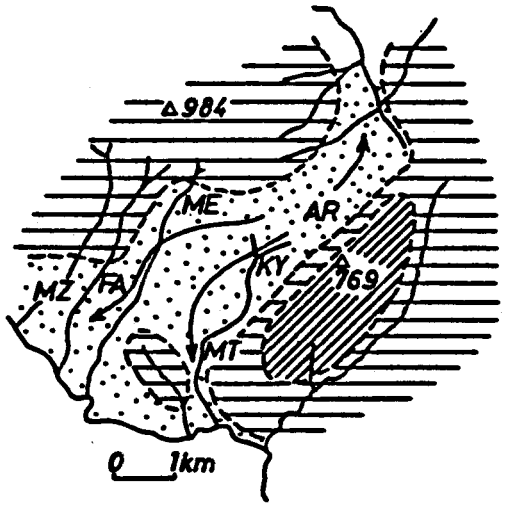

Figure 13. Specific resistivity distribution of stream flows in the Onikobe geothermal area and its surroundings, Japan (Ozaki and Kanno, 1977).

Obliquely hatched area: over 20,000 Ω-cm
Horizontally hatched area: 10,000-20,000 Ω-cm
Dotted area: less than 10,000Ω-cm
AR, KY, MT, ME, FA, MZ: see Figure 7.
Arrows indicate probable meteoric groundwater flow heated at the western side of Takahinata dacite dome.

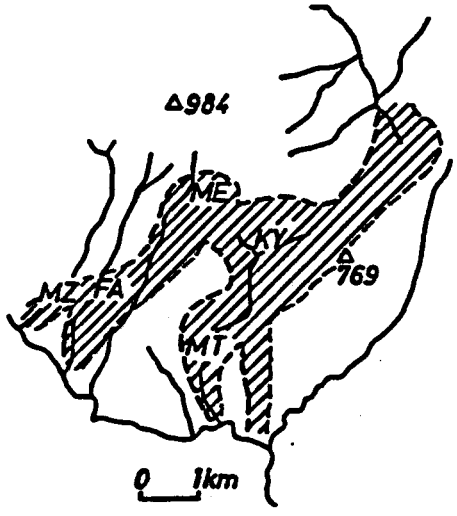

Figure 14. Specific heat discharge distribution calculated from temperatures and discharges of stream flow in the Onikobe geothermal area and its surrounding, Japan (Ozaki and Kanno, 1977)
Hatched area: over 140 kcal/sec/1 km^2
Unhatched area: less than 140 kcal/sec/1 km^2
AR, KY, MR, ME, FA, MZ: see Figure 7.

Table 9. $\delta^{34}S$ values of thermal waters from deep wells of the Onikobe geothermal area.

Well	$\delta^{34}S$
#102	+3.90
#111	+3.92
#124	+3.89
K-line (#101.102,103, 111)	+19.90
Y Line (#108,112,117)	+5.02
Z-line (#104,105,106, 120)	+16.52

Acid Thermal Water

Ozawa and Nagashima (1975), Yamada (1975), Nakamura et al. (1977) and Ozawa, Nagashima and Iwasaki (1980) have reported that the chemical characteristics of the thermal water in the Onikobe geothermal area generally change with depth as follows:

A. surface or near surface thermal water: low pH, high SO_4 and low Cl content;

B. intermediate depth water (100-500 m): neutral pH, intermediate SO_4 and intermediate Cl contents; and

C. deeper thermal water (800-1300 m): low pH, low SO_4 and high Cl contents.

Ozawa and Nagashima (1975) and Ozawa, Nagashima and Iwasaki (1980) inferred (1) the release of magmatic gas rich in HCl from depth, (2) its mixing with metoric water to form acid, high Cl thermal water and (3) the transformation of this acid thermal water to a neutral one by interaction with the rock as it comes up.

The concept of the wide distribution of acid thermal water or steam at depths of

over 800 m in the Onikobe geothermal area was born from the production of acid thermal water through some bore-holes such as G-10, G-11 and G-13 drilled to 1100-1300 m depth. JEDC once tried to get enough neutral or alkaline thermal water or steam from these deep bore-holes but later abandoned these deep wells and changed the project plan. They then began drilling relatively shallow (200-500 m) bore-holes such as #101, 102, 103 and 124 to supply neutral steam to their power plant. Thermal water and steam obtained through these shallow holes were of neutral or weakly alkaline nature (pH = 5-7) at the beginning. Several months or a year later, however, they changed to acid or weakly acid (pH = 3-4). Also, the temperature of this thermal water and steam and the amount discharged gradually or rapidly decreased and is apparently affected by precipitation of rain or melted snow.

Recently, JEDC again drilled to over 1000 m in the Z-line belt (#127) and succeeded in finding respectable amounts of neutral or weakly alkaline steam at a depth of over 1000 m in this geothermal area. All available data (drilling, petrographic and water chemistry) of bore hole #127 clearly indicate that within an over 1155m deep bore hole there must be at least two horizons in which acid thermal water is developed and hydrothermally formed calcite has been dissolved away to form highly porous rocks. We cannot expect the occurrence of acid thermal water at depths greater than 950m. Therefore, the idea of the the confined distribution of neutral pH thermal water or steam at relatively shallow depths (100-500 m) and the wide distribution of acid thermal water at greater depths within the Onikobe geothermal area was not supported by the data obtained from this #127 drilling.

The genesis and distribution of acid thermal water or steam at depth is one of the most important problems in the exploration for geothermal resources. As far as we know, the occurrence of acid thermal water is generally confined to a shallower zone above the predominant neutral or alkaline solution zone. Even when acid thermal water is found at depths of several hundred meters below the surface, the occurrence of the acid thermal water is generally rather local. Examples of the occurrence of acid thermal water at depth in some Japanese geothermal areas will be given as follows:

(1) In the Matsukawa geothermal area, Sumi and Maeda (1973) identified the presence of the following three types of thermal waters in relation to depth:

acid type (pH = 2.7-5.4): from a near surface shallow zone of about 30-150 m depth;

acid-neutral type (pH = 3.8-6.3); from "upper reservoir", developing from about 160 to 550 m in depth; and

weakly acid to alkaline type (pH = 4.0-8.6): from lower reservoir at about 550 to 1400 m in depth.

(2) Two types of thermal water, acid and neutral-alkaline, occur in the Onuma geothermal area, Japan (Ito et al,, 1977). The difference between these two types of water is chiefly due to a difference in SO_4 content. Chemical compositions of acid thermal water are almost the same as those of neutral-alkaline NaCl type thermal water plus CO_2 and SO_4. Figure 15 indicates the distribution of acid type and neutral-alkaline type thermal water in the Onuma geothermal area as confirmed by deep bore-holes. Detailed petrographic data clearly indicate that, at the depths at which acid thermal water predominates, no carbonate minerals form in the hydrothermally altered rocks (Yora et al., 1973; Ito et al., 1977a. The acid thermal water must have been formed only locally by the mixing of H_2S- and/or CO_2-rich volcanic gas migrated up through a fault (Akagawa fault) at the southern part of this geothermal area with widely distributed alkaline or neutral deep thermal water (Ito et al., 1977a).

(3) In the Kirishima geothermal area of Japan, thermal water from depths of over 20 m is neutral or weakly alkaline and becomes strongly acid or acid only near the land surface as the result of penetrated oxygen-bearing meteoric water (Yoshida, 1974). As far as observed in a drilled core sample in this geothermal area, calcite is a very common alteration mineral in cores from below 13 m depth but disappears by interaction with circulating acid thermal water in bore-hole cores from less than 13 m depth.

(4) In bore-hole AT-1 drilled in the Takinoue geothermal area of Japan from which 150°C alkaline thermal water is produced, calcite is a very common alteration mineral formed in rocks at depths of over 30 m (Kimbara and Sumi, 1975). No calcite was detected in the shallower zone where acid thermal water predominates.

(5) In the Satsunan geothermal area of Japan, thermal water from the surface is acid (Kimbara and Okubo 1978). At greater depths, neutral Na-Ca-Cl type thermal water poor in SO_4 was obtained.

(6) Koga et al. (1981) have reported a rapid lowering of the pH of thermal water coming from a depth of 1343 m through a bore in the Hatchobaru geothermal area, Japan. The thermal water obtained when the drilling of this hole was finished was neutral or weakly alkaline NaCl type water of pH = 7.5-7.7 and NaCl = 2300 ppm. Within 10 days, the pH of these thermal waters dropped down to almost 4.0. Simultaneously, the Cl/SO_4 and Ca/Mg ratios in these thermal waters decreased and the H_2SO_4 content increased. Petrographic evidence clearly indicates the presence of low pH thermal water at depths of 35-85 m and 700-850 m and the wide predominance of neutral or alkaline thermal water in the deeper part of the hole (Fujino et al., 1981). On the basis of detailed examination of technical processes and geochemical and petrographical evidence, Koga et al. (1981) concluded that the breakdown (corrosion) of casing pipe at a depth of 684-960 m led to the mixing of acid thermal water which is formed in a relatively shallow part with neutral-alkaline thermal water which came up from depths of over 960 m. This mixing must have been the major process which caused the rapid drop in the pH of the thermal water as a function of time.

The widespread occurrence of calcite in most of the core samples collected by deep drilling is a good indicator of the widespread occurrence of neutral to alkaline thermal waters at depth in the Onikobe geothermal area. For example, in bore-holes P-5, P-7, P-8, P-10, GO-7, GO-8, 123, 124 and 127 from which neutral or weakly alkaline thermal water is obtained, calcite can be widely observed as a hydrothermally formed mineral. At depths of over 800 m in GO-10 and over 600 m in GO-11, calcite was not found. These two deep wells have been abandoned or collapsed because of the predominance of acid thermal water at depth. If these two bore-holes had been drilled more deeply, perhaps to 1500 or 2000 m, however, neutral or alkaline thermal waters of over 250°C may have been obtained.

In bore-hole #127, the geothermal gradient, permeability of rocks and ditribution of calcite indicate the presence of acid thermal water at depths of about 370-470 m and

870-920 m. In this bore-hole enough high-temperature (240°C) weakly alkaline thermal water was obtained from a depth of 1000-1150 m, where calcite is one of the common hydrothermal alteration minerals.

In June to July of 1982, a new deep production hole (#128) (1255 m) (for locality see Figure 2) was successfully drilled. This new hole produces a remarkable amount of alkaline (pH: 8.3~8.5) high temperature steam and thermal water (steam 40 ton/hour, thermal water 140 ton/hour, maximum temperature 240°C).

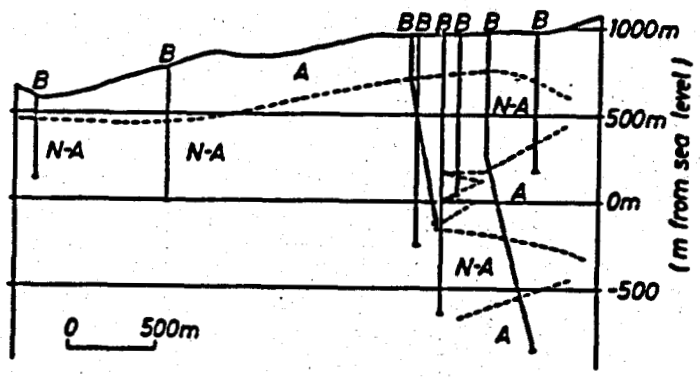

Figure 15. North-south cross section in Onuma geothermal area, Japan (Ito et al., 1977).
A: Acid thermal water zones
N-A: Neutral-alkaline thermal water zones.

LITHOLOGY AND DESCRIPTION OF SELECTED CORE SAMPLES

The rocks are an important component of the geothermal system and a detailed knowledge of the original lithologies and the secondary assemblages are necessary to determine the chemical interaction between rock and thermal waters. Petrographic and X-ray diffraction studies of the drill hole cores have identified many secondary phases. These phases and the rock type of each core sample are listed in Tables 10 to 20 for drill holes P-5, P-7, P-8, P-10, GO-7, GO-8, GO-10, GO-11, 123, 124, and 127 respectively. Three points should be mentioned for these tables: (1) Secondary minerals are listed according to the sequence of silica, clay, zeolite, feldspar, carbonate, sulfate, prehnite, epidote and opaque minerals; (2) Their modal abundances were not determined and the table simply shows that a given mineral is present in a

Table 10. Rock types and secondary minerals of bore-hole cores of #P-5, the Onikobe geothermal area, Japan.

Depth from Surface (m)	Rock Type	Cr	Qz	Ka/Py	Smectite-chlorite			Ill	Zeolites						Ab	Carb	Gyp	Anh	Alu	Ad	Pr	Ep	Mt/Hm	Pyr	Other min.
					Alk-Sm	Sm	Int-Ch		Md	Cp	Lm	Yu	Wr	Other											
22.25	AT	0	0	K		0			0								0	0						0	S,
29.3	AT	0	0			0			0							0	0	0						0	
36.0	A	0	0	K		0		0	0					Dach									(M)	0	
40.0	AT		0			0								Dach									(M)	0	
45.9	AT		0			0			0					Dach			0						(M)	0	
52.5	A		0			0					0						0						(M)	0	
55.0	AT		0	K		0		0						Dach		0	0						(M)	0	
62.0	AT		0			0		0						Dach		0	0						(M)	0	
63.35	AT		0			0								Dach										0	
72.5	AT		0			0					0			Dach		0	0						(M)	0	
148.0	AT		0			0					0					0	0					0		0	
149.0	AT		0				0				0					0	0								
179.6	AT		0				0				0					0						0	(M)	0	

Abbreviations

AT: Andesitic tuff or tuff breccia; A: Andesitic lava; DT: Dacitic tuff or tuff breccia; D: Dacitic lava; Cr: Cristobalite; Qz: Quartz; Ka: Kaolinite (K); Py: Pyrophyllite (P), Alk-sm: Alkaline smectite; Sm: Smectite, Int-ch: Chlorite/smectite interstratified mineral-chlorite, Ill: Illite, Md: Mordenite; Cp: Clinoptilolite; Lm: Laumontite; Yu: Yugawaralite; Wr: Wairakite, Dach: Dachiardite; Chab: Chabazite; Thom: Thomsonite; Nat: Natrolite; Ab: Sodic plagioclase, Carb: Calcite, Gyp: Gypsum; Anh: Anhydrite, Alu: Alunite; Ad: Adularia, Pr: Prehnite, Ep: Epidote, Mt: Magnetite, Hm: Hematite; Py: Pyrite; S: Sulfur; NaCl: Halite; Chalcopy: Chalcopyrite; Act: Actinolite, Pump: Pumpellyite, Bi: Biotite, ?: Not positively identified.

Table 11. Rock types and secondary minerals of bore-hole cores of #P-7, the Onikobe geothermal area, Japan (Symboles are same as in Table 10).

Depth from Surface (m)	Rock Type	Cr	Qz	Ka/Py	Smectite-chlorite			Ill	Zeolites						Ab	Carb	Gyp	Anh	Alu	Ad	Pr	Ep	Mt/Hm	Pyr	Other min.
					Alk-Sm	Sm	Int-Ch		Md	Cp	Lm	Yu	Wr	Other											
21.0	AT	0	0	K		0										0	0		0					0	S
26.0	DT	0	0	K		0			0					Dach		0	0						M	0	S
35.0	D	0	0	K	0					0						0							(M)	0	
39.0	AT		0	K		0					0?					0	0						(M)	0	NaCl
47.0	D		0	K		0			0														(M)	0	
50.0	DT		0	K		0			0							0							(M)	0	
57.7	DT		0													0							(M)/M	0	
70.15	DT	0	0	K		0		0								0	0						(M)/M	0	
77.25	D		0	K		0									0	0	0						(M)/M	0	
90.0	DT		0	K		0		0																0	
100.0	DT		0	K		0								Dach			0							0	
115.0	DT		0		0						0		0				0						(M)	0	
130.8	AT		0	K		0					0					0	0	0					(M)/M	0	
142.5	AT		0				0							Dach			0						M	0	
150.0	D		0				0						0	Dach	0	0	0					0	(M)	0	
170.0	D		0				0						0			0	0					0		0	
200.0	A		0				0									0						0		0	
218.0	AT		0				0	0								0				0		0	(M)	0	
250.0	AT		0				0	0								0	0	0				0	(M)	0	

Table 12. Rock types and secondary minerals of bore-hole cores of #P-8, the Onikobe geothermal area, Japan (Symboles are same as in Table 10).

Depth from Surface (m)	Rock Type	Cr	Qz	Ka/Py	Smectite-chlorite			Ill	Zeolites						Ab	Carb	Gyp	Anh	Alu	Ad	Pr	Ep	Mt/Hm	Pyr	Other min.
					Alk-Sm	Sm	Int-Ch		Md	Cp	Lm	Yu	Wr	Other											
50.0	AT	0	0			0			0							0		0					(M)	0	NaCl
50.5	A	0	0		0				0					Dach			0	0					(M)	0	NaCl
72.5	A	0	0	K		0					0			Dach		0	0						(M)	0	
85.0	AT		0			0			0		0					0								0	NaCl
95.0	A		0			0			0		0						0						(M)/H	0	NaCl
100.0	A		0			0			0					Dach									M,H		
104.15	AT		0			0			0					Dach									(M)/H	0	
111.2	AT		0	K		0		0			0			Thom		0	0						(M)	(0)	NaCl
118.05	A		0	K		0					0					0	0						(M)	0	
124.5	A		0	K		0			0					Dach		0							M	(0)	
131.8	AT		0		0				0		0					0	0						(M)	0	
140.25	A	0	0				0				0			Cheb Dach		0							M		
148.55	AT	0	0	K			0		0					Dach		0	0						(M)	0	
150.0	A		0			0			0					Dach		0						0	M	(0)	
156.25	DT	0	0				0	0	0			0		Dach		0	0						(M)	(0)	
168.55	AT		0				0	0			0		0	Dach		0	0					0	(M)	0	NaCl
180.0	A		0				0							Dach	0	0	0					0	M	0	
200.0	D		0				0							Dach	0	0	0					0	M	0	
213.9	AT		0				0				0		0		0	0	0					0	M	(0)	
250.0	A		0				0	0			0		0		0	0	0					0	M	0	
300.0	A		0				0								0							0	(M)/H	0	Act

Table 13. Rock types and secondary minerals of bore-hole cores of #P-10, the Onikobe geothermal area, Japan (Symboles are same as in Table 10).

Depth from Surface (m)	Rock Type	Cr	Qz	Ka/Py	Smectite-chlorite			Ill	Zeolites						Ab	Carb	Gyp	Anh	Alu	Ad	Pr	Ep	Mt/Hm	Pyr	Other min.
					Alk-Sm	Sm	Int-Ch		Md	Cp	Lm	Yu	Wr	Other											
25.0	DT		0	K		0										0								0	S
50.0	DT		0			0			0					{Chab, Dach		0	0	0						0	
50.5	DT		0			0								Dach		0	0							0	
51.5	A		0			0			0					Dach		0	0						(M)	0	
95.6	AT		0			0			0					Chab		0	0	0	0T					0	
100.0	AT		0			0								Dach		0	0	0					(M)	0	
110.0	A		0			0				0				Dach		0							(M)	0	
125.0	AT		0			0			0					Dach		0	0						(M)	0	
132.0	AT		0			0		0	0		0					0	0						(M)	0	NaCl
133.35	AT		0			0		0			0			Thom		0							(M)	0	NaCl
135.0	A		0			0				0				Dach		0		0					M	0	NaCl
139.25	A		0			0				0				{Dach, Thom		0	0						M		NaCl
144.25	*A		0			0					0			Dach		0	0						M	0	
148.75	AT		0			0				0						0	0					0		0	NaCl
149.0	A		0			0					0			{Dach, Thom				0					M	(0)	NaCl
152.35	AT		0			0								Dach		0	0					0	M	(0)	NaCl
160.0	D		0			0					0			Dach		0	0					0	M	0	
161.05	AT		0			0			0					Dach				0				0	(M)	0	NaCl
166.4	A		0			0					0					0	0					0		0	NaCl
171.75	AT		0			0			0		0			Dach		0							M	(0)	
183.05	AT		0			0			0		0			Dach		0							(M)	0	
194.2	AT		0			0						0	0	Dach		0	0						(M)	0	
203.0	A		0			0			0				0			0	0	0				0	(M)	0	

Table 14. Rock types and secondary minerals of bore-hole cores of #GO-7, the Onikobe geothermal area, Japan (Symboles are same as in Table 10).

Depth from Surface (m)	Rock Type	Cr	Qz	Ka/Py	Smectite-chlorite			Ill	Zeolites						Ab	Carb	Gyp	Anh	Alu	Ad	Pr	Ep	Mt/Hm	Pyr	Other min.
					Alk-Sm	Sm	Int-Ch		Md	Cp	Lm	Yu	Wr	Other											
15.0	AT		0		0				0								0						(M)	0	S,NaCl
16.0	AT		0													0							M	0	
20.5	AT		0		0				0							0	0						(M)	0	
23.0	AT		0		0				0							0							(M)/M	0	
26.5	DT	0	0		0				0							0	0						(M)/M	0	NaCl
36.0	DT		0			0										0	0						(M)	0	
107.0	DT		0	K	0				0		0					0	0		0?				M	0	
108.4	*DT		0			0					0					0	0						(M)	0	
147.0	*A		0	K		0			0		0		0			0							(M)/M	0	
175.0	A		0	K		0		0			0					0	0						M	0	NaCl
201.1	*A		0				0				0		0		0	0	0						(M)	0	NaCl
201.15	A		0				0						0	Dach	0	0	0						(M)/M	0	NaCl
243.0	A		0				0	0					0			0	0						(M)	0	
247.0	A		0				0						0			0	0						(M)	0	NaCl
263.0	DT		0				0	0					0		0	0	0						(M)	0	
276.0	DT		0				0						0			0							(M)	0	
299.3	A		0				0	0					0		0	0							(M)	0	
300.0	A		0				0						0		0	0		0					(M)	0	NaCl
300.8	A		0				0						0		0	0	0						(M)	0	NaCl
315.0	DT		0				0									0	0					0	(M)/M	0	NaCl
351.8	*DT		0				0	0					0		0	0	0						(M)	0	
352.0	AT		0				0						0		0	0	0						(M)	0	
358.5	AT		0				0						0			0	0						(M)	0	
364.0	A		0				0						0			0	0					0	(M)/M	0	
377.5	A		0				0						0			0	0				0		M	0	
381.0	A		0				0						0			0		0					M	0	
398.6	A		0				0	0					0		0	0	0				0		(M)	0	
404.0	A		0				0						0			0		0					(M)	0	
423.4	A		0				0						0			0	0					0	(M)	0	
441.0	A		0				0						0			0	0	0				0	(M)	0	
450.0	A		0				0						0				M								
450.6	A		0				0						0			0	0					0	(M)	0	
482.3	A		0				0						0		0		0	0				0	(M)	0	
498.0	A		0				0						0			0						0	M		NaCl
500.0	A		0				0	0					0				0					0	(M)	0	

Table 15. Rock types and secondary minerals of bore-hole cores of #GO-8, the Onikobe geothermal area, Japan (Symboles are same as in Table 10).

Depth from Surface (m)	Rock Type	Cr	Qz	Ka/Py	Smectite-chlorite			Ill	Zeolites						Ab	Calc	Gyp	Anh	Alu	Ad	Pr	Ep	Mt/Hm	Pyr	Other min.
					Alk-Sm	Sm	Int-Ch		Md	Cp	Lm	Yu	Wr	Other											
25.0	DT	0	0		0				0								0							0	
50.0	DT	0			0				0							0								0	
50.5	DT		0			0			0		0						0							0	
52.0	DT		0			0					0						0							0	
100.5	AT		0	K	0	0					0					0							M	0	
126.5	AT		0		0								0			0	0							0	
147.0	D		0				0									0	0						(M)	0	
147.1	DT		0				0	(0)			0		0			0	0						(M)	0	
148.0	D		0				0				0		0		0	0	0							0	NaCl
198.5	DT		0		0			(0)			0		0				0						(M)	0	
202.0	A		0				0	(0)			0		0		0	0	0							0	NaCl
247.0	A		0				0						0		0	0		0					(M)	0	NaCl
250.5	D		0				0				0		0			(0)	0							0	
265.0	DT		0				0										0							0	
297.5	AT		0				0						0		0	0	0	0						0	NaCl
350.5	A		0				0	(0)			0		0			(0)	0							0	NaCl
351.0	A		0				0	0					0		0		0						(M)	0	
402.5	AT		0				0	(0)					0			(0)	0	0						0	NaCl
403.0	A		0				0	(0)										0						0	
454.5	A		0				0						0		0	0		0				0		0	
455.5	AT		0				0	0					0		0	(0)	0	0				0		0	
455.8	AT		0				0						0			0		0						0	NaCl
500.5	AT		0				0	(0)					0		0	0		0				0		0	NaCl
501.0	D		0				0	(0)					0		0		0					0		0	NaCl
552.5	A		0				0	0					0			(0)	0							0	
597.5	A		0				0	(0)					0			(0)						0		0	
599.0	A		0				0						0			0	0					0		0	NaCl
650.5	D		0				0	0					0			(0)						0		0	NaCl
651.0	DT		0				0	0					0				0					0		0	
700.0	DT		0				0	0					0				0					0		0	
700.1	A		0				0						0		0		0					0		0	
701.3	DT		0				(0)	0							0	0	0				0	0		0	
744.6	DT		0				0	0					0									0		0	
750.0	D		0				0	(0)					0				0					0	(M)	0	
775.0	A		0				0						0		0							0		0	
799.0	D		0				0						0		0		0				0	0		0	
818.4	DT		0				0	0					0									0		0	
827.0	A		0				0								0						0	0		0	
849.9	AT		0	P			0								0									0	NaCl
869.2	A		0				0						0		0	0					0	0	(M)	0	Act
899.8	D		0				0	(0)												0				0	
950.0	DT		0	P			0											0						0	
964.0	DT		0	P			0								0			0						0	
973.0	DT		0	P			0								0								(M)	0	
993.0	DT		0	P			0						0											0	
998.0	DT		0				0	0					0		0							0	(M)	0	
998.3	DT		0	P			0	0					0		0									0	chal-copy

core sample from a certain depth; and (3) The secondary minerals occur in veins, in vesicles, in matrix, or as a replacement after feldspar, mafic minerals, or volcanic glass and such modes of occurrence are not differentiated in these tables. Their variation with depth, characteristic chemistry, and occurrences will be discussed later. In this section, general features of the altered rock types will be described first, followed by petrographic descriptions of selected rock samples.

Four rock types were identified: andesitic tuff - tuff breccia (AT), andesitic lava (A), dacitic tuff - tuff breccia (DT), and dacitic lava (D). Although pervasive hydrothermal alteration has significantly modified both primary textures and minerals for most of the core samples, many features are well preserved and they were used for distinction among these rock types. Chemical analyses of some less altered rock cores were completed and the results will be described later. In general, andesitic lava contains less SiO_2 than the dacitic rocks. Therefore, the andesitic rocks contain mainly augite $\pm$ hypersthene $\pm$ hornblende as major mafic minerals; quartz phenocrysts were not identified. On the other hand, the dacitic rocks are characterized by the presence of hornblende and quartz phenocrysts, plagioclase of lower An content, and higher contents of volcanic glassy matrix or groundmass. The primary features of the 4 rock types are briefly described below.

Andesitic tuff and tuff breccia (AT)

Tuffaceous rocks are most common in the drill hole core samples. Because they have suffered severe alteration due to the present geothemal activity, it is difficult to clearly assign the volcanic rocks into the various Plio-Pleistocene formations described in the previous sections. The andesitic tuffs consist of abundant angular andesitic fragments of various sizes and shapes in a matrix of fine-grained volcanic glass, quartz, and co-genetic minerals. Andesitic fragments even within a single tuff sample may vary significantly in textures and in primary minerals, which are similar to those of the andesitic lavas (A) described below. Because of the relative accessibility to geothermal waters, the tuffaceous rocks tend to be much more altered then their lava counterparts. Veining and fracturing are

very common. Both mafic and plagioclase phenocrysts have been altered at least in part. Slightly altered andesitic tuff contains both augite and hypersthene as phenocrysts and groundmass minerals and zoned plagioclase phenocrysts of An 85 to 35. Olivine microphenocrysts may have occurred in some mafic andesitic fragments, but they were not identified. Glass shards are irregular in form; they together with other fine-grained tuffaceous matrix material are extensively replaced by secondary phases including zeolite, chloritic clay mineral and calcite.

Andesitic lava (A)

Except for the Takahinata dacite dome, both andesitic and dacitic lavas are rare in the Onikobe geothermal area. Those that occur may cover a wide range of chemical composition and textural variations. The andesitic rocks are characterized by the common occurrence of augite phenocrysts and hypersthene as microphenocrysts or in the groundmass. Although olivine was not found, it may have occurred in some basaltic andesites and been entirely altered. Plagioclase is the most common mineral both as a phenocryst and as a groundmass constituent. Plagioclase always forms zoned crystals and its core composition may be as calcic as An 85-90. Augite most often occurs as phenocrysts and shows slight pale greenish brown to pale green pleochroism. Hornblende occurs in some andesitic core samples but is a relatively minor constituent compared to augite. Other primary phases include magnetite-ilmenite, zircon, and apatite.

Dacitic tuff and tuff breccia (DT)

Primary textures and alteration features of the dacitic tuffs from the Onikobe geothermal area are similar to those of the andesitic tuffs mentioned above. However, the dacitic rocks contain corroded quartz phenocrysts together with zoned plagioclase and mafic minerals. Augite and hypersthene may occur in the less silicic dacite, but the most abundant mafic minerals are green to greenish brown hornblendes which appear as phenocrysts and groundmass as well as crystal fragments in the matrix. Amphiboles are euhedral to subhedral in form and are commonly replaced by chloritic clay together with fine-grained sphene. Oxidized hornblende was not

Table 16. Rock types and secondary minerals of bore-hole cores of #GH-10, the Onikobe geothermal area, Japan (Symboles are same as in Table 10).

Depth from Surface (m)	Rock Type	Cr	Qz	Ka/Py	Smectite-chlorite: Alk-Sm	Sm	Int-Ch	Ill	Zeolites: Md	Cp	Lm	Yo	Wr	Other	Ab	Carb	Grp	Anh	Alu	Ad	Pr	Ep	Mi/Hm	Pyr	Other min.
55.0	D		o	K		o					o					o	o						K	o	
90.0	DT		o			o					o						o							o	
155.0	DT		o				o				o		o		o		o	o					K	o	
195.0	DT		o				o				o							o						o	
204.0	A		o				o								o									o	
235.0	A		o	K			o				o		o				o						(W)	o	
300.0	A		o			o							o											o	
321.0	A		o			o							o					o						o	
330.0	A		o				o				o		o		o		o	o						o	
355.0	A		o				o				o					o	o							o	
380.0	A		o				o				o		o											o	
400.0	A		o				o								o									o	
401.0	A		o				o					o	o		o	o	o	o						o	
435.0	A		o				o																	o	
500.0	A		o				o						o			o	o					o		o	
525.0	A		o				o						o				o							o	
600.0	A		o				o	o					o			o		o				(o)	K	o	Hcl
655.0	A		o				o																	o	
700.0	A		o				o								o		o					o	(W)	o	
725.0	A		o				o	o					o			o		o						o	
800.0	A		o	P			o	o					o		o									o	
855.0	A		o				o																	o	
900.0	A		o	P			o																(W)	o	
925.0	DT		o	PT			o	o					o				o							o	
1000.0	DT		o	P			o																	o	
1050.0	DT		o	P			o																	o	
1100.0	D		o	P			o	o					o		o									o	
1150.0	DT		o	P			o																	o	
1200.0	D		o	P			o	o							o									o	
1243.0	D		o	P			o																	o	
1277.0	D		o	P			o																	o	
1330.0	D		o	P			o	o					o		o		o							o	Act. Bi

identified. Plagioclase phenocrysts also show distinct zoning, but the core composition is less anorthitic than those in the andesitic rocks.

Table 17. Rock types and secondary minerals of bore-hole cores of #GO-11, the Onikobe geothermal area, Japan (Symboles are same as in Table 10).

Depth from Surface (m)	Rock Type	Cr	Qz	Ko/Py	Smectite-chlorite			Ill	Zeolites					Ab	Carb	Gyp	Anh	Alu	Ad	Pr	Ep	Ml/Hm	Pyr	Other min.
					Alt-Sm	Sm	Im-Ch		Md	Cp	Lm	Yu	Wr	Other										
50.0	DT		o	K		o					ot					o						M	o	Wcl
100.0	DT		o													o						M	o	
105.0	DT		o		o	o					ot				o	o	o					M	o	Wcl
150.0	DT		o	K	o	o					o				o	o						M	o	
200.0	DT		o		o	o									o	o						(M)	o	
203.0	DT		o		o			o			o		o		o	o						(M)	o	
250.0	DT		o	K			o	o			o		o									(M)	o	
300.0	DT		o										o		o	o						(M)	o	
305.0	DT		o								o		o		o	o						(M)	o	
350.0	A		o										o		o	o						(M)	o	
400.0	DT		o										o		o							(M)	o	
401.6	DT		o										o		o							(M)	o	
450.0	D		o										o		o	o					o	M	o	
500.0	A		o	K									o		o					o		M	o	
503.0	A		o					(o)					o									M	o	
550.0	A		o					o					o		o	o					o	M	o	
598.0	DT		o					(o)					o		o	o						(M)	o	
650.0	D		o					(o)					o		o	o						(M)	o	
700.0	D		o					o					o		o	o						(M)	o	
701.0	AT		o	K				o					o		o	o						(M)	o	
791.0	A		o												o	o						M	o	
800.0																								
900.0	DT		o	P			o	(o)							o	o						M	o	
902.0	DT		o				o	(o)							o	o						M	o	
1004.0	DT		o	P			(o)	(o)							o	o						M	o	Act?
1005.0	DT		o	P			(o)	(o)						o	o	o						M	o	Act?
1100.0	DT		o	P			(o)	o						o	o	o						M	o	Act?
1103.0	DT		o	P			(o)	o						o	o	o	o				o	M	o	Pump?
1200.0	DT		o	P			(o)							o	o	o	o				o	M	o	Pump?
1205.0	DT		o	P			(o)	o						o	o	o	o					M	o	Pump?
1300.0	DT		o				o	(o)						o	o	o	o					M	o	Pump?

Dacitic lava (D)

The dacitic lavas are highly vesicular and are filled with secondary phases. They are porphyritic rocks containing quartz, hornblende and plagioclase as major

Table 18. Rock types and secondary minerals of bore-hole cores of #123, the Onikobe geothermal area, Japan (Symbols are same as in Table 10).

Depth from Surface (m)	Rock Type	Cr	Qz	Ks/Py	Smectite-chlorite Alt-Sm	Sm	Irr-Ch	Ill	Zeolites Md	Cp	Lm	Ye	Wr	Other	Ab	Cord	Gyp	Anh	Alu	Ad	Pr	Ep	Ml/Hm	Pyr	Other min.
158.9	AT		o				o	(o)					o		o	o	o							o	
159.2	DT		o				o	(o)								o								o	
162.9	AT		o				o	(o)					o			o								o	
163.1	A		o				o									o								o	
165.1	DT		o				o	(o)					o		o	o	o					o	M	o	
165.2	AT		o				o						o			o								o	
169.8	AT		o				o	(o)					o			o				o				o	
173.9	AT		o			o							o			o								o	
176.8	AT	o	o				o	(o)					o		o	o	o	o						o	
179.0	AT		o				o	(o)					o		o	o	o	o			o			o	
184.7	AT		o			o					Gr	o	o			o								o	
187.6	DT		o			o					o		o			o								o	
191.8	AT		o				o	(o)					o	Thom	o	o	o	o						o	KCl
198.4	DT		o				o	(o)					o		o	o	o						(M)	o	
202.5	DT		o				o	o					o			o	o						(M)	o	
206.6	DT		o				o	(o)					o			o						o		o	
207.1	DT		o				o								o	o								o	
210.9	AT		o				o	(o)					o		o	o	o							o	
215.2	AT		o				o									o								o	
216.0	AT		o				o	o					o		o	o	o							o	
229.4	DT		o				o	(o)				o	o	Dach, Cheb	o	o	o							o	NaCl
232.4	AT		o				o									o								o	
238.6	DT		o				o	(o)						Mor	o	o	o	o		o				o	NaCl
244.9	AT		o				o						o		o	o								o	NaCl
247.6	AT		o				o	(o)					o			o								o	
253.0	A		o				o									o								o	
260.9	A		o				o	(o)					o	Dach	o	o	o	(o)						o	
262.6	A		o				o	(o)					o			o		(o)						o	
263.6	DT		o				o	(o)					o		o	o	o							o	
267.7	A		o				o									o								o	
273.6	A		o				o	(o)					o	Dach	o	o	o			o				o	
279.6	AT		o				o						o			o								o	
285.3	AT		o				o	(o)					o	Thom	o	o	o	(o)						o	NaCl
290.1	AT		o				o						o			o		o						o	
295.2	AT		o				o	(o)					o		o	o								o	
300.1	A		o				o									o								o	
303.5	DT		o				o	(o)					o	Dach	o	o	o							o	NaCl
307.5	DT		o				o	(o)					o	Dach	o	o	o							o	
308.2	A		o				o	(o)				o	o	Dach	o	o	o	o						o	
311.7	A		o				o									o								o	
313.7	A		o				o	(o)					o	Dach	o	o	o							o	NaCl
319.9	A		o				o	(o)					o	Dach	o	o	o							o	
323.8	DT		o				o									o								o	
328.6	DT		o				o	(o)					o	Dach	o	o	o	o						o	NaCl
333.3	DT		o				o	(o)					o			o	o							o	
340.6	AT		o				o	(o)					o		o	o								o	NaCl
344.6	DT		o				o	o					o			o								o	
348.5	AT		o				o	(o)					o			o								o	
353.0	AT		o				o	(o)					o		o	o								o	

phenocrysts, and glassy groundmass which is extensively replaced by secondary minerals. The silicic dacite contains biotite flakes as the only mafic phase in the groundmass; those biotites are pseudomorphed by chloritic clay ± prehnite. Hypersthene was not found and minor augite phenocrysts are common in most dacitic core samples.

Table 19. Rock types and secondary minerals of bore-hole cores of #124, the Onikobe geothermal area, Japan (Symboles are same as in Table 10).

Depth from Surface (m)	Rock Type	Cr	Qz	Ka/Py	Smectite-chlorite			Ill	Zeolites						Ab	Cord	Gyp	Ani	Alu	Ad	Pr	Ep	Mt/Hm	Pyr	Other min.
					Alk-Sm	Sm	Int-Ch		Md	Cp	Lm	Yu	Wr	Other											
158.3	AT		●				●				●			Bach, Thom		●			○?		●		N		
159.5	*DT		●				●				●				●	●			○?		●	●	N		
162.4	*AT		●				●						●	Bach, Thom	●	●					●	●	N	3	
165.6	AT		●	K			○				●		○		●	○					○		N	○	
167.3	AT		●				●						●		○	○							N	○	NaCl
172.4	A		●	K		●										○	○					○	N	○	
178.0	*A		●	K		●										○							N	(○)	
179.3	AT		●				●				●		●			○	○							○	
186.3	AT		●				●						●	Bach, Thom	●	○						○	N	○	NaCl
192.0	A		●				●				●					○				○	○		N	(○)	
193.4	AT		○	K		○	○	(○)					●			○	○			○			N	○	
200.3	A		○			●								Bach		○	○						N		
201.8	*AT		○				●				●	○	●		●	●	○				○	○		○	NaCl
209.9	DT		○				○						●		●	○	○				○	○		○	
211.1	*AT		○				●					(○)	●		●	○	○	(○)		●	○	○	N		
216.3	DT		○				○	○					●		○							○		○	NaCl
219.6	DT		○				●	●					●		●	○	○					●		○	
222.8	*DT		○				●	●			●		●		●	○	○					●		○	
227.4	A		○				●								●	○		○						○	
231.7	B		○				●	(○)							○	○	○			●				○	NaCl
235.8	DT		○				○								○	○				○				○	
239.8	DT		○				○									○	○							○	
243.0	A		○				●	(○)							●	○							N	(○)	
246.4	DT		○				●	(○)						Bach		○							N	○	
249.4	DT		○				○	(○)																○	
252.5	A		○				○						●	Bach	○	○	○						(N)	○	
254.4	DT		○				●	(○)					●	Bach	○	○	○							○	
259.4	DT		○				●	(○)					●		○	○						○		○	
259.9	*A		○				●	(○)			●		●		○	○						○		○	
264.05	AT		○				●							Bach	○	○								○	
264.4	DT		○				○									○							N	○	
270.4	DT		○				○								○	○				○			N	○	
276.9	DT		○				●	(○)					●		●									○	
286.2	AT		○				●						●			○							N	○	
288.6	DT		○				●						●											○	
291.5	*A		○	K		○			●								○							N		
294.4	A		○				○						●		○	○	○							○	
300.3	A		○				○						●			○							N	○	
307.3	A		○				●						●		○	○						○		○	
310.4	AT		○				●						●	Chab	○	○							N		
314.3	A																						N		
315.4	AT		○				○						●		○	○							N	(○)	
318.5	A		○				○						●			○						○		○	
320.4	AT		○				●	(○)					●			○		○						○	
323.7	AT		○				●						●			○	○	○						○	
324.5	A		○				●						●		○	○	○						N	○	
329.7	A		○				○						●		○	○	○					○	N	○	
331.4	AT		○				○						●		○	○							N	○	
334.7	*A		○				●						●		○	○	○				○	○		○	
339.6	A		○				●						●			○								○	
344.6	DT		○				●	(○)					●			○	○				○	○		○	
346.3	DT		○				○						●			○						○		○	
349.4	DT		○				○						●			○	○					○		○	

The petrographic features of 30 selected core samples from various drill holes in the Onikobe geothermal area are described below. The first 15 samples are less altered and were selected for analysis for major elements using a wet chemical method and the results are listed together with modal compositions (both primary and secondary) in Table 21.

No. 1, Hypersthene-augite andesite (P-8, 118.05 m): This andesitic rock from

Table 20. Rock types and secondary minerals of bore-hole cores of #127, the Onikobe geothermal area, Japan (Symboles are same as in Table 10).

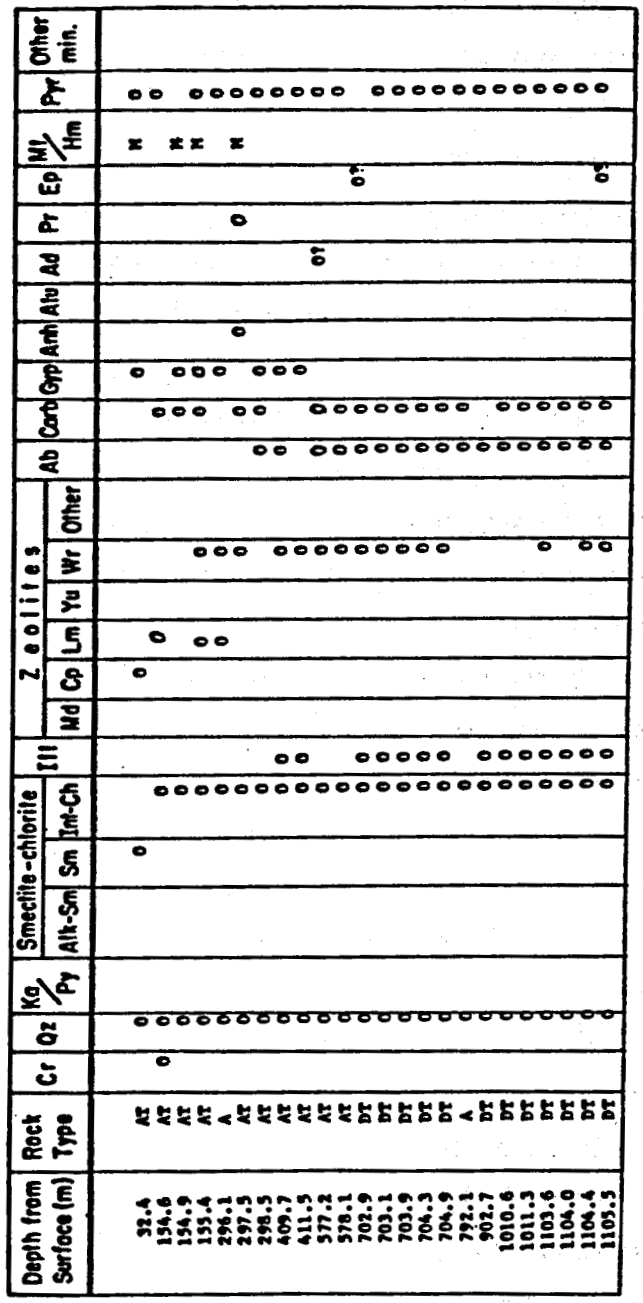

drill hole P-8 is porphyritic in texture and consists of augite, hypersthene and plagioclase as phenocrysts and fine-grained clinopyroxene, magnetite and volcanic

glass as groundmass phases. The hypersthene phenocrysts have nearly been replaced and pseudomorphed by fine-grained aggregates of brownish smectite. However, most augite phenocrysts remain fresh and some are replaced by brown smectite, leucoxene and calcite along crystal margins and cleavages. No hydrothermal alteration of plagioclase phenocrysts was found. The groundmass has been strongly altered into an assemblage of calcite, leucoxene, quartz, laumontite, smectite, pyrite, kaolinite and gypsum. Thin veins 0.3 mm wide with brown smectite, quartz and minor laumontite occur.

The strong alteration of the rock is reflected in its major chemistry with very high Al_2O_3, Fe_2O_3, Na_2O and H_2O.

No. 2, Hypersthene-augite andesite (P-10, 144.25 m): This porphyritic andesite from drill hole P-10 is similar to the rock described above. It consists of the same phenocrysts which have been subjected to a similar alteration. However, some hypersthene phenocrysts are preserved and augites are only altered along cleavage traces and crystal margins. The groundmass has been totally replaced by the assemblage quartz, laumontite, brown to brownish green smectite, calcite, dachiardite and leucoxene. No pyrite was found. Irregular amygdules 0.7 to 1.2 mm in diameter are filled with brownish green smectite at the margin and quartz at the center. Thin veins 0.3-0.5 mm wide consist of quartz, dachiardite, laumontite and brownish green smectite.

The rock has a very similar major chemistry to that of No. 1; they are both low in SiO_2 and high in Al_2O_3, Fe_2O_3 and H_2O.

No. 3, Hornblende dacite tuff (GO-7, 108.4 m): This tuff consists of abundant fragments of hornblende, plagioclase and corroded quartz phenocrysts and fine-grained plagioclase, magnetite and volcanic glass in both groundmass and tuffaceous matrix. Hornblendes are nearly completely replaced by pale brown to brownish green alkaline smectite and some strongly zoned plagioclase phenocrysts are replaced by laumontite, calcite and alkaline smectite. Both groundmass and matrix materials have been totally altered to laumontite, quartz, smectite, calcite, hematite, gypsum, pyrite and leucoxene.

This tuff is chemically characterized by higher SiO_2, Fe_2O_3 and H_2O and lower Al_2O_3, MgO, CaO and H_2O compared to the andesites described above.

No. 4, Augite andesite (GO-7, 147.0m): Augite phenocrysts in this porphyritic andesite are nearly completly replaced by brown smectite + calcite + minor leucoxene whereas plagioclase phenocrysts are still very fresh. The groundmass, which was originally composed of fine-grained augite, plagioclase, magnetite and volcanic glass, is strongly altered to calcite, quartz, mordenite, laumontite, pyrite and pale greenish brown smectite. Veins 0.7-1.0 mm thick consist mainly of quartz, calcite and wairakite whereas other veins about 0.4 mm thick consist of only anhydrite + quartz. The temporal and spatial relationship between the wairakite- and anhydrite-bearing veins is not apparent. It should also be noted that laumontite occurs in the rock and wairakite is restricted to only the veins of this rock. Some of the primary magnetite and secondary pyrite crystals have been oxidized and replaced by hematite along their crystal margins.

This andesite contains low SiO_2 and MgO and very high Fe_2O_3, CaO and CO_2.

No. 5, Augite andesite (GO-7, 201.1 m): This porphyritic andesite consists of augite and plagioclase phenocrysts and augite, plagioclase, magnetite and volcanic glass as groundmass phases. Most of the augite phenocrysts have been altered to pale brownish green chlorite/smectite, and leucoxene. Phenocrysts of plagioclase, however, are rather fresh except for partial replacement by calcite and wairakite along crystal margins or cleavage planes. The groundmass has been strongly silicified and completely replaced by laumontite, wairakite, calcite, quartz, pyrite, chlorite/smectite, leucoxene and gypsum. Amygdules are chiefly composed of quartz, calcite and wairakite. Quartz, quartz-calcite- and quartz-wairakite veins are common. This rock is higher in TiO_2, FeO, and MgO and lower in Fe_2O_3 and MgO than those described above.

No. 6, Hornblende dacite tuff (GO-7, 351.8 m): This tuffaceous rock contains abundant fragments of primary phenocrysts, but most of them have been strongly altered. For instance, most hornblende phenocryst fragments have been replaced and pseudomorphed by pale greenish brown chlorite clay, calcite and leucoxene.

Table 21. Bulk chemical and modal mineral compositions of representative altered volcanic rocks came from deep bore holes at the Onikobe geothermal area, Japan.

	1	2	3	4	5	6	7	8	9	10	11	12	13	14	15
SiO_2	49.43	48.09	53.84	44.29	46.45	60.48	56.13	53.99	51.54	48.99	59.31	63.65	53.77	51.54	55.82
TiO_2	1.04	1.02	0.86	1.61	1.77	1.12	0.82	0.83	1.06	0.89	0.65	0.37	0.88	1.06	0.79
Al_2O_3	17.73	17.28	14.22	16.98	16.74	13.35	15.71	16.09	15.95	18.32	12.68	13.78	16.01	15.95	15.63
Fe_2O_3	5.81	5.98	7.17	8.75	4.92	4.78	4.04	4.15	3.69	5.48	5.75	3.75	5.03	3.69	4.86
FeO	2.64	3.13	1.23	1.99	5.62	1.69	3.46	4.23	4.93	3.11	2.32	1.24	3.01	4.93	2.84
MnO	0.12	0.18	0.08	0.06	0.18	0.08	0.04	0.17	0.21	0.13	0.09	0.11	0.14	0.21	0.15
MgO	4.61	4.37	1.62	1.76	5.95	2.13	3.33	3.94	4.55	3.88	2.93	2.35	3.36	4.55	3.35
CaO	8.90	8.51	3.48	11.01	7.08	5.93	7.67	7.93	8.38	9.54	7.60	3.01	7.49	8.38	7.04
Na_2O	3.16	2.41	1.16	2.90	1.83	0.82	1.88	2.13	1.92	2.22	1.88	1.94	2.05	1.92	1.74
K_2O	0.21	0.50	0.51	0.15	0.81	0.25	0.81	0.80	0.49	0.26	0.19	1.88	1.28	0.49	0.97
H_2O+	2.43	5.34	7.26	4.82	3.17	7.82	4.28	3.75	2.94	5.64	5.79	5.76	5.83	2.94	4.23
H_2O-	3.74	2.96	7.24	1.60	1.77	0.73	1.51	1.88	4.19	1.11	0.59	1.93	0.94	4.19	2.27
P_2O_5	0.16	0.15	0.14	0.16	0.18	0.18	0.15	0.17	0.16	0.15	0.16	0.11	0.17	0.16	0.10
CO_2	n.d.	n.d.	0.83	3.41	0.96	0.15	n.d.	n.d.	n.d.	n.d.	n.d.	n.d.	n.d.	n.d.	n.d.
S	n.d.	n.d.	0.28	0.30	0.35	0.32	n.d.	n.d.	n.d.	n.d.	n.d.	n.d.	n.d.	n.d.	n.d.
Total	99.98	99.92	99.92	99.79	99.78	99.83	99.83	100.16	100.01	99.72	99.94	99.88	99.96	100.01	99.81
Primary phase															
Hypersthene		2													
Augite	16	17					3	1	22	2	1			19	2
Hornblende			2												
Plagioclase	28	24	20	23	11	7	22	34	36	31	4	4	19	34	27
Magnetite	2	7	1	2			3	4	3					7	

Secondary phase															
Hematite			2	4	1	2								2	
Pyrite	3		6	5	9	7		4	1	6	7	4	6		5
Leucoxene	1	1	1	1	2	2	1	1	1	1	1	1	1	1	1
Quartz	10	12	21	12	14	26	13	14	12	15	16	26	18	8	10
Mordenite-Clinoptilolite				2										18	
Laumontite	6	6	18	10	8		12			1					
Tugawaralite											1				
Wairakite				6	14	13		4		6	3	3	14		6
Kaolinite	6			3					2					2	
Smectite-chlorite	14	20	21	14	20	19	24	20	20	12	16	34	20	6	21
Illite						7						4	1		
Gypsum	4		4		4	6					2	2	2	3	2
Alunite						1	1	1							
Dachiardite		3						1							
Thomsonite								1							
Epidote						2	6	5		9	7	6	9		4
Prehnite							4	1		3	29				
NaCl	1				2					1					
Albite					8	4	9	6		10	12	14	8		10
Calcite	2	6	4	10	4	2	2	3	3	3	1	2	2		3
Vein Mineral	Qz 1	Dach-Lm-Qz 2		Wa-Calc Qz 8	Wa-Calc Qz 3	Wa-Qz 2									Wa-Calc Qz 9

1: Hypersthene-augite andesite, P-8, 118.05 m. (This paper), 2: Hypersthene-augite andesite, P-10, 144.25m. (This paper), 3: Hornblende dacite tuff, GO-7, 108.4 m. (Seki et al., 1969), 4: Augite andesite, GO-7, 147.0 m. (Seki et al., 1969) 5: Augite andesite, GO-7, 201.1 m. (Seki et al., 1969), 6: Hornblende dacite tuff, GO-7, 351.8 m. (Seki et al., 1969), 7: Augite dacite tuff, #124, 159.5 m. (This paper), 8: Augite andesite tuff, #124, 162.4 m. (This paper), 9: Augite andesite, #124, 178.0 m. (This paper), 10: Augite andesite tuff, #124, 201.8 m. (This paper), 11: Augite andesite tuff, #124, 211.1, m. (This paper), 12. Hornblende dacite tuff, #124, 222.8 m. (This paper), 13: Augite andesite, #124, 259.9 m. (This paper), 14: Augite andesite, #124, 291.5 m. (This paper), 15: Augite andesite, #124, 334.7 m. (This paper)

Plagioclase phenocryst fragments are also partly replaced by wairakite, sodic plagioclase, illite, quartz and calcite along their cleavage planes. Corroded large fragments of quartz phenocrysts are abundant. The tuffaceous matrix and groundmass have been strongly silicified and replaced by quartz and wairakite with subordinate amounts of calcite, chloritic clay, epidote, leucoxene, gypsum and pyrite. Some pyrite crystals have been oxidized to form a hematite rim. Many amygdules and veins are filled with quartz, sodic plagioclase and wairakite. An alunite vein of 0.1-0.3 mm thick is also found. This rock contains very high SiO_2 and low Al_2O_3, MgO, CaO, Na_2O and K_2O.

No. 7, Augite dacite tuff (#124, 159.5 m): Most of the primary phases of this rock are well preserved. Some augite phenocryst fragments have been partially replaced by a pale green-pale brownish green chlorite/smectite with minor amounts of epidote, calcite and leucoxene. Neither relics nor pseudomorphs after hornblende phenocrysts have been identified. Most plagioclase fragments remain fresh, while some have been partly replaced by prehnite, epidote, quartz, calcite and sodic plagioclase. Quartz fragments are irregular in shape and no overgrowth or recrystallization was found.

The groundmass, fine-grained tuffaceous matrix and tiny lithic fragments are composed of small crystals of augite, plagioclase, magnetite, quartz and volcanic glass. They have been strongly altered to the assemblage of laumontite, epidote, quartz, calcite, chlorite/smectite, prehnite and sodic plagioclase.

Some amygdules 0.3-1.3 mm in diameter are filled with quartz-laumontite, quartz-laumontite-chlorite/smectite and quartz-laumontite-prehnite-chlorite/smectite assemblages. Judged from textural relations, prehnite, laumontite and epidote seem to be stably associated in this rock.

No. 8, Augite andesite tuff (#124, 162.4 m): Augite phenocryst fragments have been extensively replaced by pale green chlorite/smectite and calcite with minor amounts of leucoxene and epidote. However, plagioclase and lithic fragments generally remain fresh and have been only partly replaced by sodic plagioclase and prehnite along cleavage planes.

The groundmass and tuffaceous matrix have been strongly altered to the assemblage of quartz, pale green chlorite/smectite, calcite, sodic plagioclase, epidote, leucoxene, wairakite and pyrite with minor amounts of prehnite. Amygdules are round in shape and filled with chlorite/smectite, wairakite and quartz.

Although X-ray diffraction patterns of the light fraction separated from rock powder by suspension indicate the presence of small amounts of thomsonite and dachiardite, their occurrence could not be confirmed by microscope.

No. 9, Augite andesite (#124, 178.0 m): The rock is porphyritic in texture with augite, plagioclase and magnetite as the main phenocryst minerals. It is a typical fresh augite andesite. Only glassy groundmass has been weakly replaced by quartz, brownish green smectite, leucoxene and kaolinite, and augites by brown smectite along crystal margins or cleavage planes.

No. 10, Augite andesite tuff (#124, 201.8 m): Augite fragments have been almost entirely replaced by pale green chlorite/smectite, leucoxene, epidote and calcite. Plagioclase fragments have also suffered alteration to sodic plagioclase, epidote, calcite, prehnite, quartz and wairakite. An unaltered plagioclase grain shows a distinct calcic core of An 88 and a sodic rim of An 32 (Table 22). The groundmass, tuffaceous matrix and fine-grained lithic fragments were strongly altered into an assemblage of quartz, calcite, wairakite, chlorite/smectite, prehnite, epidote, pyrite and sodic plagioclase.

Small vesicles 0.4 mm in diameter are filled with quartz, laumontite and pale brownish green chlorite/smectite. Bulk rock X-ray diffraction analysis indicates that NaCl is an alteration mineral in this specimen.

Vein minerals are chiefly calcite, quartz, wairakite, prehnite and chlorite/smectite; no laumontite was found. However, some of these veins clearly cut the tuffaceous matrix which has been replaced by a laumontite-bearing assemblage.

No. 11, Augite andesite tuff (#124, 211.1 m): Augite, plagioclase and coarse-grained lithic fragments have been almost completely replaced by pale

green chlorite/smectite, wairakite, prehnite, quartz, and sodic plagioclase with subordinate amounts of calcite, epidote, pyrite, gypsum and leucoxene. Similar assemblages have also replaced the glassy groundmass of volcanic fragments and fine-grained tuffaceous matrix. Microscopic observation indicates the following mineral associations are stable in this specimen: (1) chlorite/smectite + prehnite + wairakite + quartz: and (2) chlorite/smectite + sodic plagioclase + prehnite + quartz.

Epidotes in this specimen are generally brownish pistacite-rich fine-grained crystals with irregular form. The epidotes may not be stably associated with prehnite and wairakite but are relics from the replacement by prehnite and wairakite.

X-ray diffraction analysis of the light fraction separated from rock powder by a suspension method indicates the presence of yugawaralite in this specimen. Microscopic observation, however, could not positively confirm its occurrence.

No. 12, Hornblende dacite tuff (#124, 222.8 m): Fragments of mafic phenocrysts, probably of hornblende, have been completely replaced by pale green chlorite/smectite and leucoxene. Plagioclase fragments are altered to the assemblage of quartz, wairakite, sodic plagioclase, calcite and illitic clay. Relict plagioclase was analyzed and has An 39 composition (Table 22). Tuffaceous matrix has been wholly replaced by the assemblage of quartz, illitic clay, chloritic clay, sodic plagioclase, wairakite, gypsum, and calcite with minor amounts of epidote and pyrite. Idiomorphic epidote crystals are stably associated with quartz, sodic plagioclase, wairakite, illite and chlorite. Irregularly shaped cavities are filled with quartz-wairakite, quartz-wairakite-chlorite/smectite, wairakite-calcite and epidote-quartz-chlorite/smectite.

No. 13, Augite andesite (#124, 259.9 m): The original mafic phenocrysts may have contained both augite and hypersthene but they have been completely replaced by pale green chlorite/smectite, leucoxene and calcite. Plagioclase phenocrysts are also altered to a wairakite-sodic plagioclase assemblage particularly along crystal margins

Table 22. Chemical analyses of primary plagioclases in drill hole core samples from the Onikobe geothermal area.

Sample No.	124 - 165.6m	124 - 201.8m Core	124 - 201.8m Rim	124 - 222.8m	124 - 259.9m	124 - 288.6m Core	124 - 288.6m Rim	124 - 334.7m
SiO_2	51.50 - 48.59	46.41 - 60.00		58.98	61.16 - 58.90	50.90 - 48.80		49.93
Al_2O_3	30.15 - 32.03	34.62 - 26.40		26.91	26.32 - 26.51	29.71 - 31.43		31.25
Fe_2O_3*	0.97 - 0.88	0.74 - 0.18				1.25 - 0.83		0.98
MgO								
CaO	13.45 - 14.75	17.86 - 6.70		8.03	6.23 - 8.29	13.94 - 15.46		15.20
K_2O	0.18 - 0.09	0.08 - 0.13		0.15	0.85 - 0.60	0.12 - 0.13		0.10
Na_2O	3.69 - 3.32	1.37 - 7.24		6.99	7.65 - 6.60	3.52 - 2.71		2.90
Total	99.94 - 99.66	101.06 - 100.65		101.08	102.22 - 100.90	99.45 - 99.35		100.35
An	67 71	88	32	39	31 41	69	76	74

Sample No.	127 - 154.6m	127 - 298.5m	127 - 409.7	123 - 309.5m	123 - 344.6m
SiO_2	52.96 - 46.36	54.07 - 46.83	51.76 - 43.94	52.24 - 54.12	53.40 - 45.37
Al_2O_3	29.51 - 33.40	27.74 - 32.66	29.20 - 33.66	28.53 - 28.10	27.00 - 31.60
Fe_2O_3*	0.40 - 0.77	0.69 - 0.71	0.69 - 0.58	0.89 - 0.80	0.46 - 0.80
MgO	0.01 - 0.03	0.06 - 0.04	0.04 - 0.04	0.07 - 0.47	0.00 - 0.10
CaO	12.70 - 17.75	11.11 - 16.41	11.85 - 18.49	12.83 - 14.31	11.70 - 17.17
K_2O	0.09 - 0.05	0.83 - 0.06	0.23 - 0.03	0.62 - 0.08	0.10 - 0.06
Na_2O	4.18 - 1.39	4.54 - 2.13	4.50 - 0.83	3.60 - 3.21	4.77 - 1.56
Total	99.85 - 99.75	99.04 - 98.84	98.27 - 97.57	98.78 - 101.09	97.43 - 96.66
An	63 87	55 81	58 92	67 72	58 85

*Total Fe as Fe_2O_3

Table 23. Chemical analyses of clinopyroxenes in drill hole core samples from the Onikobe geothermal area.

Sample No.	124 - 165.6m	124 - 254.4m	124 - 307.5m	124 - 334.7m	124 - 349.4m	123 - 303.5m
SiO_2	53.00	52.30 - 51.79	51.81 - 51.43	51.56 - 52.14	50.90 - 50.70	50.90
TiO_2	0.50			0.51 - 0.33		
Al_2O_3	2.78	1.60 - 2.14	1.99 - 2.22	2.36 - 2.05	3.04 - 3.73	2.91
FeO*	9.39	9.92 - 12.05	10.90 - 12.17	11.40 - 12.14	10.63 - 11.29	11.93
MgO	15.25	14.71 - 14.32	14.94 - 14.62	14.39 - 14.46	14.80 - 14.15	15.07
CaO	19.96	20.54 - 19.10	19.44 - 18.60	19.83 - 19.36	19.50 - 19.55	19.30
Na_2O	0.32	0.34 - 0.29	0.27 - 0.26	0.19 - 0.23	0.25 - 0.25	0.26
Total	101.20	99.41 - 99.69	99.35 - 99.30	100.24 - 100.71	99.12 - 99.67	100.37
En	42.8	42.0 - 41.2	42.7 - 42.0	41.1 - 41.1	42.6 - 41.0	42.3
Fs	14.8	15.9 - 19.4	17.5 - 19.6	18.2 - 19.4	17.1 - 18.3	18.8
Wo	42.4	42.1 - 39.4	39.9 - 38.4	40.7 - 39.5	40.3 - 40.7	38.9

*Total Fe as FeO

and cleavage planes; some plagioclase phenocrysts have An 31-41 composition (Table 22). The groundmass has been wholly replaced by quartz, wairakite, epidote, sodic plagioclase, and illitic clay, with minor amounts of gypsum, pyrite, leucoxene and calcite. Idiomorphic epidote crystals with light yellowish green-reddish interferen color must be high in pistacite molecules.

Veins are chiefly composed of quartz and wairakite with subordinate amounts of calcite.

No. 14, Augite andesite (#124, 291.5 m): This is a relatively unaltered andesite with abundant relicts of augite and plagioclase phenocrysts. Some tabular pseudopmorphs composed of brownish green or brown smectite and leucoxene are found after hypersthene or hornblende phenocrysts. Augite phenocrysts have suffered partial alteration into brownish green smectite along their crystal margins or cleavage planes.

The groundmass has been entirely replaced by mordenite-quartz-smectite with minor gypsum and kaolinite. Round amygdules are chiefly composed of mordenite-quartz-smectite. No pyrite was found. Magnetite crystals are oxidized into hematite along their crystal margins.

No. 15, Augite andesite (#124, 334.7 m): Most of the augite phenocrysts have been replaced by pale green chlorite/smectite and leucoxene with minor calcite: unaltered augite phenocrysts have a composition of $En_{41}Fs_{19}Wo_{40}$ with about 2.4 wt% Al_2O_3 and 0.3-0.5 wt% TiO_2 (Table 23). The hydrothermal alteration of plagioclase phenocrysts is weak; only a minor replacement by wairakite, quartz and sodic plagioclase along their cleavage planes has occurred. Some of the unaltered plagioclase phenocrysts are as calcic as An 74 (Table 22). The groundmass has been totally replaced by the assemblage wairakite, sodic plagioclase, pyrite, calcite, chlorite/smectite, pistacitic epidote and minor gypsum and leucoxene.

Veins 1.7-1.9 mm thickness are composed of quartz, wairakite, calcite and prehnite.

No. 16, Dacite tuff (#124, 288.6m): This pyroclastic rock contains abundant chloritic pseudomorphs after augite and hypersthene (?) (or hornblende) phenocrysts.

In some of these pseudomorphs, relict augites were found. Plagioclase phenocrysts of An 69-76 (Table 22) are only partly replaced by wairakite along cleavages and fractures. The tuffaceous matrix has been wholly replaced by wairakite, pale green chloritic clay, pyrite and a small amount of fine-grained crystals of Fe-rich epidote. Amygdules and veins are chiefly composed of wairakite and quartz.

No. 17, Andesite tuff (#127, 154.6m): Zoned plagioclase (An 63-87)(Table 22) and augite phenocrysts in this tuffaceous rock have been partly altered to laumontite ± calcite and calcite + chlorite + leucoxene respectively. The tuffaceous matrix is extensively replaced by the assemblage calcite, cristobalite, quartz, clay mineral, laumontite and pyrite. The occurrence of cristobalite is most characteristic and this is the only sample which contains cristobalite in drill hole #127 .

No. 18, Andesite tuff (#127,155.4m): Phenocrysts of mafic minerals, probably augite and hypersthene, have completely altered into aggregates of pale green clay mineral and leucoxene. Plagioclase phenocrysts have only suffered partial replacement along cracks by laumontite, clay mineral, calcite and leucoxene. Pyrite has formed along magnetite crystal margins. Vesicles and irregularly shaped veins 0.3-0.6 mm thick are chiefly composed of quartz, calcite, and wairakite with minor amounts of clay mineral.

No. 19, Andesite tuff (#127, 297.5m): Both plagioclase and mafic pyroxene phenocrysts have been completely replaced by prehnite + sodic plagioclase + wairakite, and pale green chloritic clay + leucoxene assemblages respectively. The tuffaceous matrix and lenticular glass shards are also wholly altered to aggregates of prehnite, sodic plagioclase, wairakite, chloritic clay, anhydrite, pyrite and minor amounts of calcite.

No. 20, Andesite tuff (#127, 409.7m): Partial replacement of plagioclase phenocrysts by calcite, wairakite, illite and sodic plagioclase has occurred along cleavages and cracks. This rock contains the most calcic plagioclase (An 92)(Table 22) among the analyzed samples. Pyroxene phenocrysts have been completely replaced by a calcite-pale green chloritic clay-leucoxene assemblage. The fine-grained glassy matrix has suffered strong silicification and has been altered into the assemblage of

quartz, calcite, wairakite, sodic plagioclase, pyrite and clay minerals (chlorite/smectite interstratified mineral and illitic mineral). X-ray diffraction analysis indicates the presence of gypsum.

No. 21,22, Andesite tuff (#127, 577.2m and 578.1m): These two tuffaceous rocks are very similar and contain abundant wairakite in veins and as replacements after plagioclase and glassy matrix. Irregular veins of wairakite + sodic plagioclase within plagioclase phenocrysts are well developed. Mafic phenocrysts, probably augite and hypersthene, have been completely replaced by green to pale green chloritic clay and minor amounts of leucoxene. Veins chiefly composed of wairakite with a rim of chloritic clay cut through the tuffaceous matrix which has been almost completely replaced by wairakite, sodic plagioclase, chloritic clay, and pyrite with minor calcite. The X-ray powder pattern and microscopic observation indicate the presence of adularia as a hydrothermal mineral in this sample.

No. 23,24,25, Dacite tuff (#127, 702.9m, 703.1m and 703.9m): These three dacitic tuff core samples are very similar. They contain phenocrysts of corroded quartz, plagioclase, pyroxene and/or hornblende. Plagioclase phenocrysts have suffered partial replacement by calcite, sodic plagioclase, wairakite, and some illitic clay along cleavages and cracks. Mafic phenocrysts have been completely decomposed into a green chloritic clay-calcite-leucoxene assemblage. The tuffaceous matrix has been replaced by chloritic clay, calcite, sodic plagioclase, illitic clay, quartz, and pyrite with Fe-rich epidote. Veins and fractures are not common except in sample 703.1m in which quartz-wairakite and calcite are well developed in some vesicles and veins.

No. 26, 27, Dacite tuff (#127, 1010.6m and 1011.3m): These two core samples have identical petrographic features. Phenocrysts of a mafic mineral (probably pyroxene or hornblende) and plagioclase have been completely replaced by chloritic clay + calcite + epidote + leucoxene and sodic plagioclase + calcite + illitic clay, respectively. The tuffaceous matrix including glass shards has also suffered total replacement by chloritic and illitic clay, calcite, sodic plagioclase and pyrite. Calcite and quartz-calcite veins are common and no wairakite was found in these samples.

No. 28, 29, Dacite tuff (#127, 1103.6m and 1104.0m): These two samples are similar except for the absence of wairakite in the latter. Plagioclase phenocrysts have been completely replaced by sodic plagioclase, wairakite and illitic clay. The mafic minerals, probably hypersthene or hornblende, have also suffered total hydrothermal alteration to a chloritic clay, calcite and leucoxene assemblage. The hydrothermal alteration, including silicification, of the tuffaceous matrix into the assemblage of quartz, sodic plagioclase, illitic and chloritic clay, epidote, pyrite and leucoxene is distinct.

No. 30, 31, Dacite tuff (#127, 1104m and 1105.5m): Plagioclase phenocrysts in these two samples have been partly altered into a sodic plagioclase + wairakite + calcite assemblage with a minor amount of illitic clay along cracks or cleavages. Mafic phenocrysts, probably augite and hypersthene, are pseudomorphed by pale green chloritic clay + calcite + leucoxene. The tuffaceous matrix has been wholly replaced by quartz, calcite, wairakite, illitic clay, chloritic clay, sodic plagioclase, Fe-rich epidote and pyrite. Many vesicles of irregular shape in the original tuff are filled with the wairakite-quartz-calcite assemblage with a thin chloritic clay coating. Sample 1105.5m contains much less wairakite and much more illitic clay than sample 1104.4m.

CHEMICAL COMPOSITIONS OF SOME REPRESENTATIVE CORE SAMPLES

Chemical compositions of 15 selected core samples are listed in Table 21 together with their modal mineral compositions. As described in the previous sections, all these rocks have been extensively altered due to their interactions with geothermal waters. Secondary phases constitute more than half of the modal compositions; some of them contain even up to 93-96% secondary phases. Of course, in Table 21, all quartz contents are listed as secondary phase and in fact, some of them could be primary. Therefore, chemical compositions of the analyzed rocks cannot be considered reliably representative of the original rocks. The extensive chemical modifications during hydrothermal alteration are shown by (1) extremely high H_2O, Fe_2O_3 and S contents,

(2) high Fe_2O_3/FeO ratio, (3) low total $Na_2O + K_2O$ content, (4) variable SiO_2, MgO and total Fe as FeO* and (5) no correlation between TiO_2 and FeO*/MgO ratio. Such chemical variations are shown in the $(K_2O + Na_2O)$-SiO_2 plot of Figure 16, in the SiO_2-FeO*/MgO plot of Figure 17 and the $(Na_2O + K_2O)$-FeO*-MgO plot of Figure 18. To plot the compositions of these rocks onto these diagrams, all oxides were normalized to H_2O-free values.

According to Kuno (1950; 1959), all non-alkalic volcanic rocks of Japan can be differentiated into a hypersthene or pigeonite series. His hypersthene series is made up of rocks whose groundmass pyroxenes are both monoclinic and orthorhombic, or only orthorhombic, whereas his pigeonitic series is made up of rocks whose groundmass pyroxenes are only monoclinic (augite, ferroaugite and pigeonite). As an additional criterion, he used the occurrence of hornblende and biotite phenocrysts as being characteristic of his hypersthene series. Kuno (1959, 1968b) later regarded his hypersthene and pigeonitic series as representative of volcanic rocks of the calc-alkaline (CA) and tholeiitic (TH) series respectively. However, as pointed out by Miyashiro (1974) and others, such mineralogical and chemical correlations may not be always true. Miyashiro (1974) proposed the SiO_2-FeO*/MgO plot to differentiate CA and TH series as shown in Figure 17.

As described in the previous sections, all the andesitic and dacitic rocks from the Onikobe geothermal area contain hypersthene together with augite and hornblende as the most common mafic minerals, although they have been extensively replaced by chloritic clay. No pigeonite was found. Therefore, these rocks may belong to Kuno's hypersthene series and they may have chemical characteristics of the calc-alkaline series. According to Miyashiro (1974), the calc-alkali volcanic rocks (andesite and dacite) at a given FeO*/MgO ratio are higher in SiO_2, $Na_2O + K_2O$, and lower in FeO* contents than tholeiitic rocks. The TiO_2 content of the CA series decreases with an increase in the FeO*/MgO ratio. The compositions of the altered rocks from the Onikobe geothermal area vary significantly from their unaltered counterparts. As shown in Figures 16-18, significant leaching of SiO_2, MgO, $Na_2O + K_2O$, and oxidation of FeO must have occurred in some rocks during the hydrothermal alteration.

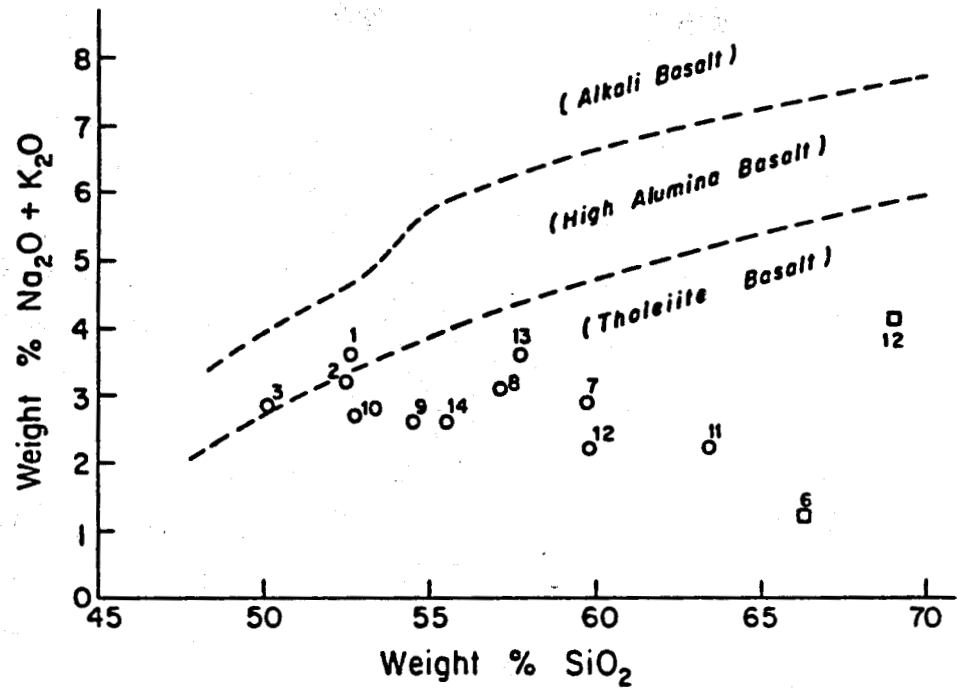

Figure 16. $(Na_2O + K_2O)$ - SiO_2 plot for selected drill hole core samples from the Onikobe geothermal area. Compositional fields for tholeiite basalt, high alumina basalt and alkali basalt are from Kuno (1966). Numbers refer to those samples in Table 21. Circles are andesitic rocks and squares are dacitic rocks.

Such chemical alteration varies from specimen to specimen. For instance, specimen No. 12 (#124-222.8m) may have gained a significant amount of SiO_2 during alteration. In contrast, a possible loss of SiO_2 in No. 5 and in Nos. 1, 2, and 10 may have occurred. Similarly, samples No. 3 and 4 contain too little MgO (hence too high FeO*/MgO) for any possible island arc volcanic rocks (see Miyashiro, 1974) and these two samples are not plotted in Figures 16-18. Apparently, significant leaching of MgO may have occurred during the hydrothermal alteration of these samples.

DISTRIBUTION OF SECONDARY MINERALS WITH DEPTH

Distributions of secondary minerals with depth for drill holes #P-5, P-7, P-8, P-10, GO-7, GO-8, GO-10, GO-11, 123, 124, 127 are listed in Tables 10 to 20. Two points should be mentioned about these tables: (1) the modal abundances of the secondary minerals were not determined and the tables simply show that given minerals

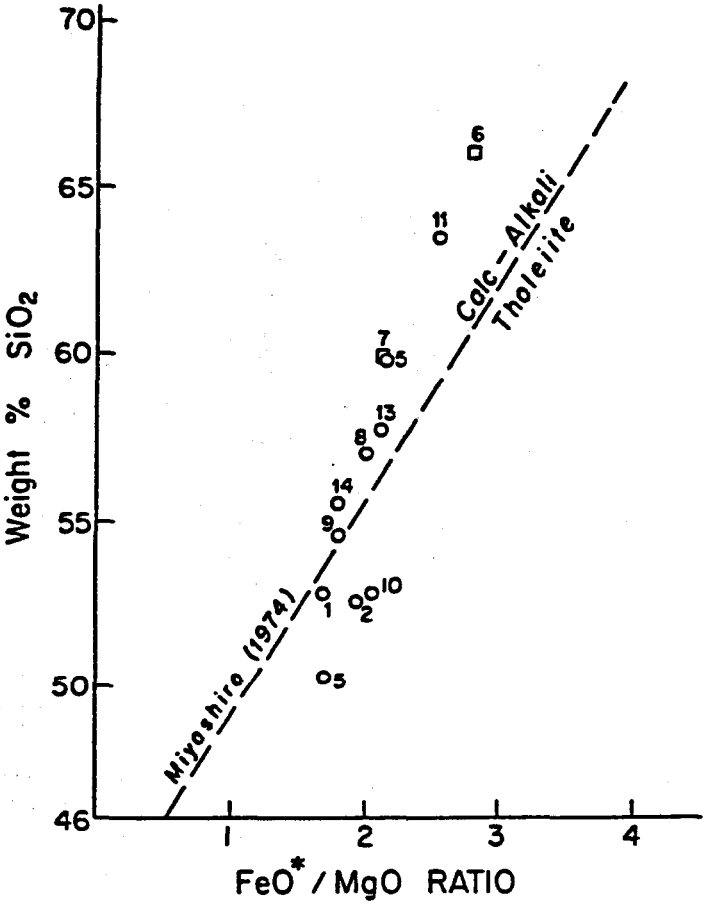

Figure 17. SiO_2 - FeO*/MgO plot for selected drill hole core samples from the Onikobe geothermal area. This diagram of Miyashiro (1974) was used to differentiate calc-alkali rocks from tholeiitic rocks. Numbers and symbols are the same as those of Figure 16.

are present in the core sample at certain depths; (2) the modes of occurrence of the secondary minerals in the pyroclastics and flows could be grouped into the following four types:

(a) Precipitation in vesicles (e.g., amygdaloidal mineral) and along fractures (e.g., vein mineral);

(b) Replacement of plagioclase phenocrysts and groundmass mostly along fractures and cleavages;

(c) Replacement of ferromagnesian minerals including hornblende, augite,

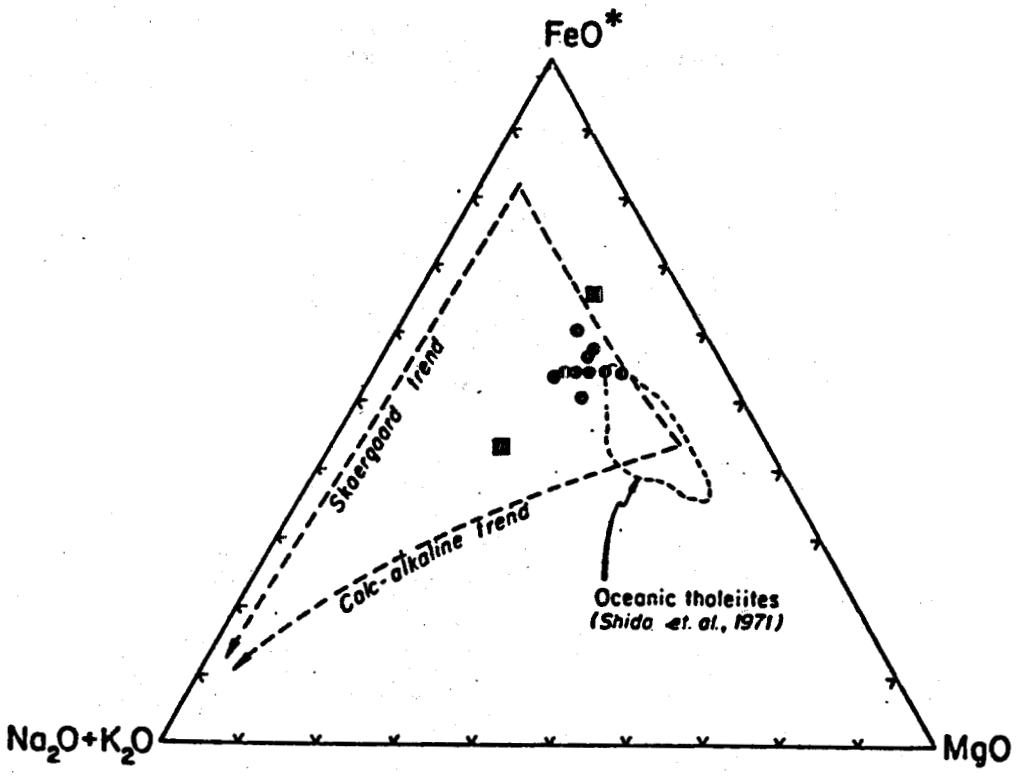

Figure 18. Compositions of selected drill hole core samples plotted onto the classical AFM diagram. Compositional field of oceanic tholeiites is from Shido et al. (1971). Closed circles are andesitic rocks and squares are dacitic rocks.

hypersthene and possibly olivine; and

(d) Replacement of volcanic glass.

Such differences in modes of occurrence were not differentiated in these tables. Therefore, a zonal distribution of secondary minerals in some drill holes is not apparent. Characteristic features for their distribution are briefly described for each bore-hole as follows:

P-5 (Table 10): Thirteen core samples were studied from this 179.6m deep pilot-hole. These samples are mainly andesitic tuff with two thin andesitic flows at 36.0m and 52.5m. Most samples are highly altered; quartz, smectite, carbonate, gypsum, and pyrite usually occur. Cristobalite was found only in samples from the

upper 36 meters along with minor secondary quartz. Kaolinite, illite and anhydrite sporadically occur in samples at shallow depth.

Native sulfur and NaCl were identified in a sample from 22.3m in depth. Three zeolite minerals occur in the drill hole core samples: mordenite at depths above 45.9m, laumontite at depths below 72.5m and dachiardite which mostly occurs as a vein mineral at depths between 36.0m and 72.5m. Poorly crystallized epidote was found in two deep samples. Smectite was widely formed above 148.0 m and chlorite/smectite interstratified minerals occur at greater depths.

P-7 (Table 11): Nineteen core samples were examined from this 250.0 m deep bore-hole. The rock types vary from andesitic to dacitic tuffs and flows, with the flows being volumetrically less important. Smectite or alkaline smectite is present to a depth of 130.8 m, with chlorite/smectite interstratified mineral then occurring to the bottom. Illitic clays occur at depths greater than 218.0 m. The zeolites exhibit a crude depth distribution, with mordenite and clinoptilolite occurring from 26.0 to 50.0 m, laumontite at 115.0 and 130.8 m, and wairakite from 115.0 to 170.0 m. Dachiardite is found between 26.0 and 150.0m, mostly as a vein-forming phase. Epidote occurs in every sample from 150.0 to 250.0 m. Cristobalite, alunite, and native sulfur are found in the upper few tens of meters. Carbonate, gypsum and pyrite are formed in most of the studied bore-hole cores. Sodic plagioclase, which was found in only two samples of dacitic nature, may not be a geothermal alteration product but of igneous origin. Adularia as an alteration mineral was found only in samples from 218.0 m.

P-8 (Table 12): Twenty-one core samples were examined from this 300.0 m deep bore-hole. The rock is predominantly andesite and andesitic tuff with two thin dacite and dacitic tuff layers. The phyllosilicates are approximately depth-zoned; kaolinite and smectite or alkaline smectite occur in the upper 150 meters, and illite and chlorite/smectite interstratified mineral occur in the lower part of the hole. Seven different zeolites are found in this hole: major

mordenite, laumontite, wairakite and dachiardite and minor yugawaralite, chabazite and thomsonite. The mordenite, laumontite, yugawaralite and wairakite show a succession with increasing depth, while dachiardite is present through most of the core. As far as observed in thin sections, dachiardite, thomsonite and chabazite occur only as vein minerals . Epidote occurs in most samples from below 95.0 m depth. Secondary albite is found in all five samples from below 180.0 m. Actinolite occurs in the 300.0 m sample which contains the alteration assemblage of actinolite + epidote + albite + chlorite + quartz + pyrite.

P-10 (Table 13): Twenty-three core samples were studied from this 203.0 m deep drill-hole. The rock is predominantly andesite and andesitic tuff with subordinate dacite and dacitic tuff. Smectite is the dominant phyllosilicate mineral throughout the core; no chlorite/smectite interstratified mineral occurs. Kaolinite and native sulfur are found at 25.0 m, and illite occurs at 132.0 and 133.35 m. Mordenite was found in core samples from deeper than 161.05 m and occurs as cavity fillings and as an interstitial phase in laumontite- or wairakite-bearing altered rocks. Most of the dachiardite, chabazite and thomsonite are found in veins. A rough depth zonation from mordenite-clinoptilolite to wairakite through laumontite and yugawaralite can be seen. Epidote occurs consistently at depths greater than 125.0 m. Carbonate, pyrite and gypsum are very common in the core specimens. No albitic plagioclase was found, even in wairakite-bearing rock.

GO-7 (Table 14): Thirty-five core samples were examined from this 500.0 m deep drill hole. The rock is predominantly andesite and andesitic tuff with minor dacitic tuff. A distinct alkaline smectite-smectite through chlorite/smectite interstratified mineral to chlorite zoning with depth is noticeable. Smectite, chlorite/smectite interstratified mineral and chloritic clay are observed at 15.0-175.0 m, 201.0 m and 243.0-423.4 m respectively, although the rock at 450.6 m contains chlorite/smectite interstratified mineral + wairakite. An equally well-developed mordenite through laumontite to wairakite

zoning with depth is also observed. Mordenite, laumontite and wairakite occur at depths at 15.0-147.0 m, 36.0-175.0 m and 201.1-500.0 m respectively. Only one sample has dachiardite as a vein mineral. Albite occurs in many samples below depths of 201.1 m and epidote is found starting at a depth of 263.0 m. Prehnite occurs at 377.5 and 398.6 m. Carbonate, pyrite and gypsum are widely found.

GO-8 (Table 15): Fifty-one samples were studied from this 998.3 m deep drill-hole. The rock consists of subequal amounts of andesite, andesitic tuff, dacite, and dacitic tuff. Smectite and alkaline smectite occur to a depth of 199.2 m, and chlorite/smectite interstratified mineral is found from 147.0 to 998.3 m. Chloritic clay is found at depths greater than 250.0 m. A progression of mordenite through laumontite to wairakite with depth is observed; mordenite, laumontite and wairakite are found at 25.0-50.5 m, 50.5 m-350.5 m and 126.5-998.3 m respectively. Albite, illite and epidote occur in most samples below 147.0 m, and prehnite is observed in four samples between 701.5 and 869.2 m depth. Actinolite associated with albite, epidote, prehnite, quartz, wairakite and chlorite was identified at 869.2 m. Pyrite occurs in all studied samples and chalcopyrite was found in the deepest sample at 998.3 m. Cristobalite occurs in only two samples in the shallowest part. The occurrence of carbonate in bore-hole cores collected at depths greater than 650 m is rather rare and pyrophyllite occurs in most samples below about 850 m. This fact must indicate the presence of neutral-alkaline thermal water and acid thermal water at relatively shallower and deeper levels of this well respectively.

GO-10 (Table 16): Thirty-two samples were examined from this 1330.0 m deep bore-hole. Approximately sixty percent of the samples are andesite with the remaining forty percent being dacite and dacitic tuff. Smectite is present in four samples above 302.0 m, chlorite/smectite interstratified mineral occurs from 155.0 to 1330.0 m, and illite is present in most samples from 655.0 to 1330.0 m. Most of the chlorite/smectite interstratified clays in rocks deeper than 330.0 m

are chloritic. Pyrophyllite occurs in most samples below 800.0 m, and biotite is present at 1330.0 m. Laumontite, yugawaralite, and wairakite display the typical zeolite zonation pattern with depth observed in many of the other cores. Albite and epidote occur sporadically at depths greater than 204.0 m, and actinolite is present in two samples at 700.0 and 1330.0 m. The 1330.0 m sample is chiefly composed of quartz, pyrophyllite, chlorite, illite, actinolite, biotite, and albite with minor amounts of wairakite and gypsum. Pyrite is found in most of the studied rocks. It must be noted that no carbonate was found in rocks deeper than 800.0 m where pyrophyllite is widely formed. Acid thermal water must also predominate at depths greater than 800 m.

GO-11 (Table 17): Thirty-one samples from this 1300.0 m deep bore-hole were studied. The rock is dominantly dacitic tuff with minor dacite, andesite, and andesitic tuff. Smectite and alkaline smectite occur from 50.0 to 203.0 m, chlorite/smectite interstratified mineral occurs from 250.0 m to the bottom of the well, and illite commonly occurs intermittently at depths greater than 203.0 m. Most of the chlorite/smectite interstratified minerals in rocks deeper than 350.0 m are chloritic. Therefore, smectite, chlorite/smectite interstratified mineral and chloritic clay form a zonal distribution with the following order: 50.0-203.0 m smectite, 250.0-300.0 m chlorite/smectite interstratified mineral and 305.0-902.0 m chloritic clay, although the clay minerals formed at depths of 1205.0 m and 1300 m are chlorite/smectite interstratified minerals. Kaolinite is present sporadically from the top of the hole to 701.0 m, and pyrophyllite occurs in seven of eight samples between 900.0 and 1205.0 m. The only two zeolites observed in this well are laumontite and wairakite, the former occurring to a depth of 305.0 m, and the latter between 203.0 and 701.0 m. One very unusual feature about this well is that wairakite is not observed anywhere over the deepest 500.0 m interval where no carbonate was found and pyrophyllite is common. An analogous pattern is observed with epidote, where this mineral is nearly ubiquitous from 300.0 to 800.0 m, but is present in only two of nine samples below this depth. Prehnite occurs at 500.0 m. Actinolite has been

tentatively identified at 800.0 and 1004.0 m, as has pumpellyite at 1103.0 and 1300.0 m. In this drill hole, the presence of acid thermal water is also expected at the depths from 600 m to the bottom.

123 (Table 18): Fifty-two samples from this 353.0 m deep well were studied. The rock is primarily andesitic and dacitic tuff with minor andesite layers. The shallowest core samples available for this well begin at a depth of 158.9 m. Smectite occurs in only three samples, at 175.9, 184.7, and 187.6 m and chlorite/smectite interstratified mineral is commonly present in other samples throughout this well. Only three specimens among forty-two specimens from depths between 158.9 m and 333.3 m have chloritic clay. Probably, the boundary between chlorite/smectite interstratified mineral zone and chlorite zone is located at about 340 m and rocks at greater depths than 340 m are characterized by the occurrence of chlorite. Illite has been identified in most of the studied samples. Seven zeolites occur in the core: wairakite, laumontite, yugawaralite, dachiardite, natrolite, chabazite, and thomsonite. Of these, only wairakite is ubiquitous throughout the core. Dachiardite is present as a vein mineral in eight samples between 238.6 and 328.6 m. The other zeolites each occur in only a few samples. Epidote and albite are present in most of the samples throughout the drill hole. Prehnite occurs in only three samples. Adularia is present in six samples between 169.8 and 279.8 m.

124 (Table 19): Fifty-six samples were studied from 158.3 to 349.4 m depths in well # 124. The rock is composed of subequal andesite and andesitic and dacitic tuffs with only one thin dacite flow. Kaolinite and smectite are intermittently present between 165.6 and 200.3 m and occur in the sole mordenite-bearing sample at 291.5 m. Chlorite/smectite interstratified mineral is present in most samples throughout the bore hole; only three specimens at 214.5, 219.6 and 227.4 m depths have chloritic clay. Illite has been tentatively identified in some of the samples at depths below 193.4 m. Laumontite and dachiardite occur sporadically between 158.3 and 264.05 m, and wairakite is found

in many core samples from depths of 162.4 to 349.4 m (bottom). Trace amounts of yugawaralite are present in only one sample from 211.1 m and chabazite and thomsonite are found in some specimens filling network cracks. Carbonates, pyrite, albite and epidote are generally present throughout the core. Prehnite is limited to the 158.3 to 211.1 m interval and to the 334.7 to 344.6 m interval. Adularia occurs in six samples between 193.0 and 270.4 m.

127 (Table 20): Twenty-four samples have been examined from this 1105.5 m deep well. The upper half of the hole is primarily composed of andesitic tuff while the lower half is composed of dacitic tuff. Smectite is only present at 32.4 m. Chlorite/smectite interstratified mineral occurs in samples collected at depths between 154.6 m and 298.5 m. Chlorites are found between 296.1 m and 1105.5 m. Chlorite and chlorite/smectite interstratified mineral are associated in three specimens at 296.1, 297.5 and 298.5 m. Illite occurs in most samples at depths greater than 409.7 m. Clinoptilolite occurs at 32.4 m, laumontite at 155.4 and 296.1 m, and wairakite in most samples at depths greater than 155.4 m. Albite is present in most samples from 298.5 to 1105.5 m. Epidote occurs at depths greater than 702.9 m and prehnite only at 297.5 m. Gypsum is limited to the upper 411.5 m. Pyrite and carbonate are observed in almost all studied specimens. Calcite commonly occurs in this bore-hole even at depths greater than 1000m, except in specimens of 409.7-411.5m and 902.7m. The daily drilling records for this bore-hole indicate that distinct leakages of cooling water occurred at depths of 390-470m and 870-910m. Figure 6 also shows that the measured bottom-temperatures were extraordinarily low at 51 hours and 99 hours after the stop of the cooling water supply. High porosity rocks occurred at these two depths due to the decomposition of calcite by acid thermal waters.

SEM AND EDAX STUDY OF CORE SAMPLES FROM DRILL HOLE #127

Twenty-three 5 to 10 mm chips of core samples from 154.6 to 1105.5m depth in

the #127 drill hole were examined using scanning electron microscopy and semi-quantitative energy-dispersive analysis. This study of core #127 was carried out for the following reasons:

(1) to better understand the paragenetic sequence of minerals;

(2) to determine if a systematic difference in phyllosilicate morphology or paragenetic sequence occurred as a function of depth;

(3) to qualitatively determine the compositions of the fine-grained phyllosilicate; and

(4) to see if this type of study would result in the discovery of secondary phases too small to be observed using optical microscopy.

Figure 19 includes many scanning electron micrographs of chips from the #127 core samples. The areas shown in the photos are typical textures or, where cavities were present, free-growing secondary phases with distinct morphologies. Tentative identifications of minerals in these photos were based on morphologies, semi-quantitative energy-dispersive X-ray analysis on the SEM, and previous thin section and X-ray diffraction identifications. Each of the samples was first completely scanned at low power (100-200X), then representative areas were observed at medium power (500-1000X), and finally specific areas were examined at high power (2000-5000X). Approximately one hour was spent examining each chip on the SEM.

The following are short individual sample descriptions keyed to the Figure 19 micrographs:

<u>154.6m</u>: Two habits of phyllosilicates are tentatively identified in the two photomicrographs: large (10-30 micron wide by 2-3 micron thick) plates of a well-crystallized phyllosilicate, and a very fine (less than 1 micron) enmeshed web of a smectite-appearing material mixed with fine acicular crystals occurring as clumps among the large plates. The fine-grained acicular crystals are a Ca-Al-Si phase based on the EDAX data. They appear to be mordenite based on morphology and qualitative composition. Mordenite was not found in thin section by petrographic microscope. The two phyllosilicates both contain Ca, Fe, Si and

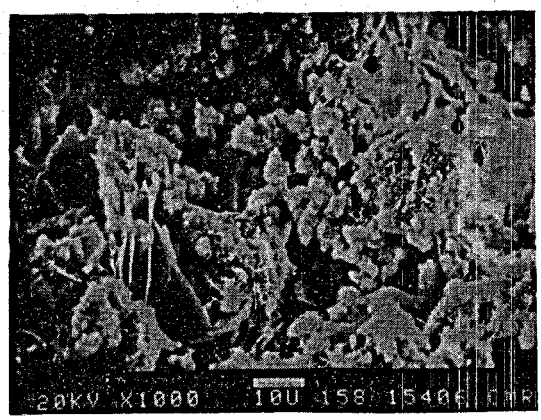

154.6m (a)

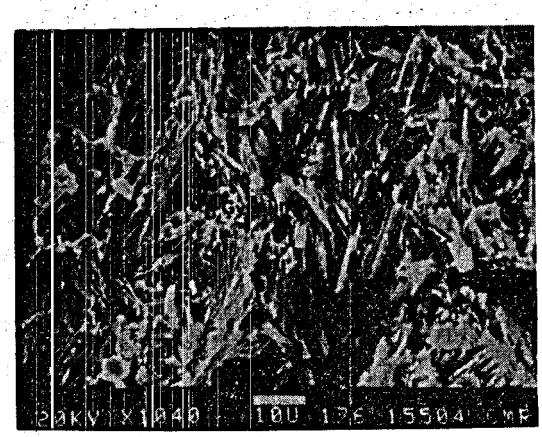

155.4m (a)

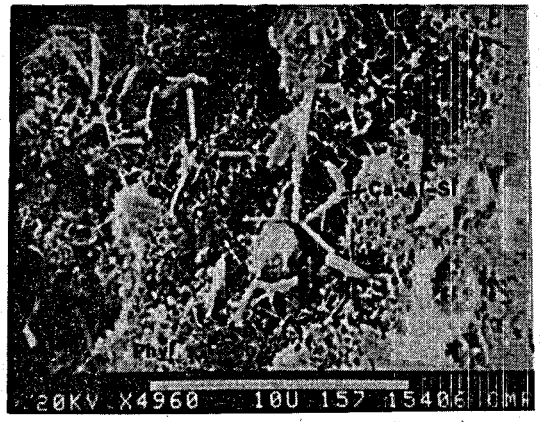

154.6m (b)

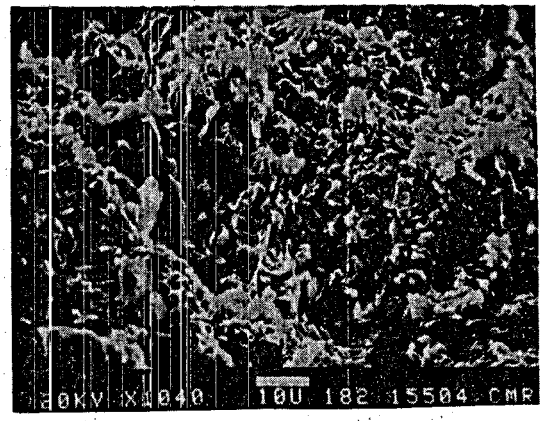

155.4m (b)

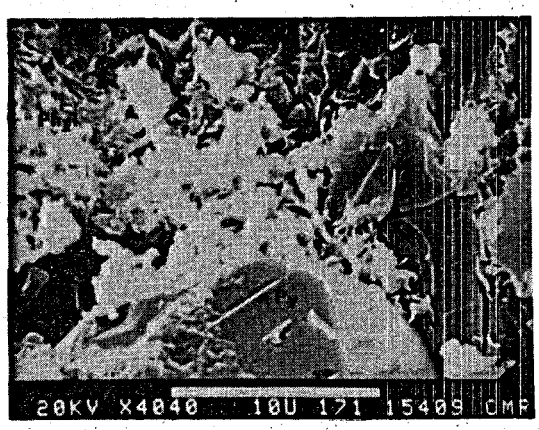

154.9m

155.4m (c)

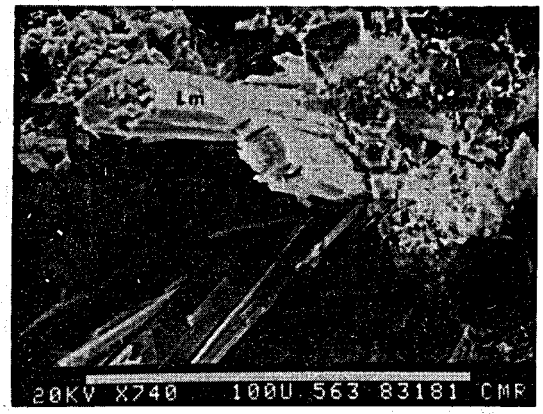

296.1m (a)

297.5m (b)

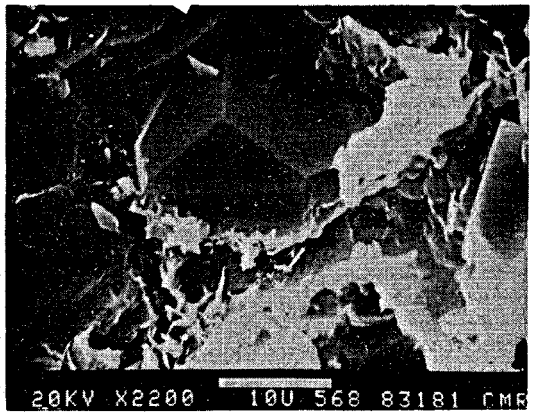

296.1m (b)

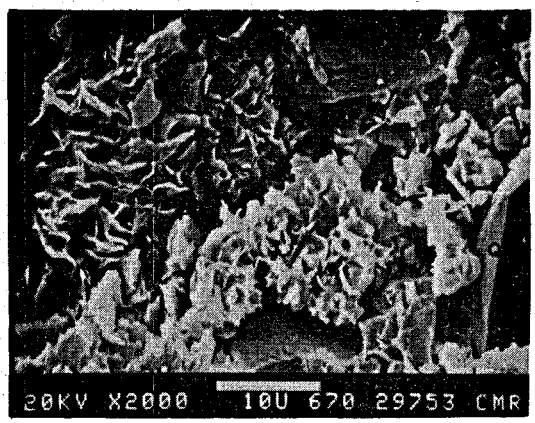

297.5m (c)

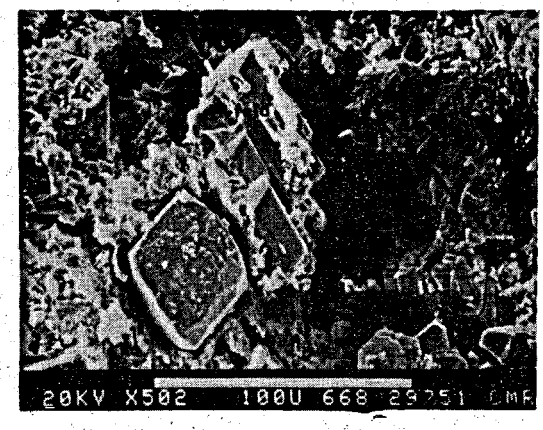

297.5m (a)

298.5m

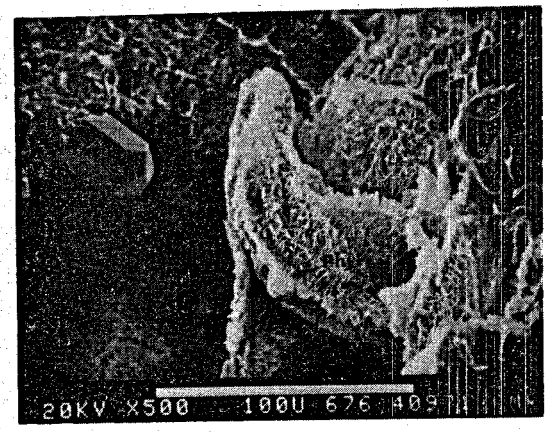

409.7m (a)

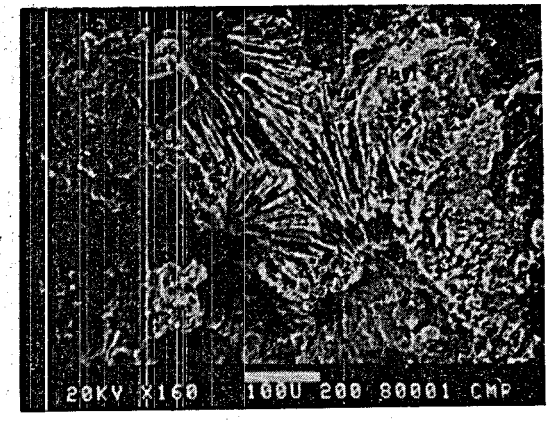

411.5m (b)

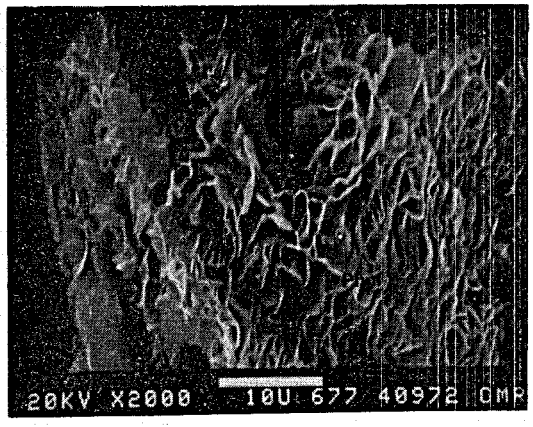

409.7m (b)

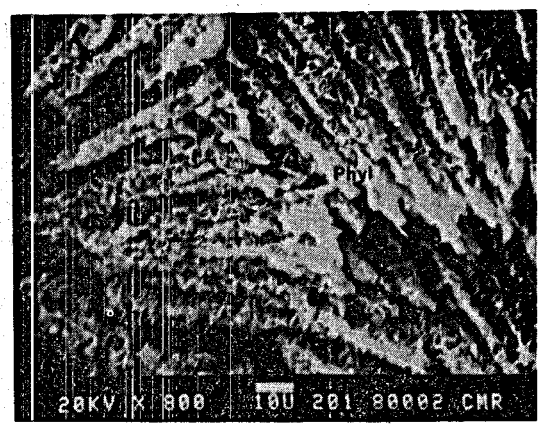

411.5m (c)

411.5m (a)

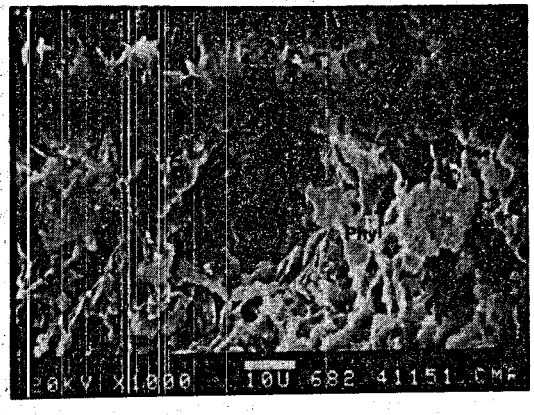

411.5m (d)

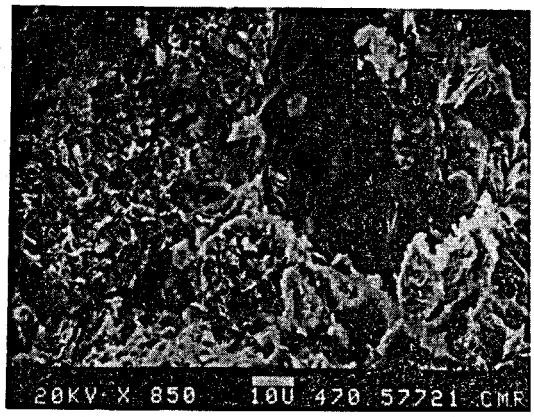

577.2m (a)

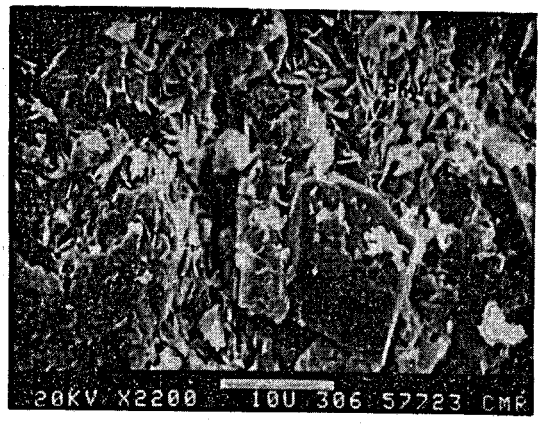

578.1m

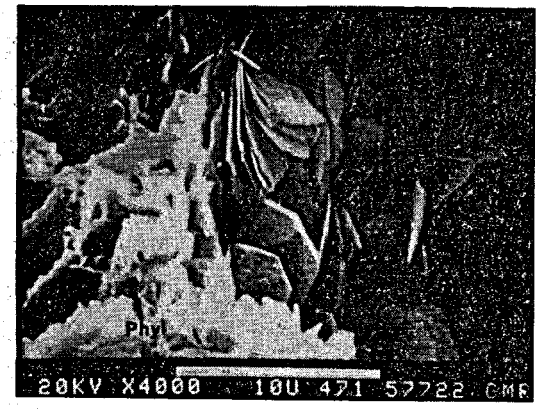

577.2m (b)

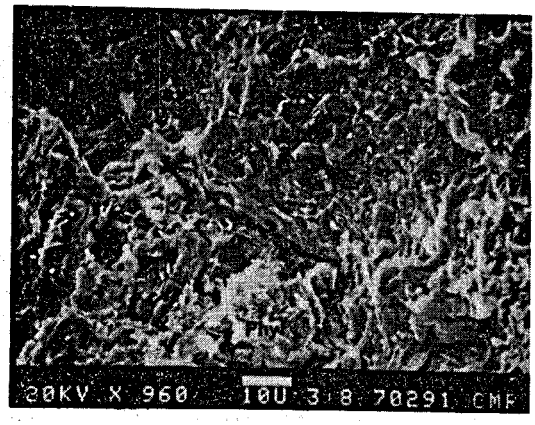

702.9m

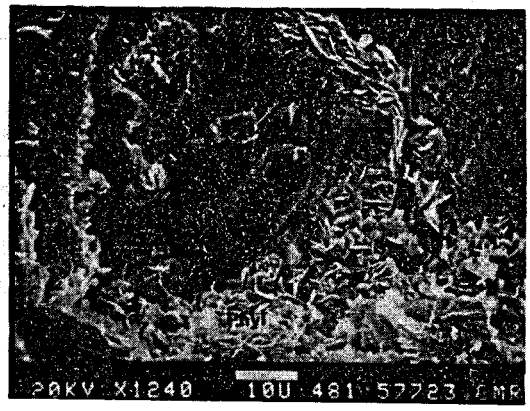

577.2m (c)

703.1m (a)

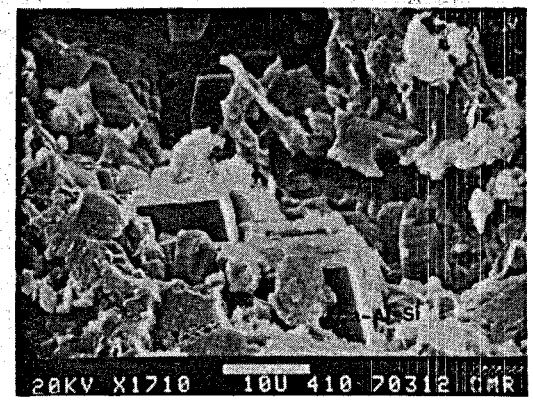

703.1m (b)

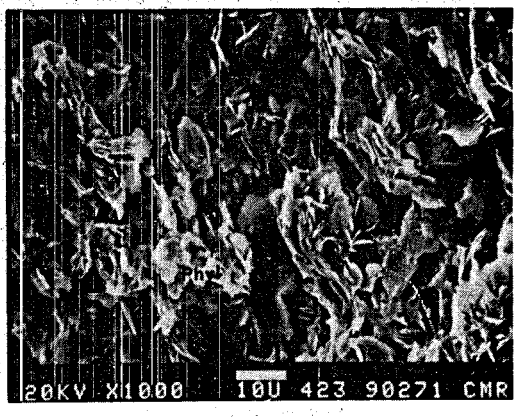

902.7m

703.9m

1011.3m

792.1m

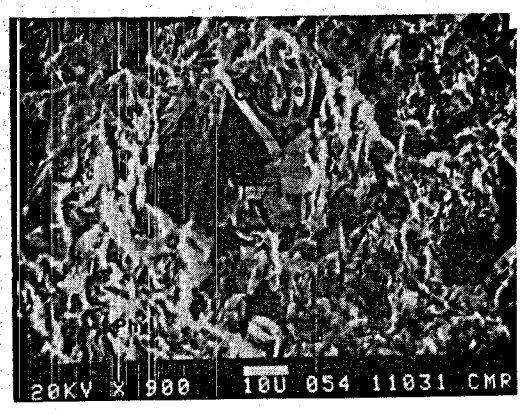

1103.6m

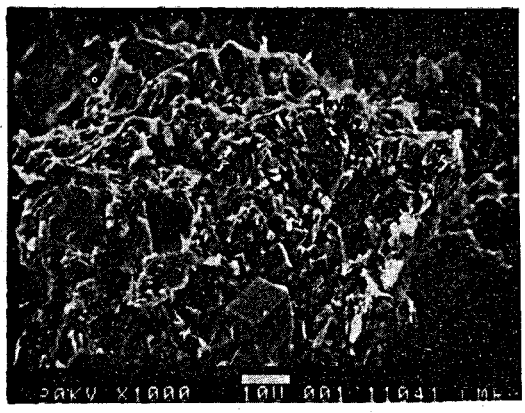

1104.0m (a)

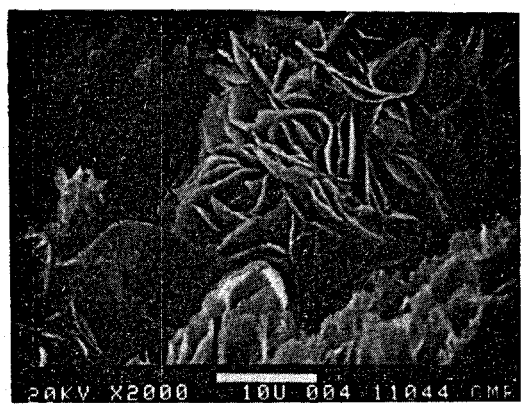

1104.0m (d)

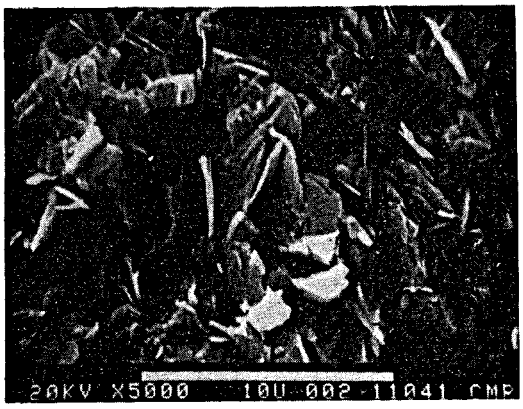

1104.0m (b)

1104.4m (a)

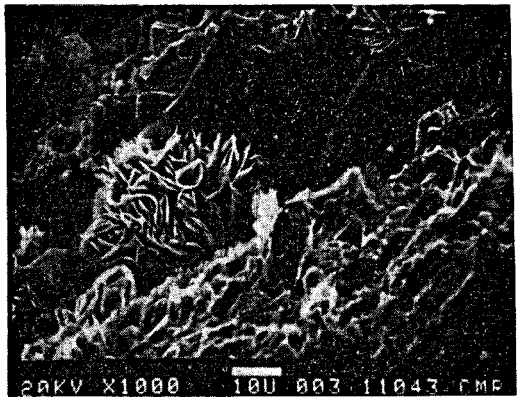

1104.0m (c)

1104.4m (b)

1105.5m (a)

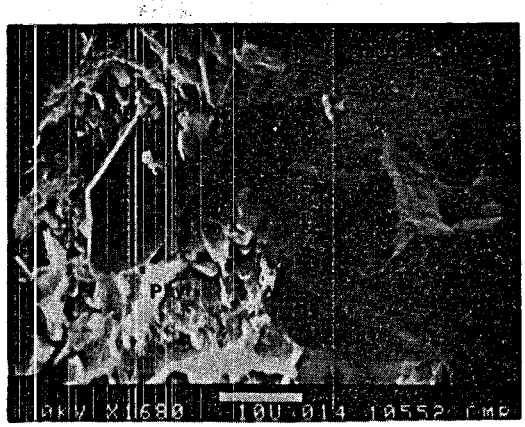

1105.5m (b)

Al.

154.9m: The phyllosilicates observed in this photomicrograph are generally uniformly coarser than in the previous sample. They also contain Ca, Fe, Si and Al. Minor acicular mordenite crystals were found. Coarse pyrite is abundant.

155.4m: Three photomicrographs are shown in Figure 19 for this sample. The phyllosilicate occurs as quite uniformly-shaped 2 to 10 micron plates clustered in the form of rosette-shaped aggregates. Gypsum can be seen in several areas on the grain.

296.1m: The minerals commonly observed in this sample are laumontite (possibly altering to leonhardite), wairakite, pyrite, and a phyllosilicate.

297.5m: In addition to quartz, phyllosilicate and pyrite, a K-Al-Si blocky, free-growing crystal is observed in one cavity. Although a K-zeolite cannot be completely eliminated, the morphology would favor its being K-feldspar, most likely adularia.

298.5m: In addition to the phases identified optically, several tapered acicular crystals are observed in cavities. EDAX indicates the major elements to be Ca, Mg, Fe, and Si. No absolute identification was possible for this phase, but low-Al amphibole is a possibility based on the morphology and the EDAX composition. Secondary amphibole was not identified by using X-ray and microscope methods and it is not common at shallow depths in geothermal drill holes.

409.7m: Coarse, lattice-like phyllosilicate occurs as a coating on matrix and apparently as a vein filler. Quartz and pyrite are ubiquitous.

411.5m: Coarse, divergent aggregates of plates are overgrown by finer phyllosilicates; pyrite is again abundant.

577.2m: Clusters of euhedral quartz crystals are very common in cavities. The phyllosilicate has much the same appearance as in the previous sample. The smaller quartz crystals intergrown with the phyllosilicate exhibit a distorted habit, being distinctly flattened parallel to the c axis.

578.1m: Phyllosilicate very similar to the last sample is observed. Pyrite

is also abundant; quartz is much less so.

702.9m: This sample is almost identical in appearance to the previous one.

703.1m: Coarse, euhedral calcite crystals are observed lining cavities; twinning striations are shown on some of the crystal faces. In addition to phyllosilicates, pyrite, calcite, and quartz, a blocky Ca-Al-Si crystal was found in one fracture. No positive identification could be made and it may be chabazite or yugawaralite.

703.9m, 704.3m (no photos), 704.9m (no photos), 792.1m, and 902.7m: These five samples are very similar in appearance. Medium-grained phyllosilicate curved aggregates are the only features seen on the surface of these chips.

1010.6m (no photos) and 1011.3m: Very fine-grained, poorly-shaped phyllosilicate is the only secondary phase observed.

1103.6m: Subhedral calcite crystals are observed in cavities. Phyllosilicates are coarser than those observed at 1011.3m.

1104.0m: Energy-dispersive analysis of some of the platy phyllosilicates in the first two photos (a,b) reveals major amounts of Al and Si but only minor amounts of other elements, suggesting that some of the platy crystals may be pyrophyllite. The very coarse rosettes in the next two photos (c,d) appear to show typical Mg-Fe-Al-Si analyses as in previous samples, indicating that they are interstratified chlorite. Calcite and a blocky Na-Al-Si phase, most likely albite, are also observed.

1104.4m: Abundant euhedral calcite crystals are visible along fractures. Distinct, well-shaped Fe-Mg-Al-Si phyllosilicates are visible intergrown with the calcites and also, apparently, on the surface of the calcites. These well-crystallized phyllosilicates could be chlorite.

1105.5m: Abundant euhedral quartz crystals and phyllosilicates are visible. EDAX indicates major Al and Si, substantial K and Fe, minor Na and Mg, and no Ca in the phyllosilicates, suggesting that they might be phengitic illites.

Concluding Remarks

Detailed examination of phyllosilicates in the core samples of drill hole #127 has yielded ambiguous results. Although a variety of phyllosilicates including smectite, alkaline smectite, interstratified chlorite, K-phyllosilicates and pyrophyllite were detected, positive identification of these phases is difficult. This is partly due to the similar morphology of all the phyllosilicates and partly due to very poor resolution of the EDAX qualitative analyses. Therefore, further SEM study of core samples from other drill holes was not continued. Several very uncommon phases are suggested to occur in the samples based on the morphology and the qualitative composition. This includes fine acicular mordenite in #154.6 and #154.9, adularia in #297.5, tremolitic amphibole (?) in #298.5, and chabazite (?) or yugawaralite (?) in #703.1 m.

PROCEDURES FOR ELECTRON MICROPROBE ANALYSES OF SECONDARY MINERALS

Electron microprobe analyses have been performed on polished thin sections from the #124 well by J.G. Liou and from the #123, #127, and #124 wells by Ray Guillemette. The #127 core samples were critically hand-chosen by Y. Seki and Ray Guillemette at Onikobe in August 1980. Only partial cores were available; and samples were chosen both at regular intervals in the available core and where changes in lithology or texture were discernible with a hand lens. The #123 and #124 core samples were similarly chosen for study by Y. Seki at earlier dates. Petrographic reconnaissance studies of polished thin sections were followed by detailed electron microprobe analyses of secondary phases observed in those thin sections. All of these analyses were designed to intermesh with the detailed petrographic and clay X-ray diffraction studies carried out by Y. Seki on another set of thin sections cut from samples collected from the same core intervals. Electron microprobe analyses were carried out both to obtain complete quantitative analyses of given minerals and to confirm tentative petrographic identifications. In the latter case, both semi-quantitative "real-time" counts and cathode-ray screen imaging techniques were used. The samples for microprobe study were prepared as standard polished thin sections at Stanford. After examination, the areas chosen for

study on each 1" by 2" slide were circled with permanent ink and photographed at 20 to 80X magnification. The photos were then marked to indicate the tentative mineral identificatons and the preferred areas for analysis. In a minority of the samples, hand-drawn sketches were used instead of photos as microprobe "maps". The preparation of the photos or diagrams was necessary in order to locate small grains for analysis under the microprobe's generally poor low-power transmitted and low and high-power reflected light optics. In addition, the exact area analyzed could be marked directly on the photos to allow the electron beam to be placed exactly on the same spot to continue the analysis. After the analyses were completed and examined, compositional patterns observed could be correlated with texture and paragenetic information by re-examining the sections petrographically. After initial examination and prior to microprobe analysis, each polished section was coated with a 125 to 175 Å thick conductive carbon film using a vacuum evaporator in order to prevent static charge build-up and beam deflection during analysis.

All of the microprobe analyses were carried out on a manual 3-channel ARL model EMX-SM microprobe at Stanford. A sample current of approximately 100nA set on a benitoite standard with an accelerating voltage of 15 kV was used for all of the analyses. A beam diameter of 20-25 microns was used whenever possible. When necessary due to a small grain size or grain inhomogeneity, a beam diameter as small as 1 to 2 microns was used. When this was done, care was exercised to see that the target area was not being destroyed. The raw counts were also especially observed as a function of time to ascertain that the diffusion of alkali metals away from the spot area was not occurring, resulting in falsely low sodium and potassium values. When this was observed in analyzing a narrow vein mineral, the sample stage was continually moved during the analysis, when possible, in order to keep the small beam on the mineral being analyzed but not always at the same spot, thus minimizing damaging heat buildup.

The ARL EMX-SM microprobe was capable of simultaneously analyzing for 3 elements. Thus, for a typical 8 or 9 element analysis, each of the spectrometers had to be manually driven to a new peak position an average of three times. This could be done in one of two ways: (1) the beam could be left on one area to be analyzed and the

Table 24A. Microprobe standards used for mineral analyses.

Mineral	Si	Ti	Al	Fe	Mn	Mg	Ca	Na	K
Albite, Plagioclase	Ab		Ab	Kb		Kaer	Kaer	Ab	Or
Pyroxene	Cp	R	Kaer	Cp		Cp	Cp	Ab	
Prehnite	Cp		Ab	Cp			Cp	Ab	Or
Epidote	Cp		Ab	Cp	Spess	Cp	Cp		
Wairakite, Laumontite, Yugawaralite	Ab		Ab	Kaer			Cp	Ab	Or
Phengitic Illites, Phyllosilicates	Kaer		Ab	Kaer	Spess	Kaer	Kaer	Ab	Or
Carbonates				Kaer	Spess	Cp	C		

Ab = albite; Or = Orthoclase; Kaer = Kaersutite; Cp = Clinopyroxene; Spess = Spessartine
C = Calcite; R = Rutile.

Table 24B. Chemical compositions of microprobe standards (wt.%)

	Albite	Orth.	Kaer.	Cpx.	Spess.	Calcite	Rutile
SiO_2	68.14	64.65	39.60	47.60	36.41		
TiO_2			4.97	1.55	1.08		100.00
Al_2O_3	19.77	17.04	13.36	9.38	20.59		
Fe_2O_3	0.01	1.87	17.38	2.78			
FeO				5.57	2.47	0.01	
MnO				0.19	40.31	0.01	
MgO			9.58	13.20		0.01	
CaO	0.38		10.07	18.70	0.62	56.03	
Na_2O	11.46	0.94	2.90	1.08			
K_2O	0.23	15.40	1.18				
CO_2						43.97	
TOTAL:	99.99	99.90	99.04	100.05	101.48	100.00	100.00

spectrometers driven to all peak positions before moving the sample to the next area; or (2) the three spectrometers could be left at one group of settings and all of the samples could be sequentially brought into analyzing position before the spectrometers were driven to new positions. At that time, the samples could again be sequentially moved into analytical position (i.e., the same 20-25 micron areas previously analyzed). Option (2) was chosen in order to minimize spectrometer reproducibility errors and excessive drive time. The detailed photographic probe "maps" allowed the exact spots analyzed to be located as many times as necessary. Table 24 lists the microprobe standards used for the analyses. An effort was made to match matrices of unknowns and standards as closely as possible in order to minimize matrix-correction errors. The ZAF computer program MAGIC IV by John Colby was used for the data reduction.

A total of 419 analyses of secondary (and a few primary) minerals were carried out on the #123, 124, and 127 core sample thin sectins by J.G. Liou and Ray Guillemette. Of these, 167 representative analyses were chosen to be included in this report. The modes of occurrence of most of the minerals analyzed are provided below the sample numbers. The characteristic compositionnl features for individual secondary minerals are described in detail in the next chapter. For both primary plagioclase and clinopyroxene, compositions were described in the previous sections.

DESCRIPTION OF SECONDARY MINERALS

Silica Minerals

Silica minerals are ubiquitous in the altered samples from the Onikobe geothermal area and include both cristobalite and quartz. Cristobalite is restricted to shallow depths and occurs as a fine-grained massive replacement after glassy groundmass, as fine-grained precipitates in vesicles, and as thin siliceous layers as the latest phase along fractures. Secondary quartz is present in every specimen. It occurs as fine-grained aggregates intimately associated with other secondary minerals in altered feldspars and glassy groundmass, as euhedral coarse-grained crystals along fractures and vesicles and as microcrystallized mosaic aggregates after primary quartz. Quartz is most

commonly associated with clays minerals, carbonates, zeolites and pyrite in the altered samples.

Kaolinite/pyrophyllite

Kaolinite is one of the most common secondary phases at the surface of fumarolic areas within the Onikobe geothermal area. However, in drill hole core samples, both kaolinite and pyrophyllite are very minor and kaolinite is restricted to shallow depth. They can only be identified in fine-grained separates by X-ray diffraction. Therefore, their occurrence and depth distribution are difficult to determine. They occur as fine-grained phases, intimately associated with other secondary minerals, in veins and as replacements after plagioclase crystals and glass shards. The kaolinite is restricted to shallow depths above 300 meters except for porous samples in GO-11 where minor kaolinite was identified in samples at depths of about 500m and 700m.

Pyrophyllite occurs in some core samples at depths greater than 800 meters in GO-8 and GO-11; an inverse correlation between pyrophyllite and wairakite may exist. Pyrophyllite is present in those drill hole core samples where wairakite is either absent or forms as a later phase. Apparently, the formation of both kaolinite and pyrophyllite is favored in rocks where an acidic aqueous solution flows. In such an acidic environment, Ca-zeolites such as laumontite and wairakite are not stable.

Clay Minerals

Clay minerals are the most common hydrothermal minerals in bore-hole cores of the Onikobe geothermal area and consist of a variety of species. Based on the X-ray diffraction characteristics, particularly the basal spacings under dry conditions and after ethylene-glycol treatment, the clay minerals in the drill hole core samples from the Onikobe geothermal area are divided into smectite, alkaline smectite, chlorite/smectite interstratified mineral, chlorite and illite. Tables 25-35 list the d_{001} values of these clay minerals under dry conditions and after ethylene glycol treatment. Below, we first describe the procedures employed for our identification of

the clay mineral species, then the general textural and compositional features of each of the clay minerals, their distribution and depth variations, and finally we correlate our results with those of other investigations in many other geothermal areas.

Procedures for Identification of Clay Minerals

It has been shown that the basal spacing d_{001} of smectite and smectite/chlorite interstratified mineral varies easily by cation exchange as well as by changes in the relative humidity under which these clays are kept. We determined the d_{001} values of clay minerals according to the following procedures:

1. The sample was ground into fine-grained powder of less than 100 microns, immersed in distilled water in a beaker, and thoroughly stirred in order to separate the clay particles from other minerals.
2. The suspension was allowed to sit for 15-30 minutes and then poured into another beaker; the light suspension contained abundant clay minerals.
3. The clay-rich suspension was left in a beaker for at least 2 days in order to deposit sufficient amounts of the suspended clay minerals at the bottom of the beaker.
4. An X-ray powder slide was prepared by smearing with a small amount of the clay-rich slurry.
5. The slide was dried and kept at room temperature for several days in an atmosphere of low relative humidity (less than 50%).
6. Muscovite powder was used as an internal standard because the d_{001} value of muscovite is well determined.
7. The slide was run in the X-ray diffractometer first from 10° to 2.5° 2θ (CuKα) at a chart speed of 0.5°/cm/min. Then it was run from 40° to 2.5° and 65° to 50° in order to determine other minerals and the (060) reflection of clay minerals, respectively.
8. The slide was placed into a sealed plastic box to which had been added 2 or 3 drops of ethylene glycol; it was then run again in the X-ray diffractometer from

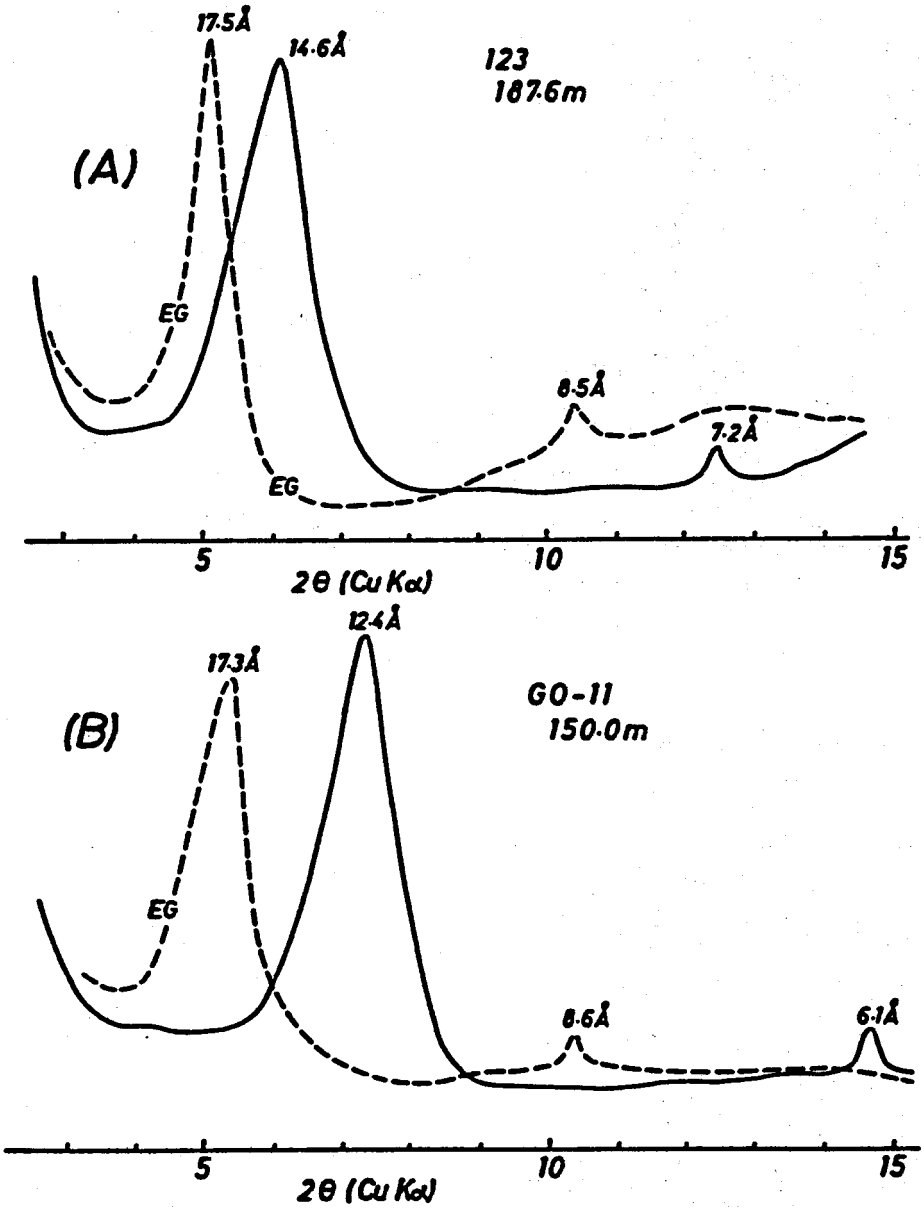

Figure 20. X-ray diffractograms of (A) smectite, (B) alkaline smectite, (C) chlorite/smectite interstratified mineral and (D) chloritic clay. Solid lines: at dry conditions; broken lines: after ethylene glycol treatment.

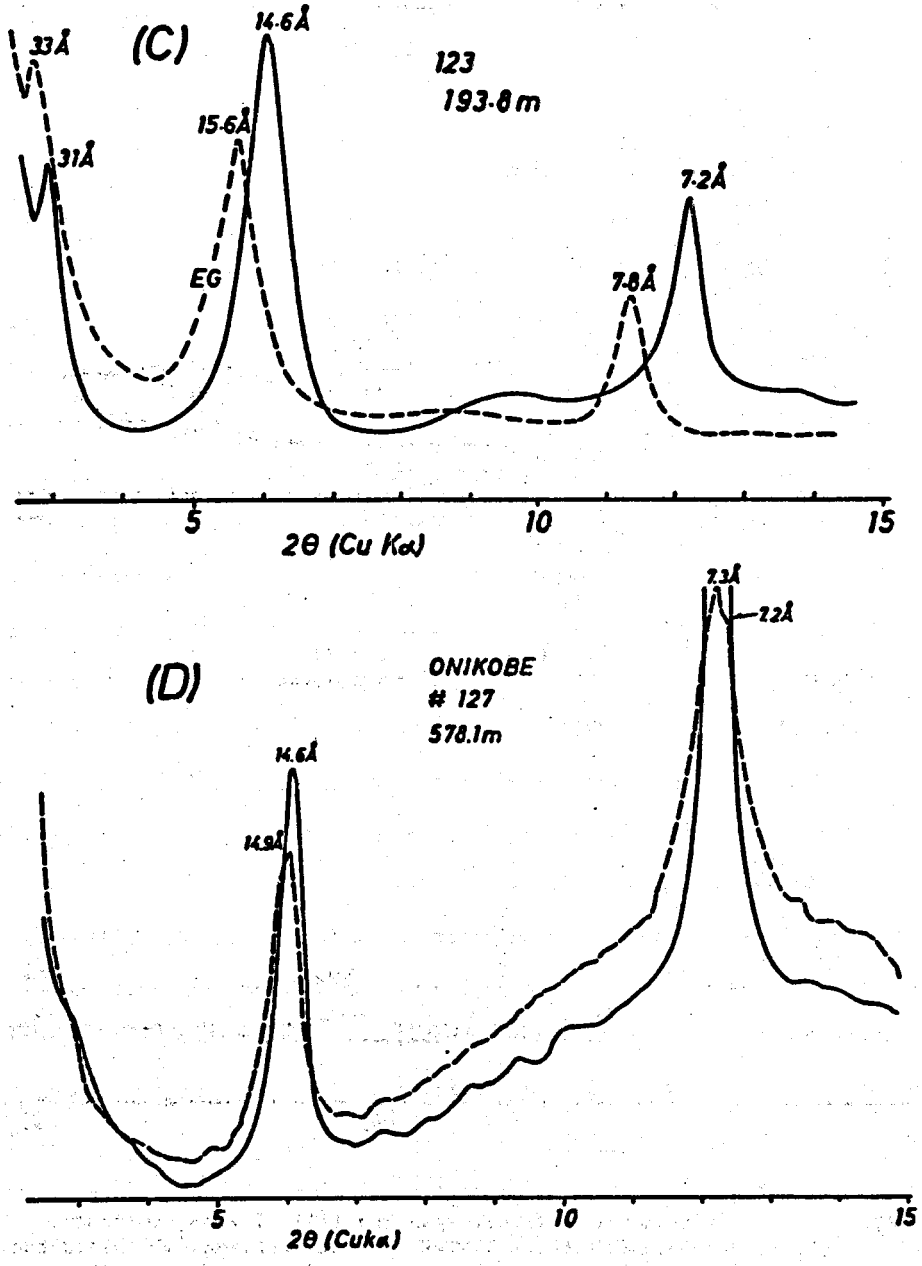
(C)
123
193.8m
14.6Å
15.6Å
33Å
31Å
EG
7.2Å
7.8Å
5
10
15
2θ (Cu Kα)
(D)
ONIKOBE
127
578.1m
7.3Å
7.2Å
14.6Å
14.9Å
5
10
15
2θ (Cukα)

15° to 2.5° 2θ (CuKα).

9. The d_{001} value was then determined in the case of smectite-chlorite mixed layer and chlorite, and their d_{001} values were calculated from their d_{002}, d_{003} and d_{004} values.

Description of Each Clay Mineral Species

Smectite (Type I Clay): The clay minerals with d_{001} values ranging from 14.3Å to 15.4Å under dry condition and 16.6 - 18Å after ethylene glycol treatment are called smectites in this paper and examples of their X-ray diffractograms are shown in Figure 20(A). The term "smectite" is a general term or group name which includes various types of expandable clay minerals such as montmorillonite, beidellite, saponite and others (Eberl, 1978; Bailey, 1980). According to Eberl (1978), the montmorillonite should be "dioctahedral" smectite in which most of the layer charges are developed by isomorphous substitution in the octahedral layer, whereas the main charge component in beidellite is tetrahedral. He recommended using the general term smectite when the differentiation between montmorillonite and beidellite is not possible. Although the name saponite was originally used as the equivalent of trioctahedral montmorillonite, many authors have used saponite as a general term to include both smectite and montmorillonite (e.g., Kimbara, 1975a,b; Sequet et al., 1975).

Smectite minerals are common in the upper 200 m of most of the drill-hole cores and are occasionally found down to a depth of 300 m. No chemical compositions were obtained by microprobe analysis as a result of the inability to locate larger isolated grains suitable for this type of analysis. No definitely-identified smectites were found in the #127 core samples examined by SEM.

Alkaline Smectite (Type I' Clay): Alkaline smectites, in which most of the Ca and Mg cations in smectites are replaced by alkaline metals such as Na and K, are characterized by d_{001} (dry) values of 12.5-13Å and an expansion to 17.0-17.6Å after ethylene glycol treatment. As shown in Figure 20(B), the alkaline smectites are easily differentiated from the smectite described above.

The d_{001} (dry) versus d_{001} (EG) diagram of clay minerals from the Onikobe drill hole core samples are summarized in Figure 21. Apparently, a significant gap between smectite and alkaline smectite exists, supporting the observation that both chemical composition and structural relations are discontinuous between the two clay minerals. Similar observations have been made in the Miocene volcanogenic sequence of the Seikan undersea tunnel area in Japan (Seki, et al., 1980).

Like Ca-Mg smectite, this variety generally occurs at depths shallower than about 200 m; it is, however, much less abundant than the former, occurring in fewer samples per hole and in a total of only 4 of 11 drill-hole cores. No microprobe or SEM analyses could be carried out.

Chlorite/Smectite Interstratified Minerals (Type II Clay): We named the clay minerals with d_{001} (dry) values of about 14-15Å and an expansion to 14-16Å by ethylene glycol treatment as chlorite/smectite interstratified minerals. These minerals consist of non-expandable layers of chlorite and expandable smectite layers. The degree of expansion by ethylene glycol treatment generally increases with the increase of interstratified expandable components. The relative intensities of the 14Å peaks and 7Å peak can be used to estimate the relative proportion of expandable layers in chlorite/smectite interstratified minerals (Weaver, 1956; Yoshimura, 1971; Yoshimura et al., 1977). With increasing chlorite content, the peak height ratio of 7Å/14Å in the X-ray diffractograms decreases continuously from about 1.5 to about 0.4 and d_{001} changes from 14Å to 15.5Å (as a result of ethylene glycol treatment). Variation in the relative intensities of the basal spacings at 14Å and 7Å of these minerals must be caused primarily by variation of cations in the octahedral layers and in the hydroxide sheet, the latter being occupied by large cations and H_2O molecules.

Most chlorite/smectite interstratified minerals from the bore-hole cores of the Onikobe geothermal area show a distinct 31Å diffraction peak, indicating that they are regularly interstratified minerals. Figure 20(C) illustrates the X-ray diffractogram for a chlorite/smectite interstratified mineral: the basal spacings represented by the three distinct peaks are respectively 31Å for (001), 14.6Å for (002) and 7.2Å for (004).

The d_{001} (dry) - d_{001} (EG) relations for chlorite/smectite interstratified

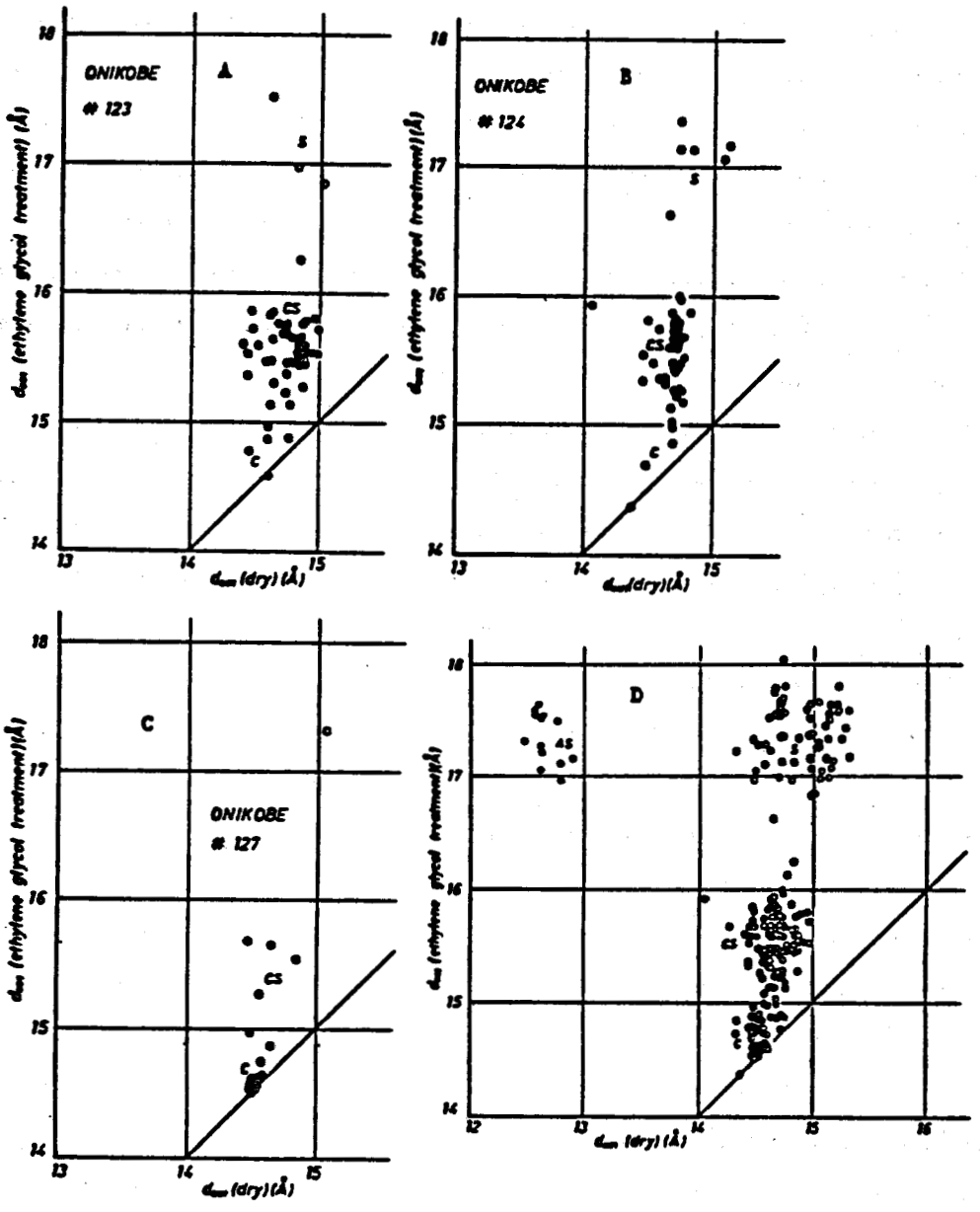

Figure 21. d_{001}(dry)-d_{001} (ethylene glycol) diagram of alkaline smectite (AS), smectite (S) and chlorite-chlorite/smectite interstratified mineral series (CS) in rocks of #123 (A), #124 (B) and #127(C) holes of the Onikobe geothermal area, Japan. (D) is a summary figure of all smectite-chlorite minerals measured from bore-hole cores of the Onikobe geothermal area.

minerals are plotted in Figure 21(A) for individual Onikobe drill cores #123, 124 and 127. From the available data shown in Figures 21(A) and (B), a small gap exists between smectite and the chlorite/smectite interstratified minerals, whereas a continuous series occurs between the chlorite/smectite interstratified minerals and chlorite.

Morphologically, the chlorite/smectite minerals observed by scanning electron microscopy in samples from core #127 occur as distinct, thin, platy and generally curved crystals. Coatings of these 2 to 10 micron crystals often display a locally sub-parallel, corrugated texture. Aggregates of curved plates in the form of rosettes are sometimes seen. Optically, the chlorite/smectite is pale green in plane light and displays low birefringence.

The chlorite/smectite interstratified minerals are the most common phyllosilicate found in the Onikobe geothermal area, occurring abundantly in drill-hole cores at depths greater than about 150 m. Selected minerals were analyzed for their major chemistry by electron microprobe. The results are listed in Tables 36 and 37 for 11 smectite/chlorite interstratified minerals and 17 chlorites. The interstratified phases are much more variable in composition than chlorite and contain mainly SiO_2 (28-33 Wt%), Al_2O_3 (9-19 Wt%), FeO* as total Fe (8-29 Wt%) and MgO (10-23 Wt%), minor amounts of MnO (0.06-2.0 Wt%) and CaO (0.1 to 2.2 Wt%) and negligible amounts of K_2O and Na_2O.

Since the chlorite group minerals can accommodate only a very limited amount of Ca in their structure, the presence of more than a few tenths of a percent of this element in an analysis indicates the occurrence of interlayered smectite. As a general rule, one can observe from Table 36 that shallower samples contain higher Ca concentrations, and, hence, a higher proportion of interlayered smectite. This trend is shown in Figure 22 for drill holes #123 and 127. A similar pattern based on the expandibility of the interstratified chlorite/smectite is observed in the X-ray diffraction results.

The modal variations among the major components SiO_2-Al_2O_3 - (FeO + MgO) for these analyses are shown in Figure 23 together with the compositional plots of smectite by Sudo and Shimada (1969), chlorite/smectite interstratified mineral by Kimbara (1975a,b) and chlorite by Shirozu et al., (1975). Apparently, the chlorite/smectite interstratified phases show significant variations in terms of these components; some of

Table 25. The d_{001} values of clay minerals from cores of P-5, the Onikobe geothermal area, Japan.

Depth (m)	Smectite		Chl/Smect - Chlorite		Illite
	Dry	EG	Dry	EG	Dry
22.2(5)	14.3(4)	17.3(5)			
29.3	14.8(2)	16.8(5)			
36.0	14.6(7)	16.9(8)			
45.9	14.7(5)	16.9(8)			
55.0	14.8(5)	17.1(4)			
62.0	14.4(0)	17.2(1)			
63.3(5)	14.5(0)	16.9(2)			
72.5	14.1(5)	17.1(8)			
148.0	14.4(3)	17.0(5)			
149.0			14.5(0)	15.4(0)	

Table 26. The d_{001} values of clay minerals from cores of P-7, the Onikobe geothermal area, Japan.

Depth. (m)	Smectite		Chl/Smect - Chlorite		Illite
	Dry	EG	Dry	EG	Dry
21.0	14.8(5)	17.3(1)			
26.0	14.6(2)	17.2(5)			
35.0	12.4(4)	17.2(5)			
39.0	14.4(8)	17.1(4)			
47.0	14.6(0)	17.1(4)			
50.0	14.4(8)	16.9(8)			
57.7					
70.15	14.1(3)	16.9(8)			
115.0	12.6(6)	17.2(5)			
130.8	14.3(6)	16.6(0)			
142.5			14.6(4)	15.3(6)	
150.0			14.3(6)	15.2(2)	
170.0			14.5(2)	15.6(3)	
200.0			14.5(0)	14.9(5)	
218.0			14.3(6)	15.3(0)	10.2(3)
250.0			14.7(9)	15.5(2)	10.3(9)

them have compositions very close to that of chlorite. Nevertheless, they contain higher SiO_2, lower (FeO + MgO) and lower CaO than chlorite. Both the smectite/chlorite interstratified mineral and chlorite are extremely low in K_2O content and are significantly different from illite and illite/smectite mixed layer silicates described later.

Chlorite Clay (Type III Clay): The d_{001} spacing of an ideal chlorite is not changed by ethylene glycol treatment (Nakamura, 1976). The occurrence of such unexpandable chlorite is extremely rare in the drill hole core samples from the Onikobe geothermal area. Most of the chlorite clays, as shown in Figure 20(D), are weakly to

Table 27. The d_{001} values of clay minerals from cores of P-8, the Onikobe geothermal area, Japan.

Depth (m)	Smectite		Chl/Smect - Chlorite		Illite
	Dry	EG	Dry	EG	Dry
50.0	15.20	17.1(8)			
50.5	12.6	17.2(5)			
72.5	14.9	17.1(1)			
85.0	14.5(2)	17.2(5)			
95.0	14.3(8)	17.0(8)			
100.0	14.9(2)	16.7(8)			
104.1(5)	14.7(0)	16.9(8)			
111.2	14.7(2)	16.9(8)			10.1(6)
118.0	14.4(5)	17.1(1)			
124.5	14.6(0)	16.7(5)			
131.8	12.8(5)	16.9(2)			
148.5(5)			14.3(6)	15.1(7)	
150.0	14.8(5)	16.9(5)			
156.2(5)			14.3(4)	15.1(5)	10.4(0)
168.5(5)			14.3(6)	15.3(3)	
200.0			14.3(6)	15.2(2)	
213.9			14.0(6)	15.6(6)	
250.0			14.3(6)	15.2(0)	10.3(9)

Table 28. The d_{001} values of clay minerals from cores of P-10, the Onikobe geothermal area, Japan.

Depth (m)	Smectite		Chl/Smect - Chlorite		Illite
	Dry	EG	Dry	EG	Dry
25.0	14.9(2)	17.4(1)			
50.0	15.1(2)	16.7(5)			
50.5	15.0(0)	17.0(5)			
51.5	14.7(2)	17.1(1)			
95.6	15.2(0)	16.7(2)			
100.0	14.9(2)	16.9(5)			
110.0	15.0(2)	16.9(2)			
125.0	14.5(5)	16.9(2)			
132.0	15.0(0)	16.9(2)			10.6(2)
133.3(5)	14.7(0)	16.7(8)			10.5(7)
135.0	15.0(7)	16.7(2)			
138.2(5)	14.8(2)	16.7(8)			
144.2(5)	14.7(0)	16.7(9)			
148.7(5)	14.8(3)	17.1(1)			
149.0	15.1(2)	16.9(8)			
152.5(5)	14.7(0)	16.9(2)			
160.0	14.7(0)	16.8(5)			
161.0(5)	14.6(2)	16.9(2)			
166.4	14.7(0)	16.7(8)			
171.7(5)	14.4(8)	16.6(6)			
183.0(5)	14.6(7)	16.9(2)			
194.2	14.6(2)	17.0(5)			
203.0	14.6(0)	16.7(8)			

Table 29. The d_{001} values of clay minerals from cores of GO-7, the Onikobe geothermal area, Japan.

Depth (m)	Smectite		Chl/Smect - Chlorite		Illite
	Dry	EG	Dry	EG	Dry
15.0	12.6(4)	16.9(5)			
20.5	12.5(8)	16.9(8)			
23.0	12.8(0)	16.9(8)			
26.5	12.5(1)	16.9(5)			
107.0	12.2(7)	17.0(5)			
147.0(8)	14.6(3)	16.9(9)			
175.0	14.6(0)	16.6(6)			10.6(0)
201.1(3)			14.4(8)	15.2(0)	
201.1(5)			14.4(3)	15.3(3)	
243.0			14.4(3)	14.6(2)	10.4(4)
247.0			14.2(2)	14.7(2)	
263.0			14.5(7)	14.6(2)	10.2(5)
276.0			14.3(6)	14.7(9)	
299.3			14.7(2)	14.9(7)	10.3(7)
300.8			14.4(3)	15.2(2)	
352.0			14.3(6)	14.7(5)	
377.5			14.4(8)	14.7(0)	
381.0			14.2(4)	14.9(7)	
398.0			14.4(0)	14.6(7)	10.4(9)
423.4			14.4(8)	14.9(7)	
450.6			14.5(2)	15.3(3)	
500.0					10.3(0)

moderately expanded by ethylene glycol treatment.

Tables 25 to 35 list the d_{001} values of clay minerals from cores of many drill holes in the Onikobe geothermal area. The data clearly indicate that the $[d_{001}(EG)-d_{001}(dry)]/\ d_{001}$ (dry) ratio decreases with increasing temperature and depth in the Onikobe geothermal area. Apparently, the chlorite/smectite interstratified mineral changes to chloritic clay, and the percentage of chlorite layers in the chlorite/smectite interstratified minerals increases with increasing depth.

Some bore-hole core samples contain both chlorite/smectite interstratified mineral and chloritic clays as shown in the X-ray diffractogram of Figure 24. Whether these two clay minerals are stable is not certain. Optical observation to reveal their genetic relationship is difficult.

Selected chlorite minerals were analyzed for their major element compositions and the results are listed in Tables 37 and 38 and graphically shown in Figures 23 and 25. Compared to those chlorite/smectite interstratified minerals described above, the chlorites have a much more restricted range of chemical compositions. The chlorites

Table 30. The d_{001} values of clay minerals from cores of GO-8, the Onikobe geothermal area, Japan.

Depth (m)	Smectite		Chl/Smect - Chlorite		Illite
	Dry	EG	Dry	EG	Dry
25.0	12.8(0)	17.3(0			
50.5	12.8(2)	17.5(9)			
100.5	14.6(7)	17.6(3)			
100.5	13.0(0)	17.6(3)			
126.5	12.6(2)	17.6(6)			
147.0	14.9(7)	17.0(8)	14.9(7)	15.6(3)	
147.1			15.0(0)	15.7(7)	
148.0			14.7(2)	15.7(7)	
199.2	15.0(0)	17.3(8)			
202.0			15.0(2)	15.7(1)	
247.0			14.7(9)	15.1(7)	
250.0			14.7(9)	14.7(7)	
250.0			14.7(9)	15.2(2)	
297.0			14.7(2)	15.3(0)	
350.9			14.5(7)	14.6(7)	
351.0			14.7(2)	14.7(2)	10.6(3)
402.5			14.6(2)	15.2(7)	
455.0			14.6(0)	14.6(7)	10.1(1)
500.5			14.6(4)	14.8(9)	
501.0			14.7(2)	14.7(7)	
552.5			14.7(0)	14.7(7)	10.3(0)
597.5			14.6(2)	14.6(2)	
599.0			14.6(0)	14.5(7)	
650.5			14.5(5)	14.5(5)	10.2(0)
651.0			14.5(0)	14.5(7)	10.1(9)
700.0			14.5(5)	14.7(0)	10.1(6)
700.1			14.5(7)	14.5(7)	
701.5					9.9(7)
750.0			14.5(2)	14.6(2)	
799.0			14.6(5)	14.5(5)	
899.8			14.6(0)	14.8(2)	11.5(2)
899.8			14.6(0)	15.4(9)	
950.0			14.7(2)	14.7(2)	10.1(2)
998.3			14.5(5)	14.5(0)	10.2(3)

contain much lower CaO and SiO_2 than the chlorite/smectite phases.

Analyses of minerals considered to be almost entirely chlorite as a result of low Ca contents are also plotted in Figure 25 (after Hay, 1954). The analyzed samples from drill holes #123, 124, and 127 all plot in the pycnochlorite and diabantite fields, following unoxidized chlorite nomenclature; the deeper samples appear to generally plot further to the left than the shallower ones as a result of lower Si contents. If oxidized chlorite nomenclature is used, then the analyses fall in the delessite and chamosite fields. Although ferric/ferrous ratios could not be obtained for these samples, the occurrence suggests that unoxidized chlorites are more likely than oxidized

Table 31. The d_{001} values of clay minerals from cores of GO-10, the Onikobe geothermal area, Japan.

Depth (m)	Smectite		Chl/Smect - Chlorite		Illite
	Dry	EG	Dry	EG	Dry
55.0	14.5(7)	17.3(2)			
155.0			14.8(2)	15.8(2)	
255.0			14.7(7)	15.7(5)	
300.0	14.7(9)	17.0(5)			
302.0	14.9(7)	17.1(1)			
330.0			14.6(2)	14.9(7)	
380.0			14.9(2)	14.7(7)	
401.0			14.7(7)	15.2(2)	
453.0			14.7(7)	15.1(0)	
535.0			14.5(7)	14.6(0)	
655.0			14.5(7)	14.5(5)	
755.0			14.4(8)	14.5(2)	10.1(1)
855.0			14.5(2)	14.5(7)	
955.0			14.5(7)	14.5(7)	10.0(9)
1050.0					10.0(6)
1100.0					10.0(6)
1330.0			14.4(5)	14.5(0)	10.1(1)

Table 32. The d_{001} values of clay minerals from cores of GO-11, the Onikobe geothermal area, Japan.

Depth (m)	Smectite		Chl/Smect - Chlorite		Illite
	Dry	EG	Dry	EG	Dry
50.0	14.1(3)	16.9(8)			
105.0	12.9(5)	17.5(2)			
105.0	14.4(3)	17.5(2)			
150.0	12.4(0)	17.3(8)			
150.0	14.4(3)	17.3(8)			
200.0	12.8(0)	17.5(9)			
200.0	14.7(2)	17.5(9)			
203.0	12.3(4)	17.2(5)			12.6(4)
203.0	15.0(2)	17.2(5)			
250.0			15.0(2)	15.8(2)	11.1(8)
300.0			14.8(9)	15.2(0)	
305.0			14.7(2)	14.9(7)	
350.0			14.6(2)	14.6(2)	
400.0			14.6(2)	14.6(2)	
401.6			14.8(7)	15.3(8)	
503.0			14.6(7)	14.7(7)	
550.0					10.9(1)
598.0			14.3(6)	14.4(3)	11.9(4)
701.0			14.6(2)	14.6(2)	10.3(2)
791.0			14.5(5)	14.6(2)	10.0(9)
800.0			14.6(2)	14.6(7)	
800.0			14.6(2)	15.7(7)	
900.0			14.4(8)	14.4(8)	
902.0			14.5(2)	14.4(3)	10.5(2)
1205.0			14.5(2)	15.7(7)	10.2(3)
1300.0			14.5(7)	15.7(7)	

Table 33. The values of clay minerals from cores of #123, the Onikobe geothermal area, Japan.

Depth (m)	Smectite		Chl/Smect - Chlorite		Illite
	Dry	EG	Dry	EG	Dry
158.9			14.4(8)	15.6(6)	
159.2			14.5(2)	15.6(0)	
159.9			14.8(7)	15.6(0)	
162.9			14.6(2)	15.8(5)	
163.1			14.6(7)	15.7(7)	
165.1			14.9(7)	15.5(2)	
169.8			14.9(7)	15.7(1)	
175.9	15.1(2)	16.8(5)			
178.8			14.8(7)	15.7(7)	
179.0			14.8(2)	16.2(6)	
184.7	14.8(2)	16.9(8)			
187.6	14.6(2)	17.5(2)			
193.8			14.6(2)	15.6(2)	
198.4			14.6(2)	15.4(9)	10.2(7)
202.5			14.8(7)	15.6(0)	
206.6			14.6(4)	15.3(0)	
207.1			15.4(8)	15.7(5)	
210.9			14.4(5)	15.3(8)	
215.2			14.4(5)	15.5(5)	
216.6			14.7(7)	14.8(7)	10.2(7)
229.4			14.6(4)	14.6(4)	10.2(7)
232.4			14.5(7)	15.4(6)	
238.6			14.7(7)	15.1(2)	
244.9			14.8(7)	15.5(5)	
247.6			14.8(2)	15.4(9)	
253.0			14.8(2)	15.6(6)	
260.9			14.9(5)	15.8(0)	
262.6			14.4(0)	15.6(0)	
263.6			14.8(2)	15.6(0)	
267.7			14.8(5)	15.4(9)	
273.6			14.8(5)	15.2(7)	
279.8			14.7(2)	15.2(2)	
285.3			14.7(9)	15.4(6)	
290.1			14.8(2)	15.5(5)	
295.2			14.8(7)	15.5(5)	
300.1			14.7(2)	15.5(2)	
303.5			14.8(2)	15.4(4)	
307.5			14.8(2)	15.6(6)	
308.2			14.7(2)	15.7(1)	
311.0			14.8(7)	15.7(7)	
313.7			14.8(7)	15.5(2)	
319.9			14.7(2)	15.3(8)	
323.8			14.6(2)	14.8(2)	10.2(7)
328.6			14.8(7)	15.5(7)	
333.3			14.7(2)	15.7(5)	
340.6			14.4(5)	14.7(8)	
340.6			14.7(2)	15.6(8)	
344.6			14.6(6)	14.9(2)	10.2(2)
348.5			14.7(7)	14.8(5)	

Table 34. The d_{001} values of clay minerals from cores of #124, the Onikobe geothermal area, Japan.

Depth (m)	Smectite		Chl/Smect - Chlorite		Illite
	Dry	EG	Dry	EG	Dry
158.3			14.7(2)	15.6(8)	
159.5			14.7(2)	15.7(1)	
162.4			14.6(7)	15.8(8)	
165.6	14.7(2)	17.3(8)			
167.3			14.6(2)	16.6(0)	
172.4	15.1(2)	17.1(8)			
178.0	14.7(2)	17.1(1)			
179.3			14.8(2)	15.8(8)	
186.3			14.7(2)	15.7(7)	
192.0			14.7(2)	16.0(0)	
193.4	14.7(7)	16.9(8)			
200.3	15.0(7)	17.0(5)			
201.8			14.4(8)	15.8(0)	
209.9			14.06	15.9(4)	
211.1			14.7(7)	15.6(8)	
214.0(5)			14.3(6)	14.3(6)	
214.3			14.7(2)	15.2(7)	10.2(8)
219.6			14.6(7)	14.9(7)	10.0(9)
222.8			14.6(7)	14.8(5)	10.2(3)
227.4			14.6(7)	15.6(0)	
231.7			14.5(7)	15.3(6)	
235.8			14.7(0)	15.2(7)	
239.8			14.6(7)	15.0(2)	
243.0			14.7(2)	15.3(0)	
245.0			14.7(2)	15.4(9)	
246.4			14.7(2)	15.4(4)	
249.4			14.7(0)	15.7(1)	
252.5			14.4(5)	15.3(3)	
253.5			14.6(2)	15.3(6)	
254.4			14.6(7)	15.4(9)	
259.4			14.7(0)	15.8(2)	
264.0(5)			14.6(7)	15.1(5)	
264.4			14.7(2)	15.3(3)	
270.4			14.7(2)	15.2(2)	
276.9			14.6(2)	15.3(3)	
286.2			14.6(7)	15.6(0)	
291.5	14.8(2)	17.1(4)			
294.4			14.7(7)	15.1(7)	
300.5			14.7(7)	15.5(2)	
307.5			14.6(7)	15.6(3)	
310.4			14.7(2)	15.4(1)	
315.4			14.7(2)	15.6(8)	
318.5			14.7(2)	15.4(4)	
320.4			14.5(7)	15.7(5)	
323.7			14.7(2)	15.8(0)	
324.5			14.7(7)	15.7(1)	
329.7			14.7(2)	15.6(6)	
334.7			14.4(5)	15.5(5)	
344.6			14.7(2)	15.7(5)	
346.3			14.5(2)	15.4(9)	
349.4			14.7(2)	15.6(3)	

Table 35. The d_{001} values of clay minerals from cores of #127, the Onikobe, geothermal area, Japan.

Depth (m)	Smectite		Chl/Smect - Chlorite		Illite
	Dry	EG	Dry	EG	Dry
32.4	15.0(2)	17.3(1)			
154.6			14.8(2)	15.5(5)	
155.4			14.5(5)	15.2(8)	
296.1			14.6(4)	15.6(6)	
296.1			14.5(0)	14.5(0)	
297.5			14.4(5)	15.6(8)	
297.5			14.5(4)	14.5(6)	
298.5			14.8(4)	15.5(5)	
298.5			14.5(2)	14.5(4)	
409.7			14.5(2)	14.6(2)	10.7(7)
411.5			14.4(8)	14.5(0)	10.5(9)
577.2			14.4(8)	14.9(7)	
578.1			14.6(4)	14.8(7)	
702.9			14.4(8)	14.5(7)	10.4(7)
703.1			14.4(8)	14.5(2)	10.5(0)
703.9			14.5(2)	14.5(2)	10.6(2)
704.3			14.5(0)	14.6(0)	10.2(7)
704.9			14.4(8)	14.5(5)	10.4(0)
792.1			14.5(7)	14.7(2)	
902.7			14.5(2)	14.5(2)	10.3(9)
1010.6			14.5(2)	14.5(5)	10.8(8)
1011.3			14.5(7)	14.5(7)	11.0(2)
1103.6			14.5(7)	14.6(2)	10.1(8)
1104.0			14.5(2)	14.6(2)	10.1(3)
1104.4			14.5(2)	14.5(2)	10.0(8)
1105.5			14.5(7)	14.5(5)	10.1(6)

ones (where, following Hay's convention, oxidized chlorites are those containing more than 4 wt.% Fe_2O_3). Table 38 lists the calculated chlorite formulas for the analyses plotted in Figure 25. Although these analyses can be successfully calculated as smectite-free chlorites, it is important to note that very few of these chlorites exhibit no expansion upon ethylene glycol treatment; the majority still show weak to moderate expansion. This is characteristic of what has been called "swelling chlorite" by a number of researchers. In addition to showing a 14-16Å reflection, the Onikobe interstratified chlorite/smectite minerals also exhibit a distinct 31Å reflection, indicating that they are regularly rather than randomly interstratified.

Illite/Smectite Interstratified Minerals and Sericite: Illitic clay minerals occur in some deep bore hole cores of the Onikobe geothermal areas. They are relatively rare compared to smectite-chlorite series clay minerals described above. The illitic clay minerals, judging from their X-ray diffraction patterns and limited microprobe

Table 36. Chemical composition of chlorite/smectite interstratified minerals in drill hole core samples from the Onikobe geothermal area, Japan.

Sample No.	#123 - 238.6m	#123 - 344.6m	#124 - 165.6m				#124 - 259.9m	#124 - 334.7m	#127 - 154.6m	#127 578.1m	
SiO_2	29.09	29.25	31.43	28.79	31.79	32.59	28.30	24.44	29.26	28.84	33.63
Al_2O_3	17.20	18.23	13.03	11.65	12.25	9.70	11.96	11.06	16.06	17.57	18.53
FeO*	19.80	13.82	29.13	26.05	27.86	22.34	11.69	22.78	17.05	11.37	8.52
MnO	0.88	0.66							0.51	2.07	1.85
MgO	16.85	22.30	12.61	12.74	11.80	11.99	19.23	10.77	16.61	20.79	18.41
CaO	0.27	0.16	1.20	1.01	1.78	2.02	0.76	0.58	0.61	1.57	2.21
K_2O	0.07	0.04	0.09	0.08	0.15	0.07	0.02	0.06	0.05	0.00	0.01
Na_2O	0.05	0.03	0.06	0.09	0.08	0.02	0.04	0.05	0.07	0.16	0.19
Anhydrous Total	84.20	84.98	87.55	80.42	85.71	78.74	71.99	69.74	80.22	82.36	83.35

*Total Fe as FeO.

Table 37. Chemical composition of chlorites in drill hole core samples from the Onikobe geothermal area, Japan.

Sample No.	#127 - 578.1m	#127 - 1010.6m						#127 - 1011.3m		#127 - 1103.6m	#127 - 1104.4m
SiO_2	29.08	27.71	27.62	27.94	26.84	28.36	27.84	28.75	28.51	25.35	29.46
Al_2O_3	14.49	18.70	18.35	18.97	18.04	17.74	18.23	18.06	18.37	17.46	19.36
FeO*	10.92	21.93	22.82	21.96	22.07	22.22	22.21	22.27	22.35	22.99	17.72
MnO	1.78	0.35	0.33	0.30	0.32	0.32	0.31	0.28	0.32	0.46	0.33
MgO	20.67	16.86	16.33	16.86	16.57	16.72	16.58	17.82	17.40	13.78	21.88
CaO	1.58	0.10	0.13	0.17	0.21	0.27	0.19	0.15	0.21	0.01	0.13
K_2O	0.01	0.06	0.06	0.04	0.06	0.05	0.06	0.03	0.09	0.02	0.03
Na_2O	0.14	0.07	0.08	0.07	0.10	0.10	0.11	0.07	0.08	0.09	0.05
Anhydrous Total	81.67	85.79	85.71	86.31	84.21	85.78	85.53	87.42	87.31	80.16	88.96

	#127 - 1104.4m					
SiO_2	29.60	29.37	29.95	29.56	28.56	29.94
Al_2O_3	18.66	19.26	18.96	18.44	19.25	18.22
FeO*	18.84	18.31	18.25	18.02	18.01	18.08
MnO	0.37	0.33	0.32	0.38	0.33	0.32
MgO	21.04	20.97	21.63	21.72	20.63	22.19
CaO	0.13	0.25	0.12	0.08	0.15	0.10
K_2O	0.05	0.04	0.04	0.04	0.01	0.01
Na_2O	0.05	0.04	0.05	0.05	0.06	0.04
Anhydrous Total	88.74	88.58	89.32	88.29	87.02	88.90

*Total Fe as FeO

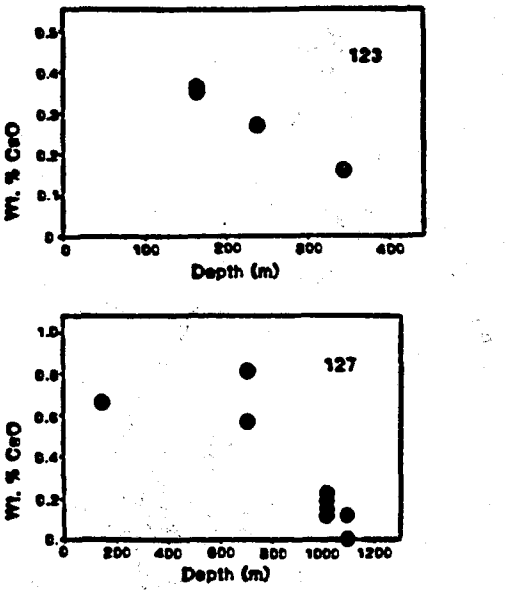

Figure 22. Plot of CaO wt% in chlorite-smectite interstratified minerals from drill hole samples in cores #123 and #127 as a function of depth. CaO was calculated on the basis of water-free totals normalized to 88%.

compositions, belong to the illite-illite/smectite interstratified mineral series. Continuous variations occur in this series; with increasing depth, as shown in Table 3[9], the difference in (001) spacings between dry condition and after ethylene glycol treatment becomes smaller. This relationship indicates that the smectite component decreases and illite becomes the major K-bearing phase for deep drill hole core samples.

An example of an X-ray diffractogram of a typical illite/smectite interstratified mineral separated from GO-11 (203.0m depth) is shown in Figure 26(A); both pre- and post-glycolation diffractograms are presented. The diffractogram exhibits the effects of two components—smectite and illite. The 27.3Å peak is due to the regular interstratification of sericite and smectite. The 12.65Å peak is due to both components, which can best be shown in the diffractogram run after glycol treatment (13.71Å for smectite component and 9.11Å for the illite component). On the other hand, as shown in Figure 26(B), the end-member illite (or sericite) exhibits a characteristic white mica pattern with 10.12Å for (001) peak and 5.06Å for (002); these reflections are not affected by ethylene glycol treatment. The (hkl) reflections in the range of 20°-35°

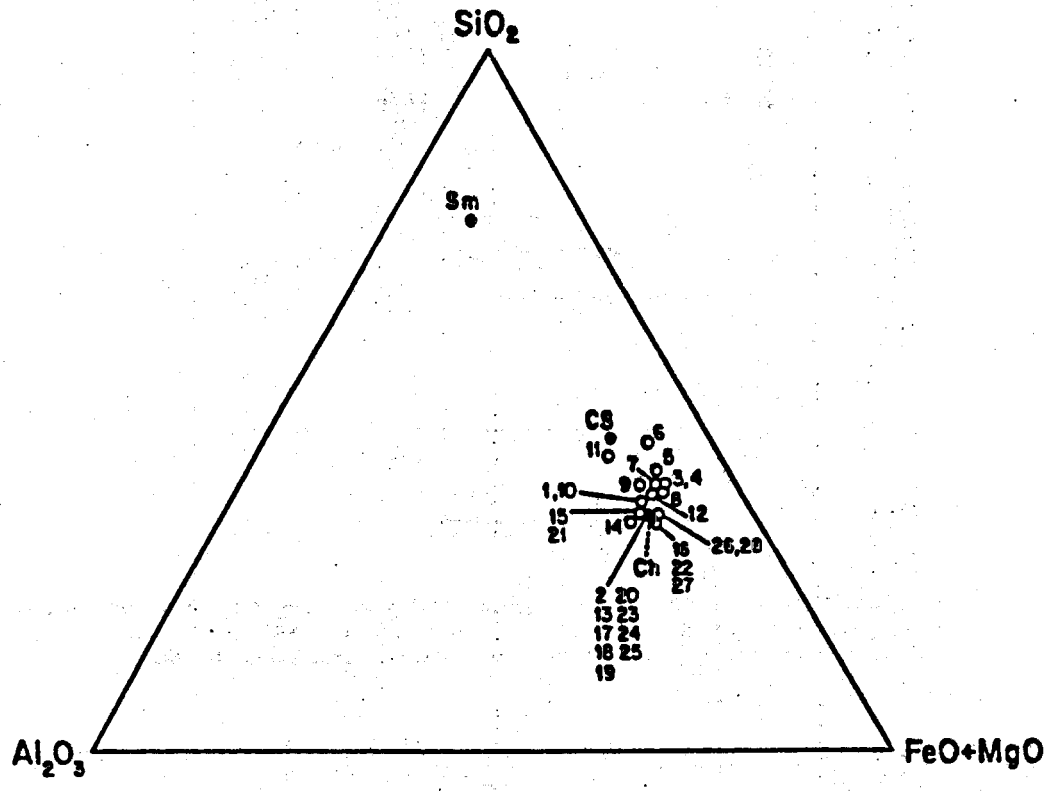

Figure 23. SiO_2 - Al_2O_3 - (FeO + MgO) diagram showing compositions of analyzed chlorite/smectite interstratified minerals and chlorites from drill hole cores of the Onikobe geothermal area. Numbers refer to those analyses in Tables 36 and 37. Sm: smectite (Sudo and Shimoda, 1969); CS: chlorite/smectite interstratified minerals (Kimbara, 1975a); Ch: chlorite (Shirozu et al., 1975).

CuKα 2θ (Yoder and Eugster, 1955) indicate that illite and illite/smectite interstratified minerals belong to the $2M_2$ and 2Md (or 1M) polytypes respectively. The values of d_{060} spacing of 1.497Å - 1.500Å suggest that the K-bearing clay minerals are dioctahedral phyllosilicates.

Some drill core samples contain both smectite-chlorite and illitic clay minerals. Both appear to be stable. Some illite crystals are coarse enough to exhibit the optical properties of phengitic mica. The phengitic phyllosilicates are colorless and have high birefrigence, whereas the chlorite-smectite minerals are light green in color and have neutral interference color. X-ray diffractograms of some samples with the 2 types of clay minerals are shown in Figure 27. The 9.82Å peak appearing after ethylene glycol

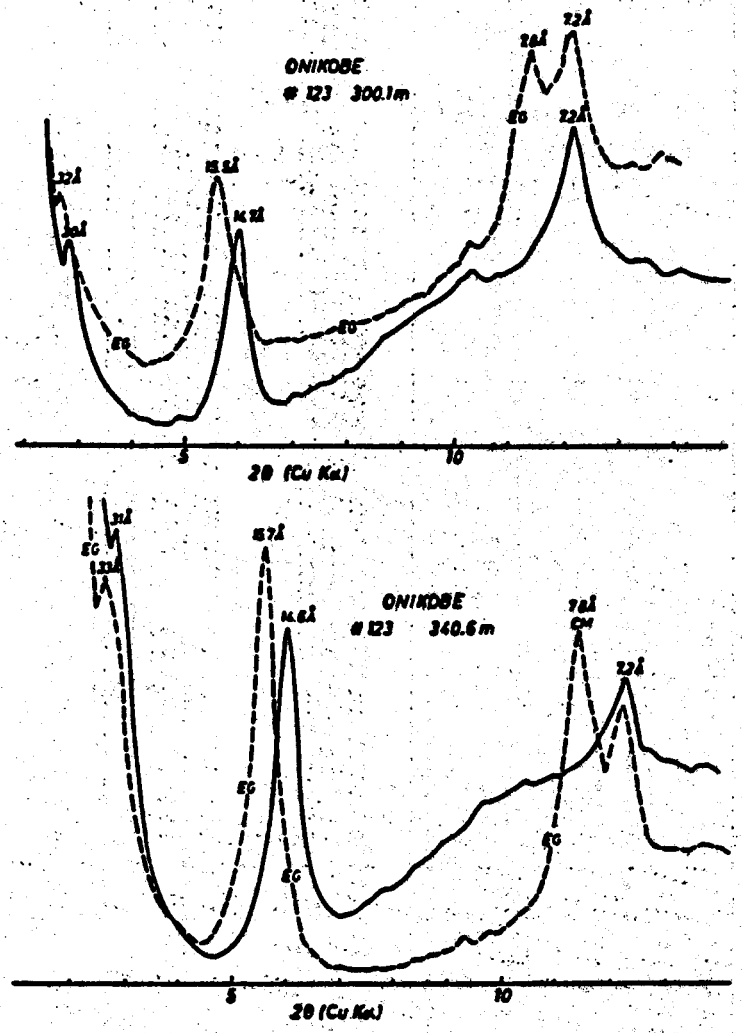

Figure 24. X-ray diffraction diagram of the mixture of chlorite and chlorite/smectite interstratified mineral from bore-hole cores (A) #123, 300.1m and (B) #123, 340.6 m of the Onikobe geothermal area, Japan. Broken line: after ethylene glycol treatment.

treatment (Figure 27(A)) is due to interference between the sericite layer and the expanded smectite layer reflections.

A few intermediate K-bearing phyllosilicates were observed in the SEM study of core #127. The morphology of the crystals appeared no different than that of the chlorite/smectite minerals. In thin secton, the coarser illitic grains were colorless to pale brown in plane light and displayed second-order interference colors under crossed

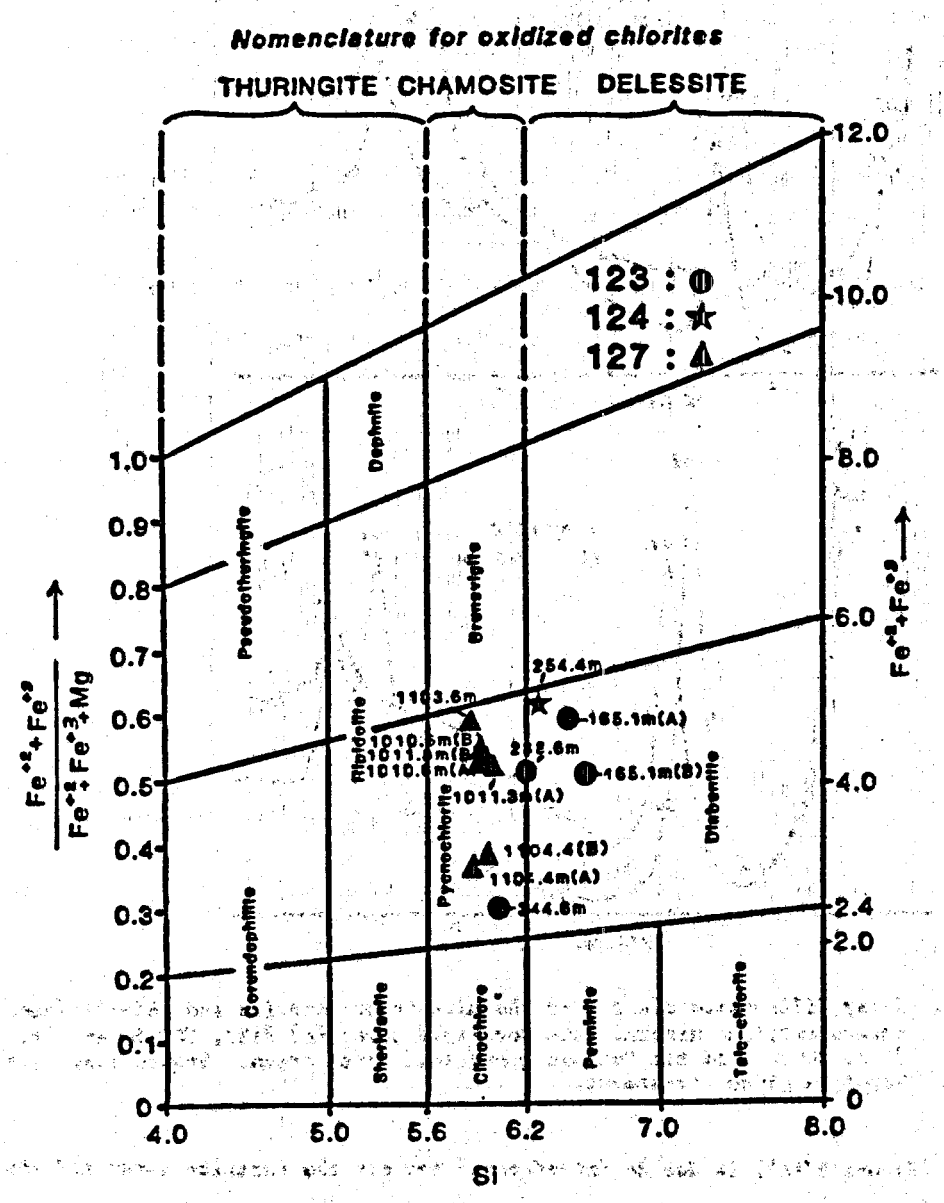

Figure 25. Plot of compositions of chlorites from cores of Nos. 123, 124, 127 bore-holes in the Onikobe geothermal area on Hay diagram.

Table 38. Calculated formulae for chlorites from the Onikobe geothermal area, Japan.

Sample	Ca	Mn	$(Mg_A$	Al_A	$Fe_A)_A$	$((Si_A$	$Al_A)_{8.0}O_{20})(OH)_{16}$		Fe/Fe+Mg
123-163.1m A	0.09	0.14	4.90	2.32	4.18	11.63*	6.43	1.57	0.46
123-163.1m B	0.10	0.18	5.31	2.35	3.42	11.36*	6.54	1.46	0.38
123-238.6m	0.06	0.16	5.36	2.52	3.53	11.63*	6.20	1.80	0.40
123-344.6m	0.04	0.11	6.95	2.37	2.36	11.83*	5.98	2.02	0.25
124-234.4m	0.05	0.09	4.88	2.23	4.52	11.77*	6.24	1.76	0.48
127-1010.6m A	0.02	0.06	5.32	2.52	3.88	11.80*	5.86	2.14	0.42
127-1010.6m B	0.03	0.06	5.18	2.48	4.06	11.81*	5.88	2.12	0.44
127-1011.2m A	0.03	0.05	5.31	2.37	3.86	11.82*	5.96	2.04	0.41
127-1011.2m B	0.05	0.06	5.39	2.43	3.89	11.82*	5.93	2.07	0.42
127-1103.6m	0.00	0.09	4.72	2.56	4.42	11.79*	5.83	2.17	0.48
127-1104.4m A	0.03	0.06	6.48	2.38	2.94	11.89*	5.85	2.15	0.31
127-1104.4m B	0.03	0.06	6.28	2.34	3.16	11.87*	5.93	2.07	0.33

* : Total includes (Mg + Al + Fe) plus Ca and Mn.

Table 39. $d_{001}{}_{dry}$; $d_{001}{}_{EG}$ and $d_{001}{}_{dry} - d_{001}{}_{EG}$ values of illitic clay minerals in bore-hole cores of #127, Onikobe geothermal area, Japan (Å).

Depth	$d_{001}{}_{dry}$	$d_{001}{}_{EG}$	$d_{001}{}_{dry} - d_{001}{}_{EG}$
411.5m	10.5_7	10.0_4	0.5_3
702.9m	10.4_7	9.92	0.5_5
703.1m	10.5_0	9.8_5	0.65
703.9m	10.6_2	9.8_5	0.7_7
704.9m	10.4_0	9.8_5	0.5_5
902.7m	10.3_9	10.0_4	0.3_5
1103.6m	10.1_8	10.1_3	0.0_5
1104.0m	10.1_3	10.1_0	0.0_3
1105.5m	10.1_6	10.1_6	0.0_0

nicols.

Some illitic clay minerals from the bore-hole cores of the Onikobe geothermal area were analyzed by the electron microprobe. The results are listed in Table 40 and graphically illustrated in Figure 28. Also shown in the diagram are compositions of saponite (Yoshimura et al., 1975), sericite (Higashi and Shirozu, 1975) and illite (Shimoda and Nishiyama, 1973). Upon examination of the reconnaissance data listed in the table and shown in the figure, several facts are deduced: (1) illitic clay minerals vary substantially in their major elements, (2) the SiO_2 content ranges from 31 to 49 wt% and increases with increasing K_2O; (3) those illite/smectite interstratified minerals are low in SiO_2 and K_2O and high in (FeO + MgO), H_2O and CaO, whereas illite minerals are high in SiO_2, Al_2O_3 and K_2O and low in (FeO + MgO) and H_2O,

Table 40. Chemical composition of illitic clay minerals in drill hole core samples from the Onikobe geothermal area, Japan.

Sample No.	#123 - 238.6m		#124 - 222.8m	#127 - 703.1m						
SiO_2	31.46	33.11	38.82	42.27	49.41	49.15	36.04	37.97	36.34	32.94
Al_2O_3	18.76	20.55	22.84	25.20	31.51	30.93	23.13	22.72	25.02	19.08
FeO*	14.03	12.19	9.17	0.32	0.24	0.23	8.53	6.60	8.31	6.56
MnO	0.66	0.73	——	——	——	——	0.18	0.29	0.12	0.11
MgO	13.13	13.33	14.52	1.56	1.35	1.21	5.71	8.85	5.55	4.33
CaO	0.29	0.26	0.17	0.51	0.09	0.07	0.50	0.75	0.45	1.84
K_2O	1.34	1.69	2.51	6.54	8.82	9.32	3.10	1.89	4.04	2.09
Na_2O	0.09	0.12	0.04	0.19	0.28	0.20	1.40	2.20	0.64	2.34
Anhydrous Total	79.76	81.99	88.17	76.59	91.94	91.94	78.61	81.33	80.47	69.28

	#127 - 703.9m		#127 - 1105.5m	
SiO_2	38.32	38.57	48.08	48.96
Al_2O_3	26.55	26.74	28.33	27.96
FeO*	14.28	14.64	3.74	3.90
MnO	0.17	0.09	0.04	0.04
MgO	5.72	5.05	1.77	1.94
CaO	0.30	0.27	0.08	0.02
K_2O	4.31	3.98	10.36	10.57
Na_2O	0.35	0.37	0.13	0.08
Anhydrous Total	89.91	89.71	92.52	93.46

*Total Fe as FeO.

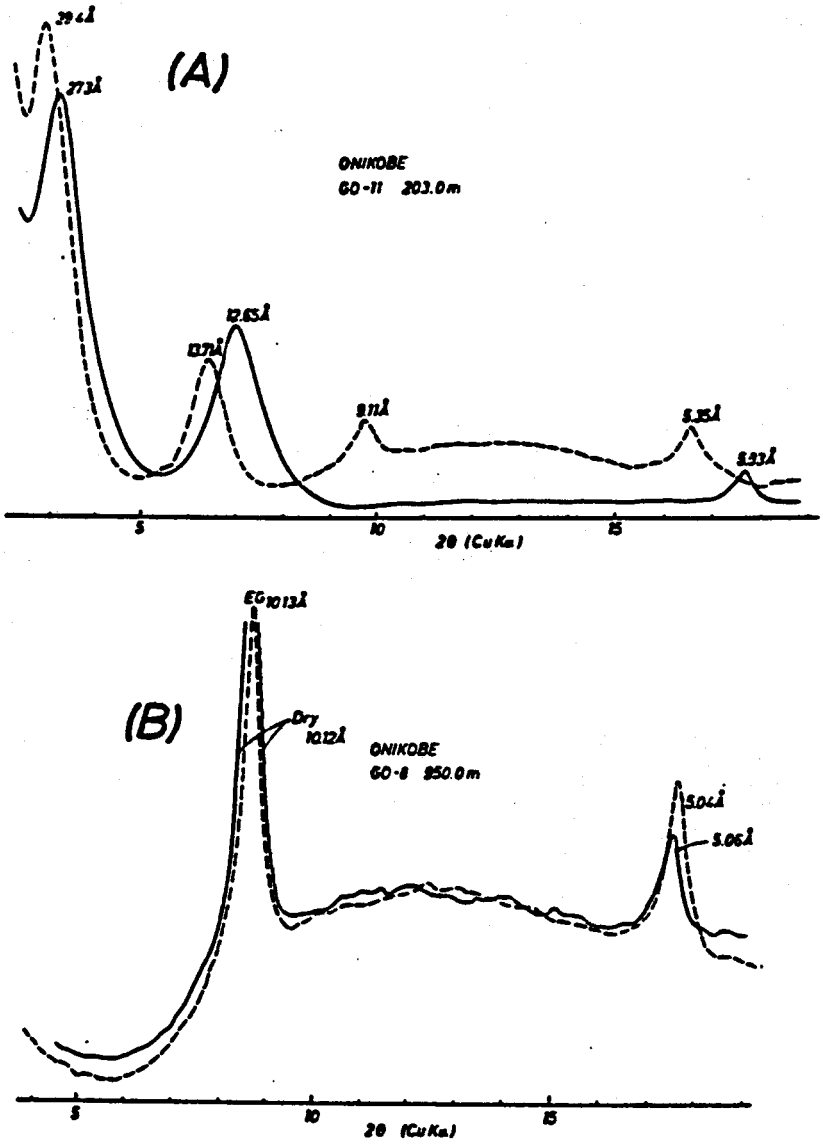

Figure 26. X-ray diffraction diagrams of (A) illite/smectite interstratified mineral (GO-11, 203.0m) and (B) illite (GO-8, 950.0m), Onikobe geothermal area, Japan. Solid line: at dry condition; broken line: after ethylene glycol treatment

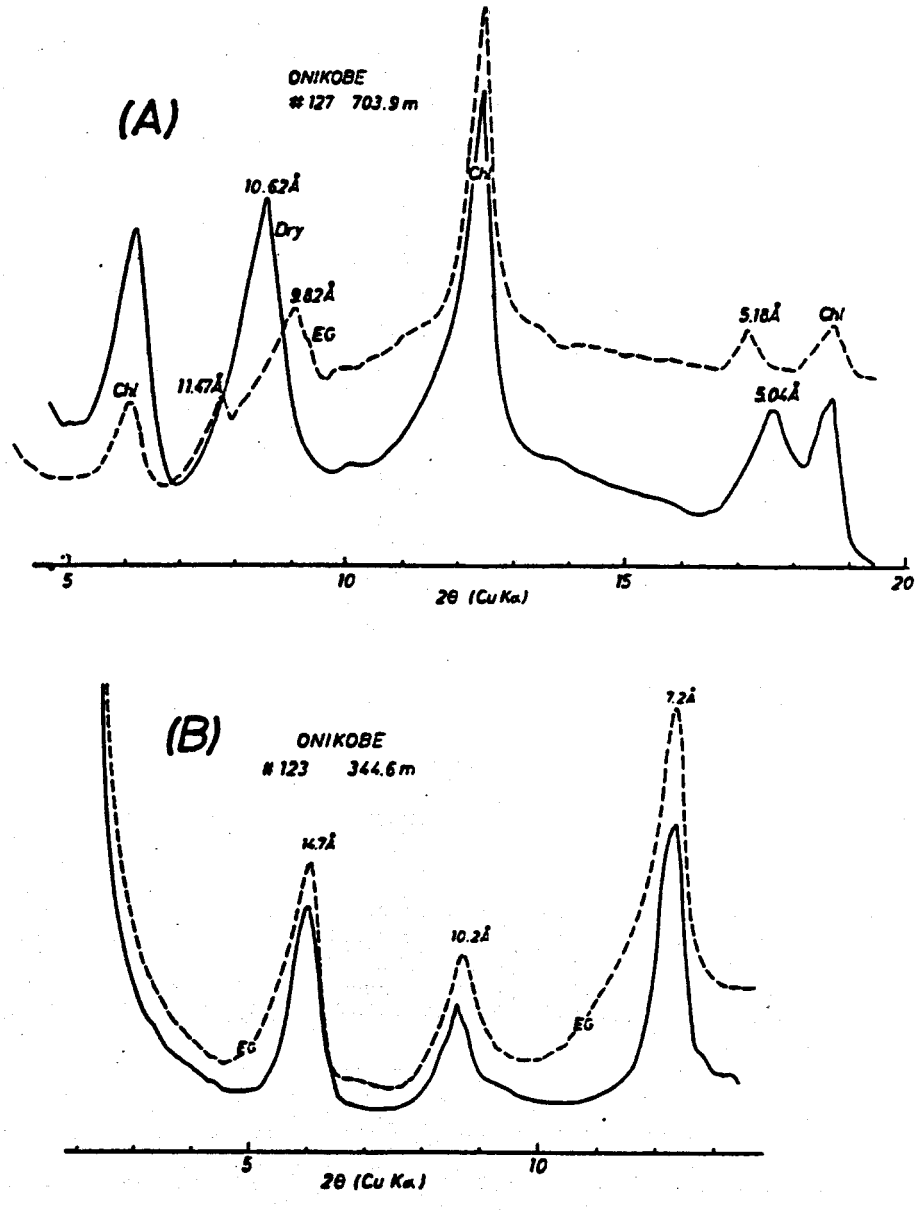

Figure 27. X-ray diffraction diagrams of (A) illite/smectite interstratified mineral associated with chlorite (#127, 703.9m), and (B) chlorite and sericite (#123, 344.6m) from the Onikobe geothermal area, Japan. Solid line: at dry condition; Broken line: after ethylene glycol treatment.

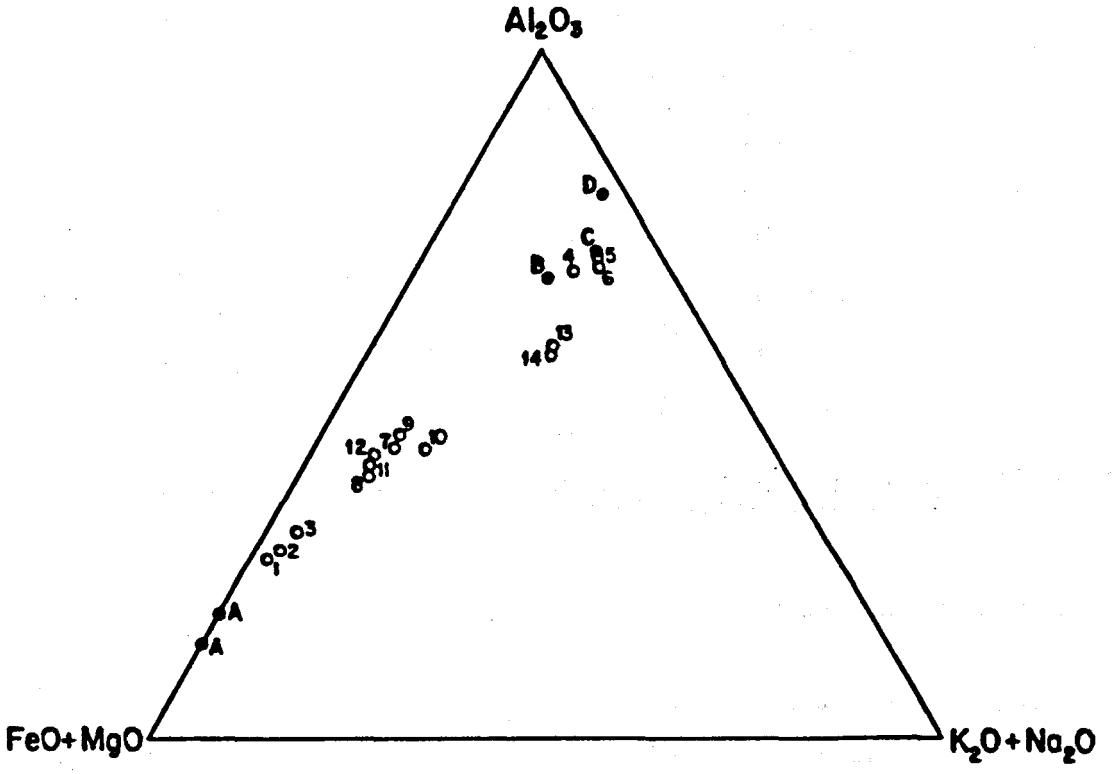

Figure 28. Al_2O_3-(FeO + MgO) - (K_2O + Na_2O) diagram showing compositions of analyzed illitic clay minerals from drill hole cores of the Onikobe geothermal area. A: "Saponite" (Trioctahedral smectite) (Yoshimura et al., 1975): B: Illite/saponite interstratified mineral (Sato et al., 1975); C: sericite (Higashi and Shirozu, 1975); D: Illite (Shimoda and Nishiyama, 1973).

(4) the analyzed compositions as shown in Figure 28 lie between those of smectite and illite with possible paired substitution of (FeO + MgO) $\rightleftharpoons$ Al_2O_3 + (K_2O + Na_2O). Such coupled substitution and increasing illite component in the illite/smectite interstratified minerals can be correlated with depth, and hence temperature of formation. Figure 29 is a plot of K concentration as a function of depth for illitic clays from holes #123 and 127. The proportion of illite making up these minerals appears to generally increase with depth. Similar observations have been made by Hower et al. (1981) from burial metamorphic sequences and from other geothermal areas.

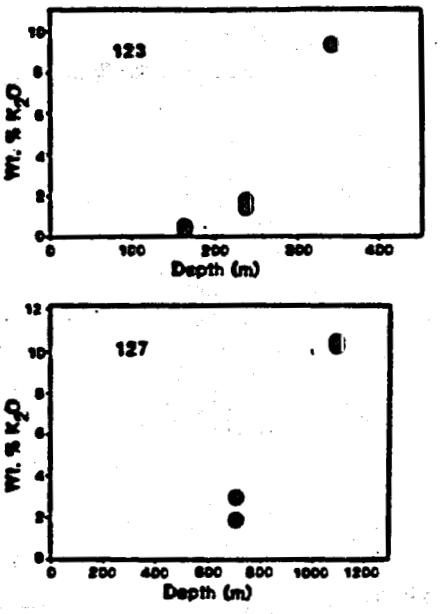

Figure 29. Plot of K_2O wt % in illitic clay minerals from some core samples of #123 and #127 as a function of depth.

A New X-ray Method to Estimate Smectite % in Illite/Smectite Interstratified Minerals

Determination of smectite content in illite/smectite interstratified minerals by X-ray diffraction data has been studied by Weaver (1956). He presented a relationship between percentage of the expandable layer and the basal spacing after ethylene glycol treatment. His method has been commonly used. For instance, Steiner (1977) estimated the % of smectite layer in illitic clay minerals in the Wairakei geothermal area and showed a decrease of smectite layer % with increasing temperature conditions. He divided illitic clay minerals in the Wairakei geothermal area into three groups: high d_{001} (10.40-11.78Å) group, intermediate d_{001} (10.28-10.40Å) group and low d_{001} (9.93-10.28Å) group, respectively, with high, intermediate, and low content of smectite layers in the interstratified minerals. Hower and Mowatt (1966) showed that the d_{001} spacing of sericite/smectite interstratified minerals under dry conditions generally increases with increasing smectite layer %. They also showed that the separation of the (001) (9-10Å) and (002)(5-6Å) peaks in 2θ (Cukα) values for these minerals after ethylene

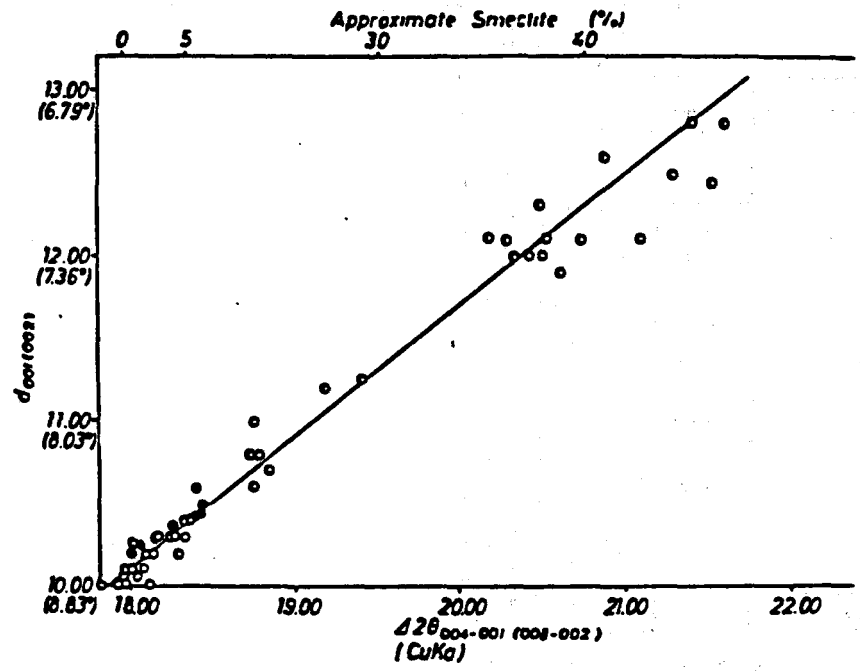

Figure 30. $\Delta 2\theta_{004-001}$ vs. d_{001} relations of sericite/smectite interstratified minerals. Open circles: published data from the Salton Sea geothermal area and the Gulf Coast (Hower et al., 1976); closed circles: clay minerals from the Onikobe geothermal area, Japan.

glycol treatment decreases with increasing content of interstratified smectite layer.

Based on the X-ray method proposed by Hower and Mowatt (1966), McDowell and Elders (1980) found that the smectite layer % in the sericite/smectite interstratified minerals from the Salton Sea geothermal field of California decreases with increasing depth and temperature. The relationships are listed below:

Depth	Temperature	% of Smectite Layer
412m	185-190°C	10-15 %
494m	210°C	5 %
620m	250°C	0-5 %
725m	275°C	0 %
1135m	325°C	0 %

Table 41. Types and K_2O of original rocks and occurrence of illitic clay minerals from Iceland, Onikobe, Hakone, Matsukawa, Otake, Wairakei and Steamboat Springs geothermal areas.

Geothermal area	Type of original rocks	K_2O in original rocks (wt.%) Range	Average	Occurrence of illitic clays
Iceland (1)	Basaltic	0.08 - 0.26	0.18	no or extremely rare
Onikobe (2)	Andesitic	0.15 - 1.88	0.67	not common
Hakone (3)	Andesitic	0.56 - 0.70	0.64	not common
Matsukawa (4)	Dacitic	0.79 - 1.20	1.00	common
Otake (5)	Andesitic	0.45 - 2.41	1.68	common
Wairakei (6)	Rhyolitic	2.0 - 3.6	2. 7	very common
Steamboat (7) Springs	Trachytic - granodiorite	2.2 - 3.2	2. 7	very common

(1) Björnsson et al., (1970), Kristmannsdóttir (1975a)
(2) Seki et al., (1969), Katsui (1955), This paper
(3) Kuno (19)
(4) Sumi (1968), Sumi and Maeda (1973)
(5) Hayashi (1973), Hayashi and Yamasaki (1975)
(6) Steiner (1977)
(7) Sigvaldson and White (1961, 1962), Schoen and White (1965, 1967)

Hower et al., (1976) studied Oligocene-Miocene core samples from a drill-hole (5776m) on the U.S. Gulf Coast and found that the smectite layer % in sericite/smectite interstratified minerals decreases from about 85% to about 20% with increase in depth and temperature. Figure 30 plotted their data from the Salton Sea geothermal area and the Gulf Coast. A similar diagram has been constructed by Boles and Franks (1979) to show the mineralogical change which occurred during the diagenesis of a 4650m thick Eocene sandstone formation in Texas.

Shirozu et al. (1972) proposed a method to estimate the amount of smectite layer interstratified with sericite by measurement of the peak width of the 10-12Å reflection at half height and of the peak position of 10-12Å reflection. Sato (1973) modified Weaver's diagram and found that the basal reflection of the sericite/smectite interstratified minerals with greater than 40% smectite layer separates into two peaks of

8.5-10Å and 16-17Å. Watanabe (1980) confirmed the finding by theoretical calculation; the difference in 2θ between the two peaks after ethylene glycol treatment increases with increase in the smectite layer. Watanabe (1981) recently proposed another diagram to identify the type of sericite/smectite interstratified minerals from X-ray powder data; the diagram indicates that the smectite layer % can be inferred from the difference in 2θ (CuKα) values of the two peaks between 9-10° and 16-17° after ethylene glycol treatment. A similar method has been proposed by Spodon (1980).

The d_{001} values under dry conditions and after ethylene glycol treatment are useful to estimate the smectite % in the sericite/smectite interstratified minerals. However, as has been shown by Steiner (1977), the d_{001} of illitic clays with less than 10-20% smectite layer does not expand but apparently shrinks after ethylene glycol treatment (Table 39). Such shrinkage must be due to the interference of the 002 reflection of the glycolated smectite layer (8.9Å) with the 001 reflection of sericite at about 10Å (Higashi, 1980).

As discussed above, several methods have been used to estimate the smectite % in the sericite/smectite interstratified clays by means of the measurement of the 2θ difference between two peaks. However, it is difficult to locate these two peaks with confidence, particularly in the samples where the illitic clays are associated with other minerals such as smectite, chlorite/smectite interstratified minerals, discrete illite and zeolites.

The d_{001} and d_{004} values of illitic clays progressively increase and decrease respectively with the increase of the proportion of interstratified smectite layer (Higashi, 1980). The shift of the 10Å peak representing d_{001} to a lower 2θ value must be due to the interference of the (001) reflection of smectite (14-15Å) with the (001) reflection of sericite (10.0Å). The shift of the 3Å peak representing d_{004} to a higher 2θ value is due to the interference of the (005) reflection of smectite (2.9-3.0Å) with the (005) reflection of sericite (3.3Å).

As shown in Figure 30, the difference in 2θ (CuK_α) between d_{004} (dry) and d_{001} (dry) for the sericite/smectite interstratified minerals increases with the increase of smectite layer. When illitic clay minerals are separated from quartz and feldspar,

reliable peak separation between $2\theta_{004}$ and $2\theta_{001}$ can be obtained. The data for the illitic clays from the drill hole core #127 in the Onikobe geothermal area are plotted in Figure 30; the results indicate that the smectite content in the interstratified illitic clays is less than 10 percent.

Occurrence of Illitic Clay and Chemical Composition of Original Rocks

It has been proposed that illite/smectite interstratified minerals and illite found at depth in geothermal areas were formed chiefly by K-metasomatism (addition of K to rocks from the fluid phase) (Steiner, 1968, 1977; Hower, et al., 1976). Steiner (1968) proposed the following sequence of hydrothermal alteration of silicic glass to illitic clay: silicic volcanic glass → Ca-smectite → sericite/smectite interstratified mineral → sericite. He concluded that the most significant factor in forming illitic clay minerals is a high mK^+/mH^+ and a low mNa^+/mK^+ ratio in the geothermal fluid. The alteration of plagioclase to illitic clays is less common but was also observed in the Wairakei geothermal area (Steiner, 1977). The introducion of K from thermal water to form illitic clays seem to be a salient chemical feature of hydrothermal alteration at Wairakei. In the Steamboat Springs geothermal area of Nevada, illite/smectite interstratified minerals are also common (Sigvaldason and White, 1962; Schoen and White, 1965, 1967). The illitic clays appear to be stable phases in most of the altered drill hole rocks in this geothermal field. Schoen and White (1965) suggested that the mK^+/mH^+ ratio of the thermal waters must be high at depth. Similarly, in the Matsukawa and Otake geothermal areas of Japan, illitic clay minerals are common (Sumi, 1968; Sumi and Maeda, 1973; Hayashi, 1973; Hayashi et al., 1978) and have been found in many more bore-hole cores than in the Onikobe and Hakone geothermal areas. On the other hand, in Icelandic geothermal areas, illitic clay minerals are either absent or present in only extremely small amounts in hydrothermally altered rocks at shallow depth, and no K-mica or K-feldspar occurs at depth. (Tómasson and Kristmannsdóttir, 1972; Arnórsson et al, 1978). The major changes in the altered basaltic rocks are hydration and oxidation, and enrichment of SiO_2 in a few samples (Kristmannsdóttir, 1975a).

Table 41 lists the type and K_2O content of original rocks and the occurrence of illitic clay minerals in geothermal areas of Iceland, Onikobe, Hakone, Matsukawa, Otake, Wairakei and Steamboat Springs. Examination of these data makes it apparent that a close correlation exists between the occurrence of illitic clays and the type and K_2O contents of original rocks. Although the addition of some K_2O from geothermal waters may be significant for the formation of illitic clays, lithological characteristics, especially the K_2O content of original rocks, must be the important factors that determine the abundance of illitic clay minerals in rocks of a geothermal system.

Zeolite Minerals

Zeolite minerals are well developed in the core samples from the Onikobe geothermal area. Some calcium zeolites are exceptionally abundant in some samples and they are easily identified by petrographic microscope; such common zeolites include mordenite, laumontite, yugawaralite and wairakite. Their zonal depth distribution in #GO-2, GO-5, GO-7 and GO-8 of this geothermal area has been described by Seki, Onuki et al. (1969). Similar plots for these and other drill holes are shown in Figure 31. Apparently, with increasing depth (hence temperature), the zeolite present varies from mordenite → laumontite → yugawaralite → wairakite. Details of such variations will be discussed later.

In addition to those common zeolites, clinoptilolite, dachiardite, chabazite, thomsonite and natrolite were also identified. They are very minor in quantity and occur sporadically in some samples. These zeolites are not described below.

Mordenite $((Na_2,K_2,Ca)Al_2Si_{10}O_{24} \cdot 7H_2O)$: Mordenite is the most common zeolite at shallow depths from the drill core samples. It characteristically occurs at depths of less than 200 meters and is most commonly found between depths of about 50 to 150 meters, depending on the geothermal gradient. It is commonly associated with clinoptilolite; optical distinction between them is difficult. Mordenite occurs as radial fan-like or spherulitic aggregates of fine prismatic crystals in veins or vesicles.

Unfortunately, no mordenite was found in core samples from drill holes #123, 124 and 127. Therefore, no microprobe analysis of mordenite was obtained. Mordenite usually contains abundant SiO_2 (e.g. 65-67 wt%) and varies significantly in terms of Ca, Al and

Figure 31. Distribution of zeolites (mordenite, clinoptilolite, laumontite, yugawaralite and wairakite) as a function of depth for drill holes P-5(a), P-7(b), P-8(c), P-10(d), #123(e), #124(f), #127(g), GO-7(h), GO-8(i), GO-10(j) and GO-11(k).

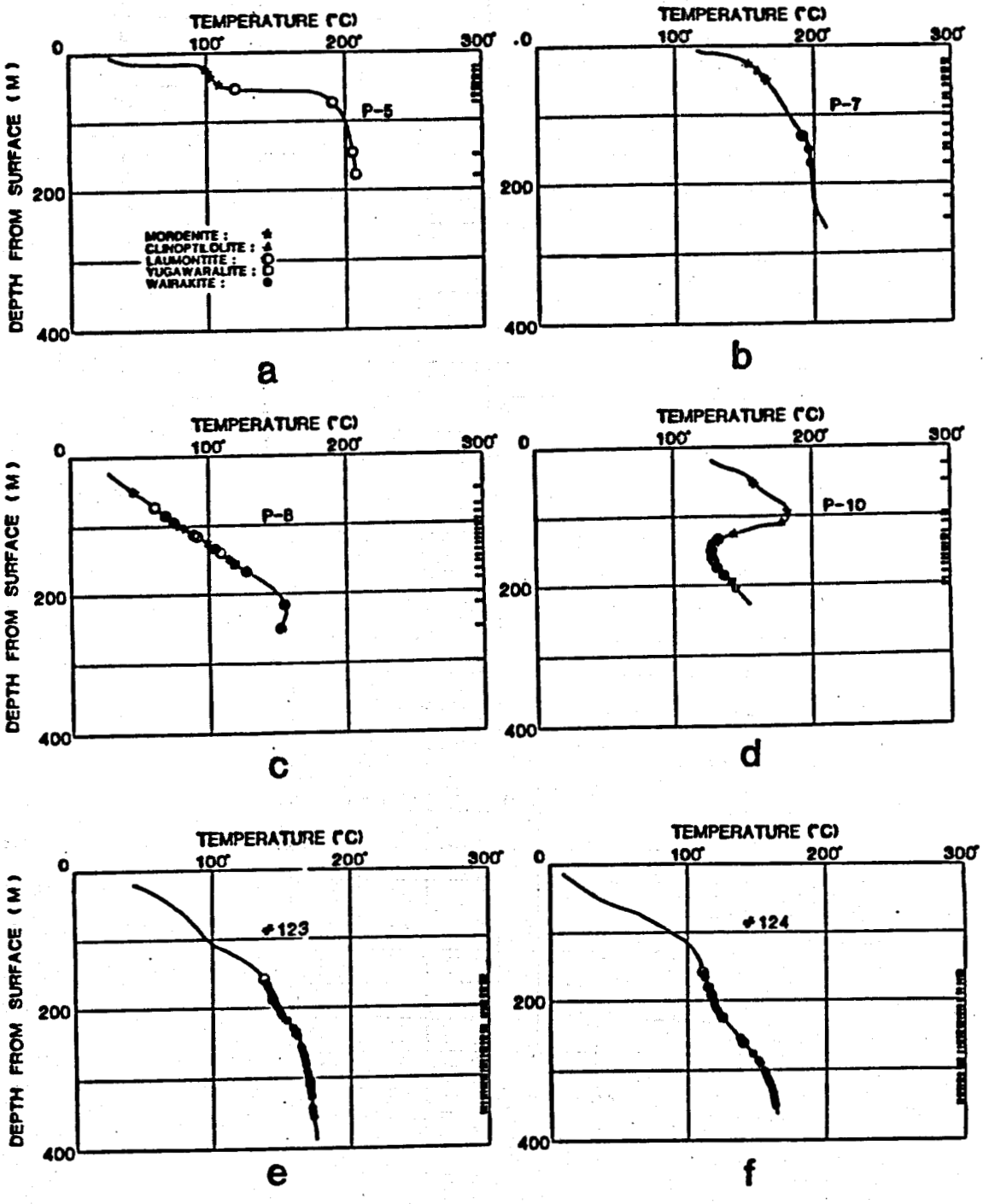

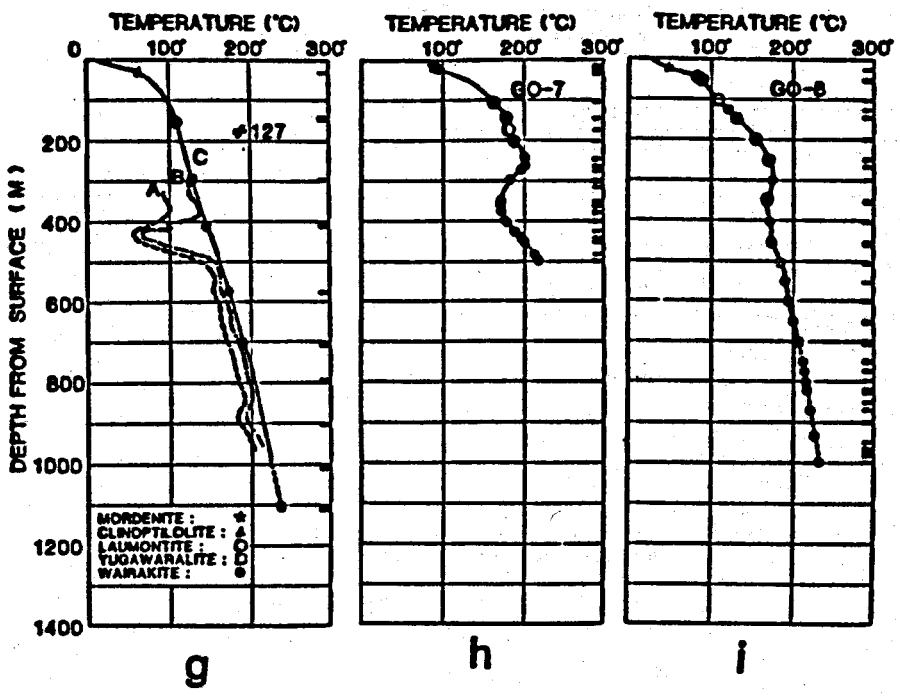
TEMPERATURE (°C)
0
100°
200°
300°
DEPTH FROM SURFACE (M)
200
400
600
800
1000
1200
1400
#127
C
B
A
MORDENITE :
CLINOPTILOLITE :
LAUMONTITE :
YUGAWARALITE :
WAIRAKITE :
GO-7
GO-8
g
h
i

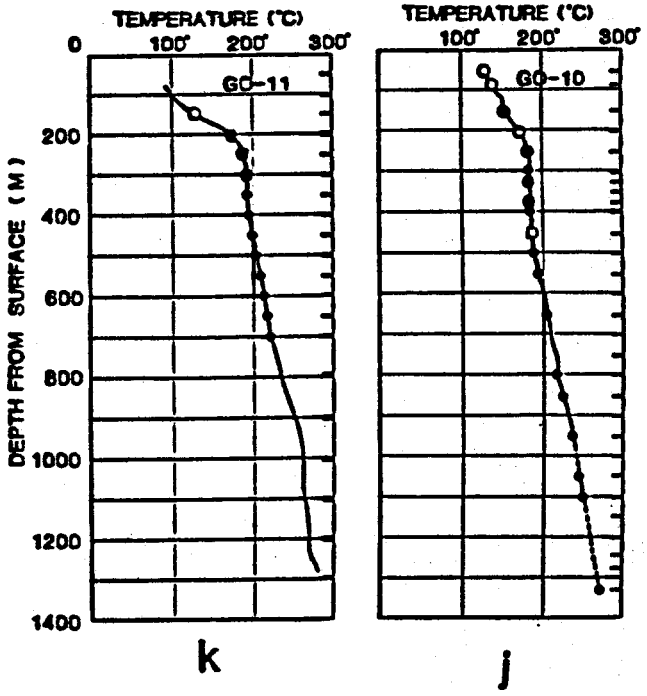
TEMPERATURE (°C)
0
100°
200°
300°
DEPTH FROM SURFACE (M)
200
400
600
800
1000
1200
1400
GO-11
GO-10
k
j

Table 42. Chemical analyses of laumontites and yugawaralite in drill hole core samples from the Onikobe geothermal area, Japan.

	Laumontite			Yugawaralite	
Sample No.	124 - 201.8m	124 - 222.8m	124 - 259.9m	124 - 201.8m	123 - 184.7m
SiO_2	53.13	53.38	53.91	61.53 - 60.23	61.06 - 61.47
Al_2O_3	21.88	21.79	22.61	17.29 - 17.89	15.72 - 16.22
Fe_2O_3*	0.03			0.05	0.06 - 0.06
CaO	11.31	11.25	11.63	9.04 - 9.58	8.62 - 8.81
K_2O	0.18	0.08	0.08	0.09 - 0.07	0.05 - 0.04
Na_2O	0.13	0.12	0.20	0.29 - 0.12	0.35 - 0.32
Anhydrous Total	86.66	86.61	88.43	88.27 - 87.89	85.86 - 86.92

*Total Fe as Fe_2O_3

Table 43. Chemical compositions of laumontite and wairakite separated from bore-hole cores of GO-7, Onikobe, Japan (Seki, Onuki et al., 1969).

	Laumontite GO-7, 108.4m	Wairakite GO-7, 397.6m
SiO_2	50.97	54.91
TiO_2	0.03	0.01
Al_2O_3	21.50	22.75
Fe_2O_3	0.10	0.64
FeO	0.11	0.44
MnO	0.02	0.01
MgO	tr.	0.23
CaO	12.22	11.69
Na_2O	0.28	0.60
K_2O	0.10	0.31
H_2O^+	14.11	8.23
H_2O^-	0.18	0.19
Total	99.72	100.01

K (e.g., Seki, 1973a).

Laumontite ($CaAl_2Si_4O_{12}\cdot 4H_2O$): Laumontite is typically found at depths greater than 50 m and shallower than 200-400 m and occurs in all eleven of the bore-hole cores studied from Onikobe. It occurs as either a vein or amygdule mineral or replacing plagioclase phenocrysts and glassy groundmass; it often takes the form of a sub-parallel lath aggregate. Because laumontite was relatively uncommon in samples from drill holes #123, 124, and 127, only a few microprobe analyses were obtained: the results are listed in Table 42. The samples analyzed from hole #124 were quite pure in composition, containing only very minor Fe_2O_3, Na_2O and K_2O. Chemical compositions of laumontites separated by heavy liquid and analyzed by wet chemical method have been reported and are shown in Table 43. The probe data contain considerably higher SiO_2 and lower CaO than the wet chemical data.

Yugawaralite ($CaAl_2Si_6O_{16}\cdot 4H_2O$): Yugawaralite has been found in six of the eleven suites of core samples. It is typically found in only one or two samples per hole, varying in depth from the shallowest occurrence in P-8 at 156.25 m to the deepest occurrence in GO-8 at 701.5m. It is most commonly found as a blocky vein mineral at the lower end of the laumontite zone and at the upper part of the wairakite zone. Four microprobe analyses are listed in Table 42; they are very close to the Ca end-member composition, containing only very minor amounts of Fe_2O_3, Na_2O and K_2O.

Wairakite ($(Ca,Na_2)Al_2Si_4O_{12}\cdot 2H_2O$): Wairakite is the most abundant zeolite mineral in the Onikobe drill-hole core samples. It occurs in most wells beginning at depths of 100-150 m and extending to the bottom of the holes. The one noticeable exception to this statement is hole GO-11, where wairakite is present between 203 and 701 m depth, but is absent from 791 to 1300 m. Wairakite most commonly occurs as a vein mineral, often filling the core of veins lined with either anhedral or euhedral quartz. It is also found as amygdule fillings, replacing plagioclase, and replacing fine-grained matrix. In all of these occurrences it exhibits typical very low birefringence and often shows cross-hatched twinning.

Wairakites of various occurrences from many core samples were analyzed for their major components (SiO_2, Al_2O_3, Na_2O, CaO, Fe_2O_3 and K_2O)(Tables 43, 44). For

Table 44. Chemical analyses of wairakites in drill hole core samples from the Onikobe geothermal area, Japan.

Sample No.	124 - 165.6m	124 - 201.8m	124 - 222.0m	124 - 254.4m	124 - 259.9m	124 - 288.5m		124 - 307.5m
	vein	vein		along vein	vein	vein	repl. plag.	vein
SiO_2	55.97 - 55.68	55.04 - 54.40	55.41 - 55.74	54.79 - 56.45	55.70 - 56.31	56.60 - 55.64	55.94 - 52.73	56.01 - 55.76
Al_2O_3	22.53 - 22.64	22.09 - 23.40	22.66 - 22.94	23.02 - 22.46	23.38 - 22.21	22.91 - 22.96	22.53 - 22.79	22.21 - 21.77
Fe_2O_3*	0.02 - 0.00	0.02 - 0.02	—	0.17 - 0.05		0.08	0.18 - 0.19	0.10 - 0.05
CaO	11.16 - 11.34	9.58 - 12.56	11.23 - 10.61	11.50 - 10.45	11.90 - 9.90	11.09 - 12.48	11.53 - 11.78	10.83 - 9.54
K_2O	0.06 - 0.05	0.07 - 0.05	0.02 - 0.11	0.02 - 0.06	0.03 - 0.03	0.07 - 0.06	0.08 - 0.09	0.05 - 0.08
Na_2O	1.45 - 1.19	2.82 - 0.31	1.20 - 1.73	0.83 - 1.88	0.75 - 2.41	1.53 - 0.48	0.59 - 0.84	1.90 - 2.22
Anhydrous Total	91.19 - 90.90	89.61 - 90.76	90.53 - 90.92	90.13 - 91.35	91.84 - 90.86	90.27 - 89.42	89.85 - 88.41	89.90 - 89.42
Si	4.066 - 4.076	4.072 - 3.981	4.052 - 4.055	4.023 - 4.088	4.023 - 4.099	4.015 - 3.975	4.023 - 3.968	4.108 - 4.118
Al	1.929 - 1.944	1.926 - 2.018	1.953 - 1.967	1.992 - 1.917	1.987 - 1.905	1.985 - 2.013	1.981 - 2.021	1.920 - 1.895
Fe^{+3}	0.001	0.001 - 0.001		0.009 - 0.003		0.004	0.010 - 0.011	0.006 - 0.003
Ca	0.989 - 0.883	0.759 - 0.995	0.888 - 0.811	0.905 - 0.811	0.920 - 0.772	0.874 - 0.993	0.921 - 0.959	0.708 - 0.735
Na	0.204 - 0.168	0.405 - 0.044	0.170 - 0.244	0.098 - 0.264	0.105 - 0.348	0.218 - 0.069	0.085 - 0.123	0.213 - 0.218
K	0.005 - 0.006	0.007 - 0.005	0.002 - 0.010	0.002 - 0.006	0.003 - 0.003	0.007 - 0.006	0.009 - 0.009	0.005 - 0.008
Or	11	14	15	16	14	11	12	11	10	10	20	6	8	11	21	30
An	89	86	85	84	86	77	91	75	90	89	80	94	92	89	79	70

Sample No.	124 - 330.7m	
	vein	repl. plag.
SiO_2	55.78 - 55.07	54.54 - 54.98
Al_2O_3	21.26 - 22.45	22.38 - 22.27
Fe_2O_3*	0.81 - 0.15	0.33 - 0.36
CaO	9.78 - 11.78	11.98 - 11.68
K_2O	0.08 - 0.06	0.06 - 0.06
Na_2O	2.51 - 0.77	0.59 - 0.73
Anhydrous Total	89.35 - 90.48	89.88 - 90.06
Si	4.131 - 4.075	4.052 - 4.068
Al	1.856 - 1.956	1.923 - 1.932
Fe^{+3}	0.000	0.018 - 0.020
Ca	0.770 - 0.915	0.937 - 0.921
Na	0.360 - 0.109	0.084 - 0.104
K	0.008 - 0.006	0.006 - 0.006
Or	44	37	92	98
An	32	11	8	10

Table 44 . (Continued)

Sample No.	127 - 133.4m		127 - 297.5m		127 - 409.7m		127 - 577.2m		127 - 578.1m	
	vein		Cracks in pyroxene		Surrounding Alt. Plag.		vein		Cracks in Anorthite Megacryst	
SiO_2	53.56 - 54.38		54.45 - 54.92		53.93 - 54.68		54.84 - 55.09		54.15 - 54.67	
Al_2O_3	23.13 - 22.96		20.78 - 20.32		21.16 - 20.65		23.84 - 21.68		22.39 - 21.90	
Fe_2O_3*	0.07 - 0.06		0.08 - 0.03		0.06 - 0.08		0.03 - 0.01		0.13 - 0.00	
CaO	12.20 - 11.85		10.65 - 10.77		12.08 - 10.92		12.66 - 11.35		11.24 - 10.64	
K_2O	0.06 - 0.05		0.07 - 0.06		0.06 - 0.06		0.02 - 0.04		0.06 - 0.07	
Na_2O	0.34 - 0.90		1.35 - 1.58		0.36 - 1.46		0.39 - 1.42		0.15 - 1.81	
Anhydrous Total	89.36 - 90.40		87.58 - 87.71		87.62 - 87.83		89.98 - 89.40		89.32 - 88.09	
Si	3.979 - 4.008		4.118 - 4.147		4.079 - 4.124		3.988 - 4.087		4.046 - 4.086	
Al	2.025 - 1.987		1.832 - 1.808		1.886 - 1.836		2.004 - 1.879		1.989 - 1.894	
Fe^{+3}	0.004 - 0.003		0.005 - 0.002		0.002 - 0.005		0.002 - 0.001		0.007 —	
Ca	0.971 - 0.932		0.862 - 0.871		0.980 - 0.882		1.001 - 0.902		0.900 - 0.852	
Na	0.049 - 0.128		0.227 - 0.233		0.053 - 0.214		0.027 - 0.204		0.217 - 0.262	
K	0.006 - 0.005		0.007 - 0.006		0.004 - 0.004		0.002 - 0.004		0.006 - 0.007	
Or	93	88	79	79	93	80	97	82	81	76	94	79	98	85
An	5	12	21	21	5	20	3	18	19	24	2	21	2	15

Sample No.	127 - 1103.6m		127 - 1105.5m	123 - 138.9m		123 - 165.1m	123 - 230.6m		
	vein		alt. lithic fragment	vein	vein	vein	in Plag.		cavity filling
SiO_2	55.32 - 56.08		55.97	53.95 - 55.81	53.53 - 53.43	54.36	54.81 - 52.92		54.58 - 55.48
Al_2O_3	22.62 - 22.40		23.67	21.44 - 21.87	21.30 - 21.41	23.89	22.44 - 23.47		22.71 - 22.12
Fe_2O_3*	0.04 - 0.04		0.16	0.53 - 0.18	1.20 - 1.25	0.04	0.03 - 0.06		0.00 - 0.01
CaO	11.74 - 11.14		11.56	10.84 - 10.24	10.93 - 10.58	12.03	11.29 - 12.45		11.14 - 10.59
K_2O	0.07 - 0.16		0.09	0.05 - 0.05	0.06 - 0.04	0.05	0.06 - 0.08		0.07 - 0.08
Na_2O	0.76 - 1.18		0.98	1.22 - 1.97	1.09 - 1.22	0.40	1.03 - 0.53		1.25 - 1.72
Anhydrous Total	90.55 - 91.80		92.23	88.03 - 88.52	88.11 - 87.93	90.17	89.76 - 89.51		89.75 - 90.00
Si	4.047 - 4.079		4.022	4.066 - 4.116	4.043 - 4.041	4.009	4.051 - 3.937		4.031 - 4.081
Al	1.950 - 1.920		1.988	1.904 - 1.858	1.896 - 1.908	2.000	1.931 - 2.058		1.977 - 1.916
Fe^{+3}	0.002 - 0.002		0.009	0.030 - 0.010	0.068 - 0.071	0.002	0.002 - 0.003		— —
Ca	0.920 - 0.868		0.890	0.875 - 0.821	0.885 - 0.857	0.947	0.892 - 0.992		0.881 - 0.835
Na	0.108 - 0.166		0.137	0.178 - 0.286	0.160 - 0.179	0.057	0.147 - 0.076		0.179 - 0.245
K	0.007 - 0.015		0.008	0.005 - 0.005	0.006 - 0.004	0.005	0.006 - 0.008		0.007 - 0.008
Or	89	84	87	83	74	85	83	94	86	93	83	77
An	11	16	13	17	26	15	17	6	14	7	17	23

Sample No.	123 - 303.5m		123 - 323.6m			123 - 344.6m			123.348.9m		
	vein		oval altered patch	amygdule core	amygdule rim	vein		alt. Plag. Phene.		repl. matrix	vein
SiO_2	54.93 - 55.18		53.19 - 54.16	53.87	53.86	54.26 - 54.33		53.54 - 53.69	55.07 - 55.31		54.90
Al_2O_3	22.17 - 21.90		21.85 - 21.33	21.27	21.14	22.04 - 21.40		22.00 - 22.09	23.34 - 23.84		23.19
Fe_2O_3*	0.03 - 0.01		0.04 - 0.04	0.17	0.26	0.17 - 0.29		0.04 - 0.02	0.04 - 0.07		0.03
CaO	11.34 - 10.14		12.42 - 10.86	11.71	10.71	11.61 - 11.17		12.43 - 12.11	12.21 - 11.65		12.37
K_2O	0.07 - 0.07		0.05 - 0.07	0.05	0.09	0.06 - 0.07		0.04 - 0.05	0.05 - 0.07		0.04
Na_2O	0.73 - 1.88		0.24 - 1.57	0.85	1.88	0.94 - 1.36		0.16 - 0.57	0.29 - 1.30		0.24
Anhydrous Total	89.27 - 89.18		87.79 - 88.23	87.92	87.96	89.08 - 88.62		88.23 - 88.33	91.00 - 91.44		90.97
Si	4.089 - 4.092		4.024 - 4.071	4.067	4.071	4.063 - 4.071		4.027 - 4.026	4.009 - 4.017		4.003
Al	1.936 - 1.914		1.948 - 1.908	1.893	1.885	1.945 - 1.890		1.930 - 1.932	2.003 - 1.972		1.993
Fe^{+3}	0.002 - 0.001		0.002 - 0.002	0.010	0.015	0.010 - 0.016		0.002 - 0.001	0.002 - 0.004		0.002
Ca	0.900 - 0.806		1.007 - 0.875	0.947	0.867	0.932 - 0.897		1.003 - 0.973	0.932 - 0.907		0.982
Na	0.105 - 0.270		0.035 - 0.229	0.124	0.276	0.136 - 0.198		0.023 - 0.083	0.041 - 0.183		0.034
K	0.007 - 0.007		0.005 - 0.007	0.005	.009	0.005 - 0.007		0.004 - 0.005	0.005 - 0.006		0.004
Or	90	75	97	79	88	76	87	82	98	92	96	83	97
An	10	25	3	21	12	24	13	18	2	8	4	17	3

*Total Fe as Fe_2O_3

Figure 32. Compositional variations of analyzed wairakites from the Onikobe geothermal area, Japan plotted in Wa-Ab'-Nat' diagram of Seki and Oki (1969). (A) all analyses from cores #123, 124 and 127. Core-rim compositions of wairakites from cores #123 (B), #124 (C) and #127 (D).

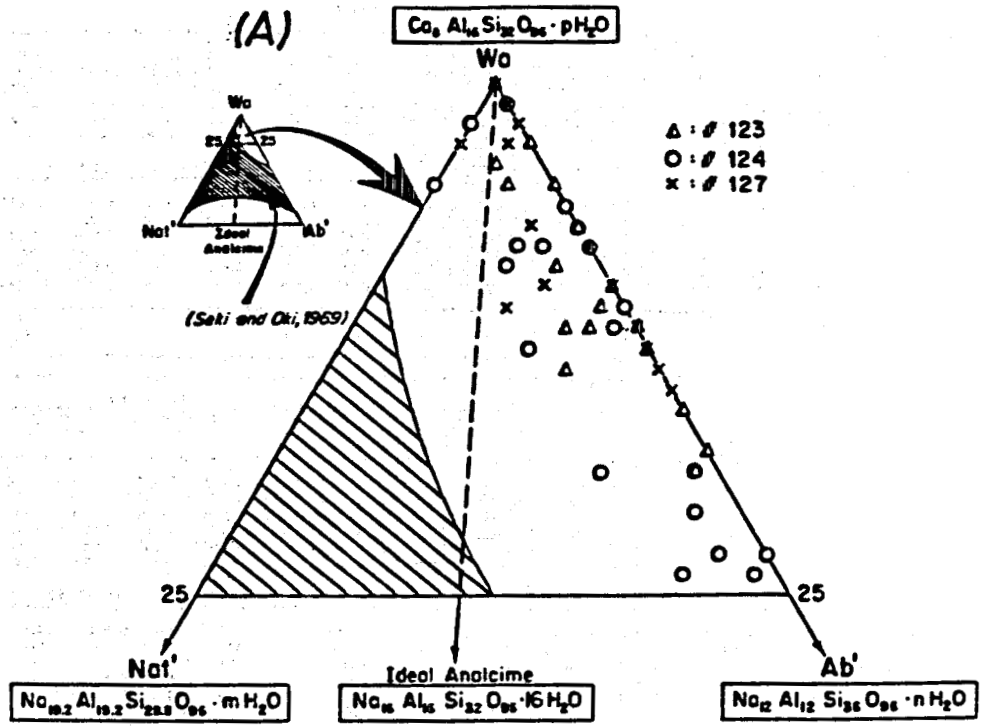

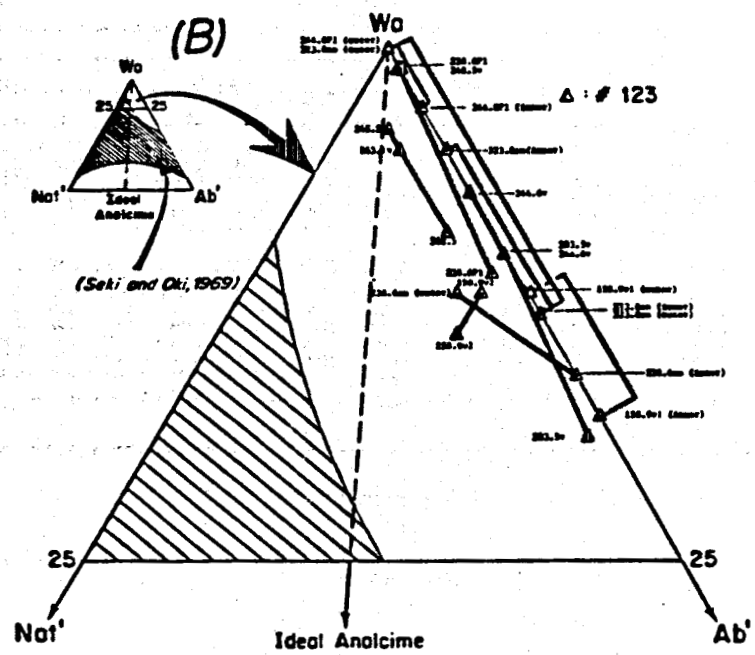

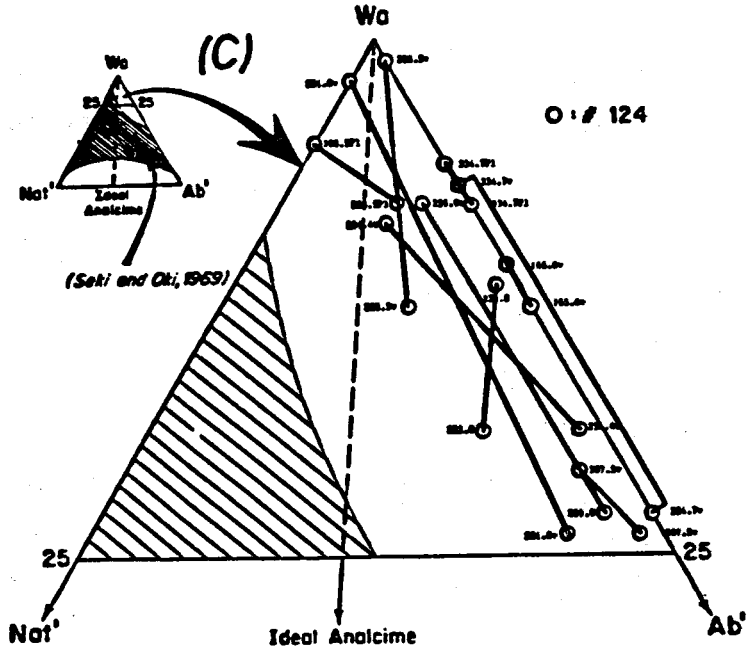
(C)
Wo
25
25
Nat'
Ab'
Ideal Analcime
(Seki and Oki, 1969)
O : # 124
Wo
25
25
Nat'
Ideal Analcime
Ab'

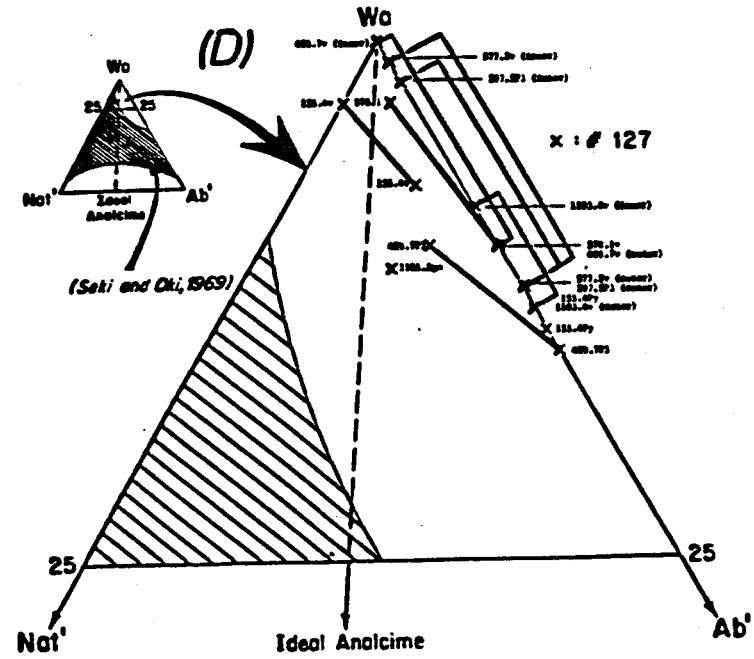
(D)
Wo
25
25
Nat'
Ab'
Ideal Analcime
(Seki and Oki, 1969)
x : # 127
Wo
25
25
Nat'
Ideal Analcime
Ab'

each sample, at least 3 crystals and 15 spot analyses were obtained. Considerable ranges of their compositions were found. Characteristically, most analyzed wairakites contain less than 0.2 wt % Fe_2O_3 as total Fe and 0.1 wt % K_2O. Some wairakite analyses (e.g., 123-158.9 m) have over 0.5 wt % Fe_2O_3 and concomitantly lower SiO_2 and Al_2O_3 contents. Such relations suggest that some Fe^{+3} substitution for Al to Si in tetahedral sites may be significant for some wairakites. Wairakite and analcime have been shown to form a solid solution series with a possible gap at intermediate compositions (Seki and Oki, 1969). Furthermore, such solid solutions exhibit a variable Al to Si ratio. In order to illustrate the range of compositions found at Onikobe, compositions obtained by electron microprobe analysis were plotted on a wairakite ($Ca_8Al_{16}Si_{32}O_{96} \cdot pH_2O$), natrolite' ($Na_{19.2}Al_{19.2}Si_{28.8}O_{96} \cdot mH_2O$), albite' ($Na_{12}Al_{12}Si_{36}O_{96} \cdot nH_2O$) triangular diagram as developed by Seki and Oki (Figure 32). The two extreme analyses for each type of occurrence (vein, amygdule, etc.) within each depth sample are connected by a line. All analyzed wairakites from holes # 123, 124 and 127 range from Wr_{100} to Wr_{76} and contain no more than 5% Nat' component. No analcime-rich compositions were found in any samples analyzed by electron microprobe. In general, there appears to be no correlation between composition of wairakite and depth of sample, nor any pattern between composition and mode of occurrence (i.e., vein, amygdule, etc.). The only trend observed was within vein minerals from hole #127. Analyzed cores of four veins showed a higher proportion of the wairakite component than did the rims. Assuming that growth occurred from the vein walls inward, this might suggest an increase of temperature with time during the deposition of the wairakite. The low Al to Si ratios seen in these analyses relative to a wairakite-ideal analcime series are consistent with that seen by Seki (1971) and Steiner (1955).

Prehnite

Prehnite sporadically occurs as fine-grained aggregates after plagioclase, discrete patches in matrix and vesicles, or as veins of variable thickness. In most samples, only a few patches of prehnite aggregates were found; thus, the occurrence of prehnite listed in Tables 10-20 may not be representative. Some core samples may contain prehnite but thin

Table 45. Chemical analyses of prehnite in drill hole core samples from the Onikobe geothermal area, Japan.

Sample No.	124 - 165.6m (amygdule)	124 - 201.8m (vein)	124 - 201.8 (amygdule)	124 - 209.9 (repl. matrix)	124 - 334.7m (repl. plag.)	124 - 349.4m (amygdule)	127 - 297.5m (vein)	123 - 303.5m (repl. matrix)	123 - 348.9m (vein)
SiO_2	43.36 - 43.47	44.45 - 44.44	43.30	43.06 - 42.98	43.62	44.29 - 43.4	43.54 - 43.20	42.58	42.69
Al_2O_3	21.06 - 20.08	23.31 - 23.14	22.46	19.69 - 18.76	21.40	23.49 - 23.9	23.26 - 21.06	19.00	21.80
Fe_2O_3*	5.27 - 6.29	1.06 - 1.20	3.00	6.51 - 8.13	4.47	1.26 - 1.00	0.03 - 2.25	7.15	2.96
CaO	26.31 - 26.26	27.07 - 26.24	25.91	25.50 - 25.17	26.45	26.09 - 25.8	26.93 - 26.35	25.37	25.99
K_2O	0.07 - 0.07	0.07 - 0.06	0.04	0.02 - 0.03	0.06		0.04 - 0.03	0.02	0.03
Na_2O	0.02 - 0.04	0.06 - 0.04	0.03	0.08 - 0.10	0.02		0.08 - 0.04	0.10	0.07
Anhydrous Total	96.08 - 96.21	96.02 - 95.12	94.94	94.86 - 95.17	96.25	95.13 - 94.1	93.80 - 92.93	94.22	93.54
Si	3.016 - 3.031	3.048 - 3.068	3.030	3.042 - 3.043	3.027	3.055 - 3.025	3.047 - 3.077	3.039	3.026
Al^{IV}	0.884 - 0.969	0.952 - 0.932	0.970	0.958 - 0.957	0.973	0.945 - 0.975	0.953 - 0.923	0.961	0.974
Al^{VI}	0.742 - 0.681	0.932 - 0.951	0.874	0.682 - 0.608	0.777	0.965 - 0.988	0.965 - 0.845	0.637	0.847
Fe^{+3}	0.276 - 0.330	0.055 - 0.062	0.157	0.346 - 0.433	0.233	0.066 - 0.053	0.002 - 0.121	0.384	0.158
Ca	1.961 - 1.962	1.989 - 1.941	1.934	1.930 - 1.909	1.967	1.928 - 1.927	2.019 - 2.011	1.940	1.974
K	0.006 - 0.006	0.006 - 0.005	0.004	0.002 - 0.003	0.005		0.003 - 0.003	0.002	0.003
Na	0.003 - 0.005	0.008 - 0.005	0.004	0.011 - 0.014	0.003		0.011 - 0.006	0.014	0.010
Fe^{+3} / $Fe^{+3}+Al$	0.138 - 0.167	0.028 - 0.032	0.078	0.174 - 0.217	0.117	0.033 - 0.026	0.001 - 0.064	0.194	0.080

*Total Fe as Fe_2O_3

sectioning may have missed the prehnite-bearing portion. Whenever it occurs, prehnite is easily identified by microscope. Anhedral platy prehnite appears as homogeneous crystal aggregates, colorless to pale green in color, and showing second-order yellow birefringence. Sample 124-209.9 m contains more than 5 volume % coarse-grained prehnite in the matrix; the prehnites are colorless to pale green and have uniform habit; some show bow-tie structure.

Prehnite-wairakite-calcite-sodic plagioclase-chlorite/smectite interstratified mineral-quartz-pyrite (± epidote) is the most common mineral association in prehnite-bearing specimens such as #124-162.4 and #124-209.9. The prehnite-laumontite-epidote-calcite-sodic plagioclase-chlorite/smectite interstratified mineral-quartz-pyrite association is also found in some specimens from relatively shallower (lower temperature) parts of bore-holes. This relationship is shown in #124 as follows:

	Prehnite	Laumontite	Wairakite	Epidote
158.3	+	+		
159.5	+	+		+
165.6	+	+	+	
192.0	+	+		
201.8	+	+ (trace)	+	+
209.9	+		+	+
211.1	+		+	+
334.7	+		+	+

Chemical compositions of prehnites in bore-hole cores of the Onikobe geothermal area are shown in Table 45. The frequency distribution is plotted against the $Fe^{+3}/(Fe^{+3} + Al^{total})$ ratio in Figure 33 and the Fe^{+3} - Al variation in the octahedral site in Figure 34. For each sample, more than 4 analyses were taken. Some have uniform composition. Others show a small range of $Fe \rightleftharpoons Al^{VI}$ substitution and such a range is listed in the table. The analyzed prehnites span a considerable range of $Fe^{+3}/(Fe^{+3} + Al)$ ratio; the most iron-rich prehnites (Fe_2O_3 6-8 wt %) occur in the matrix and appear to be stable with epidote + wairakite + quartz + chloritic clay. The veined prehnites, on the other hand, are much lower in Fe content (Fe_2O_3 less than 3 wt %) and are stable with wairakite ± carbonates + quartz. Such a difference in the Fe_2O_3

contents between matrix prehnites and veined prehnites may be due to a slight difference in f_{O_2} (and/or temperature). The matrix prehnites may have crystallized under f_{O_2} conditions buffered by highly oxidized rocks whereas the veined prehnites formed at lower f_{O_2} and higher CO_2 conditions at a later stage. The compositional range of prehnite shown in Figure 33 is consistent with analyses of prehnite from the Cerro Prieto geothermal field (Bird et al., 1983).

Figure 34 shows the variation of Fe^{+3} and Al in the octahedral sites of prehnite according to the basic formula $Ca_2(Fe, Al^{VI})(AlSi_3)O_{12}(OH)_2$. The line for unity value of the octahedral site is drawn. The sum of Fe^{+3} + Al for the matrix prehnites is greater than the unity value and the Ca cations are less than the ideal value of 2. Such relations suggest that a small amount of substitition of Fe^{+2} for Ca in the Fe-rich prehnites may have occurred.

Prehnite is known to carry an appreciable amount of Fe^{+3} in octahedral sites occupied chiefly by aluminum (Papike & Zoltai, 1967; Surdam, 1969). The maximum substitution of Fe^{+3} may be up to 10 weight percent Fe_2O_3, the phase approaching the composition $Ca_2Fe^{+3}AlSi_3O_{10}(OH)_2$. The extent of solid solutions in prehnite defined by the two end-members $Ca_2Al_2Si_3O_{10}(OH)_2$ and $Ca_2FeAl_2Si_3O_{10}(OH)_2$ has been extensively investigated. Hashimoto (1964) suggested that most prehnites have $X_{Fe}{}^{+3}$ less than 10% and some may extend to 20%. Maximum $X_{Fe}{}^{+3}$ of 20 and 25% for prehnite solid solution has been respectively reported by Surdam (1969) and Evarts and Schiffman (1983). However, Matsueda (1975) suggested that a compositional gap occurs between 8 and 13% and that the maximum substitution of Fe^{+3} for Al may be up to 10 wt. % Fe_2O_3 ($X_{Fe}{}^{+3}$ = 22%). His suggestion was not supported by a recent compilation of available compositions of natural prehnites from zeolite and prehnite-pumpellyite facies rocks by Kim et al., (in press). Their compilation indicates that no compositional discontinuity exists in the range of 8 to 13 mole %, and that prehnite contains up to 25% $X_{Fe}{}^{+3}$. More data are needed to verify this conclusion for zeolite facies prehnite.

Epidote

Epidote also occurs sporadically in Onikobe drill hole core samples as tabular

Table 46. Chemical analyses of epidote in drill hole core samples from the Onikobe geothermal area, Japan.

Sample No.	124 - 222.8m (vein)	124 - 307.5m (repl. plag.)	123 - 238.6m (repl. matrix)	123 - 323.8m (repl. matrix)	123 - 344.6m (amygdules)	123 - 348.5m (repl. matrix)
SiO_2	37.08 - 37.92	37.00	37.33	38.03	38.05 - 38.18	38.79
Al_2O_3	21.68 - 22.74	19.97	21.06	24.10	22.38 - 25.34	26.86
Fe_2O_3	13.96 - 12.40	18.57	15.49	11.46	14.34 - 10.85	9.61
MnO	0.20 - 0.19	0.20	0.20	0.47	0.54 - 0.55	0.62
MgO	0.15 - 0.21	0.07	0.16	0.12	0.06 - 0.06	0.21
CaO	23.89 - 23.15	21.95	23.07	22.85	23.47 - 23.55	22.54
Anhydrous Total	96.96 - 96.61	97.76	97.30	97.03	98.84 - 98.54	98.63
Si	6.010 - 6.104	6.004	6.040	6.069	6.038 - 5.996	6.027
Al	4.142 - 4.314	3.819	4.017	4.533	4.156 - 4.690	4.919
Fe^{+3}	1.703 - 1.502	2.268	1.886	1.376	1.713 - 1.292	1.124
Mn	0.027 - 0.026	0.027	0.027	0.064	0.073 - 0.074	0.082
Mg	0.036 - 0.050	0.017	0.039	0.029	0.014 - 0.014	0.049
Ca	4.149 - 4.314	3.816	4.000	3.907	3.990 - 3.963	3.752
Fe^{+3} / Fe^{+3}+Al	0.291 - 0.238	0.373	0.319	0.233	0.290 - 0.215	0.186

*Total Fe as Fe_2O_3

crystals or as spongy crystal aggregates replacing plagioclase and matrix or as fan-shaped coarse-grained aggregates with characteristic yellow to light yellow pleochroism. All epidote crystals possess very high birefringence suggesting a high Fe^{+3} content.

Most commonly observed associations with idiomorphic epidote are epidote-wairakite-chlorite/smectite interstratified mineral or chlorite-sodic plagioclase-calcite-quartz-pyrite. The assemblage, epidote-wairakite-chlorite/smectite interstratified mineral or chlorite-sodic plagioclase-calcite-prehnite-quartz-pyrite is also found in some specimens, such as #124-162.4. The epidote-laumontite-calcite-chlorite/smectite interstratified mineral-pyrite (± prehnite) assemblage is observed in only four specimens, including #124-159.5. No epidote was found in mordentite-bearing core samples. Epidotes from many samples were analyzed by electron microprobe (Table 46). These epidotes are all stably associated with wairakite, calcite, sodic plagioclase, chlorite/smectite interstratified mineral or chlorite, quartz and pyrite. Compositional distributions and variation of Fe^{+3}-Al in the octahedral site of these epidotes are respectively shown in Figures 33 and 34. The analyzed epidotes range in pistacite content from 19 to 37; most analyses have compositions around Ps 29 to 33. Except for the one with an extremely high Fe_2O_3 content replacing plagioclase, the compositional range of epidote from the Onikobe geothermal area is very compatible with those from Cerro Prieto (Bird, et al., 1983). The $Fe^{+3}/(Fe^{+3} + Al)$ ratio in epidotes from metamorphic terraines and geothermal areas varies, depending on metamorphic grade and oxidation state of the rock. With increasing metamorphic grade, epidote becomes more aluminous, reflecting not only the effect of temperature and total pressure but also the concomitant decrease of the oxidation state of the rocks (for details see Kim et al., in press). A systematic compositional variation of epidote with depth, and hence with temperature in the investigated samples from Onikobe is not apparent. However, it appears that epidote stably associated with wairakite + magnetite (e.g., Sample #124 - 307.5) is higher in Fe^{+3} compared to the epidote of the epidote + prehnite + wairakite assemblage. Such compositional variations related to the difference in mineral assemblage will be described in a later section.

Carbonates

Calcite is one of the most common vein minerals in the Onikobe cores. It is found starting at depths of only a few tens of meters in many holes and continuing to a maximum depth of 1100 m in #127. Compositionally, all carbonate grains analyzed by

electron microprobe and SEM were calcite, containing only a few percent Fe, Mg, and Mn; representative microprobe analyses are listed in Table 47. Some of the analyses total to less than 100% calculated carbonate as a result of difficulties in obtaining very good polishes on the small, soft grains. This is a common problem encountered when such small grains are undercut during the thin-section preparation process, resulting in a rough surface and random scattering of emitted X-rays. The ratio of one element to another within the analysis should not be severely affected.

The mineral occurs as a vein and amygdule filling and replacing fine-grained matrix and plagioclase and pyroxene phenocrysts, especially along cleavage cracks in the latter two. When it occurs as a vein mineral, it is usually observed to have been one of the last to have formed, based on textural relationships. The absence of this mineral within certain zones in the middle of some of the cores and in the bottom sections of others may be important in establishing certain hydrologic parameters in the Onikobe geothermal field. This will be discussed further later.

Sodic plagioclase

Based on petrographic observations of cores in many wells of the Onikobe geothermal area, we concluded that the replacement of primary plagioclase by sodic plagioclase seems to begin to occur when volcanic rocks were altered at temperatures of 120-180°C. At greater depth where volcanic rocks were altered at temperatures higher than 230°-240°C, some plagioclase phenocrysts have entirely been replaced by sodic plagioclase together with or without zeolitic and illitic or chloritic clay minerals. Chemical compositions of some sodic plagioclases are shown in Table 48. They are basically albitic plagioclase with an An content of less than 5 and low Fe_2O_3 and MgO contents.

Pyrite

Pyrite is one of the most common alteration minerals in bore-hole cores from the Onikobe geothermal area. Some pyrites are observed to have replaced primary magnetites and many euhedral pyrite aggregates also occur in veins, in matrix, and in the groundmass of volcanic clasts. Such pyrites must have formed by using the iron liberated from the decomposition of iron-silicates or volcanic glass. Pyrite-bearing

Table 47. Chemical analyses of carbonates in drill hole core samples from the Onikobe geothermal area, Japan.

Sample No.	127 - 154.6m (vein)	127 - 155.4m (vein)	127 - 409.7m (vein)	127 - 1010.6m (vein)	127 - 1103.6m	127 - 1104.0m (elong. grain)
FeO*	0.16 - 0.02	0.00 - 0.00	0.06	0.17 - 0.32	0.30	0.42 - 0.51
MnO	1.15 - 0.30	0.11 - 0.51	0.37	0.55 - 0.61	0.89	1.08 - 1.21
MgO	0.09 - 0.01	0.01 - 0.04	0.05	0.13 - 0.10	0.12	0.27 - 0.34
CaO	53.00 - 54.62	55.79 - 55.30	55.05	53.26 - 53.41	53.82	52.91 - 52.66
CO_2-free Total	54.40 - 54.95	55.91 - 55.85	55.53	54.11 - 54.44	55.13	54.68 - 54.72
Calc. Carb. Total	96.91 - 98.04	99.78 - 99.62	99.07	96.51 - 97.05	98.25	97.44 - 97.49

Sample No.	127 - 1104.4m (large grain, part of vein)	127 - 1105.5m (alt. lithic fragment)	123 - 184.7m (vein)	123 - 309.5m (alt. plag. pheno.)	123 - 323.8m (amygdule)
FeO*	0.13 - 0.52	0.30	0.22	0.23	0.00
MnO	0.97 - 1.41	2.30	0.66	0.25	0.31
MgO	0.12 - 0.33	0.29	0.48	0.17	0.10
CaO	53.32 - 51.70	53.57	52.01	54.43	53.42
CO_2-free Total	54.54 - 53.96	56.46	53.37	55.08	53.83
Calc. Carb. Total	97.21 - 96.10	100.44	97.27	98.29	96.07

*Total Fe as FeO

Table 48. Chemical analyses of albitic plagioclase in drill hole core samples from the Onikobe geothermal area.

Sample No.	127 - 703.9m	127 - 1104.0m	127-1105.5m
SiO_2	67.41	68.33 - 68.31	67.31
Al_2O_3	20.41	21.26 - 21.18	19.55
Fe_2O_3*	0.06	0.03 - 0.01	0.11
MgO	0.00	0.00 - 0.00	0.00
CaO	0.83	0.33 - 0.39	0.27
K_2O	0.21	0.25 - 0.08	0.30
Na_2O	11.11	11.09 - 11.38	11.64
Total	100.03	101.29 - 101.35	99.18
An content	4	2 2	2

*Total Fe as Fe_2O_3

Table 49. Comparison of SO_4 and H_2S contents of thermal water and fumarolic gas from the Onikobe and Hakone geothermal areas, Japan.

	Onikobe	Hakone
SO_4 content of thermal water (ppm)	1 - 727 (Av. 136)	51 - 369* (Av. 148)
H_2S content of thermal water (ppm)	10 - 466 (Av. 205)	0 - 44** (Av. 13)
H_2S content of fumarolic gas (vol. %)	0.02 - 0.37 (Av. 0.22)	0.01 - 0.12*** (Av.0.06)

* Nakamura, 1959a ; Hitosugi, 1969; Seki et al., 1969

** Awaya, Hirano and Kubodera, 1974

*** Hirano, Oki and Awaya, 1973; Awaya, Hirano, Suzuki and Oki, 1976

Table 50. $\delta^{34}S$ values of pyrites from bore-hole cores of the Onikobe geothermal area, Japan.

Bore-hole cores		$\delta^{34}S$
#123	178.8 m	+3.59
"	333.3 m	+3.00
#124	183.3 m	+3.38
"	331.4 m	+2.05
#127	231.7 m	+3.06
"	703.9 m	+5.43

veins of the following mineral assemblages are common:

Laumontite or wairakite-quartz-pyrite
laumontite or wairakite-calcite-quartz-pyrite } ± clay minerals
Calcite-quartz-pyrite

In the Hakone geothermal area, the occurrence of pyrite in bore-hole cores is much less common than at Onikobe, although there are no distinct differences in the petrographic and chemical characteristics, including major chemistry of thermal water, between these two geothermal areas. The occurrence of pyrite appears to be the most distinctive feature distinguishing the Onikobe geothermal area from Hakone in regard to the hydrothermally formed alteration minerals.

There is no difference in the SO_4 contents of thermal waters between Onikobe and Hakone; however, as shown in Table 49, the H_2S contents of the thermal waters and fumarolic gases of the Onikobe geothermal area are much higher than those of the Hakone geothermal area. The high H_2S concentrations in thermal waters and gases must have played the major role in producing the wide distribution of pyrite in volcanic rocks at depth in the Onikobe geothermal area. Several reactions can be written for the

crystallization of pyrite as follow:

$$Fe(rock) + 2H_2S(fluid) \longrightarrow FeS_2(rock) + 4H^+(fluid)$$

$$Fe_3O_4(magnetite\ in\ rock) + 6H_2S \longrightarrow 3FeS_2 + 4H_2O + 4H^+$$

$$FeO(silicates\ and\ glass) + 2H_2S \rightarrow FeS_2 + H_2O + 2H^+$$

The $\delta^{34}S$ values of pyrite separated from some core samples from the #123, 124 and 127 bore holes are shown in Table 50. They range from +2.05 to +3.59 at shallow depths to +5.43 at a depth of 700m. These values are almost identical to those of pyrites in altered basaltic rocks from depths of 0 to about 800m in the Reykjanes geothermal area of Iceland (Sakai et al., 1980). In the active geothermal area of the Reykjanes Peninsula where present-day seawater is actively percolating through the porous basaltic lavas at depth, the $\delta^{34}S$ value of epigenetic pyrite generally increases with increasing depth, showing a greater involvement of seawater sulfate in the deeper part. It must be noted that the hydrothermally formed pyrite at a depth of 703.9m in the Onikobe #127 well has a much higher $\delta^{34}S$ value than the pyrite from 231.7m depth in the same well and pyrites from similar depths in other wells. In the Onikobe geothermal area, the percolation of present-day seawater cannot be expected. However, fossil seawater within Miocene volcanogenic marine sediments at the basement of this geothermal area may have contributed sufficient sulfur for pyrite crystallization at depth (see Chapter 6).

Halite

The common occurrence of halite in bore-hole cores is one of the most characteristic features of hydrothermally altered rocks in the Onikobe geothermal area. This fact must be chiefly due to the high concentration of Na and Cl in the thermal waters. For example, the thermal water discharged through the GO-7 hole contains 187-213 meq Na and 302-372 meq Cl. These concentrations are over half of the present-day seawater values. The Onikobe geothermal area is also characterized by the formation of halite as a scale deposit in steam transport pipes, in injection well casing pipes and on the surface of turbin blades (Table 51). Halite has not been

Table 51. Chemical composition of scales at the Onikobe geothermal area, Japan (Hitosugi 1969).

	Black scale (1)	White scale (2)
Na	21.95	38.20
K	4.79	0.29
Ca	9.90	0.08
Mg	tr	tr
Cl	55.22	60.43
SO_4	0.13	0.08
Unsolved	4.32	0.51
	96.31	99.59

reported in bore-hole cores or as a scale depotis at any other geothermal area in Japan. The compositions of scale deposits in the Matsukawa, Odake and Onuma geothermal areas have been reported and are listed in Table 52. In Table 52, the Na, K and Cl contents of thermal waters in these geothermal areas are also shown. It is clear that the contents of chlorine and alkaline metal ions in the Onikobe thermal waters are much higher than those of other Japanese geothermal areas shown in Table 52.

PROGRESSIVE CHANGES OF MINERALS WITH DEPTH

When one examines the distribution of secondary minerals as a function of depth in drill holes of the Onikobe geothermal area, several patterns are apparent:

1. a general zoning with respect to type of phyllosilicate present.
2. a zoning with respect to zeolite minerals.
3. depth-dependent relationships for several other minerals.

Clay Minerals

The distribution of clay minerals as a function of depth is perhaps best exemplified in Table 14 for drill hole GO-7. Within the chlorite/smectite group, the following pattern is seen with increasing depth: Alkaline smectite, smectite → chlorite/smectite

Table 52. Scale deposits and N, K and Cl contents of thermal waters of Matsukawa, Odake and Onuma geothermal areas, Japan.

	Matsukawa	Odake	Onuma
Scale	Silica FeS $FeSO_4$ $CaSO_4$ Na_2SO_4 K_2SO_4	Silica $FeSO_4$	Silica Aluminous hydrosilicate
(ppm)			
Na	14-360	670-1098	345-494
K	4-250	70-320	46- 59
Cl	1- 26	1010-2317	382-447

*data from Sumi and Maeda, 1973; Hayashi, 1973; Ito, 1978; Miyamori, 1968; Fugii, 1969; Moji, 1969; Ito, 1978; Ito et al., 1977b.

interstratified mineral ⟶ chlorite.

Alkaline smectite occurs from 15.0 to 107.0 m depth, smectite from 36.0 to 175.0 m, and interstratified chlorite from 201.1 m to the bottom of the hole at 500.0 m. Kaolinite is present between 107.0 and 175.0 m, and illite occurs from 175.0 m to the bottom of the hole, roughly matching the interstratified chlorite range. In drill holes GO-8, GO-10, and GO-11, pyrophyllite occurs below depths of about 800 m. Most of the cores display considerably more overlap among the chlorite/smectite ranges than does GO-7.

As discussed previously, electron microprobe and X-ray diffraction data indicate that the proportion of the smectite component in both the chlorite/smectite and illite/smectite interstratified minerals decreases with depth. A similar pattern of increasing illite component as a function of depth was observed by Perry and Hower (1970) in Gulf Coast

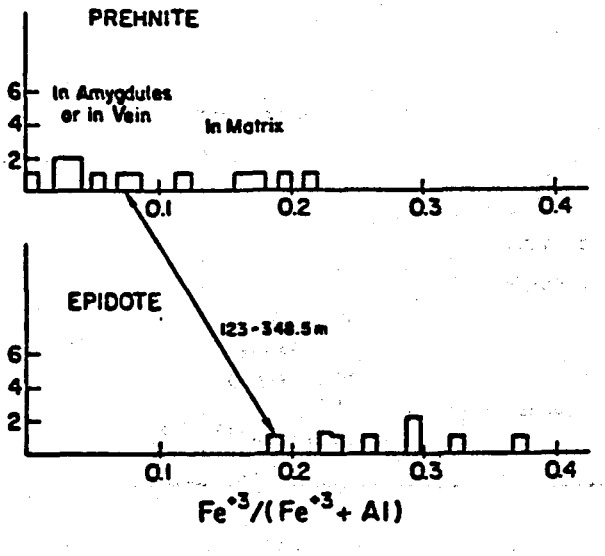

Figure 33. Number of analyses for prehnite and epidote plotted against $Fe^{+3}/(Fe^{+3} + Al)$ ratio.

sediments. They attributed this pattern to an increase in temperature with depth. Eberl and Hower (1976) performed a series of experiments on glasses and Wyoming bentonite to examine the effects of both temperature and time on this trend. They concluded that the trends observed in the Gulf Coast sediments could be explained either with a temperature-dependent equilibrium model or with a time and temperature-dependent kinetic model. Some of this same uncertainty also applies to this field relationship. We favor, however, the equilibrium model for those conditions near the bottom of the deeper drill holes as a result of the higher temperatures.

Zeolite Minerals

The zonal distribution of the four common calcium zeolites—mordenite, laumontite, yugawaralite, and wairakite is briefly described in a previous section. Figure 31(A) through (K) shows the depth distribution of these four Ca-zeolites plus clinoptilolite in drill holes GO-7, GO-8 and nine other drill holes discussed in this report. The zeolites are plotted on the geothermal gradient curves. The general pattern of mordenite→laumontite→yugawaralite→wairakite with increasing depth is observed. In addition to these 4 Ca-zeolites, clinoptilolite is also sometimes seen in this progressive

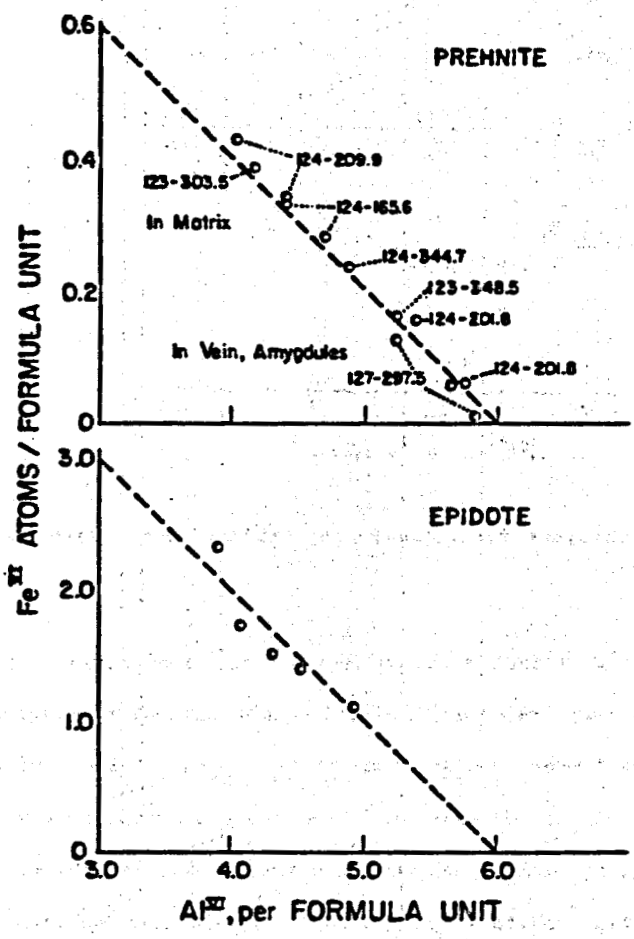

Figure 34. Fe^{+3} - Al^{VI} plot for analyzed prehnites and epidotes from the Onikobe geothermal area, Japan.

zonation and it occurs near the upper part of the mordenite zone: the following points can be made regarding these diagrams:

1. moderate to strong overlapping of zones is the rule rather than the exception in most of these diagrams.
2. not all five zeolites are usually seen in any one core, and yugawaralite is notably either absent or infrequent in all eleven of the cores.
3. the plotting of the zeolite variation along the geothermal gradient is a useful way

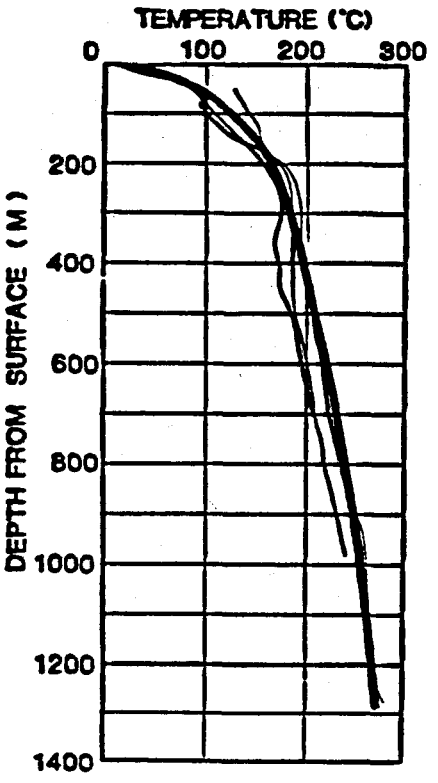

Figure 35. Estimated average geothermal gradient for the Onikobe geothermal area, Japan.

of introducing two important pieces of information. However, care must be taken in relating the zeolite present at a given depth to the corresponding gradient temperature.

The last point is true because each measured gradient curve will be partially a function of the flow regime developed in the well area as a result of drilling and subsequent pumping and may not represent the long-term, more or less steady-state temperature pattern. A better way to consider a possible temperature dependence of zeolite formation may be to construct a composite geothermal gradient for the approximately 0.25km^2 Katayama area of Onikobe. This has been done in Figure 35; the deepest two-thirds of the curve basically follows the maximum GO-8 geotherm, while the upper third is a composite constructed from the GO-8, GO-10, and GO-11 trends. This composite curve

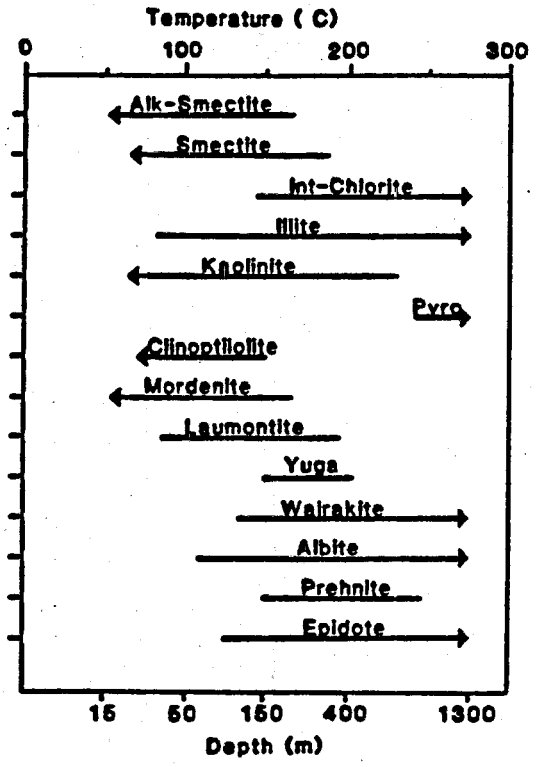

Figure 36. Distribution of secondary minerals as a function of depth and estimated temperatures from Figure 35 in the Onikobe geothermal area, Japan.

downplays the effect of "kinks" in the curves which may be due to local well-induced flow characteristics.

Figure 36, constructed using depth-temperature relations from this composite curve, shows the distribution of secondary minerals as a function of postulated present temperature in the field.

Correlation Between Clay and Zeolite Minerals

From the discussions presented in the previous sections, it is apparent that both clay and zeolite minerals change progressively in species with depth, and hence temperature, in the Onikobe geothermal area. Such changes are summarized below:

(1) Both smectite and alkaline smectite occur in the core samples from shallow depths (hence low temperatures). The most common zeolite associated with these clay minerals is mordenite (e.g., Tables 10 to 15); however, this zeolite is extremely rare in the core

Figure 37. d_{001}(dry)–d_{001}(ethylene glycol) diagrams of clay minerals associated with (A) mordenite; (B) laumontite, and (C) wairakite from bore-hole cores of the Onikobe geothermal area, Japan.

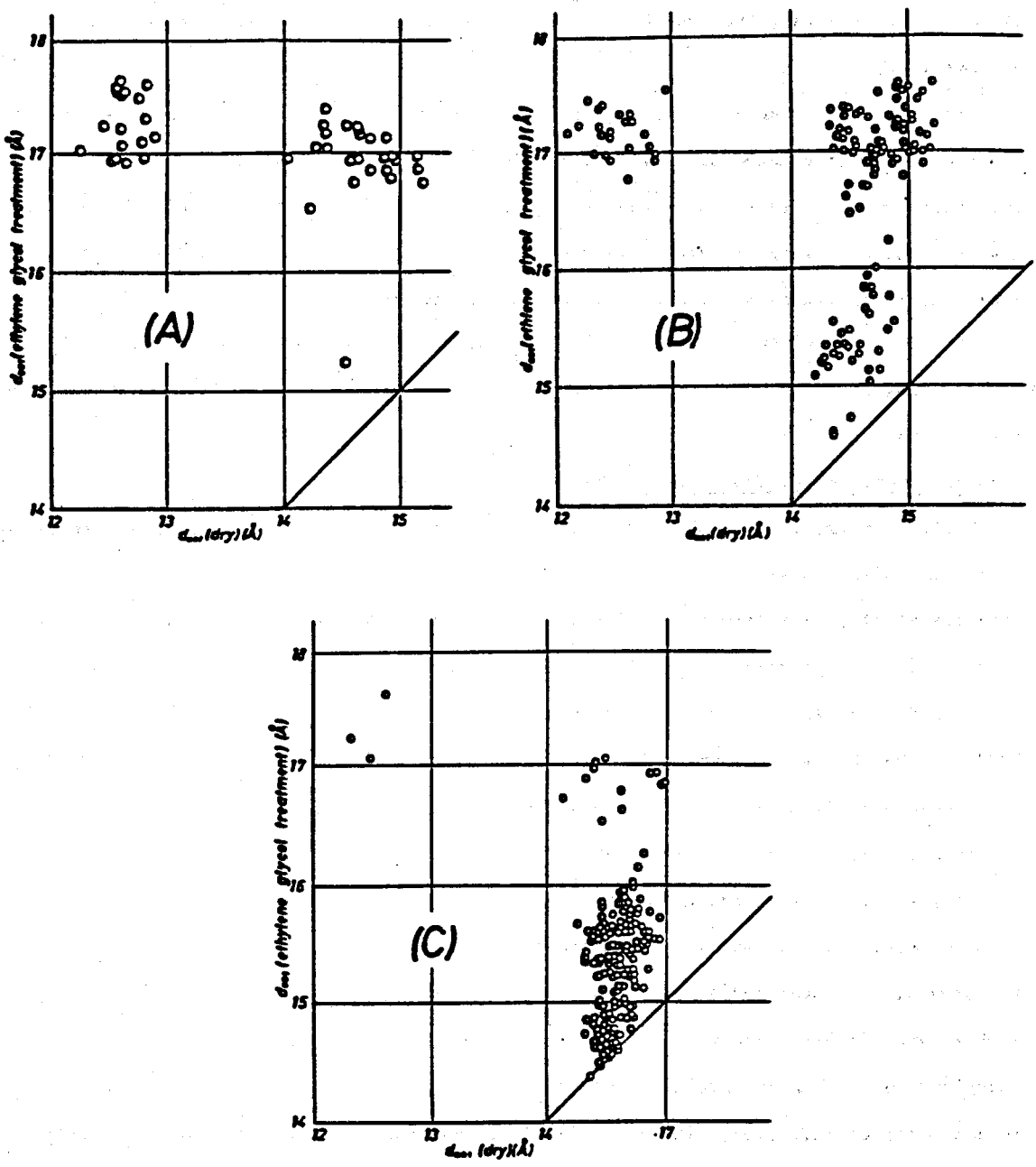

samples of drill holes #123, 124 and 127. The lack of Ca-zeolites in shallow core samples and the ubiquitousness of kaolinite-alunite in some drill holes suggests low pH thermal waters which inhibit the formation of Ca-zeolites. In the mordenite-bearing samples, as shown in Figure 37(A), the occurrence of chlorite/smectite interstratified clay mineral is extremely rare.

(2) The chlorite/smectite interstratified clay mineral occurs at intermediate depths. It is most commonly associated with laumontite and wairakite. The clay minerals identified in the laumontite-bearing drill hole cores are shown in Figure 37(B). Smectite, alkali smectite and chlorite/smectite interstratified minerals together with illite/smectite interstratified minerals were found to be stable with laumontite.

(3) The clay minerals shown in Figure 37(C), occurring at depth and stable with wairakite, are both chlorite/smectite interstratified minerals and chlorite. K-clays are also present.

Comparison with Other Geothermal Areas

Similar paragenesis of clay and zeolite minerals has been reported in other geothermal areas, including those in Japan (Hayashi et al., 1968, 1973; Hayashi and Yamasaki, 1975; Yamasaki et al., 1968; Kimbara and Okubo, 1978), in Iceland (Kristmannsdóttir, 1975a, 1975b, 1976, 1979; Tómasson and Kristmannsdóttir, 1972; Kristmannsdóttir and Tómasson, 1974, 1978; Kristmannsdóttir, 1982; Mehegan et al., 1982; Viereck et al., 1982; Exley, 1982), in New Zealand (Steiner, 1968, 1977) and in the United States (McDowell and Elders, 1980, Sheridan and Maisano, 1975; Bargar and Beeson, 1981).

Such systematic variations of clay minerals from smectite to chlorite through chlorite/smectite interstratified minerals with increasing depth in stratigraphic horizon or with increasing metamorphic grade have been studied in most detail in the Miocene volcanogenic sediments of Japan. The systematic associations of clay and zeolite minerals such as smectite and alkaline zeolites (mordenite, clinoptilolite and analcime), chlorite/smectite interstratified mineral and laumontite, and chlorite and wairakite are common (Seki et al., 1969; Kimbara, 1970, 1973; Shirozu, 1974; Kimbara and Sudo, 1973; Nakamura, 1976; Yoshimura and Kimbara, 1974; Yoshimura et al., 1977). For instance, from detailed examinations of the modes of occurrence and associated minerals of

chlorite/smectite interstratified minerals in the Japanese Miocene volcanogenic formation, Yoshimura and Kimbara (1974) reached the following conclusions: (1) There must be a P-T stability field for the interstratified minerals in between those of smectite and non-expandable clay minerals such as chlorite and sericite; (2) the chlorite/smectite interstratified minerals occur in intimate association with laumontite; almost all of the laumontite-bearing rocks in the Green Tuff region contain chlorite/smectite interstratified minerals. The occurrence of the interstratified mineral-heulandite association is extremely rare; (3) the associations of chlorite/smectite interstratified minerals with smectite and those of chlorite/smectite interstratified minerals with chlorite have been found, respectively, in the rocks transitional between the smectite zone and chlorite/smectite interstratified mineral zone and the rocks between the chlorite/smectite interstratified mineral zone and chlorite zone. Chemical reactions for the transitions among smectite, chlorite/smectite interstratified mineral and chlorite have been suggested as follows:

(A) $2.65\ (Si_{3.2}Al_{0.8})\ (Mg_{1.5}\ Fe_{1.1}Al_{0.3})\ O_{10}(OH)_2 4H_2O \longrightarrow$
(Smectite)
$(Si_{6.4}Al_{1.6})\ (Mg_{4.0}Fe_{2.9}Al_{1.3})\ O_{20}\ (OH)_{10} 4H_2O + 2.1SiO_2 + 4H_2O$
(Chlorite/smectite interstr. mineral)

(B) $0.65\ (Si_{6.4}Al_{1.6})\ (Mg_{4.0}Fe_{2.9}Al_{1.3})\ O_{20}\ (OH)_{10} 4H_2O) \longrightarrow$
(Chlorite/smectite interstr. mineral)
$(Si_{3.1}Al_{0.9})\ (Mg_{2.6}Fe_{1.9}Al_{1.0})\ O_{10}\ (OH)_8 + 1.1SiO_2 + 2H_2O$
(Chlorite)

A progressive change of Mg smectite → chlorite/smectite interstratified mineral → chlorite with increasing temperature has also been experimentally investigated (Eberl, 1978; Eberl et al., 1978). Similarly, the change of smectite to sericite through sericite/smectite interstratified mineral with increasing metamorphic temperature has also been reported in some Neogene diagenetic sequences (Dunoyer de Segonzac, 1970; Shirozu and Higashi, 1974; Higashi, 1980; Hoffman and Hower, 1979; Pevear et al., 1980) and synthesized in the laboratory (Eberl, 1978; Eberl et al., 1978).

In the Icelandic geothermal areas, the occurrence of 'swelling chlorite' is confined almost exclusively to a transitional zone between the high temperature

chlorite-epidote zone (230-280°C) and the low temperature smectite-zeolite zone (lower than 200°C) (Tómasson and Kristmannsdóttir, 1972; Kristmannsdóttir, 1975a). The "swelling chlorite" was identified by the increase of d_{001} value from 14.0-14.6Å to 15.0-17.0Å after ethylene glycol treatment and the complete disappearance of 14Å peak after heat treatment at 600°C for 2 hours. At the Wairakei geothermal area, Steiner (1968, 1977) reported the occurrence of "long-spacing regular mixed layer swelling chlorite" in a strongly sheared breccia zone. The 14.5Å peak of this "swelling chlorite" expands to 15.5Å after ethylene glycol treatment and collapses to 13.4Å after heat treatment at 600°C for 1 hour. The DTA patterns and infrared spectra of the chlorite/smectite interstratified minerals are quite similar to those of the "swelling chlorite' in Icelandic geothermal areas. Kristmannsdóttir (1976) suggested that some of the "swelling chlorites" in Icelandic geothermal areas could be thermally unstable smectite and/or thermally unstable chlorite/smectite interstratified minerals. Apparently different definitions and mineralogical characteristics of the "swelling chlorite" have been proposed. Stephen and MacEwan (1951) are among the first to suggest that the 14Å reflection of the "swelling chlorite" shifts to 17.8Å after glycol treatment and collapses to 13.8Å after 500°C heat treatment. Brindley (1961) reported that the "swelling chlorite" may be a kind of chlorite in which hydroxide sheets occur as island-like imperfect layering between silicate layers. Shimoda (1970) reported all expandable "swelling chlorite" characterized by peak shifts of 14.8Å to 15.5Å (ethylene glycol) and 14.8Å to 14.2Å (600°C heat treatment) and intensity ratio of 7Å/14Å of 0.60. He later concluded that the "swelling chlorite" may not belong to the chlorite/smectite interstratified mineral and the presence of imperfect brucite layers between silicate sheets of smectite has resulted in a chlorite-like structure of swelling behavior. In short, the definition, identification method, chemical characteristics and crystal structure of the swelling chlorite have not yet been established. Many problems remain unsolved and should be studied in the future.

Zen (1967) suggested that the interstratified mineral should be treated as a

thermodynamically stable phase and the disappearance of the mineral in diagenesis might be one of the sensitive indicators of metamorphic grade. Sudo (1968) agreed, and proposed a new facies, namely, the interstratified clay facies, characterized by the widespread occurrence of interstratified clay. As has been noted previously in this section, the variation of smectite→interstratified minerals→chlorite and sericite is closely related to the variation of zeolites from mordenite, clinoptilolite, stilbite, heulandite through laumontite to wairakite and other minerals such as sodic plagioclase, prehnite, epidote and pumpellyite. The stability fields of chlorite/smectite and illite/smectite (sericite/smectite) interstratified minerals which can be established by detailed petrographic and chemographic analyses must be one of the most interesting problems related to low-grade metamorphism.

CHEMOGRAPHIC RELATIONS AND PHASE EQUILIBRIA

From detailed descriptions of secondary phases in the previous sections, it is apparent that most drill hole core samples consist of 2 to 3 Ca-Al hydrous silicates together with abundant quartz, carbonate, chlorite-smectite and pyrite and minor albite, illitic clay, sphene, magnetite and sulfates. Common Ca-Al hydrosilicates includes Ca-zeolites (laumontite, yugawaralite, wairakite), prehnite and epidote. Ca-zeolites are most abundant and occur in more than 80 % of the investigated samples. Prehnite and epidote are minor. Pumpellyite was not positively identified, trace actinolite occurs in some deeper core samples and garnet was not found.

Compositions of all these secondary phases can be defined by a system including, K_2O, Na_2O, CaO, MgO, FeO, Fe_2O_3, Al_2O_3, TiO_2, SiO_2, H_2O, S, CO_2 and SO_4 as components; there are too many to be graphically shown in their phase relations. The total number of components can be reduced to 4 with the following assumptions:

(1) The system has an excess of fluid and quartz phases and the fluid phase is composed mainly of H_2O, CO_2, S and SO_4. Respectively S, SO_4 and CO_2 are

tied with pyrite, gypsum (and/or anhydrite) and carbonate;

(2) All minor K_2O, Na_2O and TiO_2 are respectively fixed in minor illitic clay, albite and sphene;

(3) the only phase showing significant FeO and MgO substitution is chloritic clay mineral. Although, minor actinolite also shows such substitution but it will not be included in the present discussion. We combine FeO + MgO as one component because systematic variation of FeO/MgO in chloritic clay with depth is not apparent and because we have treated chlorite as an excess phase in our discussion.

With these assumptions, the system is simplified to be $CaO - Fe_2O_3 - Al_2O_3 - (FeO+MgO)$. Compositions of the common secondary phases are plotted in the tetrahedron of Figure 38. The ranges of solid solutions for epidote, prehnite, grandite garnet, pumpellyite and chloritic clays are shown. In order to systematically illustrate the variation of mineral assemblages and compositional changes of epidote and prehnite with depth, the $Ca-Al-Fe^{+3}$ plane was selected as the projection plane and chlorite of fixed composition as the projection point.

This simplification is justified by a number of factors listed below: (1) chloritic clay minerals are ubiquitous; (2) compositional variations of epidote, prehnite, garnet and even pumpellyite is defined mainly by $Fe^{+3} - Al$ substitution; (3) analyzed zeolites (laumontite and wairakite) contain very minor Na_2O and they are plotted on the join between 2Al and Ca; and (4) compositions of Ca-zeolites and other Ca-Al hydrous silicates lie on or very close to the projection plane. Hence, the compositional change of chloritic clay minerals does not significantly affect their dispositions onto the ternary diagram.

The resultant projection of hematite, kaolinite, pyrophyllite, laumontite, wairakite, epidote, pumpellyite, prehnite, garnet, calcite and sulfates on the diagram $2Fe^{+3}-2Al-Ca$ are shown in Figure 39. Except for the Ca-Al silicates which show significant extents of solid solution as solid lines, the other phases shown in the diagram have fixed compositions. It should be mentioned that pumpellyite contains considerable amounts of (Fe+Mg)O and the position of its projection is highly dependent on the composition of chloritic phase. If the

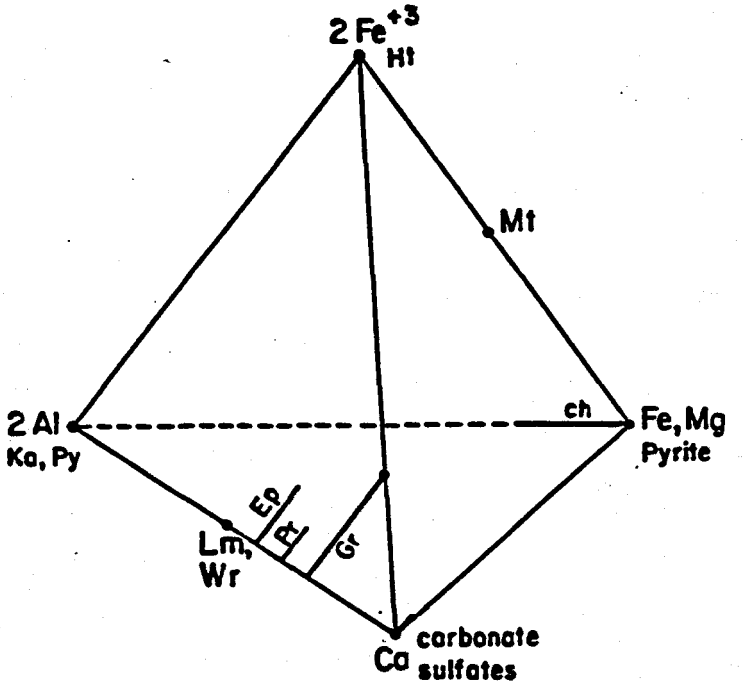

Figure 38. Compositions of common calcium zeolites, epidote, prehnite, grandite, and chlorite together with other common secondary phases (kaolinite, pyrophyllite, carbonate, sulfate, pyrite, magnetite and hematite) were plotted in a tetrahedron Ca-(Fe,Mg)-2Al-2Fe^{+3} diagram (+ albite, quartz, illite, sphene, fluid).

composition of Al-chlorite is used as a projection point, then pumpellyite is overlapped with prehnite. This problem does not exist in the present discussion because pumpellyite was not positively identified in any core samples from the Onikobe geothermal system.

This projection applies only to the phase relations at the f_{O_2} values where hematite is stable. However, in most drill core samples from the Onikobe geothermal area, magnetite is a stable iron oxide. Therefore, we have to treat the phase relations at f_{O_2} lower than the hematite-magnetite buffer. Figure 40 is a tetrahedron showing the phase relations of prehnite, epidote, garnet and iron oxides as a function of f_{O_2} in the system $CaO-FeO-Fe_2O_3-Al_2O_3-SiO_2-H_2O$ in the presence of excess quartz and fluid at a given P_{fluid}. Compositional shifts for magnetite, epidote, prehnite and grandite with decreasing f_{O_2} are shown by

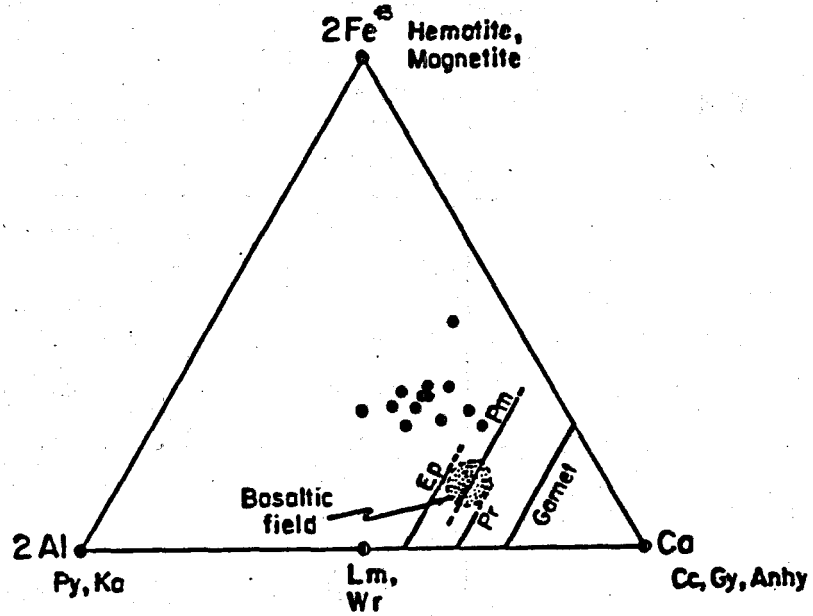

Figure 39. Ca - 2 Al - 2 Fe^{+3} diagram showing compositional variations of common Ca-Al silicates. Compositions of analyzed core samples (Table 21) from the Onikobe geothermal area and basaltic field are shown (+quartz, albite, chlorite, sphene, illite, pyrite).

arrows. This diagram illustrates the effect of f_{O_2} on compositions of Ca-Al silicates and the similarities in mineral assemblages at various f_{O_2} values. For instance, at the f_{O_2} defined by the HM buffer, the assemblage hematite + magnetite (b) together with epidote (c) + prehnite (d) or epidote (c) + andradite (e) or prehnite (d) $\pm$ andradite (e) are possibly stable in certain P-T ranges. At lower f_{O_2} conditions, the assemblage magnetite (b') + epidote (c') + prehnite (d') + grandite (e') is stable. Because of the similarity in mineral assemblages at various f_{O_2} conditions, in the following discussion, magnetite and hematite are plotted in the Fe_2O_3 corner of the Fe^{+3}-2Al-Ca diagram.

Bulk chemical compositions of representative altered core samples listed in Table 21 and basalt field are also plotted in Figure 39. The whole rock Al contents were readjusted in accordance with the presence of excess albite, and chloritic and illitic clays. Compared to unaltered basaltic rocks, the drill hole core samples from the Onikobe geothermal area are higher in Fe^{+3} and lower in Ca

Table 53. Equilibrium mineral assemblage for core samples from Drill Hole #123 and 124 of the Onikobe geothermal Area.* (All assemblages + chloritic clay + quartz ± pyrite ± albite).

depth	#123	depth	#124
238.6m	Ep(32**)+Wr	165.8m	Wr+Pr(14-17)
303.5	Pr(19)+Wr		
323.8m	Ep(23)+Wr	201.8m	Wr+Pr(3-8)+Cc
344.6m	Ep(22-29)+Wr	209.9m	Wr+Pr(17-22)+Ep(?)
348.5m	Ep(19)+Pr(8)(?)+Wr	222.8m	Ep(26-29)+Wr
		307.5m	Wr+Ep(37)
		334.7m	Wr+Pr(12)
		349.4m	Wr+Pr(3-4)+Cc

* Wr+Cc assemblages are not listed; they formed much later.
** The numbers in ( ) refer to $Fe^{+3}/(Fe^{+3}+Al) \times 100$.

Abbreviation: Ep = epidote; Wr = wairakite; Pr = prehnite; Cc = calcite.

with compatible Al contents. Such a difference is reflected in higher hematite (+ magnetite) and very minor prehnite and epidote in core samples compared to low-grade metabasites.

Two points need to be emphasized when the parageneses of observed secondary phases are discussed in terms of these plots. (1) Bulk chemical compositions for the core samples are extremely heterogeneous inasmuch as the geothermal system is open for chemical exchanges. Depending on the difference in the extents of hydrothermal alteration in rock types and in brecciations and veinings, each domain of a simple core specimen can be very different in bulk composition. Therefore, correlation of an observed mineral assemblage with bulk chemical composition could be misleading.

(2) Secondary minerals identified in a single core sample may have formed at a

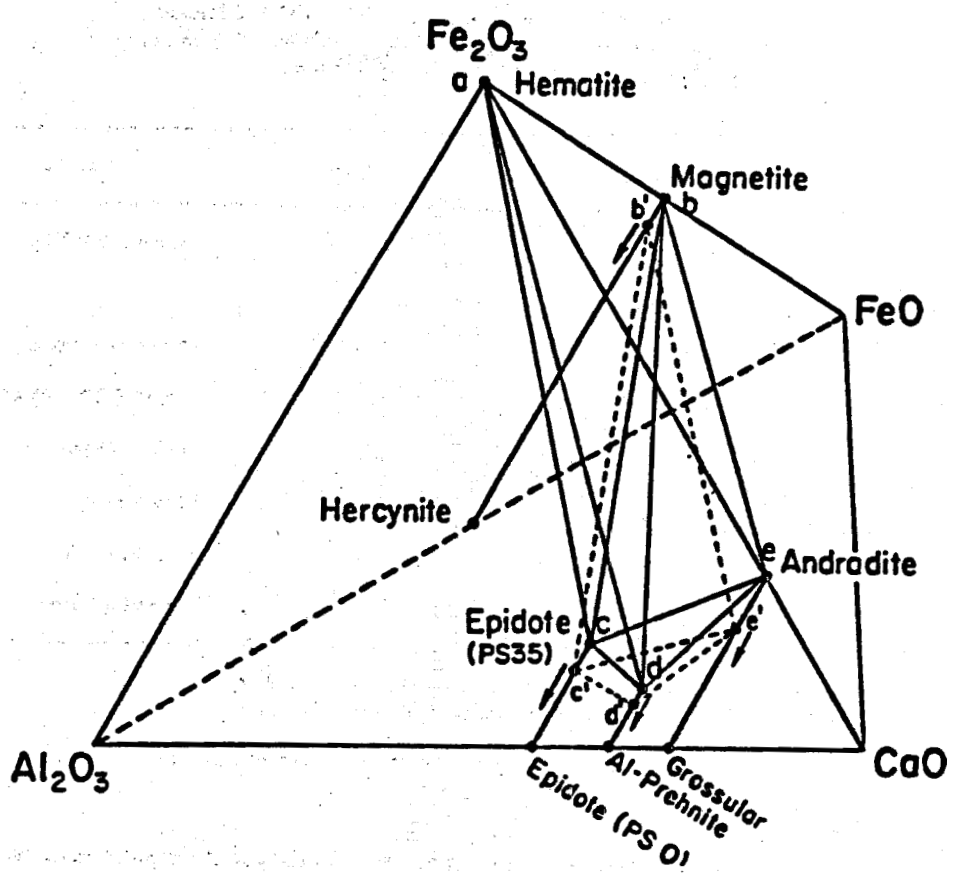

Figure 40. Tetrahedral projection showing phase relations of prehnite, epidote, garnet, hematite and magnetite as a function of f_{O_2} in the system $CaO-FeO-Fe_2O_3-Al_2O_3$ with excess SiO_2 and H_2O at a particular but unspecified P_{fluid}. Tetrahedrons abce, abde and bcde are for the systems controlled by the HM buffer. Tetrahedron b'c'd'e' is for the NNO, QMF and IM buffer systems.

different time and at different physico-chemical conditions (see Exley, 1982 for Iceland geothermal system). They occur in veins, in vesicles, as aggregates in matrix or in groundmass, and even as replacement products of some primary and early formed phases. Textural relations suggest that some of them are not in equilibrium, hence many secondary phases are listed in Tables 10-20 for each specimen. For instance, carbonate veins are found to cut wairakite crystals in the matrix suggesting carbonate formed later under different physical conditions; yet wairakite has metastably persisted. Therefore, in the following discussion, phase

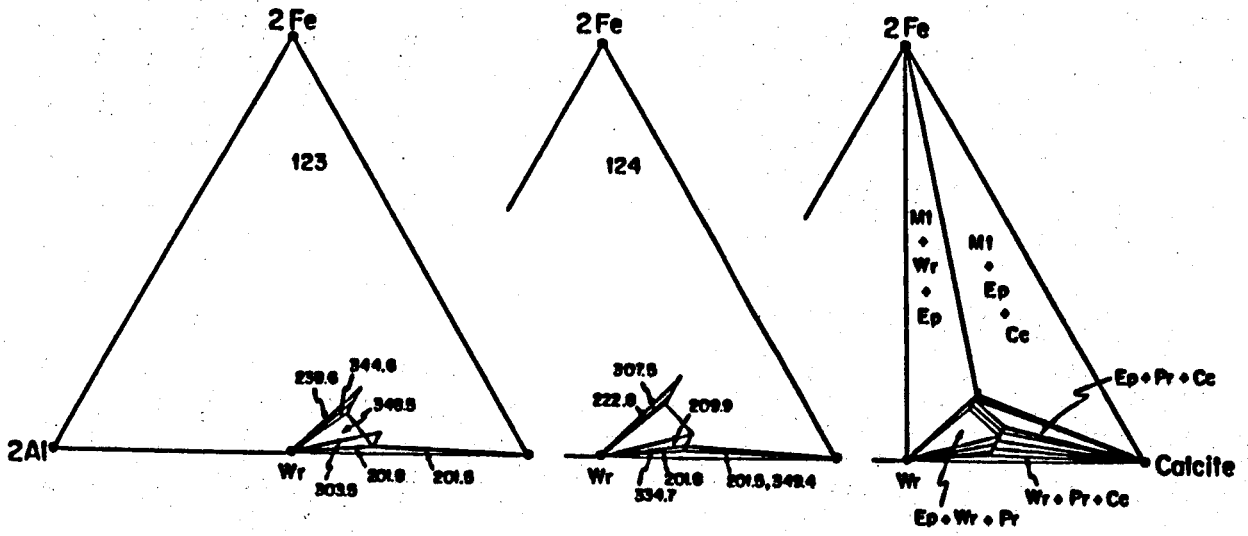

Figure 41. Ca-2Al-$2Fe^{+3}$ plots showing compositions of analyzed epidotes and prehnites and mineral assemblages from drill holes #123(A) and #124(B). Interpretative relationships for 3-phase and 2-phase assemblages are shown in (C).

relations are presented only for those minerals that exhibited grain contacts in a one-inch diameter polished section. Difficulties in establishing what constitutes an "equilibrium mineral assemblage" in low-grade metamorphic rocks have already been documented (Zen and Thompson, 1974).

Mineral assemblages which have shown grain contact relations are listed in Table 53. Compositions of epidote and prehnite were analyzed and their $Fe^{+3}/(Fe^{+3}+Al)$ ratios are listed within the parentheses along with each phase. Because these assemblages formed over the small temperature interval of 110-170°C and at the depths of 166-350 m, they are plotted in the isobaric-isothermal diagrams of Figure 41(A) and 41(B) respectively for drill holes # 123 and 124. The 2-phase assemblages wairakite + epidote and wairakite + prehnite occur in a number of samples whereas the 3-phase assemblages epidote + prehnite + wairakite and wairakite + prehnite + calcite have very restricted occurrence. Tie lines for the coexisting phases are drawn according to the analyzed compositions of epidote and prehnite.

Those samples with the 3-phase assemblage prehnite + wairakite + epidote need to be described, because for the 3-component system, compositions of the 3 phases should be invariant at constant P and T. The assemblage of a sample #124-209.0m was formed at temperature of about 115°C and contains abundant coarse-grained prehnite and wairakite in matrix with minor very fine-grained epidote. Both prehnite and wairakite were analyzed and the prehnite ranges its $Fe^{+3}/(Fe^{+3}+Al)$ ratio from 0.17 to 0.22. However, the epidote is too fine-grained to be analyzed. From compositions of epidotes in other samples in the drill hole # 124, composition of the epidote for the 3-phase assemblage was estimated to be about $X_{Fe^{+3}} = 0.26$. For sample # 123-348.5m at 170°C, the limiting compositions of both epidote and prehnite were analyzed and respectively are $X_{Fe^{+3}} = 8$ for prehnite and $X_{Fe^{+3}} = 19$ for epidote.

The deduced phase relationships for assemblages of these 2 drill hole cores are

summarized in Figure 41(C) at T of 110-170°C and depth of 200-350m. Five 3-phase assemblages were delineated: they are magnetite + epidote + wairakite, magnetite + epidote + calcite, wairakite + epidote + prehnite, epidote + prehnite + calcite, and wairakite + prehnite + calcite. These assemblages have been recorded in other geothermal areas and in low-grade meta-basalts, (e.g., Salton Sea, Bird et al., 1983; Karmutsen metabasalt, Maruyama and Liou, unpublished results).

It should be pointed out that laumontite is rather common at shallow depths in geothermal systems. As a matter of fact, laumontite and wairakite occur together in many samples. The laumontite-hematite-epidote assemblage has been found at Tatun and in other geothermal areas (e.g., Lan et al., 1980). In the investigated samples from Onikobe drill holes 123 and 124, no textural relations suggested the occurrences of laumontite + epidote + hematite, laumontite + prehnite + epidote and laumontite + prehnite + calcite. These assemblages may occur at lower temperatures and higher f_{O_2} conditions.

From the phase relations shown in Figure 41, three conclusions are drawn: (1) Both prehnite and epidote are restricted to Fe-rich composition at low temperatures and become Al-rich with increasing temperature. Such features are apparent in assemblages formed at 110°C for # 124-209.9m and 170°C for # 123-348.5m. (2) The Al-end member of both prehnite and epidote are not stable under the physico-chemical conditions defined by the assemblages in drill holes # 123 and 124. Al-prehnite was replaced by the wairakite + calcite assemblage which is common in the Onikobe geothermal system. (3) The Fe-Al partitioning between epidote and prehnite suggests that the epidote always contains higher Fe than the coexisting prehnite.

The conclusions described above are consistent with those data derived from hydrothermal experiments (e.g., Liou et al., in press), from thermodynamic calculations (e.g., Bird & Halgeson, 1978) and from natural parageneses in burial metamorphic sequence (e.g., Evarts & Schiffman, 1983) and in other geothermal areas (e.g., the Salton Sea, Bird et al., 1983). The phase relationships shown in Figure 41 apply to environments with a very low activity of CO_2. In higher

CO_2-bearing geothermal fluids, the Ca-Al silicates including epidote, prehnite, wairakite and laumontite are not stable and are replaced by a carbonate-chloritic clay assemblage. Many investigated samples lack the Ca-Al silicates, particularly those from drill hole # 127. The significant effect of CO_2 on mineral assemblages in the Onikobe geothermal area will be discussed in a later section.

INTERPRETATION OF DEPTH ZONATIONS OF MINERALS

General Factors

Zonal distributions of minerals and phase relationships described in the previous sections are controlled by a complex interplay of many factors. The most important one is temperature. Figure 36, constructed using depth-temperature relations from the composite curve of Figure 35, shows the distribution of secondary minerals as a function of postulated present temperature in the field. Each mineral occurs over a considerable range of temperature and depth intervals and shows significant overlapping with the other phases. In order to assess the role of temperature in these zonations, we must also consider the effects of other variables including (a) solution chemistry, (b) bulk rock chemistry, (c) rock permeability and texture, (d) load pressure, (e) P_{H_2O}/P_{total}, (f) solid solutions in secondary minerals, (g) kinetics, and others. These controls on the genesis of secondary minerals in geotheraml systems have been reviewed by Browne (1978); they are briefly summarized below:

Solution chemistry is one of the most important variables in the formation of secondary mineral assemblages. The fluid's pH and P_{CO_2} are two of the most important factors. For example, Zen (1961), and Thompson (1971) have postulated that a high P_{CO_2} may inhibit the formation of calcium zeolites at given P and T conditions as shown by the following reaction: Clay + Calcite = Ca-zeolite + CO_2. Likewise, by the law of mass action, a low pH would favor reactions that would consume H^+. Details of $T\text{-}X_{CO_2}$ relations of hydrous Ca-Al silicates in

geothermal systems and the pH effect on the relative stability between Ca-zeolites and carbonate will be discussed later.

In closed or low permeability strata, the solution chemistry may be strongly affected by the local bulk-rock chemistry. The effect of the bulk rock chemistry would be much less important in high-flow, permeable situations. All the drill hole core samples from the Onikobe geothermal area have similar andesitic-dacitic compositions.

The effect of load pressure differences will be quite small given the relatively shallow depths of the wells. However, given the presence of major fluid components other than H_2O in geothermal systems, the effect of $P_{H_2O}/P_{fluid} < 1$, may often be important. Values as low as 0.3 P_{H_2O}/P_{total} ratio have been postulated for typical geothermal systems (Coombs et al., 1959). These lower ratios significantly restrict the stability fields of the hydrous phases toward lower temperatures.

Experimental studies have usually been carried out with pure end-member compositions. If an appreciable amount of solid solution occurs within a given mineral in a geothermal system, then its stability range will be expanded relative to the studied pure end-member and interpretations will have to be modified. An example dealing with prehnite-epidote equilibrium will be discussed later.

The effect of kinetics is a controversial and not easily definable problem. At low temperatures ($\lesssim$50-100°C), it is generally acknowledged that kinetic constraints are often important. At intermediate temperatures found in geothermal wells, however, the situation is much more ambiguous, especially given the variable lengths of time for which such systems operate. It is interesting to note that zeolite assemblages have been observed to become simpler with increasing age and that zeolites are generally not found in rocks older than early Paleozoic (Hay, 1966).

Relevant Experimentally Determined Stabilities of Some Hydrous Aluminumsilicates

Ca-zeolites: If we now examine available data from experimental stability studies on some of these minerals, we may be able to set some limits on their

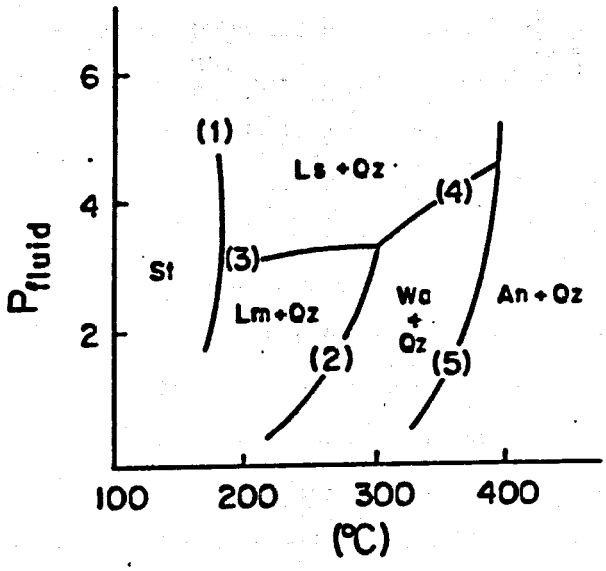

Figure 42. Experimentally determined P_{fluid}-T relations among stilbite (St), laumontite (Lm), wairakite (Wa) and lawsonite (Ls) in the presence of excess quartz (Qz) and H_2O (Liou, 1970, 1971a,b). Reaction 1: St = Lm + 3 Qz + 3 H_2O, 3: Lm = Ls + 2 Qz + 2 H_2O, 4: Wa = Ls + 2 Qz, and 5: Wa = An + 2 Qz + 2 H_2O.

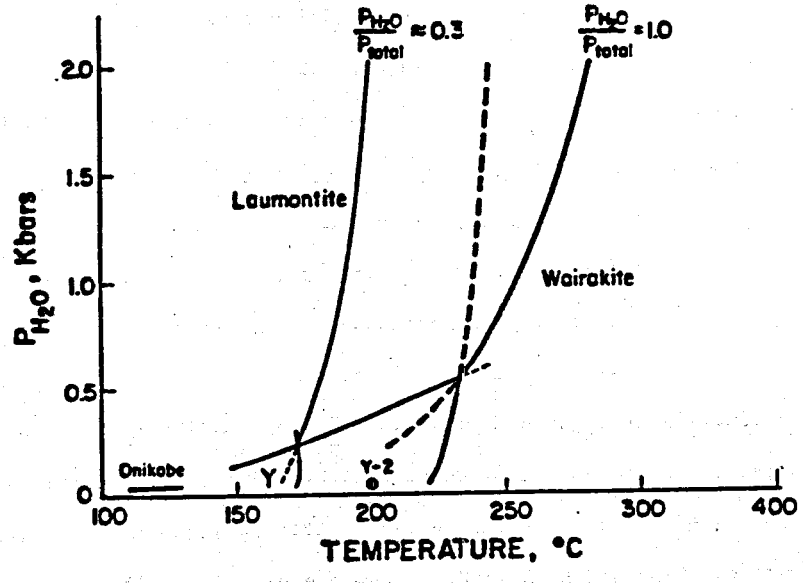

Figure 43. P_{fluid}-T diagram showing the stability relations among yugawaralite(Y), laumontite, and wairakite in the presence of excess quartz and fluid at P_{H_2O}/P_{total} = 1.0 and 0.3. The recorded temperatures and depths for yugawaralite occurrences in Onikobe (Seki et al., 1969) and in Y-2 hole of Yellowstone geothermal systems are also plotted for comparison (for details see Zeng and Liou, 1982).

conditions of formation. Figure 42 shows stability fields for the minerals laumontite, lawsonite and wairakite at $P_{fluid} = P_{total}$ (from Liou, 1970, 1971, a, b) as experimentally determined for the following reactions:

(1) stilbite = laumontite + 3 quartz + 3 H_2O,

(2) laumontite = wairakite + $2H_2O$,

(3) laumontite = lawsonite + 2 quartz + $2H_2O$, and

(4) wairakite = anorthite + 2 quartz + 2 H_2O.

In the Onikobe wells, where fluid pressure is less than total pressure and the H_2O activity is less than one due to dissolved substances, these zeolites would occur at lower P-T conditions than those determined by the experiments. One would thus expect the laumontite-wairakite transition to occur at somewhat less then 200°C. Using Figure 36, we find that laumontite occurs over the 85° to 195° range and that wairakite occurs from 130° to >275°C. The upper limit of laumontite is in good agreement with the experimental value, but the lower limit of wairakite isn't; furthermore, substantial overlap occurs between the laumontite and wairakite fields within most wells. This could be explained in at least three ways:

1. microprobe analyses of wairakite indicate up to about 23 mole % analcime component; this should extend the wairakite stability field to lower temperatures and explain the overlap of Na-bearing wairakite and laumontite.

2. some of the wairakite occurs in veins or open fractures where P_{fluid}/P_{total} may often be less than unity, also favoring the formation of the less-hydrated wairakite at lower temperatures.

3. the minerals at a given depth may not have equilibrated at one temperature but may instead be the composite products of a changing temperature regime. The systematic zoning of wairakite veins in well # 127 may support this point.

Figure 43 from Zeng and Liou (1982) shows the experimentally-determined and calculated stability relations among yugawaralite, laumontite and wairakite at $P_{H_2O}/P_{total} = 1.0$ and 0.3. The reaction: yugawaralite = wairakite + $2SiO_2$ + $2H_2O$ was experimentally determined and the phase relationships among the three Ca-zeolites under geothermal conditions of $P_{H_2O} = 0.3 * P_{total}$ were

estimated. In geothermal systems such as the Onikibe geothermal system where the fluid phase contains abundant other components in addition to H_2O, and where P_{fluid}/P_{total} ratios may be approximately 0.3, yugawaralite stability will be restricted to depths shallower than 500m.

From Figure 36 we find that yugawaralite occurs over the temperature range of 150-205°C in the Onikobe cores, spanning almost the entire overlap area between laumontite and wairakite. This would correspond to a P_{H_2O}/P_{total} ratio intermediate between 0.3 and 1.0. The relatively narrow stability range of yugawaralite at low P_{H_2O}/P_{total} values would help to explain its relative paucity in the Onikobe cores and in other geothermal areas.

As shown in Figure 43, the paragenetic depth sequence of Ca-zeolites in a geothermal system is highly dependent on the imposed thermal gradient, on the P_{H_2O}/P_{total} ratio, and on other factors, including solution composition (e.g., Giggenbach, 1981). In a geothermal system with a relatively high geothermal gradient and a high P_{H_2O}/P_{total} ratio, yugawaralite may be stable and the depth sequence could be mordenite→laumontite→yugawaralite→wairakite. On the other hand, in regions with a lower geothermal gradient and a lower P_{H_2O}/P_{total} ratio, yugawaralite is not stable and the zonation of Ca-zeolites could be mordenite→laumontite→wairakite. Because many geologic, solution and hydrologic conditions may control both the P_{H_2O}/P_{total} ratio and the geothermal gradient, different depth zonation patterns of Ca-zeolites may occur even in a single geothermal system. Such variations have been recorded in the Onikobe geothermal area by Seki et al., (1969b).

Clay Minerals: Figure 44 shows the experimentally-determined transformation of kaolinite to pyrophyllite represented by the equation: kaolinite + 2 quartz = pyrophyllite + H_2O (A.B. Thompson, 1970). At $P_{H_2O} = P_{total}$ of a few hundred bars, the transformation temperature is given as approximately 300°C. The upper limit for kaolinite postulated at Onikobe is 275°C. The lack of an apparent overlap may be due to the fact that kaolinite is very infrequent at depth, and pyrophyllite is only found in three wells. The lower transition temperature at

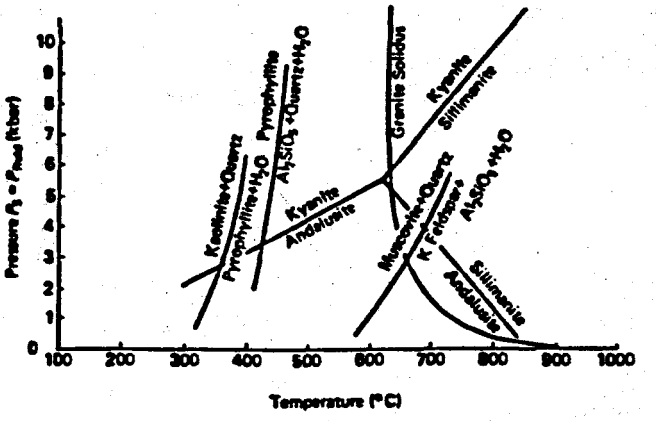

Figure 44. Kaolinite-pyrophyllite stability diagram after Thompson (1970), with stability relations of other minerals (Holdaway, 1971; Kerrick, 1971).

Onikobe could once again be due to a low P_{H_2O}/P_{total} value.

The occurrence of kaolinite or pyrophyllite is strongly influenced by solution chemistry. According to Hemley (1964), both kaolinite and pyrophyllite are stable only under acid conditions. His experimental conclusion is supported by our observations in the Onikobe area. Kaolinite is generally found only at or near the surface, where acid-sulfate waters occur as a result of H_2S and pyrite oxidation. Pyrophyllite is often found with mineral assemblages characteristic of acidic conditions. In the deeper than 800m segments of wells GO-10 and GO-11 where pyrophyllite is most abundant, calcite is almost always absent and wairakite is erratic in GO-10 and completely absent in GO-11.

Relatively little experimental work exists at low to medium temperatures for interstratified clays due to both the sluggish reaction rates and to the compositional and structural complexity of clay minerals. Eberl and Hower (1976) have examined the kinetics of illite formation from interstratified smectite/illite for several compositions. Extrapolation from their data indicates that at temperatures above about 150°C, less than 1000 years would be required to produce a 20% expandable illite/smectite from a 100% expandable smectite of K-beidellite composition. If these data are applicable to the Onikobe area, this would indicate that kinetic constraints are not the most important factor in illite formation for

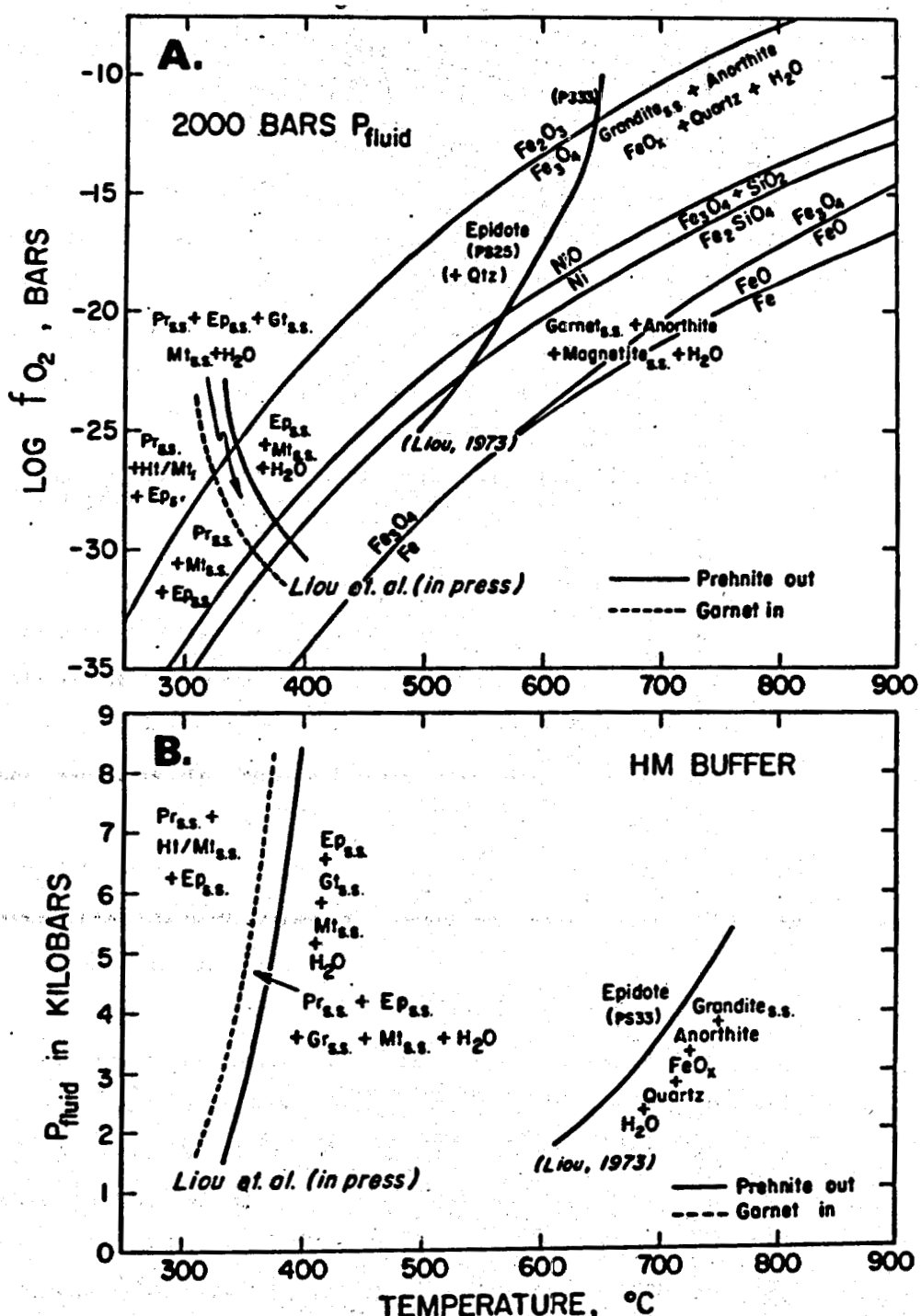

Figure 45. A. log f_{O_2}-T diagram (P_{fluid} = 2 Kb) and B. P_{fluid}-T diagram (f_{O_2} = HM buffer) for the garnet-in discontinuous and prehnite-out continuous reactions (Liou et al., in press). The previously determined curve for the maximum stability of epidote from Liou (1973) is also shown for comparison.

most of the length of the drill cores. However, Eberl and Hower (1976) and Eberl (1978b) also found that the persence of other interlayer cations such as Na and Cs appeared to substantially retard the conversion of smectite to smectite/illite and eventually to illite. Although insufficient data exists to quantitatively assess this effect, it may be of major importance in determining whether illite will form over the time intervals of interest in geothermal systems. Thus, facturs such as solution and bulk rock chemistry would be important in considering the formation of illite.

Albite, Prehnite and Epidote: These three minerals show notable depth-dependent behavior. Liou (1971) experimentally determined the stability curve for the reaction: analcime + quartz = low albite + H_2O. The presence of a sodium-bearing wairakite instead of analcime makes it dangerous to extrapolate between the two systems. In the Onikobe area, albite apparently occurs from temperatures as low as 110°C to as high as or greater than 275°C. Again, low P_{H_2O}/P_{total} would favor albite in a dehydration reaction. The observed occurrence of albite formed below 50°C in saline lakes (Hay, 1977) and in the Green River formation would indicate that fluid composition or kinetic factors may play a very large role in albite stability.

The prehnite-epidote equilibria have been recently determined for a bulk composition of Ps 33 + excess H_2O by Kim et al., (in press). The epidote of Ps 33 can be related to prehnite by a simple reaction: epidote (Ps 33) + H_2O = prehnite + hematite; however, the reaction relationship is not that straightforward. Instead, the reaction passes through a P-T transition zone in which both compositions and proportions of prehnite and epidote vary continuously with changing temperature and oxygen fugacity. Such continuous reactions are very common in low-grade mineral paragenesis.

Examples of P-T, f_{O_2}-T and T-X diagrams are illustrated in Figures 45 and 46 together with the maximum stability limit of epidote experimentally determined by Liou (1973). As shown in Figure 46, epidote has a wide stability field with a temperature range of $< 300°$-550°C, 2-8 Kb P_{fluid} and over a

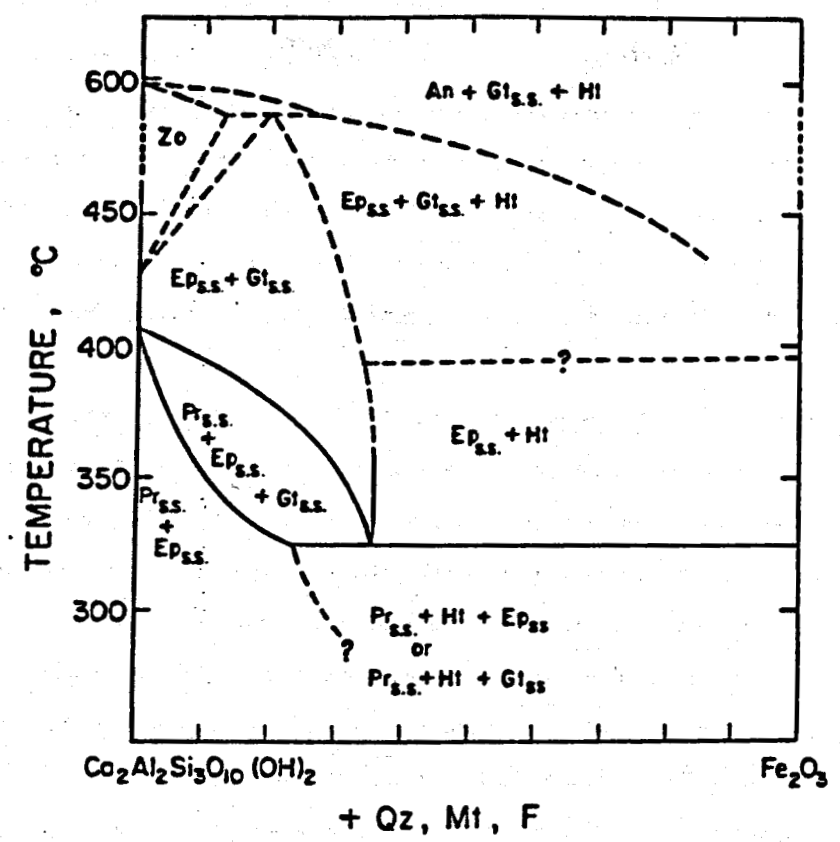

Figure 46A T-X diagram for the system Fe_2O_3-$Ca_2Al_2Si_3O_{10}(OH)_2$ with excess quartz, magnetite and fluid showing the relations among prehnite, epidote, garnet and hematite at 2000 bars P_{fluid} and f_{O_2} of the HM buffer. The system is pseudobinary only in the P_{fluid}-T regions where garnet solid solutions form (after Liou et al., in press).

range of f_{O_2} values. Two reactions were delineated at low temperatures: the garnet-in reaction defines the minimum stability for the garnet-bearing assemblages and the prehnite-out reaction the maximum stability for the prehnite-bearing assemblages. A transition zone occurs between these two assemblages where the three phases epidote + prehnite + garnet are stable and the compositions of these phases vary according to the P_{fluid}-T-f_{O_2} conditions. With successive increase in temperature and decrease in f_{O_2}, both epidote and prehnite become progressively more aluminum-rich and the coexisting garnet moves toward the grossular end-member. At temperatures below 325°C, the assemblage

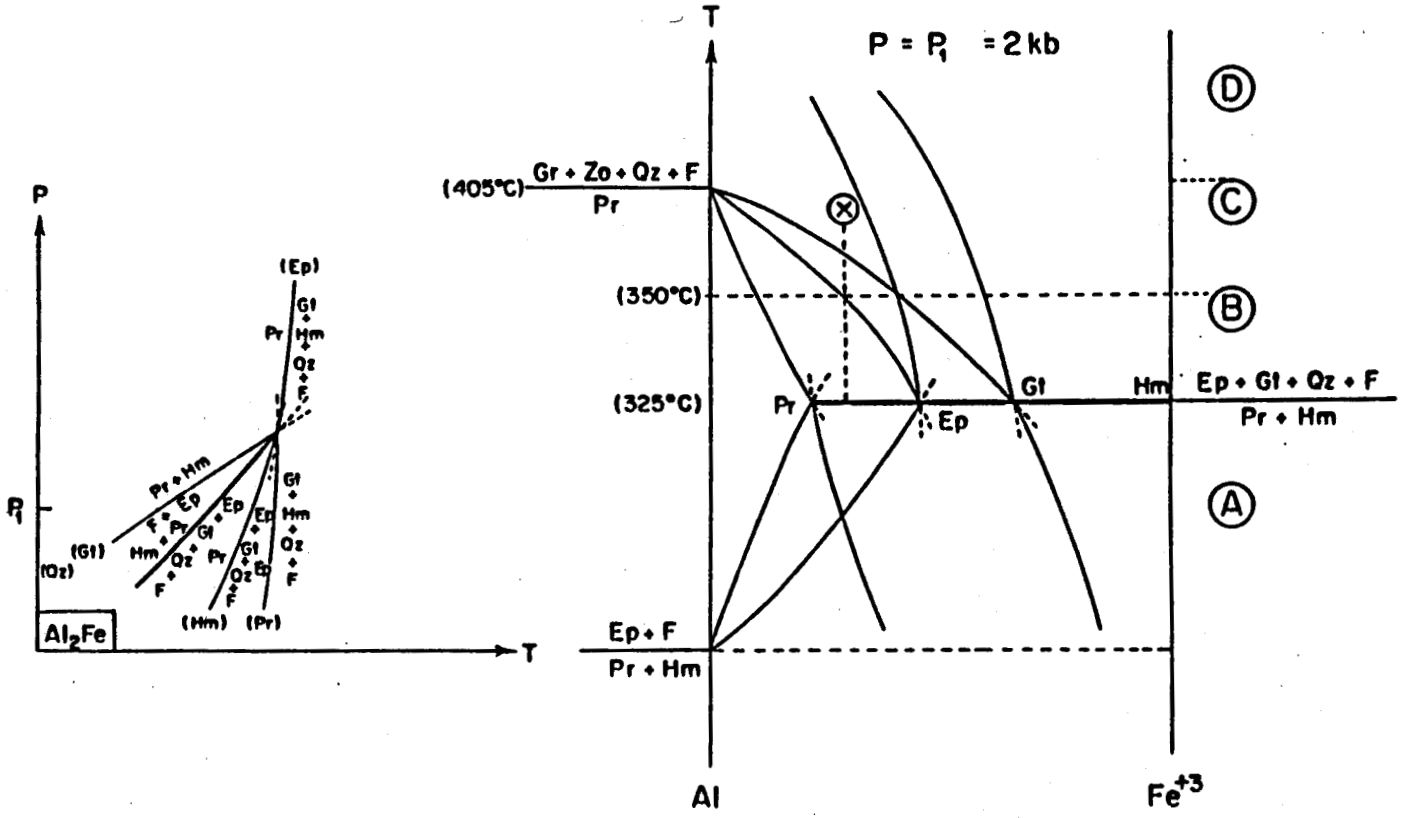

Figure 46B Schematic P-T and T-X_{Fe-Al} diagrams showing 5 continuous (light lines) and one discontinuous (heavy line) reactions relating prehnite, epidote, garnet, iron oxide, quartz and fluid in system $CaO-Fe_2O_x-Al_2O_3-SiO_2-H_2O-O$ following the procedure of Thompson (1976). Mineral compositions and assemblages shown in Figure 47A,B,C, and D are indicated. X is the starting composition. Temperatures shown on the diagram are from the present data and Liou (1971). (After Liou, et al., in press).

epidote-prehnite-garnet is not stable and both prehnite and epidote in the 3-phase assemblage epidote-prehnite-hematite decrease their Fe^{+3} content with decreasing temperature. In other words, in the presence of epidote, prehnite reaches its maximum Fe^{3+} content at the temperature defined by the discontinuous reaction. At lower temperatures, prehnite composition is highly dependent on the mineral assemblage. If prehnite coexists with garnet (or another Ca-Al phase) and hematite, it may have higher X_{Fe}^{3+} than the prehnite coexisting with epidote-hematite-quartz.

Phase relations of prehnite, epidote, garnet and hematite as a function of temperature in the pseudo-ternary system $CaO-Fe_2O_3-Al_2O_3$ with excess quartz, and fluid at 2 Kb P_{fluid} and f_{O_2} defined by the HM buffer are shown in Figure 47. With increasing temperature, four isobaric-isothermal sections are drawn in order to show the compositional relations among garnet, epidote, prehnite and hematite for both three-phase and two-phase assemblages. These diagrams were constructed based on experimental results and on deduced natural paragenesis and mineral compositions and show the following: (1) Within the temperature interval 325-550°C, the range of grandite solid solution remains complete in the system with the presence of excess quartz, whereas the ranges of solid solutions for epidote and prehnite become very restricted with increasing temperature. (2) The tie lines for 2-phase and 3-phase regions show the equilibrium compositions for the coexisting phases. These data are deduced from experimental results, available analyses of natural co-existing phases (e.g., Coombs et al., 1977) and from thermodynamic calculations (e.g., Bird & Helgeson, 1978). (3) The discontinuous reaction at 325°C representa a tie-line cross type and the continuous reaction at 350°C relates the shift of a 3-phase field to a 2-phase region. Respectively, these two reactions are equivalent to the garnet-in and prehnite-out reactions shown in Figure 45.

It is apparent that the phase relations of Figures 45, 46 and 47 apply to temperatures greater than 325°C and that at low CO_2 activity calcite is not stable. Hence they cannot directly appply to the phase relations described for the

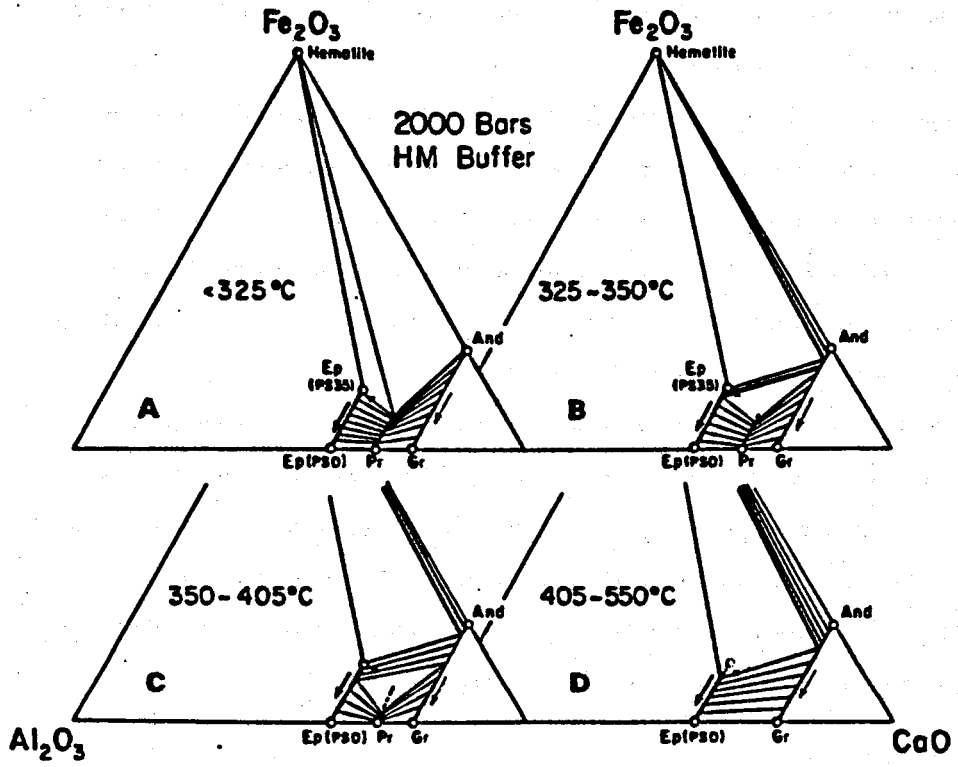

Figure 47. Phase relations of prehnite, epidote, garnet and hematite as a function of temperature in the system $CaO-Fe_2O_3-Al_2O_3-SiO_2-H_2O$ with escess quartz, and fluid at 2000 bars P_{fluid} and f_{O_2} of the HM buffer. Positions of tie lines are qualitative. X was the starting composition for the experimental study of Liou et al. (in press) and arrows indicate the shift of composition with increasing temperature.

Onikobe geothermal system. However, the principle for the sliding equlibria and compositional trends of both epidote and prehnite together with hematite or magnetite are consistent with those described in the previous sections. For instance, in comparing Figures 41(C) and 47(A), it is evident that at the conditions of the Onikobe geothermal system, (1) garnet is not stable and calcite is ubiquitous, (2) the 3-phase assemblage Ep + Pr + Hm (or Mt) was not found in the available core sample, (3) compositions of coexisting epidote and prehnite in the 3-phase assemblage Ep + Pr + Wr are lower in Fe^{+3} contents than those in Ep + Pr + Cc, (4) both epidote and prehnite have much restricted compositions compared to those

in high-temperature conditions and Al-end members of epidote (clinozoisite) and prehnite are not stable and (5) epidote is consistently higher in Fe^{+3} content than the coexistent prehnite.

In summary, one can observe that the apparent observed temperature ranges over which minerals are found in the Onikobe area are generally broader than those expected from experimental studies. This may be explained in at least 3 ways:

1. The equilibrium studies may essentially explain the observed temperature relationships if variables such as changes in solution and bulk rock chemistry, rock texture, and P_{H_2O}/P_{total} are considered.

2. The equilibrium studies may explain the observed relationships if the minerals are considered to have formed under equilibrium conditions at different times, with the temperature varying at a given depth as a function of time. As the conditions changed, some of the minerals continued to persist metastably.

3. Metastable reactions may be important in the formation of many of the phases observed, especially at temperatures below about 150°C.

Effects of CO_2 and SO_4 on Mineral Assemblages

The thermal waters from the Onikobe geothermal area described in the previous sections contain significant amounts of CO_2, SO_4, NaCl and other impurities. High concentrations of these components have resulted in the crystallization of carbonate, gypsum or anhydrite and halite at the expense of Ca-Al silicates and in the lowering of the temperature of appearance of some index minerals. A detailed discussion of their effects will not be presented here; the importance of the CO_2 concentration in the fluid phase will be used to exemplify their significance.

The role of CO_2 in low-grade metamorphism has been recently reviewed (Seki & Liou, 1981). Previous experimental and theoretical studies indicate that the breakdown of Ca-bearing silicates and their assemblages into calcite-bearing assemblages will occur as a result of increasing mole fraction of CO_2 in the fluid phase to over 0.1 at temperatures below 400°C.. For example, at $P_{total}=P_{fluid}=2$ kb, laumontite can only be stable at temperatures below 350°C

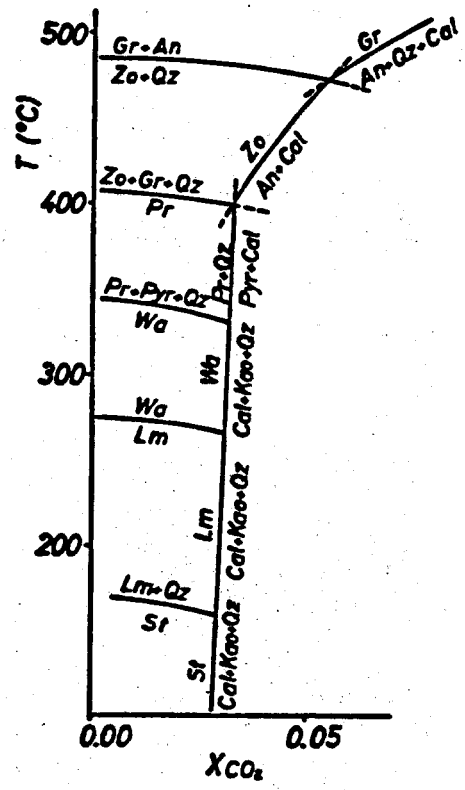

Figure 48. Probable temperature X_{CO_2} diagram in the $CaO-Al_2O_3-SiO_2-CO_2-H_2O$ system ($P_{total} = P_{fluid} = 2$ kb)(Seki and Liou, 1981).

1: 4 Zoisite + Quartz $\rightleftharpoons$ Grossularite + 5 Anorthite + $2H_2O$
2: Anorthite + Quartz + 2 Calcite $\rightleftharpoons$ Grossularite + $2CO_2$
3: 3 Anorthite + Calcite + $H_2O \rightleftharpoons$ 2 Zoisite + CO_2
4: 5 Prehnite $\rightleftharpoons$ 2 Zoisite + 2 Grossularite + 3 Quartz + $4H_2O$
5: 2 Calcite $\pm$ Pyrophyllite $\rightleftharpoons$ Prehnite + Quartz + CO_2
6: 2 Wairakite $\rightleftharpoons$ Prehnite + Pyrophyllite + Quartz + $2H_2O$
7: Calcite + Kaolinite + 2 Quartz $\rightleftharpoons$ Wairakite + CO_2
8: Laumontitie $\rightleftharpoons$ Wairakite + $2H_2O$
9: Calcite + Kaolinite + 2 Quartz + $2H_2O \rightleftharpoons$ Laumontite + CO_2
10: Stilbite $\rightleftharpoons$ Laumontite + 3 Quartz + $3H_2O$
11: Calcite + Kaolinite + 5 Quartz + $5H_2O \rightleftharpoons$ Stilbite + CO_2

Reactions 5, 7, 9 and 11 limiting X_{CO_2} are not continuous.

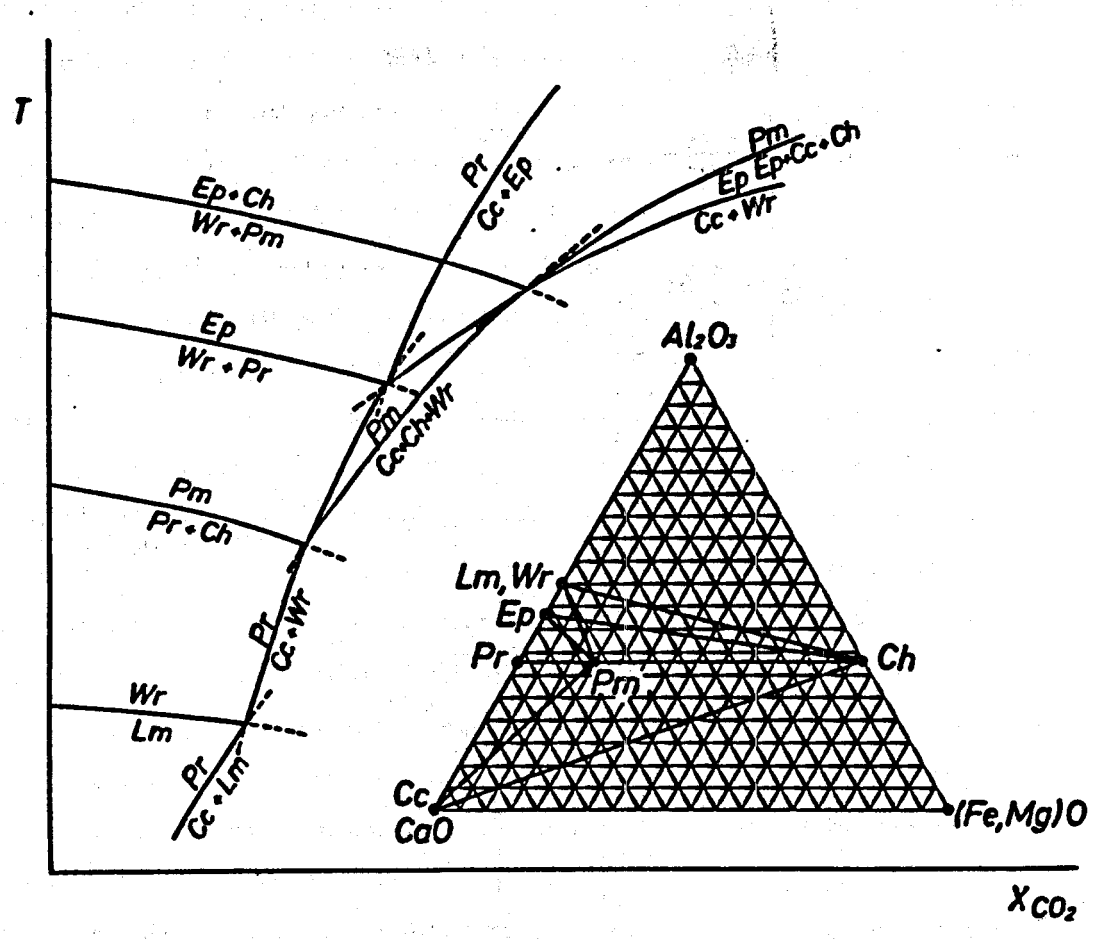

Figure 49. Schematic T-X_{CO_2} relations for Ca-zeolites (laumontite, wairakite), prehnite, pumpellyite, epidote, chlorite and calcite in a simple system Al_2O_3-CaO-(Fe, Mg)O-SiO_2-H_2O-CO_2. The geometric relations are constructed under the assumptions that (1) chlorite is amesitic in composition, (2) pumpellyite lies on the joint chlorite and prehnite, and (3) quartz and fluid are present in excess. In geothermal systems where Fe_2O_3 is ubiquitous in the Ca-Al silicates, the simplified relations could be significantly modified.

at extremely low CO_2 concentrations in the fluid (X_{CO_2} = 0.0075 - 0.02) (Ivanov and Gurevich, 1975). These theoretical and experimental studies also indicate that the equilibrium temperatures at which carbonate-bearing assemblages and carbonate-free assemblages coexist shift significantly by small changes in X_{CO_2}.

Petrographic evidence also clearly indicates the importance of CO_2 in the

fluid phase for causing differences in low-grade assemblages. The most important effects of CO_2 on low-grade metamorphic parageneses would be to: (1) decrease the dehydration temperatures of Ca-Al and other hydrosilicates; and (2) stablize Ca (and also Mg and Fe) in carbonates at the expense of epidote, prehnite, pumpellyite and Ca-zeolites. The mole fraction of CO_2 in the fluid phase attending low-grade metamorphism has generally been assumed to be very low. Coombs et al. (1976) postulated that the X_{CO_2} for pumpellyite-actinolite facies metamorphism in the Loeche area, Switzerland is lower than 0.02. X_{CO_2} attending regional metamorphism of a Triassic formation in the Swiss Alps at about 200-550°C and 1-5 kb was estimated to be lower than 0.2 (Frey, 1978). X_{CO_2} in fluids attending low-grade metamorphism to form zeolites and clay-carbonate assemblages in Cretaceous non-marine sediments of Alberta, Canada was inferred to be lower than 0.0075 (Ghent and Miller, 1974). In the fossil geothermal area in Reydarfjordur, Iceland, mineral parageneses suggest that early deposition of a clay and calcite assemblage occurred at higher X_{CO_2} and was succeeded by the later crystallization of zeolites, prehnite and epidote at reduced X_{CO_2} conditions (e.g., Mehegan et al., 1982). Similarly, the less common occurrence of wairakite, prehnite and epidote in the Ohaki-Broadlands geothermal area, New Zealand compared to the Wairakei area has been attributed to a high concentration of CO_2 in thermal waters in the former area (Browne & Ellis, 1970).

As shown in Figures 48 and 49, the most characteristic Ca-silicates in low-grade metamorphism are stable at X_{CO_2} values of less than 0.1. The CO_2 content of the fluid phase controls not only the equilibrium temperature for successive mineralogical zones but also the appearance of the calcite + clay association at the expense of Ca-Al silicates. Moreover, the CO_2 concentration strongly affects the pH value of a hydrothermal solution. Zeolite and other Ca-Al silicate assemblages are believed to develop mainly in alkaline environments. In contrast, the characteristic assemblage formed under acidic conditions is a clay + carbonate assemblage. The generally accepted idea that the Ca-Al silicates are stable at a low activity of CO_2, hence in slightly alkaline solution, is

confirmed by observations of mineral parageneses in geothermal areas.

The mineral assemblages identified in the Onikobe samples may have formed at T-X_{CO_2} conditions very close to that of the (Pm) invariant point of Figure 49, inasmuch as pumpellyite was not found. It should be emphasized that Figure 49 is very schematic and the system applies only to phases having ideal compositions. If components such as Fe_2O_3 are introduced, most of the reactions would shift toward higher X_{CO_2} and lower temperature conditions than those shown in the figure. For example, the reaction: prehnite + CO_2 + H_2O = wairakite + calcite + quartz would expand significantly toward higher X_{CO_2} conditions if the prehnite contains a sufficient amount of Fe_2O_3. In essence, the Al-prehnite (as well as the clinozoisite and pumpellyite) may have a very restricted T-X_{CO_2} stability field; this may explain why these phases were not found in the Onikobe samples.

Because of the importance of CO_2 in low-grade metamorphism, more extensive investigations with experimental techniques that control P_{H_2O}/P_{CO_2} under hydrothermal conditions are necessary to yield further information on the stability relations between zeolites, prehnite and other minerals and carbonate assemblages, which in turn may be correlated with natural mineral associations.

Figure 50 is a log $[Ca^{2+}]$ - pH diagram of Oki and Hirano (1976) used to illustrate the stability relations of calcite-laumontite-anhydrite at 150°C in terms of pH, activities of Ca^{2+} and SO_4, partial pressure of CO_2, and activity ratio of $Al(OH)_4^-$ / H_4SiO_4. This diagram was constructed on the basis of thermodynamic calculations and was used to explain the parageneses of minerals from the Yugawara geothermal area, Japan. (A circle represents the field of Yugawara thermal waters). Depending on these variables, the laumontite, calcite and anhydrite stability fields overlap considerably. Selected analyses of thermal waters from the Onikobe geothermal system are plotted onto this diagram. The results indicate that the Onikobe system waters contain a higher P_{CO_2}, a lower activity of SO_4, a lower activity ratio of $Al(OH)^-$ / H_4SiO_4, and lower pH, compared to those of the Yugawara geothermal system. Therefore, laumontite

No.	pH	log[Ca]	logPco2
GO-2	8.47	-2.25	0.28
GO-3A	7.26	-4.34	-1.22
GO-3B	7.54	-3.84	-2.28
GO-3C	6.04	-3.63	0.50
GO-3D	7.11	-3.88	-1.37
GO-4	7.61	-4.11	-2.15
GO-5	8.54	-2.62	0.49
GO-6	7.75	-4.01	-2.54
GO-7A	6.58	-2.64	-1.57
GO-7B	6.18	-2.72	-0.67
GO-7D	5.72	-1.93	-0.55
GO-8A	6.22	-2.49	-1.00
GO-8C	6.29	-2.14	-1.47
#111	6.67	-2.28	-2.09
#127	7.28	-3.01	-2.59
Y-line	6.42	-2.55	-1.33

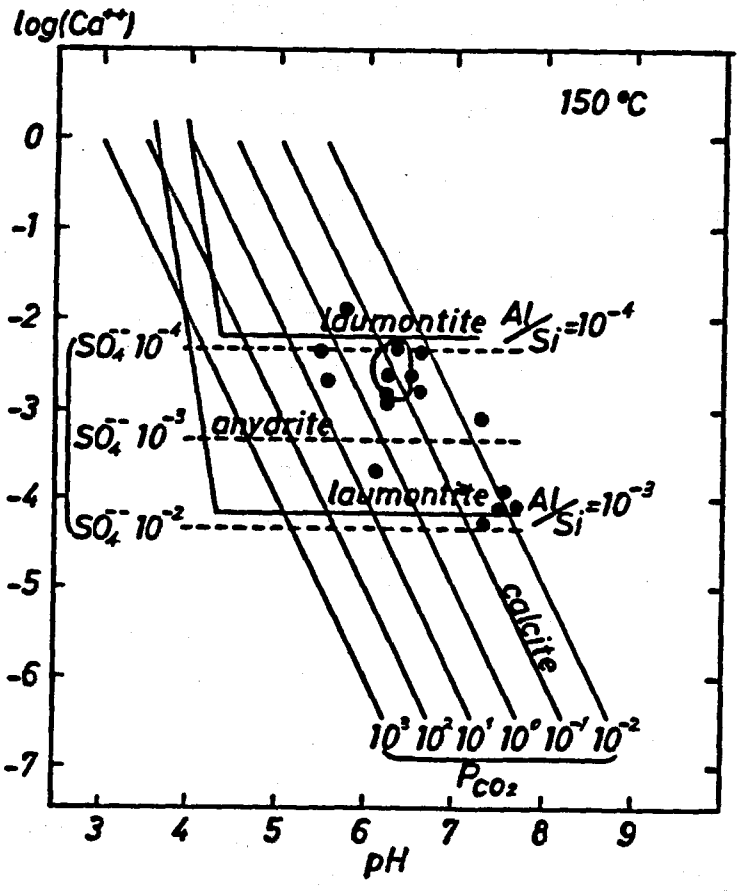

Figure 50. Geothermal waters of Onikobe area in log $[Ca^{2+}]$ versus pH diagram. Activity coefficient for each ion is calculated by the Debye-Hückel equation. An area circled by solid line indicates the field of thermal water of Yugawara geothermal are (Oki et al., 1976).

(and other Ca-Al silicates) and calcite are more common, whereas gypsum (or anhydrite) is less common in the Onikobe core samples. However, it should be emphasized that these interdependent variables and temperatures change with time and depth even in a single well. Therefore, correlation of the occurrences of Ca-Al silicates, carbonates and sulfates between different geothermal systems must be done with caution.

Summary

The distribution of secondary phases with depth in the Katayama area, Onikobe is primarily controlled by changes in temperature. Other factors which are important either locally or with regard to certain minerals are the following: the P_{water}/P_{total} ratio, solution and bulk rock chemistry, rock permeability, and kinetic constraints. Depth-dependent zonation patterns are observed for the calcium zeolites, interlayered clay minerals, and several other minerals.

ORIGIN AND DISTRIBUTION OF SOLUTION TYPES

As was shown in Table 3, many of the geothermal wells in the Onikibe geothermal area discharge acid-chloride type solutions, characterized by a high chloride to sulfate ratio and a low pH of 2 to 4.5. The presence of these acidic fluids in the geothermal field and their utilization for generating electric power has been a major problem throughout the development of the field. Figure 51 shows the major solution types that have been discharged by each well or drill-hole plotted on the drill hole distribution map. Figure 52 shows the same type of information for thermal springs at the same Onikobe area. It can be seen that the acid-chloride water type is limited to drill-holes in the Katayama and Megama areas.

In order to understand the possible origins of the acid-chloride water type, it is also necessary to examine the origins of the other major water types. They are briefly described below:

(1) Alkali chloride waters are generally high-temperature fluids produced at

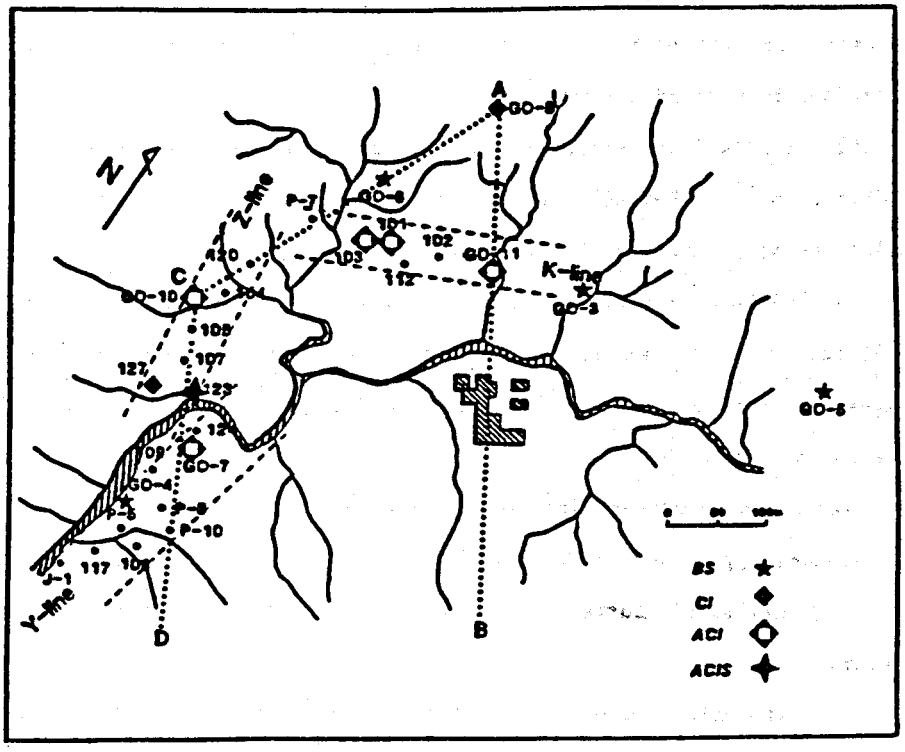

Figure 51. Distribution of solution types in Katayama area of Onikobe geothermal area, Japan (see Figure 2).

Bs: Bicarbonate type
Cl: Alkali-chloride type
ACI: Acid chloride type
ACIS: Acid chloride sulfate type

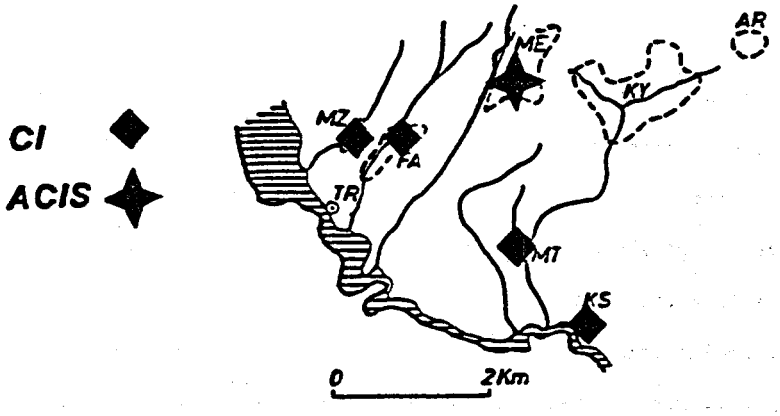

Figure 52. Distribution of hot-spring thermal water types in Onikobe geothermal area. Cl: Alkali-chloride type. ACIS: Acid chloride sulfate type. Solution types in Katayama area (KY) is shown by Figure 51. (AR,ME, KY, MZ, FA, TR, MT, KS: see Figure 7).

depth in many geothermal systems primarily as a result of meteoric water and volcanic rock interaction. Reactions with silicate minerals buffer the pH of the solutions to near neutral values.

(2) Acid sulfate waters originate near the surface as a result of the condensation of H_2S-bearing steam into surface waters and the subsequent oxidation of the H_2S to sulfate (Ellis and Mahon, 1977).

(3) Bicarbonate and bicarbonate-sulfate waters may form by near-surface condensation of CO_2 and H_2S-bearing steam and subsequent reaction with rocks. These waters have also been postulated to form organic water in silty layers within the Akazawa Formation.

(4) Acid chloride-sulfate waters may form by a number of different mechanisms, as proposed by Ellis and Mahon (1977):

1. mixing of neutral alkali chloride waters with near-surface acid sulfate waters.

2. the oxidation of sulfide to bisulfate at depth, resulting in a buffered near-neutral solution at depth which converts to an acidic solution because of the dissociation of bisulfate upon cooling.

3. the hydrolysis of sulfur to H_2S and sulfate at depth by high-temperature alkali chloride waters.

4. near-surface condensation of supercritical "steam" from a shallow magma body.

(5) Acid chloride waters merge in composition with acid chloride-sulfate waters by a slight to moderate increase in sulfate content. Several possibilities exist for the origin of the former:

1. Ozawa and Nagashima (1975) and Ozawa, Nagashima, and Iwasaki (1980) postulated that the acid-chloride water type was the prevalent one at depth in the Onikobe area, having formed by the mixing of magmatic HCl with meteoric water at depth. It is converted to the alkali chloride type as a result of buffering reactions with silicates on its way to the surface.

2. Acid chloride waters could form by the mixing of near-surface acid sulfate

waters with alkali chloride waters. The former could be transported to depth along faults which, after a time, could act as insulating passageways for the downward movement of acid near-surface waters without neutralizing them.

3. Acid chloride waters could form by the mixing of the same two solutions types as in the previous case in or along the drill hole itself as a result of casing failure.

Faults have been suggested as major pathways of fluids by several previous investigators (Matsuno and Nishimura, 1965; Hitosugi, 1969; and Nakano, 1981). However, no clear surface faults have been located and investigation of the #123, 124, and 127 core samples has also failed to reveal obvious fault features such as brecciation, slickensides, etc. This may not be surprising considering the intense level of hydrothermal alteration that the entire area has undergone. Other ways may exist of trying to determine probable fault locations and orientation if they do indeed exist:

1. the distribution of stream channels and surface expressions of hydrothermal activity related to the general topography.

2. variations in temperature vs. depth plots in drill holes; abrupt changes in the temperature of fluids as a function of depth may indicate a change in the flow regime. Two possible causes of this would be a highly permeable fault zone or a permeable ash-flow tuff horizon.

Figure 53 shows a possible fault model superimposed on the Katayama area drill hole distribution map. The postulated set of faults was located based on the existence of sub-parallel stream patterns north of the power plant area. Furthermore, the most intense hydrothermal surface activity occurs along the northern valley following proposed fault α on the map. Proposed dips on the faults were obtained using two lines of reasoning:

1. The faults found in a geological setting such as the Onikobe caldera are most likely to be high angle normal faults. Yamada (1972) measured dips of 70° or greater on faults located southwest of the Katayama area.

2. Geothermal gradients measured for each of the eleven drill holes often

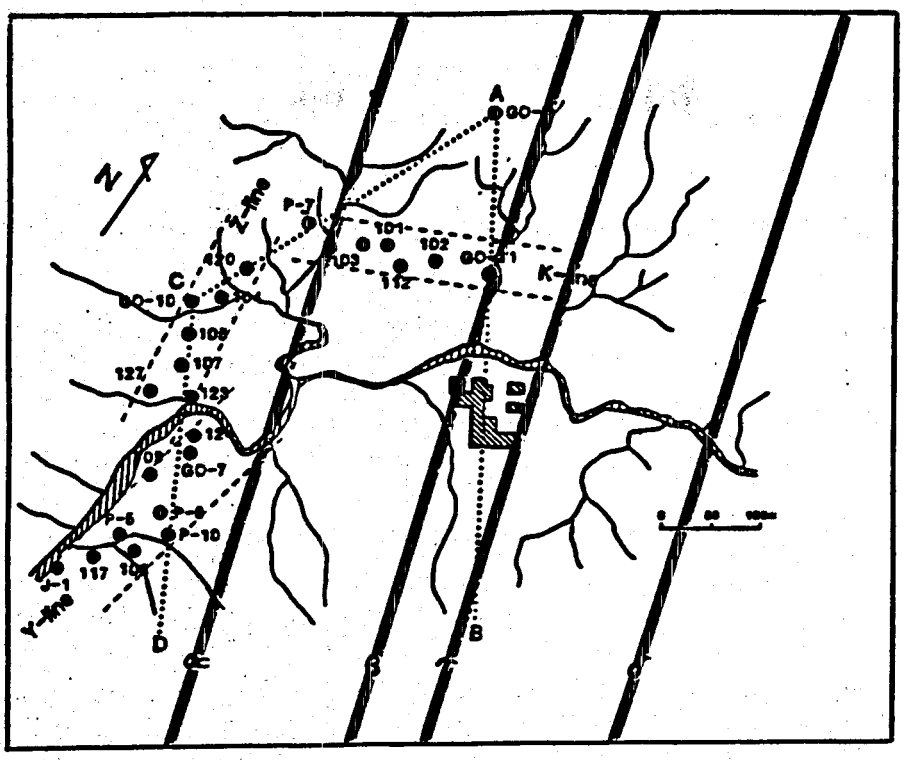

Figure 53. Localities of proposed faults in Katayama area of the Onikobe geothermal area, Japan (see Figure 2).

show abrupt temperature variations (see Figure 31). These were postulated to be due to the presence of permeable flow channels and were marked by shaded bars along drill holes on the three cross-sections across the Katayama field (Figure 54, cross sections DC, CA, and AB). Different dips on the fault set were then evaluated to see which one would best fit the data, especially for the better-characterized #127 well and the rest of the Y line. Postulated faults at depth were then drawn on all three cross-sections.

The following points were followed in constructing this model:

1. All faults in the set were assumed to be parallel to one another.
2. All faults were assumed to be planar.

The following results are obtained from this model:

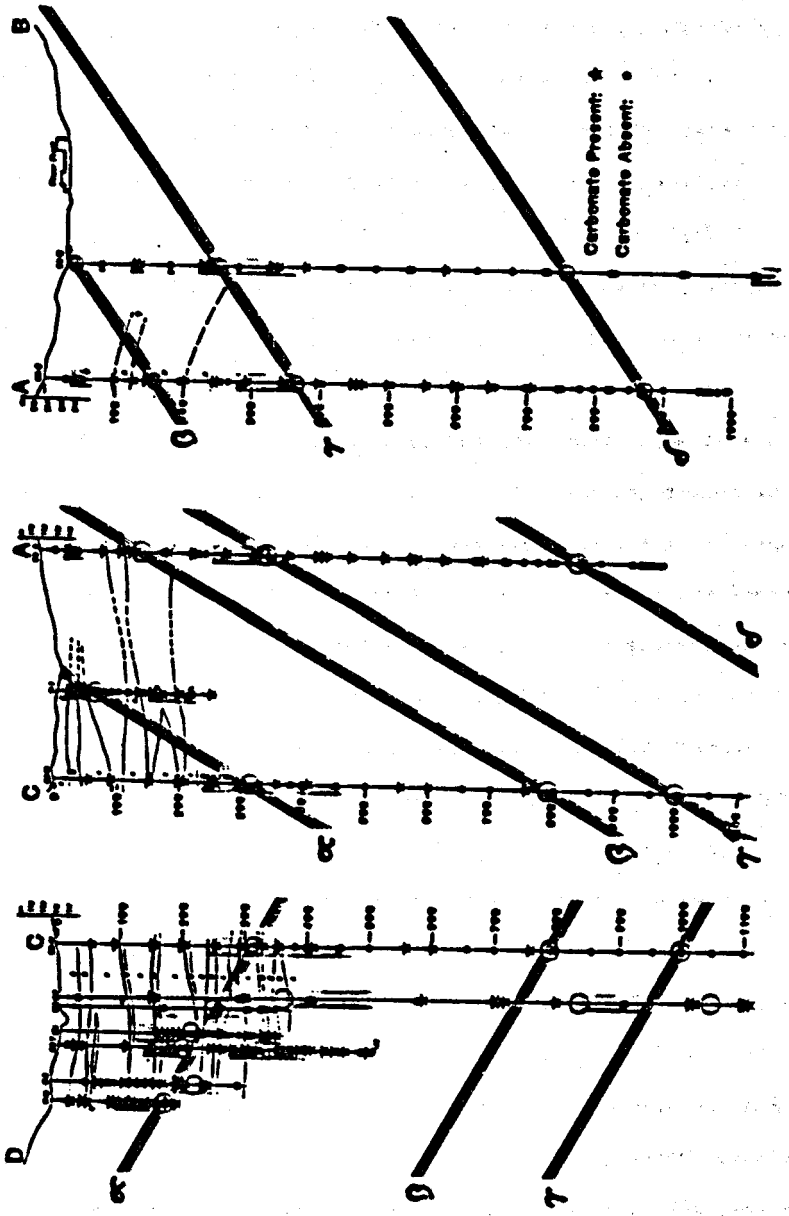

Figure 54. Schematic cross sections of proposed faults in Katayama area of the Onikobe geothermal area, Japan.

1. The location and orientation of fault α based only on the topography and on a typical dip value proposed by Yamada (1972) result in an apparent dip on the DC cross-section which roughly matches the depths and northward-dipping trend observed for the geothermal gradient irregularities in wells P-10 through GO-10. Well #127 is located farther west than the other wells on the cross-section and as such will exhibit deeper intersections when a westward-dipping fault is considered.

2. Fault β correlates well with the geothermal gradient anomaly observed at about 900m in well #127.

3. For cross sections CA and AB, the proposed faults match some of the features observed but leave others unexplained.

In order to make some statements concerning the origin of acid chloride type waters, it is important to consider two other factors: possible recharge sites for the meteoric water in the geothermal system, and the hydrologic gradient in the Onikobe area. Ozaki and Kanno (1977) and Ozaki (1981) have proposed a northeast to southwest hydrologic gradient. This is supported by the behavior of the two holes used as re-injection wells. Drill hole GO-11 was initially used for this purpose; however, this use resulted in interference with the K-line production wells to the west. When the J-1 reinjection well was used, however, no interference occurred with the Y-line wells to the northeast. Therefore, recharge of the field may occur roughly from the topographic high to the north-northwest.

This fault model could be interpreted in the following two ways regarding the origin of the acid-chloride waters:

1. The faults could act as passageways to allow either the passage of HCl-bearing magmatic fluids up from depth or the downwards flow of acid sulfate fluids from shallower levels.

2. The intersection of the faults with the land surface immediately to the north-northwest could furnish a mechanism for the local recharge of the system with contaminating acid sulfate waters. The steeply-dipping faults themselves would, after an initial reactive period, provide relatively non-reactive pathways to allow

acidic fluids to reach the subsurface.

We propose that an acid sulfate mixing model is more likely than a magmatic HCl model for the following two reasons. First, in those areas where magmatic HCl is being evolved, volcanic activity is generally still continuing and a shallow magma body is believed to exist (Ellis and Mahon, 1977). This is not the case for Onikobe; the last volcanic activity here is believed to have occurred 350,000 years ago with the formation of the Takahinata volcanic dome.

Secondly, some of the 200-400m deep wells at Onikobe geothermal area have shown a change in solution chemistry as a function of time. Initially neutral to weakly-alkaline wells have become acidic after several months to a year and flow has apparently become dependent on short-term precipitation patterns. This relationship could be interpreted as favoring the introduction of more acidic fluids from shallower levels rather than deeper.

The extensive absence of carbonate at depth in wells GO-10 and GO-11 might be explained by variations in rock properties. We have noted that the carbonate and wairakite-free zones are characterized by exceptionally porous rock.

The major solution types found at Onikobe are equivalent to those from other geothermal areas. The distribution pattern of solution types discharged by drill holes, however, seems to be complicated. The complication occurring here is the withdrawal of acidic solutions from wells as deep as over 1000 m. The origin of this acid fluid could be explained either by a deep-seated magmatic HCl source or by the contamination of neutral chloride waters with a small amount of near-surface derived acid-sulfate water. The latter could be due to steeply-dipping recharge faults or to corrosion of the well casing. The acid sulfate explanation is favored because of the relative volcanic inactivity of the area and the general hydrologic patterns observed in the Onikobe region.

REFERENCES

Arnórsson, S., K. Grönvold and S. Sigurdsson, 1978: Aquifer chemistry of four high temperature geothermal systems in Iceland, Geoch. Cosmoch. Acta, 42, pp. 527-536.

Awaya, T., T. Hirano and K. Kubodera, 1974: Hydrogen sulfide contents in hot springs and waters heated with volcanic steam, Hakone volcano (in Japanese with English abstract) Bull. Hot Spr. Res. Inst., 6, pp. 11-30.

Awaya, T., Hirano, T., Suzuki, T., and Oki, Y., 1976: Distribution of hydroxen sulfide in the air, Hakone volcano (in Japanese with English abstract). Bull. Hot Spr. Res. Inst., 7, pp. 27-42.

Bailey, S., 1980: Summary of recommendations of AIPZA nomenclature committee of clay minerals. Amer. Min., 65 pp. 1-7.

Bargar, K. and M. Beeson, 1981: Hydrothermal alteration research drill hole Y-2, Lower Geyser Basin, Yellowstone National Park, Wyoming. Amer. Min., 66, pp. 473-490.

Bickle, M. and R. Powell, 1977: Calcite-dolomite geothermometry for iron-bearing carbonates. Contr. Mineral. Petrol., 59, pp. 281-292.

Bird, D.K. and H.C. Helgeson, 1978: Chemical interaction of aqueous solutions with epidote-feldspar mineral assemblages in geologic systems: 1. Thermodynamic analyses of phase relations in the system $CaO-FeO-Fe_2O_3-Al_2O_3-SiO_2-H_2O-CO_2$. Amer. Jour. Sci., 280, pp. 907-941.

Boles, J. and S. Franks, 1979: Clay diagenesis in Wilcox sandstones of southwest Texas: implications of smectite diagenesis on sandstone cementation. Jour. Sed. Petr., 49, pp. 55-70.

Brindley, G., 1961: Chlorite minerals in "The X-ray identification and crystal structures of clay minerals" (ed. G. Brown). Min. Soc. London, pp. 242-296.

Browne, P.R.L., 1978: Hydrothermal alteration in active geothermal fields. Annual Review of Earth and Plan. Sci., 6, pp. 229-250.

Browne, P.R.L. and A.J. Ellis, 1970: The Ohaki-Broadlands hydrothermal area, New Zealand: Mineralogy and related geochemistry. Amer. Jour. Sci., 269, pp. 97-131.

Coombs, D.S., A. Ellis, W.S. Fyfe and A.M. Taylor, 1959: The zeolite facies, with comments on the interpretation of hydrothermal syntheses. Geochim. Cosmochim. Acta, 17, pp. 53-107.

Coombs, D.S., Y. Nakamura and M. Vangnat, 1976: Pumpellyite-actinolite facies schists of the Taveyanne Formation near Loeche, Valais, Switzerland. Jour. Petr., 17, pp. 440-471.

Coombs, D.S., Y. Kawachi, B.F. Houghton, G. Hyden, I.J. Pringle and J.G. Williams, 1977: Andradite and andradite-grossular solid dolutions in very low-grade regionally metamorphosed rocks in southern New Zealand. Contr. Min. Petr., 63, pp. 229-246.

Dunoyer de Segonzac, G., 1970: The transformation of clay minerals during diagenesis and low-grade metamorphism: a review. Sedimentology, 15, pp. 281-346.

Eberl, D., 1978a: Reaction series for dioctadedral smectites. Clay and Clay Minerals, 26, pp. 327-340.

Eberl, D., 1978b: The reaction of montmorillonite to mixed-layer clay: the effect of interlayer alkali and alkaline earth cations. Geoch. Cosmo. Acta, 42, pp. 1-7.

Eberl, D. and J. Hower, 1976: Kinetics of illite formation. Geol. Soc. Amer. Bull., 87, pp. 1326-1330.

Eberl, D., G. Whitney and H. Khoury, 1978: Hydrothermal reactivity of smectite. Amer. Min., 63, pp. 401-409.

Ellis, A.J. and W.A.J. Mahon, 1977: Chemistry and geothermal systems. Academic Press, pp. 1-392.

Evarts, R.C. and P. Schiffman, 1983: Submarine hydrothermal metamorphism of the Del Puerto ophiolite, California. Amer. Jour. Sci., 283, pp. 289-341.

Exley, R.A., 1982: Electron microprobe studies of Iceland research drilling project high-temperature hydrothermal mineral geochemistry. Jour. Geophys. Res., 87, 6547-6558.

Frey, M., 1978: Progressive low-grade metamorphism of a Black Shale formation, central Swiss-Alps, with special reference to pyrophyllite and margarite-bearing assemblages. Jour. Petr., 19, pp. 93-135.

Fujii, Y., 1969: On the scale deposits at production well and geothermal power plant of Matsukawa (in Japanese). Jap. Geoth. Energ. Assoc. Journ., No. 21, pp. 30-34.

Fujino, T., Y. Taguchi, M. Hayashi and T. Yamasaki, 1981: Geothermal geology of Test-well No. 3 (HT-3) and No. 4 (HT-4) at Hatchobaru geothermal area, Japan (in Japanese) Journ. Geoth. Res. Soc. Japan, 2, pp. 153-154.

Ghent, E.D. and B.E. Miller, 1974: Zeolite and clay-carbonate assemblages in the Blairmore Group (Cretaceous) southern Alberta, Foothills, Canada. Contr. Min. Petr., 44, pp. 313-329.

Giggenbach, W.F., 1981: Geothermal mineral equilibria. Geochim. Cosmochim. Acta, 45, pp. 393-410.

Hashimoto, M., 1964: The chemistry and optics of prehnite. Jour. Geol. Soc., Japan, 70, pp. 180-183.

Hay, R.L., 1977: Geology of zeolites in sedimentary rocks in "Mineralogy and Geology of Natural Zeolites: (ed. F.A. Mumpton) Min. Soc. Amer. Short Course Notes 4, pp. 53-63.

Hay, R.L., 1966: Zeolites and zeolitic reactions in sedimentary rocks. Geol. Soc. Amer. Spec. Paper No. 85, pp. 1-130.

Hayashi, M., 1973: Hydrothermal alteration in the Otake geothermal area, Kyushu. Jap. Geoth. Energ. Assoc. Jour., 10, pp. 9-41.

Hayashi, M. and T. Yamasaki, 1975: Interstratified mineral of mica-montmorillonite from the Otake geothermal area, Oita prefecture and its environmental conditions of formation (in Japanese with English abstract). Mem. Volume for Professor T. Sudo, pp. 48-53.

Hayashi, M., T. Yamasaki and Y. Matsumoto, 1968: Secondary minerals of drilling cores from test borings T-1 and T-2 in the Otake geothermal area, Kujyu volcano group, Kyushu (in Japanese with English abstract). Geoth., No. 17, pp. 93-111.

Hey, M.H., 1954: A new review of the chlorites. Min. Mag., 30, pp. 277-292.

Higashi, S., 1980: Mineralogical studies of hydrothermal dioctahedral mica minerals. Mem. Fac. Sci. Kochi Univ., 1, pp. 1-39.

Higashi, S. and H. Shirozu, 1975: On sericite minerals associated with Kuroko deposits (in Japanese with English abstract). Clay Science, 15, pp. 78-85.

Hitosugi, T., 1969: Present status of the geothermal exploration at Onikobe (in Japanese). Jap. Geoth. Energ., Assoc. Journ., No. 19, pp. 25-30.

Hitosugi, T., 1970: Report of the boring of GO-10 and GO-11 at Onikobe (in Japanese). Jap. Geoth. Energ., Assoc. Journ., No. 25, pp. 3-10.

Hitosugi, T., 1976: Geophysical prospecting in Onikobe geothermal field (in Japanese). Geoph. Prosp., 29, pp. 89-96.

Hitosugi, T. and M. Yoneya, 1972: On the drillings of the shallow wells in Onikobe (in Japanese). Jap. Geoth. Energ., Assoc. Journ., No. 32, pp. 3-14.

Hoffman, J. and J. Hower, 1979: Clay mineral assemblages as low-grade metamorphic geothermometers: application to the thrust faulted disturbed belt of Montana, U.S.A. in "Aspects of Diagenesis" (ed. by Scholle and Schluger). Spec. Publ. 26, Soc. Econ. Paleont. Min., pp. 55-79.

Hower, J., 1981: X-ray diffraction of mixed clay minerals. Mineral. Assoc. Canada, short course handbook, 7, pp. 39-58.

Hower, J., E. Eslinger, M. Hower and E. Perry, 1976: Mechanism of burial metamorphism of argillaceous sediment: 1. Mineralogical and chemical evidence. Bull. Geol. Soc. Amer., 87, pp. 725-737.

Hower, J. and T. Mowatt, 1966: The mineralogy of illites and mixed-layer illite/montmorillonites. Am. Min., 51, pp. 825-854.

Ishihara, S., 1974: Magmatism of the Green Tuff tectonic belt, Northeast Japan, in, Geology of Kuroko Deposits (Eds., Ishihara et al.), Mining Geology, special Issue No. 6, pp. 235-249.

Ito, J., 1978: The cleaning of silica scale settled in the transportation-pipes of the geothermal hot water of the Onuma geothermal power station (in Japanese with English abstract. Jap. Geoth. Energ. Assoc. Journ., 15, pp. 1-7.

Ito, J., Y. Kubota and M. Kurosawa, 1977a: On the geothermal water flow of the Onuma geothermal reservoir (in Japanese with English abstract) Geoth., 14, pp. 15-27.

Ito, J., Y. Kubota and M. Kurosawa, 1977a: On the geothermal water flow of the Onuma geothermal reservoir (in Japanese with English abstract) Geoth., 14, pp. 15-27.

Ito, J., Y. Kubota and M. Kurosawa, 1977b: On the silica scale of the Onuma geothermal power plant (in Japanese with English abstract). Jap. Geoth. Energ. Assoc. Journ., 14, pp. 1-7.

Ivanov, I.P., and L.P. Gurevich, 1975: Experimental study of T-X_{CO_2} boundaries of metamorphic zeolite facies. Contr. Min. Petr., 53, pp. 55-60.

Katayama, N. and K. Umezawa, 1958: Geological Map of the Onikobe, Scale 1: 75,000 and its Explanation Text (in Japanese with English Abstract). Geol. Surv. Japan.

Katsui, Y, 1955: A petrographical note on the welded tuff around Onikobe caldera (in Japanese with English abstract). Jour. Jap. Assoc. Min. Petr. Economic Geol., 39, pp. 190-194.

Katsui, Y., Oba, Y., Ando, S., Nishimura, S., Masada, Y., Kurasawa, H., and Fujimaki, H., 1974: Petrochemistry of the Quaternary volcanic rocks of Hokkaido, North Japan. Japanese-Soviet Seminar, Tokyo, Geodynamic Project, pp. 1-36.

Katsumoto, N. and H. Shirozu, 1973: Chlorite minerals associated with the gypsum deposits of the Wanibuchi mine, Shimane Prefecture (in Japanese with English abstract). Sci. Rept. Dept. Geol., Kyushu Univ., 11,pp. 231-241.

Kim, H.S., J.G. Liou, and S. Maruyama, in press: Prehnite-epidote equilibria and their petrologic applications. Jour. Petrol.

Kimbara, K., 1973: Clay minerals in the Miocene low-grade metamorphic rocks, Tanzawa Mountains, Kanagawa Peefecture, central Japan. Jour. Assoc. Jap. Min. Petr. Econ. Geol., 68, pp. 311-328.

Kimbara, K., 1975a: Chlorite, saponite and regularly interstratified chlorite-saponite in the Miocene pyroclastic sediments (Green Tuff) at Taiheizan, Akita Prefecture, Japan (in Japanese with English abstract). Mem. Vol. for Professor T. Sudo, pp. 42-48.

Kimbara, 1975b: Regularly interstratified clay minerals of chlorite and saponite ("Corrensite") in the Miocene Green Tuff formation in Japan. Bull. Geol. Surv. Japan., 26,pp. 669-679.

Kimbara, K. and T. Okubo, 1978: Hydrothermal altered rocks found in an exploration bore-hole (No. SA-1), Satsunan geothermal area, Japan (in Japanese with English abstract). Jour. Assoc. Jap. Min. Petr. Econ. Geol., 73, pp. 125-136.

Kimbara, K. and T. Sudo, 1973: Chloritic clay minerals in tuffaceous sandstone of the Miocene Green Tuff Formation, Yamanaka district, Ishikawa Prefecture, Japan (in Japanese with English abstract). Jour. Assoc. Jap. Min. Petr. Economic Geol., pp. 246-258.

Kimbara, K. and K. Sumi, 1975: Hydrothermal alteration minerals in the core-samples at Takinoue geothermal area, Shizukuishi, Iwate Prefecture — with special reference to the interstratified clay mineral of sericite and montmorrillonite (in Japanese with English abstract). Jap. Geoth. Energ. Assoc. Journ., 12, pp. 59-68.

Koga, A. and T. Noda, 1975: New geochemical exploration methods for geothermal sources in vapour-dominated field (in Japanese with English abstract) Geoth., 12, pp. 21-28.

Koga, A., T. Noda, I. Sonoda and T. Iwaki, 1981: Acidification of thermal waterr from Test-well No. 3 at Hatchobaru geothrmal. (in Japanese) Jour. Geoth. Res. Soc. Japan., 2, pp. 152.

Kohyama, N., S. Shimoda, and T. Sudo, 1973: Iron-rich saponite (ferrous and ferric forms). Clays and clay minerals, 21, pp. 228-237.

Kristmannsdottir, H., 1975a: Hydrothermal alteration of basaltic rocks in Icelandic geothermal areas. Proc. 2nd Un. Symp. Dev. Use Geoth. Res., pp. 441-445.

Kristmannsdóttir, H., 1975b: Clay minerals formed by hydrothermal alteration of basaltic rocks in Icelandic geothermal fields. Geol. För. Stockholm För., 97, pp. 289-292.

Kristmannsdóttir, H. 1976: Types of clay minerals in hydrothermally altered basaltic rocks, Reykjanes, Iceland. Jokull, 26, pp. 30-39.

Kristmannsdóttir, H., 1978: Alteration of basaltic rocks by hydrothermal activity at 100-300°C. Proc. Intern. Clay Conf., pp. 359-367.

Kristmannsdóttir, H., 1979: Alteration of basaltic rocks by hydrothermal activity at 100-300°C, in International Clay Conference 1978 (edited by M.M. Mortland and V.C. Farmer). Elsevier, New York, pp. 359-367.

Kristmannsdóttir, H. 1982: Alteration in the IRDP drill hole compared with other drill holes in Iceland. Jour. Geophys. Res., 87, pp. 6525-6531.

Kristmannsdóttir, H.and J. Tomasson, 1974: Nesjavellir-hydrothermal alteration in a high temperature area. Proc. Water-Rock Interaction Intern. Symp. Praha, pp. 170-177.

Kristmannsdóttir, H. and J. Tómasson, 1978: Zeolite zones in geothermal areas in Iceland. "Natural zeolites, occurrence, properties and use" (ed. by Sand and Mumpton), pp. 277-284.

Kuno, H., 1950: Petrology of Hakone volcano and the adjacent areas, Japan: Geol. Soc. Amer. Bull., 61, pp. 957-1220.

Kuno, H., 1952: Cenozoic volcanic activity in Japan and surrounding areas. Trans. New York Acad. Sci., ser. II, 14, pp. 225-231.

Kuno, H., 1953: Formation of calderas and magmatic evolution. Trans. Am. Geoph. Union, 34, pp. 267.

Kuno, H., 1959: Origin of Cenozoic petrographic provinces of Japan and surrounding areas: Bull. Volcanol., ser. 2, 20, pp. 37-76.

Kuno, H., 1966: Lateral variation of basalt magma type across continental margins and island arcs. Bull. Volcanol., 29, pp. 195-222.

Kuno, H., 1968a: Differentiation of basaltic magmas, in Hess, H.H., and Poldervaart, A., eds., Basalts 2, New York, Interscl. Publishers pp. 623-688.

Kuno, H., 1968b: Origin of andesite and its bearing on the island arc structure. Bull. Volcanol., ser. 2, 32, pp. 141-176.

Lan, C.Y., Liou, J.G., and Seki, Y., 1980: Investigation of drill hole core samples from Tatun geothermal area, Taiwan. Proc. 3rd Intern. Symp. Water-Rock Interact. Edmonton, pp. 183-185.

Liou, J.G., 1970: Synthesis and stability relations of wairakite, $CaAl_2Si_4O_{12} \cdot 2\ H_2O$. Contr. Mineral. Petrol., 27, pp. 259-282.

Liou, J.G., 1971a: P-T stabilities of laumontite, wairakite, lawsonite and related minerals in the system $CaAl_2Si_2O_8$-SiO_2-H_2O. Jour. Petrol., 12, pp. 370-411.

Liou, J.G., 1971b: Stilbite-laumontite equilbrium. Contr. Mineral. Petrol., 31, pp. 171-177.

Liou, J.G., 1973: Synthesis and stability relations of epidote, $Ca_2Al_2FeSi_3O_{12}.(OH)$. Jour. Petrol., 14, pp. 381-413.

Liou, J.G., 1979: Zeolite facies metamorphism of basaltic rocks from the East Taiwan ophiolite. Amer. Mineral., 64, pp. 1-14.

Macqueen, R.W., and E.D. Ghent, 1970: Electron microprobe study of magnesian distribution in some Mississippian echinoderm limestones from western Canada. Canadian Jour. Earth Sci., 7, pp. 1307-1316.

Matsubaya, O., and H. Sakai, 1973: Oxygen and hydrogen isotopic study on the water of crystallization of gypsum from the Kuroko-type mineralization. Geochem. Jour., 7, pp. 153-165.

Matsueda, H., 1975: Iron-rich prehnite from the skarn of Sampo Mine, Okayama Prefecture, Japan. Sci. Rept. Geol., Kyusu Univ., 12, pp. 91-100.

Matsumoto, R., 1978: Occurrence and origin of authigenic Ca.Mg.Fe carbonates and carbonate rocks in the Paleogene coalfield regions in Japan. Tokyo Univ. Fac. Sci. Jour. Sect., II, 19, pp. 335-367.

Matsuno, K. and K. Nishimura, 1965: On the Geology and Geological structure of the Onikobe area, Miyagi Prefecture (in Japanese with English abstract). Bull. Geol. Surv. Japan, 16, pp. 353-363.

Mehegan, J.M., P.T. Robinson, and J.R. Delaney, 1981: Secondary mineralization and hydrothermal alteration in the Reydarfjordur, eastern Iceland. Jour. Geophys. Res., 87, pp. 6511-6524.

McDowell, S. and W. Elders, 1980: Authigenic layer silicate minerals in borehole Elmore 1, Salton Sea geothermal field, California, U.S.A. Contr. Min. Petr., 74, pp. 293-310.

Miyamori, Y., 1968: Chemical properties of geothermal steam and water obtained by drillholes within geothermal areas in Matsukawa, Iwate Prefecture (in Japanese with English abstract). Jap. Geoth. Energ. Assoc. Journ., No. 16, pp. 15-24.

Miyashiro, A., 1974: Volcanic rock series in island arcs and active continental margins. Amer. Jour. Sci., 274, pp. 321-355.

Moji, T., 1969: On the scale in transportation pipes at Odake geothermal power plant (in Japanese). Jap. Geoth. Energ. Assoc. Journ., No. 21, pp. 35-39.

Nakamura, H., 1959a: Geothermal conditions in the Onikobe basin, Miyagi Prefecture, Japan. Jap. Assoc. Min. Petr. Econ. Geol. Journ., 43, pp. 158-166.

Nakamura, H., 1959b: Relation of the geological structure to the occurrence of natural steam in the Onikobe basin, Miyagi Prefecture (in Japanese with English abstract). Bull. Geol. Surv. Japan, 10, pp. 575-600.

Nakamura, H., 1967: Geothermal exploration and subsurface structure of Matsukawa area, northeast Japan (in Japanese). Jap. Geoth. Energ. Assoc. Journ., No. 10, pp. 13-34.

Nakamuta, Y., 1976: Zeolites and clay minerals in th Tertiary sedimentary rocks in Tsuyazaki area, Fukuoka Prefecture (in Japanese with English abstract). Jour. Jap. Assoc. Min. Petr. Economic Geol., 71, pp. 147-156.

Nakamura, H., K. Sumi and T. Ozawa, 1977: Characteristics of geothermal resources from geological and geochemical viewpoints in Japan. Jap. Geoth. Enert. Assoc. Journ., 14, pp. 3-19.

Nakamura, H., Yanagihara and S. Takagi, 1961: The third drilling for geothermal investigations in the Onikobe basin, Miyagi Prefecture (in Japanese with English abstract). Bull. Geol. Surv. Japan, 12, pp. 499-502.

Nakano, 1981: Deep fracture zone to control the geothermal system of Onikobe area (in Japanese). Journ. Geoth. Res. Soc. Japan, 2, pp. 142-143.

Oki, Y., Hirano, T., Suzuki, T., 1976: Hydrothermal metamorphism and vein minerals of the Yugawara geothermal area, Japan. Proc. First Internat. Symposium On Water-Rock Interaction, Praha, pp. 209-222.

Ozaki, T., 1981: Hot spring observation in Onikobe geothermal area (in Japanese). Journ. Geoth. Res. Soc. Japan, 2. pp. 148.

Ozaki, T. and T. Kanno, 1977: Hydrological investigation of stream flow in the Onikobe geothermal area (in Japanese with English abstract). Bull. Geol. Surv. Japan, 28, pp. 35-38.

Ozawa, T. and S. Nagashima, 1975: Geochemical studies for geothermal activity on Onikobe basin (in Japanese with English abstract). Jap. Geoth. Energ. Assoc. Journ., 12, pp. 35-38.

Ozawa, T., S. Nagashima and I. Iwasaki, 1980: Geochemical studies for geothermal activity on Onikobe basin. Bull. Volc., 43, pp. 207-223.

Papike, J.J., and T. Zoltai, 1967: Ordering of tetrahedral aluminum in prehnite $Ca_2(Al \cdot Fe^{3+})(Si_3AlO_{10})(OH)$. Amer. Mineral., 52, pp. 974-984.

Perry, E.A., Jr., and J. Hower, 1970: Burial diagenesis of Gulf Coast pelitic sediments. Clays & Clay Min., 18, pp. 165-177.

Pevear, D. V. Williams and G. Mustoe, 1980: Kaolinite, smectite and K-rectorite in bentonites: relation to coal rank at Tulameen, British Columbia. Clays and Clay minerals, 28, pp. 241-254.

Sakai, H. and F.W. Dickson, 1978: Experimental determination of the rate and equilibrium fractionation factors of sulfur isotope exchange between sulfate and sulfide in slightly acid solutions at 300°C and 1000 bars. Earth and Planetary Sci. Letters, 329, pp. 151-161.

Sakai, H., E. Gunnlaugsson, J. Tómasson and J.E. Rouse: Sulfur isotope systematics in Icelandic geothermal systems and influence of seawater circulation at Reykjanes. Geoch. Cosmoch. Acta, 44, pp. 1223-1231.

Sakai, H., and O. Matsubaya, 1974: Isotopic geochemistry of the thermal waters of Japan and its bearing on the Kuroko ore solutions. Econ. Geol., 69, pp. 974-999.

Sakai, H., T. Takenaka, and N. Kishima, 1980: Experimental study of the rate and isotope effect in sulfate reduction by ferrous iron oxides and silicates under hydrothermal conditions. Proc. 3rd Internat. symposium on Water-Rock Interaction, Edmonton, Canada, pp. 75-76.

Sato, M., 1973: X-ray analysis of mixed layer minerals (in Japanese with English abstract). Clay Science, 13, pp. 39-47.

Sato, M., Y. Goto, Y. Kizaki and S. Matsuda, 1975: An interstratified mineral of illite-montmorillonite from Wakobara, Kusatsu district, Gunma Prefecture (in Japanese with English abstract). Mem. Volume for Professor T. Sudo, pp. 54-58.

Schoen, R. and D. White, 1965: Hydrothermal alteration in GS-3 and GS-4 drillholes, Main Terrace, Steamboat Springs, Nevada. Econ. Geol., 60, pp. 1411-1421.

Schoen, R. and D. White, 1967: Hydrothermal alteration of basaltic andesite and other rocks in drillhole GS-6, Steamboat Springs, Nevada. U.S. Geol. Surv. Res., 575-B, pp. 110-119.

Seki, Y., 1970: Alteration of bore-hole cores in mordenite-bearing assemblages in Atosanupuri active geothermal area, Hokkaido, Japan. Jour. Geol. Soc. Japan, 76, pp. 605-611.

Seki, Y., 1971: Some physical properties of analcime-wairakite solid solutions. Jour. Geol. Soc. Japan, 73, pp. 1-8.

Seki, Y., 1972: Lower grade stability limit of epidote in the light of natural occurrences. Jour. Geol. Soc. Japan, 78, 405-413.

Seki, Y., 1973a: Ionic substitution and stability of mordenite. Jour. Geol. Soc. Japan, 79, pp. 669-676.

Seki, Y., 1973b: Metamorphic facies of propylitic alteration. Jour. Geol. Soc. Japan, 79, pp. 771-780.

Seki, Y. and J.G. Liou, 1981: Recent study of low-grade metamorphism. Geol Soc. China, Memoir, No. 4, pp. 207-228.

Seki, Y., J.G. Liou, Y. Oki, F. Dickson, H. Sakai and T. Hirano, 1980: The interaction between Miocene volcanogenic rocks and seawater-meteoric water mixtures in near coast undersea part of the Seikan Tunnel, Japan. Hydrosci. Geotech. Lab., Saitama Univ. Mem. No. 1, pp. 1-123.

Seki, Y., and K. Okumura, 1968: Yugawaralite from Onikobe active geothermal area, mortheast Japan. Japanese Assoc. Min. Petrol. and Econ. Geol. Jour., 60, pp. 27-33.

Seki, Y. and Y. Oki, 1969: Wairakite-analcime solid solutions from low-grade metamorphic rocks of the Tanzawa Mountains, Central Japan. Min. Journal, 6, pp. 36-45.

Seki, Y., H. Onuki, K. Okumura and I. Takashima, 1969: Zeolite distribution in the Katayama geothermal area, Onikobe, Japan. Jap. Journ. Geol. Geogr., 15, pp. 63-79.

Seki, Y., Y. Oki, T. Matsuda, K. Mikami and K. Okumura, 1969: Metamorphism in the Tanzawa Mountains, central Japan. Jour. Assoc. Jap. Min. Petr. Economic Geol., 61, pp. 1-25, 50-75.

Sequet, H., C. de la Calle and H. Pezerat, 1975: Swelling and structural organization of Saponite. Clays and Clay Minerals, 23, pp. 1-9.

Sheridan, M. and M. Maisano, 1975: Zeolite and sheet silicate zonation in a late-Tertiary geothermal basin, near Hassayampa, central Arizona. Proc. 2nd UN Symp. Develop. Use Geoth. Res., 1, pp. 597-607.

Shido, F., A. Miyashiro and A. Ewing, 1971: Crystallization of abyssal tholeiites. Contr. Mineral. Petr., 31, pp. 251-266.

Shimoda, S., 1970: An expandable chlorite-like mineral from the Hanaoka Mine, Akita Prefecture, Japan. Clay Minerals, 8, pp. 352-359.

Shimoda, S., 1974: Some properties of the so-called swelling chlorite (in Japanese with English abstract). Clay Science, 14, pp. 79-89.

Shimoda, S. and T. Nishiyama, 1973: An example of illitic clay mineral from Shakanai Mine, Akita Prefecture (in Japanese with English abstract). Clay Science, 13, pp. 10-16.

Shirozu, H., 1974: Clay minerals in altered wall rocks of the Kuroko-type deposits. Min. Geol. Special Issue, No. 6, pp. 303-310.

Shirozu, H., T. Date and S. Higashi, 1972: Clay minerals associated with the Kuroko deposits in the Hokuroku district, with special reference in relation between X-ray patterns and modes of occurrence of sericite minerals (in Japanese with English abstract). Min. Geol., 22, pp. 393-402.

Shirozu, H. and S. Higashi, 1974: Modes of occurrence of interstratified minerals in th alteration zones of the Kuroko deposits (in Japanese with English abstract). Jour. Min. Soc. Jap., 11, pp. 180-184.

Shirozu, H., T. Sakasegawa, N. Katsumoto and M. Ozaki, 1975: Mg-chlorite and interstratified Mg-chlorite/saponite associated with Kuroko deposits. Clay Science, 4, pp. 305-321.

Sigvaldason, G. and D. White, 1962: Hydrothermal alteration in drill holes GS-5 and GS-7, Steamboat Springs, Nevada, U.S. Geol. Surv. Prof. Paper, 450-D, pp. 113-117.

Spodon, J., 1980: Precise identificaton of illite/smectite interstratifications by X-ray powder diffraction. Clays and Clay Minerals, 28, pp. 401-411.

Steiner, A., 1955: Wairakite, the calcium analogue of analcime, a new zeolite mineral. Mineral. Mag. 30, pp. 691-698.

Steiner, A., 1968: Clay minerals in hydrothermally altered rocks at Wairakei, New Zealand. Clays and Clay Minerals, 16, pp. 193-213.

Steiner, A., 1977: The Wairakei geothermal area, North Island, New Zealand. Bull. N. Z.Geol. Surv., No. 90, pp. 1-136.

Stephen, I. and D. MacEwan, 1951: Some chlorite clay minerals of unusual type, Clay. Min. Bull., 1, pp. 157-162.

Sudo, T., 1968: Problems in alteration viewing from the point of interstratified clay minerals (in Japanese). "Alteration in the Green Tuff Region", pp. 171-193.

Sudo, T., and S. Shimoda, 1969: Some articles of mineralogical interests in the clays of Japan. The Clay of Japan, Geol. Surv. Japan, pp. 155-166.

Sumi, K., 1968: Hydrothermal rock alteration of the Matsukawa geothermal area, northeast Japan. Geol. Surv. Japan, Rept., No. 225, pp. 1-42.

Sumi, K. and K. Maeda, 1973: Hydrothermal alteration of main productive formation of the steam for power at Matsukawa, Japan. Proc. Symp. Hydrogeoch. Biogeoch., 1, pp. 211-228.

Surdam, R.C., 1969: Electron microprobe study of prehnite and pumpellyite from the Karmutsen Group. Vancouver Island, British Columbia. Amer Mineral., 54, pp. 256-266.

Tani, M., H. Natori and E. Yamada, 1968: Tectonic and geochemical studies of the hot-spring and geothermal areas in Miyagi Prefecture (in Japanese). Tohoku-Kaihatsu Center Report, pp. 1-41.

Thompson, A.B., 1971: P_{CO_2} in low-grade metamorphism: zeolite, carbonate, clay mineral, prehnite relations in the system $CaO-Al_2O_3-SiO_2-CO_2-H_2O$. Contr. Mineral. Petrol., 33, pp. 145-161.

Thompson, A.B., 1976: Mineral reactions in pelitic rocks: I. Prediction of P-T-X(Fe-Mg) phase relations. Amer. Jour. Sci., 276, pp. 401-424.

Tómasson, J. and H. Kristmannsdóttir, 1972: High temperature alteration minerals and thermal brines, Reykjanes, Iceland. Contr. Min. Petr., 36, pp. 123-134.

Viereck, L.G., B.J. Griffen, H.U. Schmincke, and R.G. Pritchard, 1982: Volcaniclastic rocks of the Reydarfjordur drill hole, eastern Iceland. 2. Alteration. Jour. Geophys. Res., 87, pp. 6459-6476.

Watanabe, T., 1980: On the component layer of interstratified illite/montmorillonite. Rept. Fac. Sci. Kyushu Univ., 13, pp. 225-231.

Watanabe, T., 1981: Identification of illite/montmorillonite interstratifications by X-ray powder diffraction (in Japanese with English abstract). Jour. Min. Soc. Japan, 15, pp. 32-41.

Weaver, C., 1956: The distribution and identification of mixed-layer in sedimentary rocks. Amer. Min., 41, pp. 202-221.

White, D.E., 1965: Metal contents of some geothermal fluids. Proc. Symp. Problems of Postmagmatic Ore Deposition, Praha, 2, pp. 432-443.

Yamada, E., 1972a: Study on the stratigraphy of Onikobe area, Miyagi Prefecture, Japan. Bull. Geol. Surv. Japan, 23, pp. 217-231.

Yamada, E., 1972b: Geological map of Onikobe, 1:25,000, Geol. Surv. Japan.

Yamada, E., 1973: Subaqueous pumice flow deposits in the Onikobe caldera, Miyagi Prefecture, Japan. Jour. Geol. Soc. Japan, 79, pp. 585-597.

Yamada, E., 1975: Geological development of the Onikobe caldera and its hydrothermal systems. Proc. 2nd U.N. Symp. on the Development and Use of Geothermal Resources, 1, pp. 665-672.

Yamada, E.H., Okada, S. Nishimura, M. Taniguchi and H. Natori, 1978: Hydrothermal alterations of Katayama and Narugo Geothermal areas, Tamatsukuri-gun, Miyagi Prefecture (in Japanese with English abstract). Rept. Geol. Surv. Japan, No. 259, pp. 341-375.

Yamasaki, T., Y. Matsumoto and M. Hayashi, 1968: Geology of the Otake geothermal area, Kuju Volcano group, Kyushu (in Japanese with English abstract). Geoth., No. 14, pp. 1-12.

Yoder, H. and H. Eugster, 1955: Synthetic and natural muscovites. Geoch. Cosmoch. Acta, 7, pp. 225-280.

Yora, M., K. Wakita and S. Honda, 1973: Exploration of Onuma geothermal field, northeastern Japan (in Japanese with English abstract). Geoth., 10, pp. 27-44.

Yoshida, T., 1974: Alteration zones in the Kirishima geothermal area (in Japanese with English abstract). Geoth., 11, pp. 35-45.

Yoshimura, T., 1971: Interstratified clay minerals in the Miocene pyroclastic formations from Oshima-Fukushima, Hokkaido. Sci. Rept. Niigata Univ., No. 2, pp. 1-26.

Yoshimura, T. and K. Kimbara, 1974: Interstratified chlorite-expandable layer clay minerals in the Green Tuff formation (in Japanese). Jour. Min. Soc. Japan, Special Issue, 11, pp. 135-142.

Yoshimura, S. Tanaka, N. Ito and S. Wakabayashi, 1975: Iron-rich saponites in the Green Tuff formation (in Japanese with English abstract). Mem. Volume for Professor T. Sudo, pp. 115-122.

Yoshimura, H. Shiroishi and H. Adachi, 1977: Clay minerals in the Neogene pyroclastic rocks in the Yamagata-Yoshino district, with special reference to interstratified mineral of chlorite and saponite (in Japanese with English abstract). Jour. Min. Soc. Jap., 13, pp. 226-239.

Zen, E-an, 1961: The zeolite facies: an interpretation. Amer. Jour. Sci., 259, pp. 401-409.

Zen, E-an, 1967: Mixed-layer minerals as one-dimensional crystals. Amer. Min., 52, pp. 635-660.

Zen, E-An and Thompson, A.B., 1974: Low grade regional metamorphism, mineral equilibrium relations: Ann. Rev. Earth Planet. Sci., 2, pp. 179-212.

Zeng, Y., and J.G. Liou, 1982: Experimental investigation of yugawaralite-wairakite equilibrium. Amer. Mineral., 67, pp. 937-943.

Compositions and Parageneses of Secondary Minerals in the Onikobe Geothermal System, Japan

by

J.G. Liou[1], Yotaro Seki[2], R.N. Guillemette[3], Hitoshi Sakai[4]

(1) Dept. of Geology, Stanford University, Stanford, CA 94305, USA.

(2) Hydroscience and Geotectonic Lab, Saitama University, Urawa, Japan.

(3) Dept. of Geology, Southern Illinois University Carbondale, IL 62901, USA.

(4) Institute for Thermal Spring Research, Okayama University Misasa, Japan

Chemical Geology (in Press)

March 20, 1984

ABSTRACT

Parageneses and chemical compositions of secondary minerals in many core samples of the Onikobe geothermal system, Japan were investigated in detail in order to evaluate the controls of geothermal waters on alterations of andesitic-dacitic rocks. Depth zonations of secondary minerals were delineated for calcium zeolites as mordenite→laumontite→yugawaralite→wairakite and clay minerals as smectite (± alkaline smectite)→chlorite/smectite→chlorite. Compositional variations with depth (hence temperature) are apparent for smectite/chlorite and illite/chlorite interstratified clay minerals but not for wairakite. Both prehnite and epidote at depth have Fe-rich compositions and become more aluminous with increasing depth. The ubiquitous occurrence of pyrite and rare magnetite and the absence of hematite suggest that the Onikobe system had f_{S_2}-f_{O_2} conditions within the pyrite stability field. The occurrence of abundant calcite and Ca-zeolites indicates that thermal waters at depth are neutral to slightly alkaline and X_{CO_2} is very low to stabilize Ca-Al silicates. This conclusion is consistent with the production of a remarkable amount of alkaline high-temperature steam and thermal waters in a newly drilled production well.

INTRODUCTION

Continuous exploration and development for geothermal power in active volcanic areas such as the Japanese Islands have provided excellent opportunity to investigate water-rock interactions in geothermal systems. Our basic premise is that the changing composition and temperature of geothermal fluids as a function of time is recorded by the parageneses, compositions and isotopic properties of the associated mineral assemblages, and that the mineral parageneses and compositions can be used to reconstruct the evolution of a geothermal system. Hence, a detailed mineralogical-petrological-geochemical investigation of drill hole core samples is necessary to fully understand the complex effects of water-rock interactions in the geothermal systems.

The Onikobe geothermal area, which has been recognized as one of the geothermal systems in Japan, is selected for detailed study because many pilot, exploratory and producing wells ranging from 200 to 1300 meters in depth have been drilled and geological-geochemical-geophysical information and nearly complete drill hole core samples are available. Mineralogical and petrological examinations of core samples from two 350 m drill holes (Nos. 123 and 124) and a 1155 m hole (No. 127) were completed; compositions of secondary minerals were obtained and their parageneses identifed. Several selected samples were investigated by SEM and mass spectrometer. These data together with available water chemistries and petrological-mineralogical data from other drill hole cores in the Onikobe geothermal area were used to outline the effects of several controlling factors on the alteration of the reservoir rocks by geothermal fluids. Details are described in Seki et al., (1983). This paper summarizes petrochemical features and mineral parageneses related to water-rock interactions in the Onikobe geothermal system.

GEOLOGICAL STRUCTURE AND SURFACE ALTERATION

The Onikobe caldera is located in north-central Honshu of Japan and forms an approximately 10 km diameter depression containing central peaks of up to 400-500 m above the basin floor. The caldera is a late-Pliocene to middle Pleistocene edifice which has formed at the extreme eastern edge of the Miocene Green Tuff metamorphic belt.

The stratigraphy of the Onikobe caldera area has been studied in detail by Yamada (1972). Rocks of the Onikobe area can be divided into two major lithologic groups: basement rocks and basin deposits. The basement rocks consist of Paleozoic schists, Mesozoic granodiorite and Miocene volcanogenic marine sediments (so-called green tuffs). The biotite-hornblende granodiorite is exposed within the caldera in the fault-bounded Zanno-Mori block whereas the schists are only exposed along the northwest outer caldera rim (Fig. 1). The green tuff makes up most of the Zanno-Mori block and is also abundant outside the caldera. The basin deposits consist of a number of marine and submarine volcanogenic formations. The Kitagawa dacitic welded tuff, the oldest Quaternary volcanic rock in the Onikobe area, crops out only outside of the basin proper. The other basin deposits, with the exception of the Takahinata dacite, consist of subaerially and lacustrine-deposited flows, pumices, and ash flows and their locally-derived sedimentary deposits from conglomerates through siltstones. The Takahinata dacite dome of 350,000 year B.P. (Yamada et al., 1978) occurs in the extreme southeast area of the caldera. The only younger formation within the caldera is the Onikobe Formation, which consists of 24,000 year B.P. lacustrine sediments.

The most prominent structural feature of the Onikobe caldera is the Zanno-Mori block in the northwestern corner. This 3.0 by 2.5 km fault-bounded block was uplifted during the deposition of the Kawakurazawa Formation. This uplifting may have occurred as a result of the reactivation of high-angle normal faults formed early in the development of the Onikobe basin.

Minor faults, joints, and clastic dikes are well developed within the caldera. A study of faults and fractures by Yamada (1975) indicates that older NW-SE trending faults are cut by younger NE-SW faults. In the Katayama area, where the strongest geothermal activity is centered, fractures are oriented in multiple directions; however, those with N 20-60°W strike are dominant, those striking N 60-90°W are common, and fractures striking N 34° E also occur. Many of these fractures have greater than 70° dip. In the Arayu area, fractures and clastic dikes with about N 60° W strike dominate and fractures with N 30° E are less common.

The most active and widespread area of hydrothermal activity within the Onikobe caldera occurs in the extreme northern portion (the Arayu area) and along the northwestern edge (the Katayama area) of the Takahinata dacite dome. These two areas merge to form a continuous, approximately 3 by 1 km NE-SW trending zone of obvious surface alteration and active steam and gas emission; numerous boiling mud pots, steam vents, and sulfur-depositing fumaroles occur. Rocks at the surface have been pervasively altered and contain abundant kaolinite, alunite, and native sulfur. Two other smaller hydrothermally-altered areas occur to their west: the Ogama-Megama and Fukiage areas. In the Katayama area itself, the most active surface expressions occur along a valley which strikes approximately N 20° W. Fig. 2 shows the location of some of the exploration, production, and re-injection wells drilled to date in the Katayama geothermal area. Successful production wells appear to cluster along three roughly linear trends, referred to as the K, Y and Z lines.

In spite of the pervasive hydrothermal alteration, four rock types were identified among those drill hole core samples: andesitic tuff and lava, and dacitic tuff and lava. The andesitic rocks contain mainly augite ± hypersthene ± hornblende as major mafic minerals and the dacitic rocks are characterized by

the presence of hornblende and quartz phenocrysts and higher contents of glassy matrix or groundmass. Both pyroclastic and lava rocks are highly vesicular; abundant secondary minerals occur in vesicles. Fifteen less altered core samples have been analyzed (see Table 21 and Figs. 16-18 of Seki et al., 1983); their results indicate that the compositions of the altered rocks vary significantly from their unaltered equivalents. Leaching of SiO_2, MgO, Na_2O and K_2O, addition of H_2O and S, and oxidation of FeO have occurred during hydrothermal alteration, such a chemical alteration varies from specimen to specimen. Nevertheless, these rocks have chemical characteristics of the calc-alkaline series.

THERMAL WATERS

Thermal waters from the Onikobe geothermal area have been extensively investigated (Ozawa and Nagashima, 1975; Yamada, 1975; Nakamura et al., 1977; Ozawa et al., 1980; Seki et al., 1983). They belong to the Na-Cl or Na-Ca-Cl type and may have evolved from contamination of HCO_3 and magmatic NaCl-rich solutions with meteoric water. However, our new $\delta^{34}S$ values together with Cl contents listed in Table 1 suggest that the thermal waters of the K-line and Z-line have $\delta^{34}S$ values as high as +19.90 which approach the $\delta^{34}S$ value of seawater sulfates. The Cl contents of K-line and Z-line thermal waters have over two to three times the Cl content of Y-line thermal water. These data indicate that a considerable amount of fossil seawater from Miocene basement volcanogenic sediments must have incorporated in fluids from some deep wells of the Onikobe geothermal area.

Previous investigators (e.g., Ozawa et al., 1980) have described the variation of thermal waters in the Onikobe geothermal area with depth as follows: (A) Surface or near surface thermal waters have low pH, high SO_4 and

low Cl contents; (B) intermediate depth waters (100-500 m) have neutral pH and intermediate SO_4 and Cl contents; and (C) deeper thermal waters (800-1300 m) have low pH, low SO_4 and high Cl contents. They explained such depth variation as being caused by (1) the release of magmatic gas rich in HCl from depth, (2) its mixing with meteoric water to form acid, high Cl thermal water and (3) the transformation of this acid thermal water to neutrality by interaction with the rock as it comes up. 246

The concept of the wide distribution of acid thermal water or steam at depths of over 800 m in the Onikobe geothermal area was born from the production of acid thermal water through some deep bore-holes to 1100-1300 m depth. Electric Power Development Corporation (EPDC) once tried to get enough neutral or alkaline thermal water or steam from these deep bore-holes which were later abandoned. They then began drilling relatively shallow (200-500 m) bore-holes to supply neutral steam to their power plant. Thermal waters and steam obtained through shallow holes were initially of a neutral to weakly alkaline nature (pH = 5-7) and changed to acid or weakly acid (pH = 3-4) several months or a year later. Also, their temperature and discharge rates were modulated by precipitation and snow melt events.

Recently, in the Z-line belt (#127), EPDC succeeded in finding respectable amounts of neutral to weakly alkaline steam at a depth of over 1000 m. The occurrence of acid thermal water at depths greater than 950 m is not consistent with our petrological study. Therefore, the idea of the confined distribution of neutral pH thermal water or steam at relatively shallow depths (100-500 m) and the wide distribution of acid thermal water at greater depths within the Onikobe geothermal area was not supported by our petrological data or by a new deep production hole (#128) (1255 m) drilled in June to July of 1982, which produces a remarkable amount of alkaline (pH = 8.3 to 8.5) high-temperature steam and thermal water..

The widespread occurrence of calcite in most of the deep core samples is a good indicator of the widespread occurrence of neutral to alkaline thermal waters at depth in the Onikobe geothermal area. For example, in bore-holes from which neutral or weakly alkaline thermal water is obtained, calcite commonly occurs as a hydrothermal mineral. At depths of over 800 m in GO-10 and over 600 m in GO-11, calcite was not found. These two deep wells have been abandoned or collapsed because of the predominance of acid thermal water at depth. If these two bore-holes had been drilled more deeply, perhaps to 1500 or 2000 m, however, neutral or alkaline thermal waters of over 250°C may have been obtained. In bore-hole #127, the geothermal gradient, permeability of rocks and ditribution of calcite indicate the presence of acid thermal water locally at depths of about 370-470 m and 870-920 m. High-temperature (240°C) weakly alkaline thermal water was obtained from a depth of 1000-1150 m, where calcite is common.

SECONDARY MINERALOGY

Secondary minerals in core samples have been studied in detail by Seki and Okumura (1968) and Seki et al. (1969, 1983) for eleven drill holes in the Katayama, Onikobe area. These studies consisted of hand-specimen, petrographic, X-ray diffraction, and SEM observations. A total of 419 analyses of secondary (and a few primary) minerals were carried out on the #123, 124 and 127 core samples by electron microprobe. Analytical and petrographic data and analytical accuracies are described in Seki *et al.* (1983). Only clay and zeolite minerals, prehnite, epidote and some other phases are described below in order to correlate their parageneses with the controls acting on the geothermal system.

The minerals produced by hydrothermal alteration depend on mode of occurrence (vein filling, amygdules, replacement), composition and texture of host rock and chemical composition of the fluids. Near the surface, particularly in fumarolic areas, where vigorous boiling occurs and mixing with atmospheric oxygen is possible, the rocks altered to a soft siliceous material containing clays, opaline silica, alunite, sulfur and pyrite. At deeper levels, the mineral assemblages are different and zonal distribution of secondary minerals with depth occurs. Secondary minerals in bore-hole cores form by (a) precipitation in vesicles and along fractures, (b) replacement of plagioclase and mafic phenocrysts, and (c) replacement of groundmass or volcanic glass.

Clay Minerals

Clay minerals are the most common hydrothermal minerals in bore-hole cores of the Onikobe geothermal area and consist of a variety of species. Based on the X-ray diffraction characteristics, particularly the basal spacings under dry conditions and after ethylene-glycol treatment, the Onikobe clay minerals are divided into smectite, alkaline smectite, chlorite/smectite interstratified mineral, chlorite, illite/smectite interstratified mineral, and illite.

Smectite has d_{001} values ranging from 14.3Å to 15.4Å under dry condition and 16.6 - 18Å after ethylene glycol treatment (Fig. 3). Smectite minerals are common in the upper 200 m of most of the drill-hole cores and are occasionally found down to a depth of 300 m.

Alkaline Smectite, in which most of the Ca and Mg cations in smectites are replaced by alkaline metals such as Na and K, is characterized by d_{001} (dry) values of 12.5-13Å and an expansion to 17.0-17.6Å after ethylene glycol treatment (Fig. 3). A significant gap between smectite and alkaline smectite

exists, supporting the observation that both chemical composition and structural relations are discontinuous between the two clay minerals. Similar observations have been made in the Miocene volcanogenic sequence of the Seikan undersea tunnel in Japan (Seki et al., 1980). Like Ca-Mg smectite, this clay generally occurs at depths shallower than about 200 m; it is, however, much less abundant than the former.

Chlorite/Smectite Interstratified Minerals have d_{001} (dry) values of about 14-15Å which expanded to 14-16Å by ethylene glycol treatment. The degree of expansion generally increases with the increase of expandable components. The relative intensities of the 14Å and 7Å peaks can be used to roughly estimate the relative proportion of expandable layers. With increasing chlorite content, the peak height ratio of 14Å/7Å decreases continuously from about 1.5 to about 0.4 and d_{001} changes from 14Å to 15.5Å. In general, these ratios decrease with increasing depth of bore holes.

Most chlorite/smectite interstratified minerals from the Onikobe bore-hole cores show a distinct 31Å peak for (001), 14.6Å for (002) and 7.2Å for (004), indicating that they are regularly interstratified minerals. Fig. 3 shows that a small gap exists between smectite and the chlorite/smectite interstratified minerals, whereas a continuous series occurs between the chlorite/smectite interstratified minerals and chlorite.

The chlorite/smectite interstratified minerals are the most common phyllosilicates in drill-hole cores at depths greater than about 150 m. They occur as distinct, thin, platy and generally curved pale green crystals and as aggregates of curved plates in the form of rosettes. Eleven smectite/chlorite interstratified minerals and 17 chlorites were analyzed. The interstratified phases are much more variable in composition than chlorite and contain mainly

SiO_2 (28-33 Wt%), Al_2O_3 (9-19 Wt%), FeO as total Fe (8-29 Wt%) and MgO (10-23 Wt%), minor amounts of MnO (0.06-2.0 Wt%) and CaO (0.1 to 2.2 Wt%) and negligible amounts of K_2O and Na_2O.

Since chlorite can accommodate only a very limited amount of Ca in its structure, the presence of more than a few tenths of a percent of this element indicates the presence of interlayered smectite. It was observed that shallower samples contain higher Ca concentrations, and hence, a higher proportion of interlayered smectite which is consistent with the X-ray diffraction results.

The chemical variations among the major components SiO_2-Al_2O_3 - (FeO + MgO) for their compositions are shown in Fig. 4(A) together with the compositional plots of smectite, chlorite/smectite interstratified mineral and chlorite. Apparently, the chlorite/smectite interstratified phases show significant chemical variations; some of them have compositions very close to that of chlorite. Nevertheless, they contain higher SiO_2, lower (FeO + MgO) and higher CaO than chlorite. Both the smectite/chlorite interstratified mineral and chlorite are extremely low in K_2O content and are significantly different from illite and illite/smectite mixed layer silicates described below.

Chlorite of non-expandable d_{001} spacing is extremely rare in the Onikobe drill hole cores. Most of the chloritic clays, as shown in Fig. 3, are weakly expanded by ethylene glycol treatment. Our data clearly indicate that the chlorite/smectite interstratified mineral changes to chloritic clay, and the percentage of chlorite layers in the chlorite/smectite interstratified minerals increases with increasing depth.

Selected chlorite minerals were analyzed (Fig. 4(A)). Compared to chlorite/smectite interstratified minerals described above, the chlorites have a much more restricted range of chemical compositions. The chlorites contain much lower CaO and SiO_2 than the chlorite/smectite phases. The deeper samples appear to have lower Si contents.

Illite/Smectite Interstratified Minerals and Illite occur in some deep bore hole cores. They are relatively rare compared to smectite-chlorite series minerals. These illitic clay minerals, judging from their X-ray diffraction patterns and limited microprobe compositions, belong to the illite-illite/smectite interstratified mineral series. Continuous variations occur in this series; with increasing depth, the difference in (001) spacings between their dry condition and after ethylene glycol treatment becomes smaller. This relationship indicates that the smectite component decreases and illite becomes the major K-bearing phase for deep bore-hole core samples.

Some illitic clay minerals were analyzed; the results are graphically illustrated in Fig. 4(B) together with compositions of saponite, sericite and illite. Upon examination of the reconnaissance data, several facts are deduced: (1) illitic clay minerals vary substantially in their major elements, (2) the SiO_2 content ranges from 31 to 49 wt% and increases with increasing K_2O; (3) those illite/smectite interstratified minerals are low in SiO_2 and K_2O and high in CaO, (FeO + MgO), and H_2O whereas illite minerals are high in SiO_2, Al_2O_3 and K_2O and low in (FeO + MgO) and H_2O, (4) most analyzed compositions shown in Fig. 4(B) lie between that of smectite and illite with possible paired substitution of (FeO + MgO) = Al_2O_3 + (K_2O + Na_2O). Such coupled substitution and increasing illite component in the illite/smectite interstratified minerals can be correlated with depth, and hence temperature of formation. The proportion of illite appears to generally increase with depth. Similar observations have been made by Hower et al. (1976) from burial metamorphic sequences and from other geothermal areas.

Occurrence of illitic clay appears to be correlated with host rock composition as shown in Table 2 which lists the type and K_2O content of original rocks and the occurrence of illitic clay minerals in geothermal areas

of Iceland, Onikobe, Hakone, Matsukawa, Otake, Wairakei and Steamboat Springs. Examination of these data makes it apparent that a close correlation exists between the occurrence of illitic clays and the type and K_2O contents of original rocks. Although the addition of some K_2O from geothermal waters may be significant for the formation of illitic clays, lithological characteristics, especially the K_2O content of original rocks, may determine the abundance of illitic clay minerals in rocks of a geothermal system.

Zeolite Minerals

Zeolite minerals are well developed in the core samples from the Onikobe geothermal area. Some Ca-zeolites are exceptionally abundant; such common zeolites include mordenite, laumontite, yugawaralite and wairakite. Their zonal depth distribution has been delineated; with increasing depth (hence temperature), the zeolite varies from mordenite → laumontite → yugawaralite → wairakite.

In addition to those common zeolites, clinoptilolite, dachiardite, chabazite, thomsonite and natrolite were also identified. They are very minor in quantity and occur sporadically in some samples. These zeolites are not described.

Mordenite $(Na_2,K_2,Ca)Al_2Si_{10}O_{24}\cdot 7H_2O$ is a common zeolite at shallow depths from the drill core samples. It characteristically occurs at depths of less than 200 m and is most commonly found between depths of about 50 to 150 m, depending on the geothermal gradient. It is associated with clinoptilolite and optical distinction between them is difficult. Mordenite occurs as radial fan-like or spherulitic aggregates of fine prismatic crystals in veins or vesicles. Unfortunately, no mordenite was found in core samples from drill holes #123, 124 and 127. Therefore, no microprobe analysis of mordenite was obtained.

Laumontite $(CaAl_2Si_4O_{12}\cdot 4H_2O)$ is typically found at depths greater than 50 m and shallower than 200-400 m (Seki et al., 1983). It occurs as either a vein or amygdule mineral or replacing plagioclase phenocrysts and glassy

groundmass; it often takes the form of a sub-parallel lath aggregate. The analyzed laumontites are quite pure in composition, containing only very minor Fe_2O_3, Na_2O and K_2O. Chemical compositions of laumontites separated by heavy liquid and analyzed by wet chemical method have been reported (Seki et al., 1969). The probe data contain considerably higher SiO_2 and lower CaO than the wet chemical data.

Yugawaralite ($CaAl_2Si_6O_{16}\cdot 4H_2O$) occurs as a blocky vein mineral in only one or two samples per hole, varying in depth from the shallowest occurrence in P-8 at 156.25 m to the deepest occurrence in GO-8 at 701.5m (Seki et al., 1983). Four microprobe analyses indicate that they are very close to the Ca end-member composition, containing only very minor amounts of Fe_2O_3, Na_2O and K_2O.

Wairakite ($(Ca,Na_2)Al_2Si_4O_{12}\cdot 2H_2O$) is the most abundant zeolite mineral in the Onikobe drill-hole cores. It occurs in most wells beginning at depths of 100-150 m and extending to the bottom of the holes except in GO-11, in which wairakite is present between 203 and 701 m depth, but is absent from 791 to 1300 m (Seki et al., 1983). Wairakite most commonly occurs as a vein mineral, often filling the core of veins lined with either anhedral or euhedral quartz, as amygdule fillings, replacing plagioclase, and replacing fine-grained matrix. In all of these occurrences, they exhibit characteristic very low birefringence and often shows cross-hatched twinning.

Wairakites of various occurrences were analyzed; considerable compositional variation was found. Most of the analyzed wairakites contain less than 0.2 wt % Fe_2O_3 as total Fe and 0.1 wt % K_2O. Some analyses (e.g., #123-158.9 m) have over 0.5 wt % Fe_2O_3 and concomitantly lower SiO_2 and Al_2O_3 contents. Such relations suggest that some Fe^{+3} substitution for Al in tetahedral sites may be significant for these wairakites. Wairakit and analcime have been shown to form a solid solution series with a possible immiscibility

gap at intermediate compositions (Seki and Oki, 1969). Furthermore, such solid solutions exhibit a variable Al to Si ratio. Wairakite analyses are plotted in Fig. 5 and show low Al to Si ratios relative to a wairakite-ideal analcime series.

All analyzed wairakites range from Wr_{100} to Wr_{76} and contain no more than 5% Nat' component. No analcime-rich compositions were found in any analyzed samples. In general, there is no correlation between composition of wairakite and depth of sample, nor any pattern between composition and mode of occurrence. The only observed trend was within vein minerals from hole #127. Central parts of four veins showed a higher proportion of the wairakite component than the rims. Assuming that the growth occurred from the vein walls inward, this trend suggests an increase of temperature with time during the deposition of the wairakite.

Other Minerals

Prehnite sporadically occurs as fine-grained aggregates after plagioclase, discrete patches in matrix and vesicles, or as veins of variable thickness. In most samples, only few patches of prehnite aggregates were found. Anhedral platy prehnite appears as homogeneous crystal aggregates, colorless to pale green in color, and showing second-order yellow birefringence. Sample #124-209.9 m contains more than 5 volume % of coarse-grained prehnite in the matrix; the prehnites are colorless to pale green and have uniform habit; some show bow-tie structure. Prehnite-wairakite-calcite-albite-chlorite/smectite interstratified mineral-quartz-pyrite (± epidote) is the most common mineral assemblage in prehnite-bearing specimens. The prehnite-laumontite assemblage is also found in some specimens from shallow bore-holes.

Microprobe analyses of some prehnites were done. Some prehnites have uniform composition but others show a small range of $Fe \rightleftarrows Al^{VI}$ substitution. The most iron-rich prehnites ($Fe_2O_3 \approx$ 6-8 wt %) occur in the matrix and appear to be stable with epidote + wairakite + quartz + chloritic clay. The veined prehnites, on the other hand, are much

lower in Fe content (Fe_2O_3 less than 3 wt %) and are stable with wairakite ± carbonates + quartz. Such a difference in the Fe_2O_3 contents between matrix prehnites and veined prehnites may be due to a slight difference in f_{O_2} (and/or temperature). The matrix prehnites may have crystallized under f_{O_2} conditions buffered by highly oxidized rocks whereas the veined prehnites formed at lower f_{O_2} and higher CO_2 conditions at a later stage.

Epidote also occurs sporadically as tabular crystals or as spongy crystal aggregates replacing plagioclase and matrix or as fan-shaped coarse-grained aggregates with characteristic yellow to light yellow pleochroism. All epidote crystals possess very high birefringence suggesting a high Fe^{+3} content. Most commonly observed associations are epidote-wairakite-chlorite/smectite mineral (or chlorite)-albite-calcite-quartz-pyrite. The assemblage, epidote-wairakite-chlorite/smectite mineral (or chlorite)-albite-calcite-prehnite-quartz-pyrite is also found in some specimens. The epidote-laumontite-calcite-chlorite/smectite mineral-pyrite (± prehnite) assemblage is observed in only four specimens. No epidote was found in mordentite-bearing core samples.

Epidotes were analyzed by EPMA method. These epidotes are all stably associated with wairakite, calcite, albite, chlorite/smectite mineral (or chlorite), quartz and pyrite. The analyzed epidotes range in pistacite content from 19 to 37; most analyses are around Ps 29 to 33. Except for the one with an extremely high Fe_2O_3 content (replacing plagioclase), the compositional range of epidote from the Onikobe geothermal area is very compatible with those from Cerro Prieto (Bird, et al., in press). The $Fe^{+3}/(Fe^{+3} + Al)$ ratio in epidotes from metamorphic terraines and geothermal areas varies, depending on metamorphic grade and oxidation state of the rock. With increasing metamorphic grade, epidote becomes more aluminous, reflecting not only the effect of temperature and total pressure but also the concomitant decrease of the oxidation state of the rocks (for details see Liou et al., 1983). A systematic compositional variation of epidote with depth, and

hence with temperature in the investigated samples from Onikobe is not apparent. However, it appears that epidote stably associated with wairakite + pyrite (e.g., Sample #124 - 307.5) is higher in Fe^{+3} compared to the epidote of the epidote + prehnite + wairakite assemblage.

Calcite is a common vein mineral in the Onikobe cores. It is found at depths of only a few tens of meters to a maximum depth of 1100 m in #127. Compositionally, all analyzed carbonate grains are calcite, containing only a few percent of Fe, Mg, and Mn.

Calcite occurs as a vein and amygdule filling and replacing fine-grained matrix and plagioclase and pyroxene phenocrysts, especially along cleavage cracks in the latter two. When it occurs as a vein mineral, it is one of the last phases to have formed. The absence of this mineral within certain zones may be important in establishing certain hydrologic parameters in the Onikobe geothermal field (for discussion, see Seki et al., 1983).

Albite replaces primary plagioclase and begins to occur when volcanic rocks were altered at temperatures of 120-180°C. At greater depth where volcanic rocks were altered at temperatures higher than 230°-240°C, some plagioclase phenocrysts have entirely been replaced by albite ± wairakite and illitic or chloritic clay minerals. Some analyzed albites have An content less than 5 mol% and low Fe_2O_3 and MgO contents.

Pyrite is very common in the Onikobe bore-hole cores. Some pyrites have replaced primary magnetites; many euhedral pyrite aggregates also occur in veins, in matrix, and in the groundmass of volcanic clasts. Only one sample #124-200.3 contains pyrite, magnetite and chalcopyrite; magnetite is rare in the Onikobe geothermal core samples.

The $\delta^{34}S$ values of some pyrites are shown in Table 3 and range from +2.05 to +3.59 at shallow depths to +5.43 at a depth of 700 m. These values are almost identical to those of pyrites in altered basaltic rocks from surface to depths of about 800 m in the Reykjanes geothermal area of Iceland, where present-day seawater is actively percolating through the porous basaltic lavas at depth (Sakai et al., 1980). In Onikobe, the percolation of

present-day seawater cannot be expected. However, fossil seawater within Miocene basement volcanogenic marine sediments may have contributed sufficient sulfur for pyrite crystallization.

DISCUSSION

Progressive Changes of Minerals with Depth

When one examines the distribution of secondary minerals as a function of depth in drill holes of the Onikobe geothermal area, two patterns are apparent:

1. a general zoning with respect to type of phyllosilicate present.
2. a zoning with respect to zeolite minerals.

Within the chlorite/smectite group, the following pattern is seen with increasing depth: smectite (± alkaline smectite) → chlorite/smectite → chlorite.

In the GO-7 core, for example, alkaline smectite occurs from 15.0 to 107.0 m depth, smectite from 36.0 to 175.0 m, and interstratified chlorite from 201.1 m to the bottom of the hole at 500.0 m. Kaolinite is present between 107.0 and 175.0 m, and illite occurs from 175.0 m to the bottom of the hole, roughly matching the interstratified chlorite range

Pyrophyllite occurs in some holes below depths of about 800 m. Most of the cores display considerable overlap among the chlorite/smectite ranges.

As discussed previously, the proportion of the smectite component in both the chlorite/smectite and illite/smectite minerals decreases with depth. A similar pattern of increasing illite component as a function of depth was observed by Perry and Hower (1970) in Gulf Coast sediments and has been attributed to an increase in temperature with depth and/or time-dependent kinetic effects (Eberl and Hower, 1976).

The zonal distribution of the four zeolites (mordenite, laumontite, yugawaralite, and wairakite) was briefly described in a previous section. The following points can be made regarding their distributions:

1. Moderate to strong overlapping of zones is the rule rather than the exception in most of these diagrams.
2. Not all four zeolites occur in any one core. The occurrence of yugawaralite is much less compared to those of other zeolites.
3. The plotting of the zeolite variation along the geothermal gradient is a useful way of presenting this data. However, care must be taken in relating the zeolite present at a given depth to the corresponding gradient temperature.

From the discussions presented in the previous sections, it is apparent that both clay and zeolite minerals change progressively in species with depth, and hence temperature. Such changes are summarized below and can be correlated with other geothermal areas in Japan, Iceland, New Zealand and the U.S.A.:

(1) Both smectite and alkaline smectite occur in the shallow core samples. The most common zeolite associated with these clay minerals is mordenite; however, in general, zeolites are extremely rare in shallow core samples. This together with the ubiquity of kaolinite-alunite in some drill holes suggests low pH thermal waters which inhibit the formation of Ca-zeolites (see Fig. 7). In the mordenite-bearing samples, the occurrence of chlorite/smectite mineral is extremely rare.

(2) The chlorite/smectite interstratified mineral occurs at intermediate depths. It is most commonly associated with laumontite and wairakite. Smectite, alkali smectite and chlorite/smectite interstratified minerals together with illite/smectite interstratified minerals were found to be stable with laumontite.

(3) The clay minerals occurring at depth and stable with wairakite are both chlorite/smectite interstratified minerals and chlorite. Illitic clays are also present.

Depth Zones of Ca-Zeolites

Stability relations among laumontite, yugawaralite and wairakite--at P_{H_2O}/P_{total} = 1.0 and 0.3 have been experimentally-determined (see Figs. 42 and 43 of Seki et al., 1983). In the Onikibe geothermal system where the fluid phase contains abundant components in addition to H_2O, and where P_{fluid}/P_{total} ratios may be approximately 0.3, yugawaralite stability is restricted to depths shallower than 500 m. The Onikobe yugawaralite occurs over the temperature range of 150-205°C, spanning almost the entire overlap area between laumontite and wairakite. This range would correspond to a P_{H_2O}/P_{total} ratio intermediate between 0.3 and 1.0. The narrow stability range of yugawaralite at low P_{H_2O}/P_{total} values explains its relative paucity in the Onikobe cores and in other geothermal areas (e.g., Zeng and Liou, 1982).

The paragenetic depth sequence of Ca-zeolites in a geothermal system is highly dependent on the imposed thermal gradient, on the P_{H_2O}/P_{total} ratio, and on other factors, including solution composition (e.g., Giggenbach, 1981). In a system with a relatively high geothermal gradient and a high P_{H_2O}/P_{total} ratio, yugawaralite may be stable and the depth sequence could be mordenite→laumontite→yugawaralite→wairakite. On the other hand, in regions with a lower geothermal gradient and a lower P_{H_2O}/P_{total} ratio, yugawaralite is not stable and the zonation of Ca-zeolites could be mordenite→laumontite→wairakite. Different depth zonation patterns of Ca-zeolites may occur even in a single geothermal system because both the P_{H_2O}/P_{total} ratio and the geothermal gradient are controlled by many geologic, solution and hydrologic conditions (Seki et al., 1983).

Parageneses of Ca-Al Silicates

Chemographic relations of common Ca-Al hydrosilicates (Ca-zeolites, epidote and prehnite) together with quartz, calcite and chlorite/smectite were delineated in a simplified system $CaO-Fe_2O_3-Al_2O_3-(FeO + MgO)-SiO_2-H_2O-CO_2-S$. (For

detailed assumptions, procedure of projection and effect of f_{O_2} on phase relations see Seki et al., 1983). The associations of epidote, wairakite, prehnite and calcite in some cores of drill-holes #123 and #124 are listed in Table 4. Because these assemblages formed over a small temperature interval of 110-170°C and depths of 166-350 m, they are plotted on an isobaric-isothermal Ca-2Fe-2Al diagram of Figs. 6(A) and 6(B) respectively for drill holes # 123 and # 124. The 2-phase assemblages wairakite + epidote and wairakite + prehnite occur in a number of samples whereas the 3-phase assemblages epidote + prehnite + wairakite and wairakite + prehnite + calcite have very restricted occurrence. Tie lines for the coexisting phases are drawn according to the analyzed compositions of epidote and prehnite.

The deduced phase relationships for assemblages of these two drill hole cores are summarized in Fig. 6(C) at temperature of 110-170°C and depth of 200-350m. Five 3-phase assemblages were delineated: they are pyrite + epidote + wairakite, pyrite + epidote + calcite, wairakite + epidote + prehnite, epidote + prehnite + calcite, and wairakite + prehnite + calcite. These assemblages have been recorded in other geothermal areas and in low-grade meta-basalts, (e.g., Cerro Prieto, Bird et al., in press; Karmutsen metabasalt, Maruyama and Liou, unpublished data).

It should be pointed out that laumontite is rather common at shallow depths in geothermal systems. In fact, laumontite and wairakite occur together in many samples. The laumontite-hematite-epidote assemblage has been found at Tatun and in other geothermal areas (e.g., Lan et al., 1980). In the investigated samples from Onikobe drill holes 123 and 124, the assemblages laumontite + epidote + pyrite, laumontite + magnetite + epidote and laumontite + prehnite + calcite were not observed. These assemblages may occur at lower temperatures and higher f_{O_2} conditions.

From the phase relations shown in Fig. 6, three conclusions are drawn: (1) Both prehnite and epidote are restricted to Fe-rich composition at low temperatures and become Al-rich with increasing temperature. (2) The Al-end member of both prehnite and epidote are not stable under the physico-chemical conditions defined by the assemblages in drill holes # 123 and # 124. Al-prehnite was replaced by the wairakite + calcite assemblage which is common in the Onikobe geothermal system. (3) The Fe-Al partitioning between epidote and prehnite suggests that the epidote always contains higher Fe than the coexisting prehnite.

The conclusions described above are consistent with those data derived from hydrothermal experiments (e.g., Liou et al., 1983), from thermodynamic calculations (e.g., Bird & Helgeson, 1978), and from natural parageneses in hydrothermal metamorphic sequence (e.g., Evarts & Schiffman, 1983), and in other geothermal areas (e.g., Cerro Prieto, Bird et al., in press). However, there are some differences. At the conditions of the Onikobe geothermal system, (1) garnet is not stable, calcite is ubiquitous, hematite was not found, magnetite is not common and pyrite is abundant, (2) the 3-phase assemblage Ep + Pr + Hm (or Mt) recorded in experimental study and in other geothermal areas (e.g., the Salton Sea) was not found in the available core samples, (3) compositions of coexisting epidote and prehnite in the 3-phase assemblage Ep + Pr + Wr are lower in Fe^{+3} contents than those in Ep + Pr + Cc, and (4) both epidote and prehnite have much more restricted compositions than those in high-T conditions.

Stabilities of Ca-zeolites-clay mineral-calcite-anhydrite

The Onikobe thermal waters described in the previous sections contain significant amounts of CO_2, SO_4, NaCl and other dissolved constituents. High concentrations of these three components have resulted in the crystallization of carbonate and gypsum (or anhydrite) at the expense of Ca-Al silicates and in lowering the formation temperature of some index minerals.

The role of CO_2 in low-grade metamorphism has been recently reviewed (e.g., Zen & Thompson, 1974; Seki & Liou, 1981). Previous experimental and theoretical studies indicate that the breakdown of Ca-bearing silicates and their assemblages into calcite-bearing assemblages will occur as a result of increasing the mole fraction of CO_2 in the fluid phase to over 0.1 at temperatures below 400°C. For example, at $P_{total}=P_{fluid}=2$ kb, laumontite can only be stable at temperatures below 350°C at extremely low CO_2 concentrations in the fluid (X_{CO_2} = 0.0075 - 0.02) (Ivanov and Gurevich, 1975). These theoretical and experimental studies also indicate that the equilibrium temperatures at which carbonate-bearing assemblages and carbonate-free assemblages coexist shift significantly by small changes in X_{CO_2}. The mole fraction of CO_2 in the fluid phase attending low-grade metamorphism has generally been assumed to be very low. In the fossil geothermal area in Reydarfjordur, Iceland, mineral parageneses suggest that early deposition of a clay and calcite assemblage occurred at higher X_{CO_2} and was succeeded by the later crystallization of zeolites, prehnite and epidote at reduced X_{CO_2} conditions (e.g., Kristmannsdottir, 1982; Mehegan et al., 1982). Similarly, the less common occurrence of wairakite, prehnite and epidote in the Ohaki-Broadlands geothermal area, New Zealand compared to the Wairakei area has been attributed to a high concentration of CO_2 in thermal waters (Browne and Ellis, 1970).

As demonstrated by Seki et al. (1983), the most characteristic Ca-silicates in low-grade metamorphism and geothermal systems are stable at X_{CO_2} values of less than 0.1. The CO_2 content of the fluid phase controls not only the equilibrium temperature for successive mineralogical zones but also the appearance of the calcite + clay assemblage at the expense of Ca-Al silicates. Moreover, the CO_2 concentration strongly affects the pH value of a hydrothermal solution. Zeolite and

other Ca-Al silicate assemblages are believed to develop mainly in alkaline environments. Recent calculations by Crossey et al. (in press) indicate that at T = 100-200°C, laumontite is stable only in the fluids of high pH and low P_{CO_2}. Similar relations for laumontite at 150°C and 500 bars, and for wairakite at 250°C and 500 bars were calculated using thermodynamic data of Helgeson et al. (1978). The results are shown in Fig. 7 to illustrate the effects of pH, Ca^{+2} concentration and P_{CO_2} on the stability of Ca-zeolites in general. It is also apparent from these diagrams that the characteristic assemblage formed under acidic and higher CO_2 conditions is a clay + carbonate assemblage. The generally accepted idea that the Ca-Al silicates are stable at a low activity of CO_2, hence in slightly alkaline solution, is confirmed by the observations of the Onikobe mineral parageneses and by the phase relationships shown in Fig. 7.

Oki et al. (1974) used a log $[Ca^{2+}]$ - pH diagram to illustrate the stability relations of calcite-laumontite-anhydrite at 150°C in terms of pH, activities of Ca^{2+}, and SO_4, partial pressure of CO_2, and activity ratio of $[Al(OH)_4]/[H_4SiO_4]$. Depending on these variables, the laumontite, calcite and anhydrite stability fields overlap considerably. The Onikobe thermal waters possess a higher P_{CO_2}, lower activity of SO_4, lower activity ratio of $[Al(OH)^-]/[H_4SiO_4]$, and lower pH, compared to those of the Yugawara geothermal system. Therefore, laumontite (and other Ca-Al silicates) and calcite are more common, whereas gypsum (or anhydrite) is rare in the Onikobe core samples. However, it should be emphasized that these interdependent variables and temperatures change with time and depth even in a single well. Therefore, correlation of the occurrences of Ca-Al silicates, carbonates and sulfates between different geothermal systems must be done with caution.

f_{O_2}-f_{S_2} Relations of Pyrite, Magnetite, Anhydrite and Calcite

Isothermal-isobaric log f_{O_2}-f_{S_2} relations among common Fe-oxides and sulfides were calculated at 200°C, 500 bars and concentrations of Ca^{+2}, K^+,

and total C and S representative of the Onikobe thermal waters. Thermodynamic data are from Helgeson et al. (1978) and the calculations were based on the computer code of SUPCRT of Helgeson et al. (1978) and EQ 3/6 of Wolery (1979). The results are shown in Fig. 8. Stability fields of pyrite, pyrrhotite, magnetite, hematite, calcite and anhydrite are shown. Superimposed on the relations are (a) stability of sulfur species in aqueous solutions, and (b) pH effects on the stabilities of S species, calcite, anhydrite, K-feldspar and muscovite. It is apparent from this diagram that, at the specified physical-chemical conditions of the Onikobe System, (1) calcite is stable only in the the presence of thermal waters with pH greater than 7.4, (2) assemblages of magnetite + pyrrhotite, magnetite + pyrite and magnetite + hematite are not stable with anhydrite, (3) kaolinite is stable only in the solution with pH less than 4.3 and cannot coexist with calcite.

As discussed in the previous sections, the Onikobe drill cores from depths greater than 200 m are characterized by (1) abundant pyrite, rare magnetite and absence of hematite and (2) ubiquitous occurrence of calcite, rare anhydrite and absence of kaolinite. Such mineralogical characteristics suggest that (A) the Onikobe geothermal system had f_{O_2}-f_{S_2} condition within the pyrite stability field; some assemblages fall along the magnetite-pyrite buffer curve, and (B) the pH of geothermal water for the coexistence of calcite and anhydrite at 200°C depth may be around 7-8. These conclusions are consistent with the stability of laumontite shown in Figs. 7 and 8 and with the suggestions made by Seki et al. (1983) that the neutral to slightly alkaline thermal waters must be predominant at depth in the Onikobe geothermal system. It also concurs with the production of alkaline (pH = 8.3 to 8.5) thermal waters at a depth of 1255 m in a new deep production hole (#128).

CONCLUSIONS

The distribution of secondary minerals with depth in the Katayama area, Onikobe is primarily controlled by changes in temperature. Other factors, which are important either locally or with regard to certain minerals, include the P_{H_2O}/P_{total} ratio, solution and bulk rock chemistry, rock permeability, and kinetic constraints. Depth-dependent zonation patterns are observed for the calcium zeolites, interlayered clay, and several other minerals. Main conclusions are itemized below:

1. Depth zonations of secondary minerals are particularly clear:
   (a) Smectite ($\pm$ alkaline smectite)→chlorite/smectite→chlorite; and
   (b) Mordenite→laumontite→yugawaralite→wairakite.
2. Compositional variations with depth are apparent also for smectite/chlorite and illite/smectite but not for $wairakite_{solid\ solution}$. Both chlorite and illite components of the interstratified clays increase with depth. Hence Ca-content decreases in smectite/chlorite and K-content increases in illite/smectite with increasing temperature.
3. Other Ca-Al silicates include prehnite and epidote:
   (a) They are restricted to Fe-rich composition at low-temperature and become Al-rich with increasing depth;
   (b) Their Al-end members are not stable at the conditions of the Onikobe geothermal system;
   (c) Epidote contains higher Fe than the coexisting prehnite and their relations are defined by continuous reaction.
4. Ubiquitous occurrence of pyrite and rare magnetite and absence of hematite suggest the Onikobe system had f_{S_2} - f_{O_2} conditions within the pyrite stability field; some are close to the pyrite-magnetite buffer curve.

5. Occurrence of abundant calcite and Ca-zeolites indicates thermal waters at depth are neutral to slightly alkaline and X_{CO_2} is low enough to stabilize Ca-Al silicates. 266

6. $\delta^{34}S$ values of thermal waters and pyrite suggest contamination of fossil seawaters within Miocene sediments with meteoric and magmatic waters in the Onikobe geothermal system.

ACKNOWLEDGEMENTS

This report presents research accomplished during the tenure of a United States-Japan scientific cooperative project, supported by NSF EAR 77-23173, DOE-SC07-80ID-12145 and JSPS (Grant 4-R039). Facilities at Stanford University, Saitama University, the Hot Spring Research Institute of Hakone and Institute for Thermal Spring Research, Japan provided bases for the laboratory and analytical studies. Our investigations benefited at all stages from the association with many geologists and civil engineers, particularly Dr. T. Hitosugi, of the Electric Power Development Co., Japan (EPDC). EPDC provided core specimens and many thermal water samples and allowed us to use much of their geological and technological information. Figs. 7 and 8 were respectively calculated by M. Cho and D. Pohl of Stanford University. This manuscript was critically reviewed and materially improved by Peter Schiffman and Isao Takashima.

We thank the above mentioned institutions and their personnel and the individuals for their support, comments and advice. J.G. Liou is grateful to the John Simon Guggenheim Memorial Foundation for gracious and unencumbered support during 1978-1979.

REFERENCES

Bird, D.K. and Helgeson, H.C., 1978. Chemical interaction of aqueous solutions with epidote-feldspar mineral assemblages in geologic systems: I. Thermodynamic analyses of phase relations in the system $CaO-FeO-Fe_2O_3-Al_2O_3-SiO_2-H_2O-CO_2$. Am. J. Sci., 280: 907-941.

Bird, D.K., Schiffman, P., Elders, W.A., Williams, A.E. and McDowell, S.D. (in press) Calc-silicate mineralization in active geothermal system. Econ. Geol.

Browne, P.R.L., 1978. Hydrothermal alteration in active geothermal fields. Annual Review of Earth and Plan. Sci., 6: 229-250.

Browne, P.R.L. and Ellis, A.J., 1970. The Ohaki-Broadlands hydrothermal area, New Zealand: Mineralogy and related geochemistry. Am. J. Sci., 269: 97-131.

Crossey, L.J., Frost, B.R., and Surdam, R.C., in press. Secondary porosity in laumontite-bearing sandstones, in AAPG Special Publication on Clastic Diagenesis.

Eberl, D. and Hower, J., 1976. Kinetics of illite formation. Geol. Soc. Am. Bull., 87: 1326-1330.

Evarts, R.C. and Schiffman, P., 1983. Submarine hydrothermal metamorphism of the Del Puerto ophiolite, California. Am. J. Sci., 283: 289-341.

Giggenbach, W.F., 1981. Geothermal mineral equilibria. Geochim. Cosmochim. Acta, 45: 393-410.

Hayashi, M., 1973. Hydrothermal alteration in the Otake geothermal area, Kyushu. Jap. Geoth. Energ. Assoc. Jour., 10: 9-41.

Hayashi, M. and Yamasaki, T., 1975. Interstratified mineral of mica-montmorillonite from the Otake geothermal area, Oita prefecture and its environmental conditions of formation (in Japanese with English abstract). Mem. Volume for Professor T. Sudo: 48-53.

Helgeson, H.C., Delany, J.M., Nesbitt, W.H. and Bird, D.K., 1978. Summary and critique of the thermodynamic properties of rock forming minerals. Am. J. Sci., 278A: 1-220.

Higashi, S. and Shirozu, H., 1975. On sericite minerals associated with Kuroko deposits (in Japanese with English abstract). Clay Science, 15: 78-85.

Hower, J., Eslinger, E., Hower, M. and Perry, E., 1976. Mechanism of burial metamorphism of argillaceous sediment: 1. Mineralogical and chemical evidence. Geol. Soc. Amer. Bull., 87: 725-737.

Hower, J. and Mowatt, T., 1966. The mineralogy of illites and mixed-layer illite/montmorillonites. Am. Mineral., 51: 825-854.

Ivanov, I.P. and Gurevich, L.P., 1975. Experimental study of T-X_{CO_2} boundaries of metamorphic zeolite facies. Contr. Mineral. Petrol., 53: 55-60.

Katsui, Y, 1955: A petrographical note on the welded tuff around Onikobe caldera (in Japanese with English abstract). Jour. Jap. Assoc. Min. Petr. Economic Geol., 39: 190-194.

Kimbara, K., 1975. Chlorite, saponite and regularly interstratified chlorite-saponite in the Miocene pyroclastic sediments (Green Tuff) at Taiheizan, Akita Prefecture, Japan (in Japanese with English abstract). Mem. Vol. for Professor T. Sudo: 42-48.

Kristmannsdottir, H., 1975. Hydrothermal alteration of basaltic rocks in Icelandic geothermal areas. 2nd U.N. Symp. on Development and Use of Geoth. Res. Proc.: 441-445.

Kristmannsdottir, H., 1982. Alteration in the IRDP drill hole compared with other drill holes in Iceland. J. Geophys. Res. 87: 6525-6531.

Kuno, H., 1950. Petrology of Hakone volcano and the adjacent areas, Japan: Geol. Soc. Am. Bull., 61: 957-1220.

Lan, C.Y., Liou, J.G., ans Seki, Y., 1980. Investigation of drill hole core samples from Tatun geothermal area, Taiwan. Proc. 3rd Intern. Symp. Water-Rock Interact. Edmonton: 183-185.

Liou, J.G., Kim, H.S. and Maruyama, S., 1983. Prehnite-epidote equilibria and their petrologic applications. J. Petrol., 24: 321-342.

Mehegan, J.M., Robinson, P.T. and Delaney, J.R., 1981. Secondary mineralization and hydrothermal alteration in the Reydarfjordur, eastern Iceland. J. Geophys. Res. 87: 6511-6524.

Nakamura, H., Sumi, K. and Ozawa, T., 1977. Characteristics of geothermal resources from geological and geochemical viewpoints in Japan. Jap. Geoth. Enert. Assoc. J., 14: 3-19.

Oki, Y., Hirano, T. and Suzuki, T., 1974. Hydrothermal metamorphism and vein minerals of the Yugawara geothermal area, Japan. Proc. First Internat. Symp. Water-Rock Interaction, Prague: 202-222.

Ozawa, T. and Nagashima, S., 1975. Geochemical studies for geothermal activity on Onikobe basin (in Japanese with English abstract). Jap. Geoth. Energ. Assoc. J., 12: 35-38.

Ozawa, T., Nagashima S. and Iwasaki, I., 1980. Geochemical studies for geothermal activity on Onikobe basin. Bull. Volc., 43: 207-223.

Perry, E.A., Jr., and Hower, J., 1970. Burial diagenesis of Gulf Coast pelitic sediments. Clays & Clay Min., 18: 165-177.

Sakai, H., Takenaka, T. and Kishima, N., 1980. Experimental study of the rate and isotope effect in sulfate reduction by ferrous iron oxides and silicates under hydrothermal conditions. Proc. 3rd Internat. symp. on Water-Rock Interaction, Edmonton, Canada: 75-76.

Sata, M., Goto, Y., Kizaki, Y., and Matsuda, S., 1975. An interstratified mineral of illite-montmorillonite from Wakobara, Kusatsu district, Gunma Prefecture (in Japanese with English abstract). Mem. Volume for Professor T. Sudo: 54-58. 270

Schoen, R. and White, D., 1965. Hydrothermal alteration in GS-3 and GS-4 drillholes, Main Terrace, Steamboat Springs, Nevada. Econ. Geol., 60: 1411-1421.

Schoen, R. and White, D., 1967. Hydrothermal alteration of basaltic andesite and other rocks in drillhole GS-6, Steamboat Springs, Nevada. U.S. Geol. Surv. Res., 575-B: 110-119.

Seki, Y., 1973: Ionic substitution and stability of mordenite. J. Geol. Soc. Japan, 79: 669-676.

Seki, Y. and Liou, J.G., 1981. Recent study of low-grade metamorphism. Geol Soc. China, Mem. 4: 207-228.

Seki, Y. and Oki, Y., 1969. Wairakite-analcime solid solutions from low-grade metamorphic rocks of the Tanzawa Mountains, Central Japan. Mineral. J. 6: 36-45.

Seki, Y. and Okumura, K., 1968. Yugawaralite from Onikobe active geothermal area, mortheast Japan. Japanese Assoc. Min. Petrol. and Econ. Geol. J., 60: 27-33.

Seki, Y., Onuki, H., Okumura, K. and Takashima, I., 1969. Zeolite distribution in the Katayama geothermal area, Onikobe, Japan. Jap. J. Geol. Geogr., 15: 63-79.

Seki, Y., Liou, J.G., Oki, Y., Dickson, F., Sakai, H. and Hirano, T., 1980. The interaction between Miocene volcanogenic rocks and seawater-meteoric water mixtures in near coast undersea part of the Seikan Tunnel, Japan. Hydrosci. Geotech. Lab., Saitama Univ. Mem. 1: 1-123.

Seki, Y., Liou, J.G., Guillemette, R., Sakai, H., Oki, Y., Hirano, T. and Onuki, H., 1983. Investigation of geothermal systems in Japan, I. Onikobe geothermal area. Hydrosci. Geotech. Lab., Saitama Univ. Mem. No. 2, 206 p. 271

Shimoda, S. and Nishiyama, T., 1973. An example of illitic clay mineral from Shakanai Mine, Akita Prefecture (in Japanese with English abstract). Clay Science, 13: 10-16.

Shirozu, H., Sakasegawa, T., Katsumoto, N. and Ozaki, M., 1975. Mg-chlorite and interstratified Mg-chlorite/saponite associated with Kuroko deposits. Clay Sci., 4: 305-321.

Sigvaldson, G. and White, D., 1962. Hydrothermal alteration in drill holes GS-5 and GS-7, Steamboat Springs, Nevada, U.S. Geol. Surv. Prof. Pap., 450-D: 113-117.

Steiner, A., 1977. The Wairakei geothermal area, North Island, New Zealand. New Zeal. Geol. Surv. Bull. 90: 1-136.

Sudo, T., and Shimoda, S., 1969. Some articles of mineralogical interests in the clays of Japan. The Clay of Japan, Geol. Surv. Japan: 155-166.

Sumi, K., 1968. Hydrothermal rock alteration of the Matsukawa geothermal area, northeast Japan. Geol. Surv. Japan, Rept., 225: 1-42.

Sumi, I. and Maeda, K., 1973. Hydrothermal alteration of main productive formation of the steam for power at Matsukawa, Japan. Proc. Symp. Hydrotech. Biogeoch., 1: 211-228.

Wolery, T.J., 1979. Calculation of chemical equilibrium between aqueous solution and minerals: the EQ3/6 software package. Lawrence Livermore Laboratory UCRL-52658.

Yamada, E., 1972. Study on the stratigraphy of Onikobe area, Miyagi Prefecture, Japan. Geol. Surv. Japan, Bull. 23: 217-231.

Yamada, E., 1975. Geological development of the Onikobe caldera and its hydrothermal systems. Proc. 2nd U.N. Symp. on the Development and Use of Geothermal Resources, 1: 665-672.

Yamada, E., Okada, H., Nishimura, S., Taniguchi, M., and Natori, H., 1978. Hydrothermal alterations of Katayama and Narugo Geothermal areas, Tamatsukuri-gun, Miyagi Prefecture (in Japanese with English abstract). Rept. Geol. Surv. Japan, 259: 341-375.

Yoshimura, T., Tanaka, S., Ito, N., and Wakabayashi, S., 1975. Iron-rich saponites in the Green Tuff formation (in Japanese with English abstract). Memo Volume for Professor T. Sudo: 115-122.

Zeng, Y. and Liou, J.G., 1982. Experimental investigation of yugawaralite-wairakite equilibrium. Am. Mineral., 67: 937-943.

Table 1. $\delta^{34}S$ values and Cl contents of thermal waters from deep wells of the Onikobe geothermal area.

Well	$\delta^{34}S$	Cl^- (meq)
#102	+3.90	
#111	+3.92	59.92
#124	+3.89	
K-line (#101,102,103 111)	+19.90	85.30
Y-line (#108,112,117)	+5.02	36.44
Z-line (#104,105,106 120)	+16.52	145-150

Table 2. Types and K_2O of original rocks and occurrence of illitic clay minerals from Iceland, Onikobe, Hakone, Matsukawa, Otake, Wairakei and Steamboat Springs geothrmal areas.

Geothermal area	Type of original rocks	K_2O in original rocks (wt.%) Range	Average	Occurrence of illitic clays
Iceland (1)	Basaltic	0.08 - 0.26	0.18	no or extremely rare
Onikobe (2)	Andesitic	0.15 - 1.88	0.67	not common
Hakone (3)	Andesitic	0.56 - 0.70	0.64	not common
Matsukawa (4)	Dacitic	0.79 - 1.20	1.00	common
Otake (5)	Andesitic	0.45 - 2.41	1.68	common
Wairakei (6)	Rhyolitic	2.0 - 3.6	2. 7	very common
Steamboat (7) Springs	Trachytic - granodiorite	2.2 - 3.2	2. 7	very common

(1) Kristmannsdóttir (1975)
(2) Seki et al. (1969), Katsui (1955), This paper
(3) Kuno (1950)
(4) Sumi (1968), Sumi and Maeda (1973)
(5) Hayashi (1973), Hayashi and Yamasaki (1975)
(6) Steiner (1977)
(7) Sigvaldson and White (1962), Schoen and White (1965, 1967)

Table 3 $\delta^{34}S$ values of pyrites from bore-hole cores in Onikobe geothermal area.

Bore-hole cores		$\delta^{34}S$
#123	178.8 m	+3.59
"	333.3 m	+3.00
#124	183.3 m	+3.38
"	331.4 m	+2.05
#127	231.7 m	+3.06
"	703.9 m	+5.43

Table 4. Equilibrium mineral assemblages for core samples from Drill Holes #123 and 124 of the Onikobe geothermal Area.* (All assemblages + chloritic clay + quartz ± pyrite ± albite).

depth	#123	depth	#124
238.6m	Ep(32**)+Wr	165.8m	Wr+Pr(14-17)
303.5	Pr(19)+Wr		
323.8m	Ep(23)+Wr	201.8m	Wr+Pr(3-8)+Cc
344.6m	Ep(22-29)+Wr	209.9m	Wr+Pr(17-22)+Ep(?)
348.5m	Ep(19)+Pr(8)(?)+Wr	222.8m	Ep(26-29)+Wr
		307.5m	Wr+Ep(37)
		334.7m	Wr+Pr(12)
		349.4m	Wr+Pr(3-4)+Cc

* Wr+Cc assemblages are not listed; they formed much later.
** The numbers in ( ) refer to $Fe^{+3}/(Fe^{+3}+Al) \times 100$

Abbreviation: Ep = epidote; Wr = wairakite; Pr = prehnite; Cc = calcite

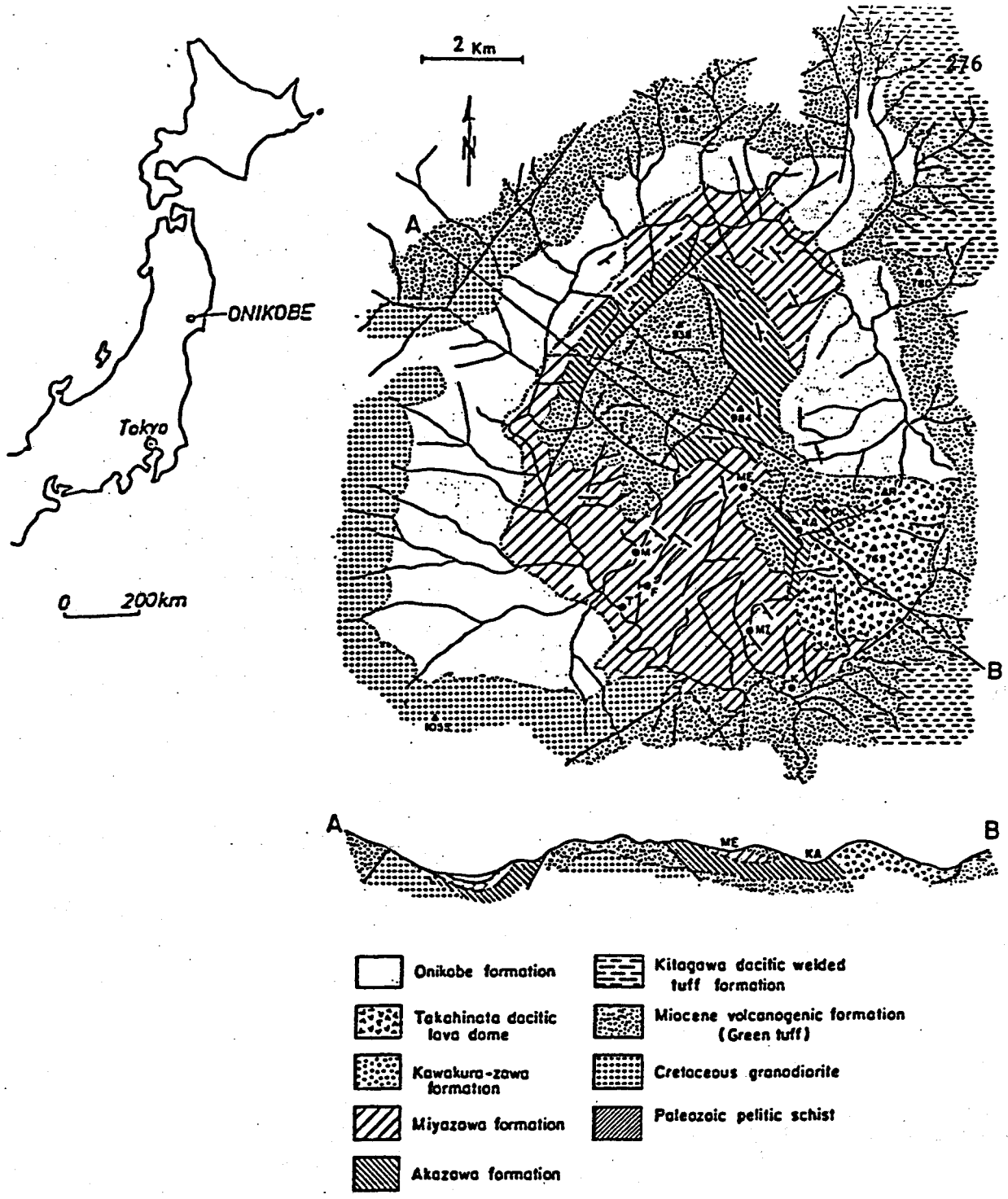

Figure 1. Location and geologic map of the Onikobe Caldera, Japan (modified after Yamada et al., 1978). KA: Katayama fumarolic area; OK: Okuno-in fumarolic area; AR: Arayu fumarolic area; ME: Megama fumarolic area; MI: Mitaki Spa; K: Kanisawa Spa; T: Todoroki Spa; F: Fukiage Spa; M: Miyazawa Spa.

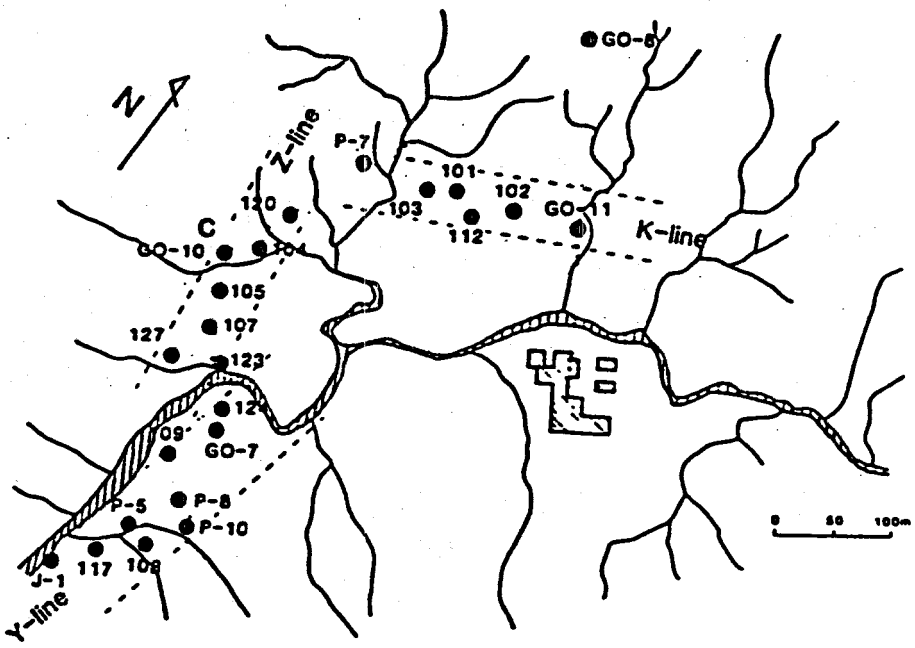

Figure 2. Distribution of bore holes in the Onikobe geothermal area, Japan.

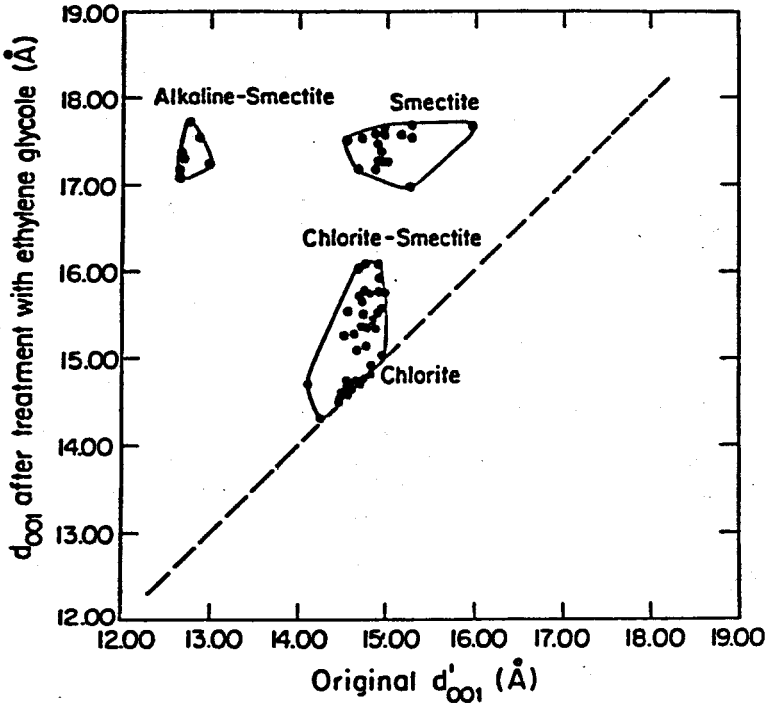

Figure 3. d_{001}(dry)-d_{001} (ethylene glycol) diagram of alkaline smectite, smectite, chlorite and chlorite/smectite interstratified mineral series in the Onikobe geothermal area, Japan.

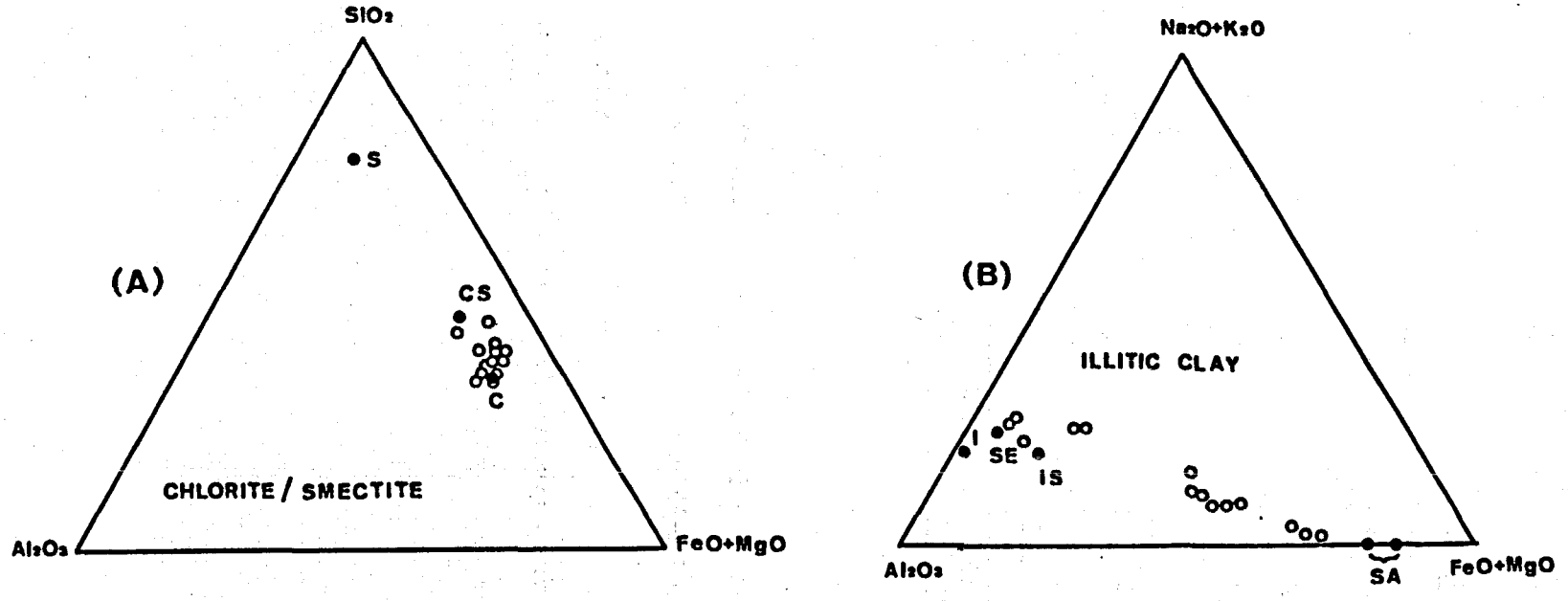

Figure 4. SiO_2 - Al_2O_3-(FeO + MgO) and (K_2O + Na_2O)-Al_2O_3-(FeO + MgO) diagrams showing compositions of analyzed chlorite/smectite and illitic clay minerals from drill hole cores of the Onikobe geothermal area (open circles). Compositions of smectite(S) from Sudo and Shimoda (1969), chlorite/smectite(CS) interstratified minerals from Kimbara (1975a), chlorite(C) from Shirozu et al. (1975), saponite(SA) from Yoshimura et al. (1975), illite/saponite interstratified mineral(IS) from Sata et al. (1975), sericite(SE) from Higashi and Shirozu (1975) and illite(I) from Shimoda and Nishiyama (1973) are shown by solid circles.

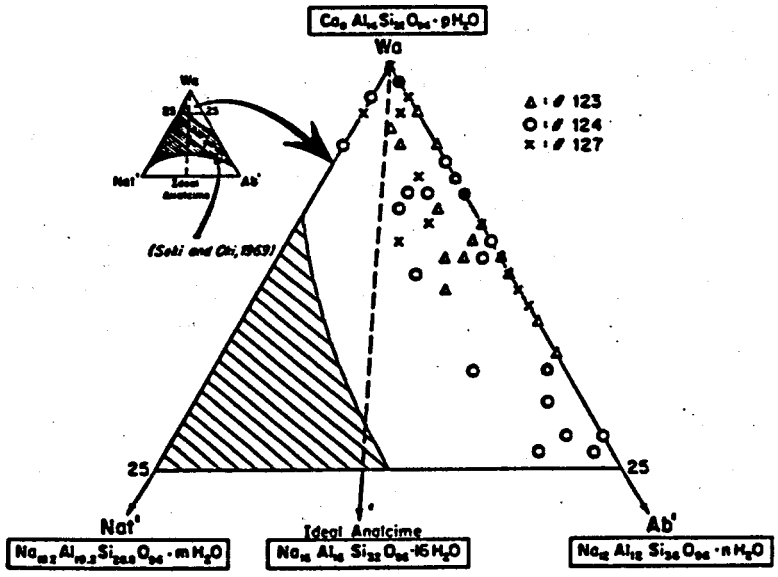

Figure 5. Compositional variations of analyzed wairakites from the Onikobe geothermal area, Japan plotted in Wa-Ab'-Nat' diagram of Seki and Oki (1969).

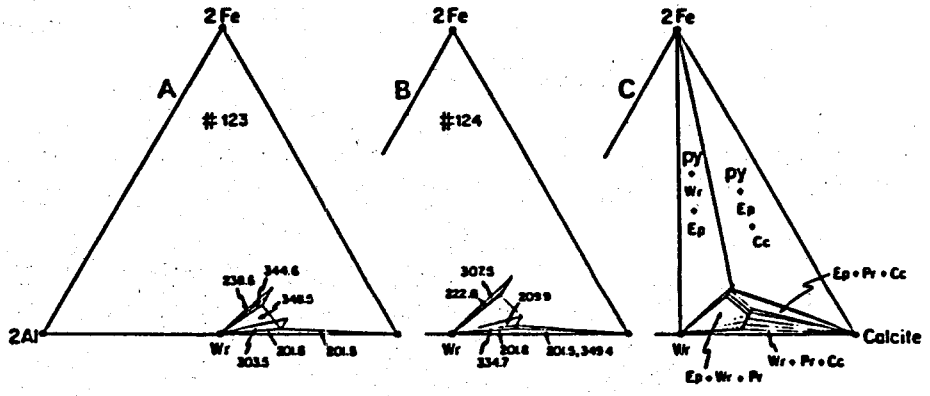

Figure 6. Ca-2Al-$2Fe^{+3}$ plots showing compositions of analyzed epidotes and prehnites and mineral assemblages from drill holes #123(A) and #124(B). I terpretative relationships for 3-phase and 2-phase assemblages are shown in (C).

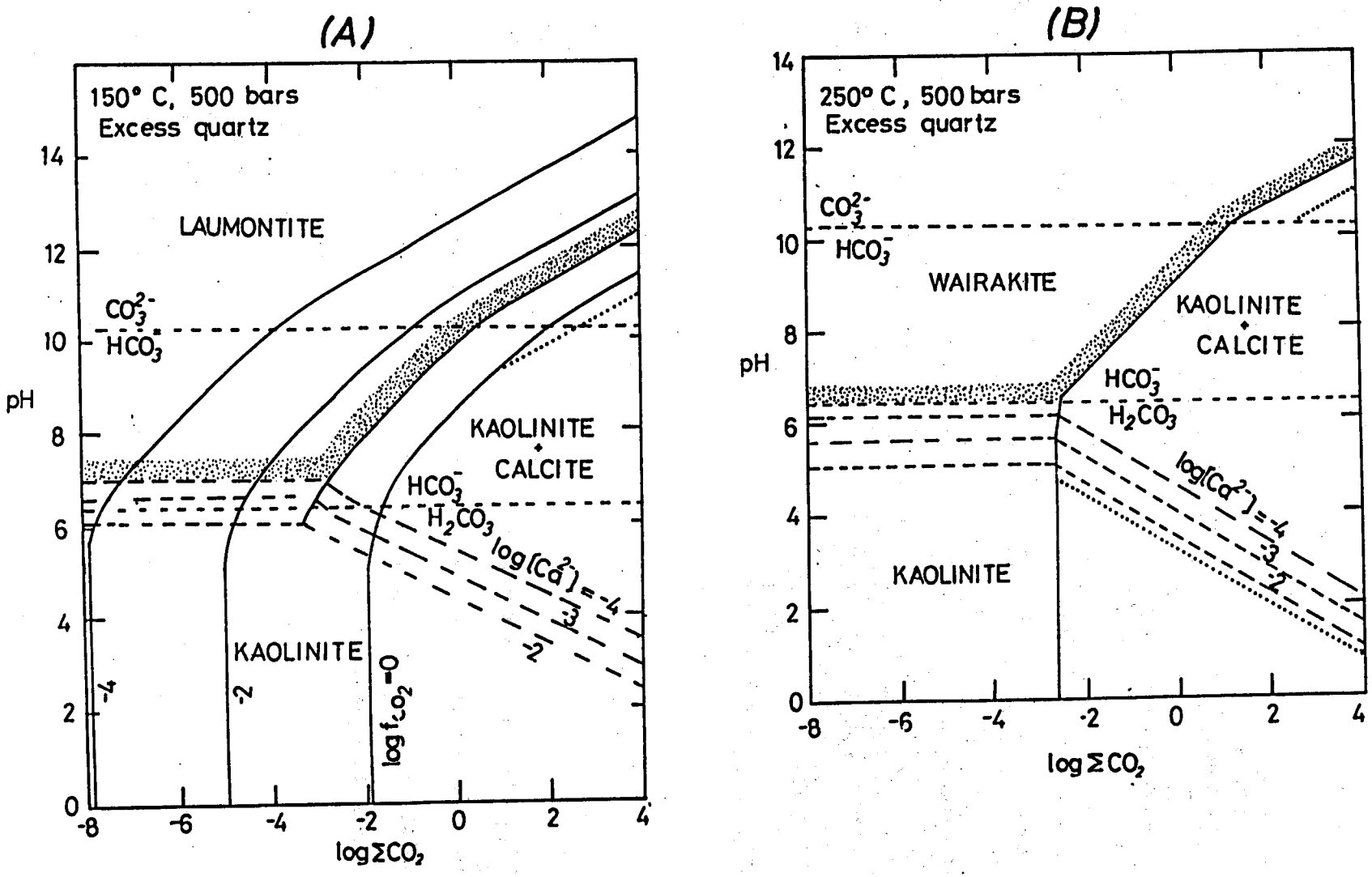

Figure 7. pH - Log Σ CO_2 stability diagrams for laumontite (A), wairakite (B), calcite + kaolinite and kaolinite. Solid lines represent f_{CO_2} isopleths, heavy dashed lines represent contours of constant Ca activity, and light dashed lines separate the pH regions where different carbonate species are dominant.

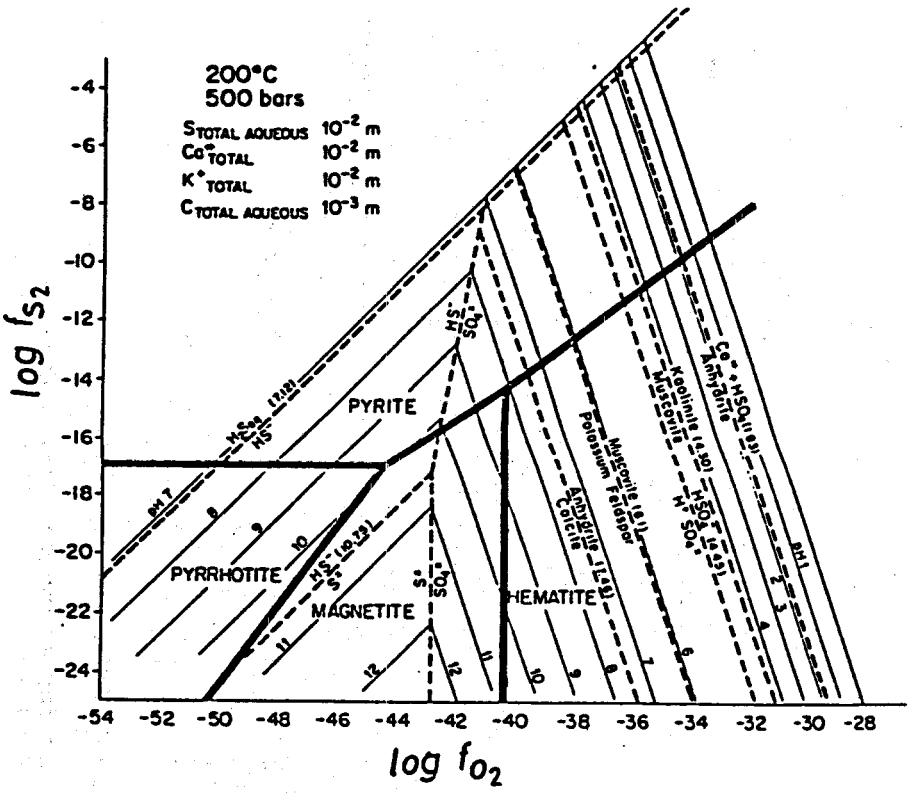

Figure 8. Log f_{O_2}-f_{S_2} stability diagram for pyrite, pyrrhotite, magnetite and hematite. Superimposed are (a) the pH isopleths and (b) stability fields for calcite, anhydrite, muscovite, and various species for S in aqueous solution.

FOURTH INTERNATIONAL SYMPOSIUM

ON

WATER-ROCK INTERACTION

August 29 - September 3, 1983

Misasa, JAPAN

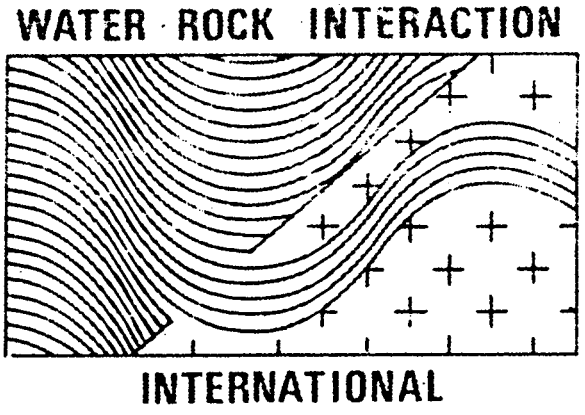

Institute for Thermal Spring Research
Okayama University

International Association of Geochemistry
and Cosmochemistry

COMPOSITIONS AND PARAGENESIS OF SOME HYDROUS CA-Al SILICATES IN THE ONIKOBE GEOTHERMAL SYSTEM, JAPAN.

J.G. Liou & Ray Guillemette, Dept. of Geology
Stanford University, Stanford CA 94305, USA
Y. Seki, Hydroscience and Geotectonic Lab
Saitama University, Urawa, Japan

Hydrothermal alteration of deep-hole cores of the Onikobe geothermal area was selected for detailed study in order to understand rock-water interaction in classic island-arc geothermal systems. More than 100 core samples from two drill holes with depths to 350m and one down to 1155m were examined; paragenesis and compositions of secondary minerals were identified and analyzed. These newly collected chemistries together with available water compositions and petrological-mineralogical data of other drill hole cores from the Onikobe geothermal area were used to outline the effects of geothermal waters and other controls in the alteration of the enclosing rocks. Details are described in Seki et al., (in press).

The Onikobe caldera is on the eastern edge of the Green Tuff basin in north central Honshu and has an oval-shaped depression about 10 Km in diameter. The caldera formations are Plio-Pleistocene in age and consist of both marine and non-marine volcanogenic tuffs and lavas of andesitic to dacitic composition. After the deposition of the caldera sediments and lavas, a dacitic lava dome of 0.35 m.y. age was intruded into the southern part of the Onikobe basin. Associated with the intrusion were the normal faulting and hydrothermal alteration. The magmatic activity related to the dome formation is believed to be the major heat source for the present-day geothermal activity and associated hydrothermal manifestations in the Onikobe area.

Thermal waters from the Onikobe geothermal area have been analyzed; they belong to the Na-Cl or Na-Ca-Cl type. They may have evolved from meteoric waters which have been contaminated with magmatic NaCl-rich solution and fossil seawater from Miocene Green Tuff. Acidic thermal waters with high SO_4 and low Cl contents apparently are confined to shallow depths; this was supported by the widespread occurrence of calcite in deep drill-hole samples and by drilling of a new production hole at 1255m which produced a remarkable amount of alkaline (pH = 8.3 to 8.5) high-T thermal waters.

The zonal distributions of clay and zeolite minerals were identified and are schematically shown in Fig. 1. With increasing depth, the zonal patterns are simplified as follows: alkaline smectite or smectite → chlorite/smectite interstratified mineral→chlorite for clay minerals and mordenite→laumontite→yugawaralite→wairakite for zeolites. We consistently found the general associations that alkaline smectite and smectite occur with mordenite, chlorite/smectite interstratified phase with laumontite, and chlorite with wairakite. Minor zeolites include clinoptilolite, dachiardite, chabazite, thomsonite and natrolite. Prehnite, epidote and phyllosilicates such as illite, illite/smectite, kaolinite and pyrophyllite also occur.

Zeolite minerals are well developed and some are exceptionally abundant. Laumontite is typically found at depths greater than 50m and shallower than 400m and yugawaralite at the lower end of the laumontite zone. The analyzed laumontite and yugawaralite have nearly stoichiometric compositions with very minor amounts of Fe_2O_3, Na_2O and K_2O. Wairakite is the most abundant zeolite mineral and occurs in most wells at depths greater than 100m. Many wairakites were analyzed and the results were plotted on a wairakite', natrolite' and albite' triangular diagram (Fig. 2). The wairakites have considerable ranges of compositions with less than 0.2 wt% Fe_2O_3 as total Fe and 0.1 wt% K_2O. Main variations are defined by 2 end-members "wairakite" and "analcime" with Al/Si ratios lower than the Wr-Am ideal series. All analyzed wairakites range from Wr_{100} to Wr_{76} and contain no more than 5% Nat' component; no analcime-rich composition was found. There appears to be no correlation between

Fig. 1 Distribution of secondary minerals as a function of depth and estimated temperatures from Fig. 39 in the Onikobe geothermal area, Japan.

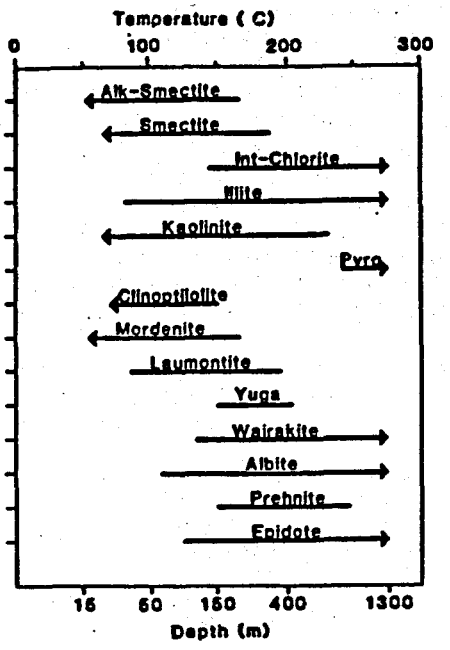

Fig. 2 Compositional variations of analyzed wairakites from the Onikobe geothermal area, Japan plotted in Wr-Ab'-Nat' diagram of Seki and Oki (1969).

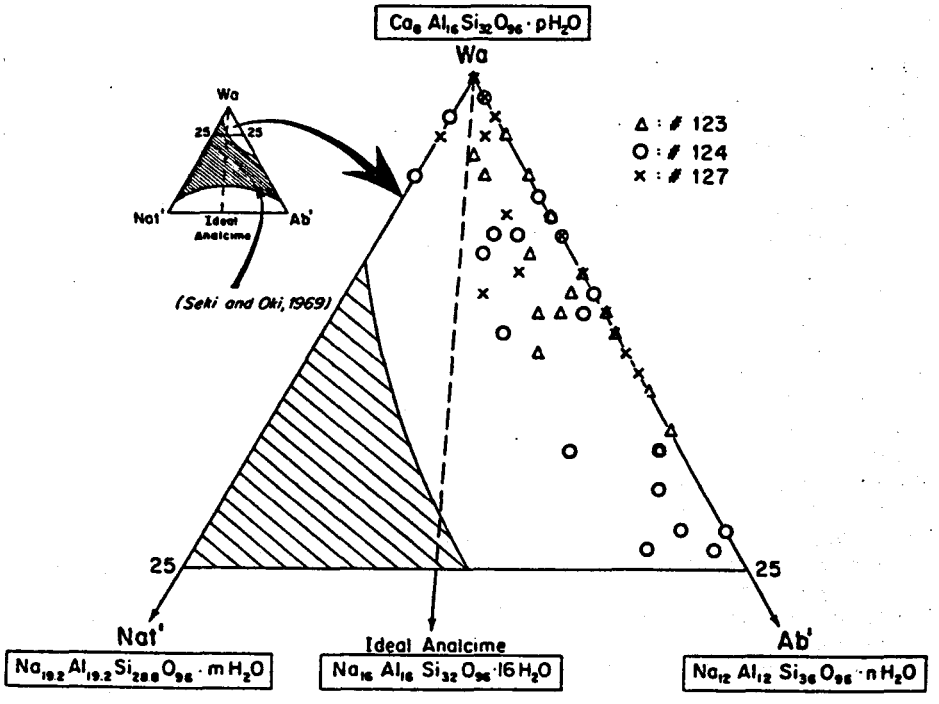

composition of wairakite and depth of its occurrence, nor any pattern between composition and mode of occurrence (i.e., vein, amygdule).

Other Ca-Al silicates include minor prehnite and epidote in association with albite-chlorite/smectite-quartz-pyrite. Prehnite-wairakite-calcite (± epidote) is the most common mineral association in prehnite-bearing samples. The prehnite-

laumontite-epidote-calcite association is also found in some specimens from relatively shallower (lower temperature) parts of bore-holes. Table 1 lists the equilibrium assemblages and analyzed Fe/Al ratios. The analyzed prehnites span a considerable range of $Fe^{+3}/(Fe^{+3}+Al)$ ratios; the most iron-rich prehnites in the matrix contain 6-8 wt% Fe_2O_3 and appear to be stable with epidote + wairakite + quartz + chloritic clay. The veined prehnites are much lower in Fe content and are stable with wairakite ± calcite + quartz. No epidote was found in mordenite-bearing samples and the epidote from laumontite-bearing samples is too fine-grained to be analyzed. The analyzed epidotes range from Ps 19 to 37 and most analyses are around Ps 29 to 33. The compositional range of epidote is very compatible with those from other geothermal areas (e.g., Cerro Prieto). The analyses of epidote and prehnite suggest that no immiscibility gap exists for these phases.

Table 1. Equilibrium mineral assemblage for core samples from Drill Hole #123 and 124 of the Onikobe geothermal area (All assemblages + chloritic clay + quartz + pyrite + albite)*.

Depth (m)	#123	Depth (m)	#124
238.6	Ep(32**) + Wr	165.8	Wr + Pr(14-17)
303.5	Pr(19) + Wr	201.8	Wr + Pr(3-8) + Cc
323.8	Ep(23) + Wr	209.9	Wr + Pr(17-22) + Ep(?)
344.6	Ep(22-29) + Wr	222.8	Wr + Ep(26-29)
348.5	Ep(19) + Pr(8) + Wr	307.5	Wr + Ep(37)
		334.7	Wr + Pr(12)
		349.4	Wr + Pr(3-4) + Cc

* Wr + Cc assemblages are not listed; they formed much later.
** The numbers in ( ) refer to $Fe^{+3}/(Fe^{+3}+Al) \times 100$.
Abbreviations: Ep=epidote; Wr=wairakite; Pr = prehnite; Cc = calcite.

Chemographic relations of common Ca-Al hydrosilicates (Ca-zeolites, epidote and prehnite) together with quartz, carbonate and chlorite/smectite were delineated in a simplified system $CaO-Fe_2O_3-Al_2O_3-(FeO+MgO)-SiO_2-H_2O-CO_2$. Compositions of prehnite and epidote are plotted in a ternary diagram $CaO-Al_2O_3-Fe_2O_3$ (Fig. 3) and tie lines for the coexisting phases in the 2-phase assemblages (wairakite + epidote and wairakite + prehnite) and the 3-phase assemblages (epidote + prehnite + wairakite and wairakite + prehnite + calcite) are drawn. The deduced phase relationships at T of 150-200°C and depth of 200-350m yield five 3-phase assemblages which have been recorded in other geothermal areas and in low-grade metabasalts. Three conclusions are made from such chemographic relations: (1) Both prehnite and epidote are restricted to Fe-rich compositions at low temperatures and become Al-rich with increasing temperature, (2) the Al end member of both prehnite and epidote are not stable under the physico-chemical conditions of the Onikobe geothermal system, and (3) the Fe-Al partitioning between epidote and prehnite suggests that the epidote always contains higher Fe than the coexisting prehnite. Such conclusions are consistent with those data deduced from hydrothermal experiments (Liou et al., 1983), thermodynamic calculations (e.g., Bird & Helgeson, 1978), and natural observations (Evarts & Schiffman, 1983; Bird et al., in press).

Zonal distributions of minerals and phase relationships observed in the Onikobe geothermal area are mainly controlled by changes in temperature and are restricted to low X_{CO_2} conditions. Other factors which are important either locally or with regard to certain minerals are the following: the P_{H_2O}/P_{Total} ratio, water and bulk rock chemistry, rock permeability, and kinetic constraints (e.g., Browne, 1978). Because of these effects, the apparent observed temperature ranges over which minerals are found in the Onikobe area as shown in Fig. 1 are generally broader than those expected from the experimental studies.

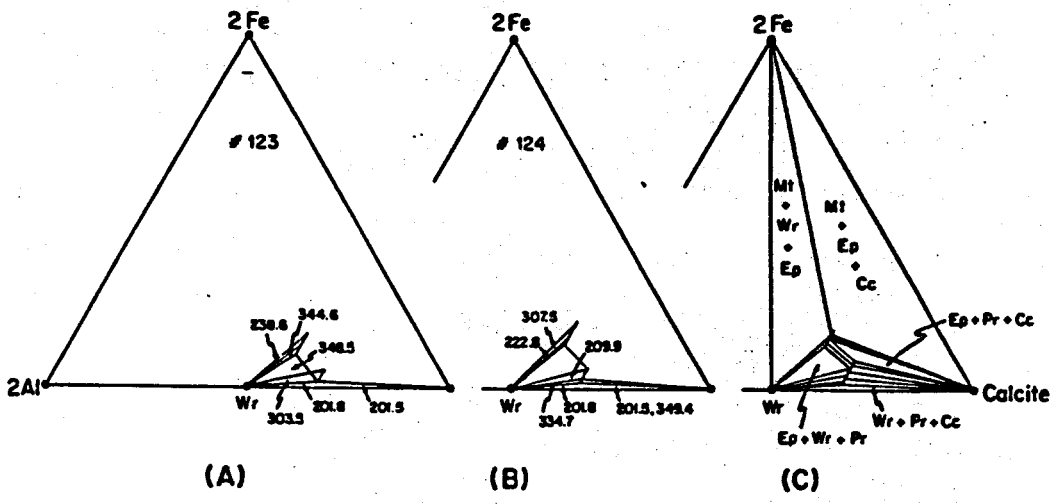

Fig. 3 Ca-2Al-$2Fe^{+3}$ plots showing compositions of analyzed epidotes and prehnites and mineral assemblages from drill hole #123(A) and #124(B). Interpretative relationships for 3-phase and 2-phase assemblages are shown in (C).

This abstract is condensed from a long report which describes research accomplished during the tenure of a U.S.-Japan cooperative project, supported by NSF 82-04298, DOE-SC07-12145 and JSPS (Grant 4 R039).

References

Bird, D.K. and Helgeson, H.C. (1978) Chemical interaction of aqueous solutions with epidote-feldspar mineral assemblages in geologic systems: 1. Thermodynamic analyses of phase relations in the system $CaO-FeO-Fe_2O_3-Al_2O_3-SiO_2-H_2O-CO_2$. Am. J. Sci. 280, 907-941.

_____, Schiffman, P., Elders, W.A., and Williams, A.E. (in press) Calc-silicate mineralization in the Cerro Prieto geothermal field, Baja California, Mexico compared with other active geothermal systems. Econ. Geol.

Browne, P.R.L. (1978) Hydrothermal alteration in active geothermal fields. Annual Review of Earth and Planet. Sci., 6, 229-250.

Evarts, R.C. and Schiffman, P. (1983) Submarine hydrothermal metamorphism of the Del Puerto ophiolite, California. Am. J. Sci., 283, 289-341.

Liou, J.G., Kim, H.S. and Maruyama, S. (in press) Prehnite-epidote equilibria and their petrologic applications. J. Petrol.

Seki, Y., Liou, J.G., Guillemette, R. and Sakai, H. (in press) Mineralogical and petrological investigations of drill hole core samples from the Onikobe geothermal system, Japan. Hydroscience and Geotechnology Lab., Saitama Univ. Memoir No. 3.

Seki, Y. and Oki, Y. (1969) Wairakite-analcime solid solutions from low-grade metamorphic rocks of the Tanzawa Mountains, central Japan. Min. Jour. 6, 36-45.

INTERNATIONAL ASSOCIATION OF GEOCHEMISTRY AND COSMOCHEMISTRY

AND

ALBERTA RESEARCH COUNCIL

3rd INTERNATIONAL SYMPOSIUM ON WATER-ROCK INTERACTION

PROCEEDINGS

Edmonton, Canada
July 14 to 24, 1980

Investigation of Drillhole Core Samples from Tatun Geothermal Area, Taiwan

C.Y. Lan, J.G. Liou*, and Y. Seki**

Mining Research and Service Organization; No. 1, Tun-Hwa South Road, Taiwan, ROC
*Department of Geology, Stanford University, Stanford, CA 94305, United States of America
**Department of Hydroscience and Geotectonics, Saitama University, Japan

The Tatun geothermal area of northeastern Taiwan, about 3 x 18 km^2 in dimension, is covered by a thick sequence of Pleistocene andesitic lavas and pyroclastics. The andesites belong to the hypersthene series and range in composition from mafic augite-hypersthene andesite to silicic biotite-hornblende andesite. The volcanic rocks are unconformably underlain by Miocene sandstones, conglomerates, and shales. The sandstones are coarse-grained and very permeable (with porosity greater than 10 percent) and have been suggested to be deep geothermal reservoirs with temperatures greater than 250°C and areal distribution greater than 20 km^2. Many hot springs and fumaroles occur, but those with the most impressive discharges of thermal fluids are concentrated within a NE-striking fault zone about 4 km wide and 18 km long. Spring waters with temperatures of 40°C – 120°C are mostly the acid sulfate chloride type and have extremely low pH values from 1 to about 3 (Chen, 1975). The acid nature is apparently restricted to surface zones where oxidation of volcanic gases such as H_2S prevails. At depth, as discussed later, the pH of waters must be higher as evidenced by the ubiquitous occurrence of calcite. Secondary minerals resulting from near-surface water/rock interactions include various silica minerals (opal, cristobalite, tridymite, and quartz), alunite, kaolinite, allophane, montmorillonite, pyrite, sulfur, and others. The mineral assemblages are characteristic of high S_2 and O_2 fugacities, high SiO_2 and total dissolved sulfur contents in the hydrothermal fluids (Wang, 1973).

The geothermal exploration of the Tatun area began in 1965 and, thus far, 62 gradient holes and 20 exploratory holes have been drilled. The gradient holes, of 35 to 622 m in depth and 2 to 3 inches in diameter, are mainly for collecting data on geothermal gradients and geology, whereas the exploratory holes up to 1510 m deep and 8.5 inches in diameter are mainly for collecting information about variation in geology, mineralogy, temperature, flow rate, and composition of fluid with depth. Core samples have been collected and temperature variations with depth have been recorded. Core samples from five drillholes were selected for detailed investigation in order to understand mineral parageneses of hydrothermal alteration and to compare them with those from Hakone and Onikobe, Japan (Seki, *et al.*, 1969; Oki and Hirano, 1974). The secondary minerals identified, together with recorded temperature gradients, are plotted versus depth in figure 1. Because temperatures fluctuated with time, temperatures shown in the figure represent the most recent measurement. A maximum temperature of 290°C has been recorded at a depth of 1200 m.

Three alteration zones were recognized based on the occurrence of kaolinite, alunite, Ca-zeolites, epidote, and the types of smectite-chlorite. Zone 1, restricted to near-surface depths of about 200 m or less, is characterized by the presence of kaolinite, alunite, pyrite, and gypsum. The original textures of andesite are totally obscured, and primary minerals have been entirely replaced. Core samples were recovered with difficulty, and secondary minerals are very similar to those at the effusive areas of hot springs and fumaroles. Zone 2, the intermediate zone between about 200 to 500 m, is characterized by the sporadic occurrence of laumontite, analcime, and hematite, together with abundant smectite-chlorite, anhydrite, quartz, carbonate, and pyrite. Alunite, wairakite, Type III chlorite and secondary albite were not found. Primary textures and minerals of the andesitic rocks are well preserved. Plagioclase (An 42 to 68) was mainly replaced by carbonates and anhydrite and locally by laumontite, whereas both hornblende and pyroxenes were mainly replaced by smectite-chlorite, illite, carbonate, pyrite, and hematite. Zone 3, below about 500 m, is characterized by the appearance of epidote, wairakite, chlorite, albite in addition to anhydrite, illite, quartz, and pyrite. The hornblende-two pyroxene andesitic core samples within this zone (for example, E-205 and E-208) are extensively altered and veined by secondary minerals. The primary porphyritic texture is modified by aggregates of saussurite + carbonate + anhydrite pseudomorphs after plagioclase and chlorite + pyrite + magnetite + sphene after mafic minerals. Plagioclases (An 44 to 66) were locally replaced by wairakite and epidote. Major vein minerals are carbonates, quartz, and anhydrite; wairakite and chlorite are also present.

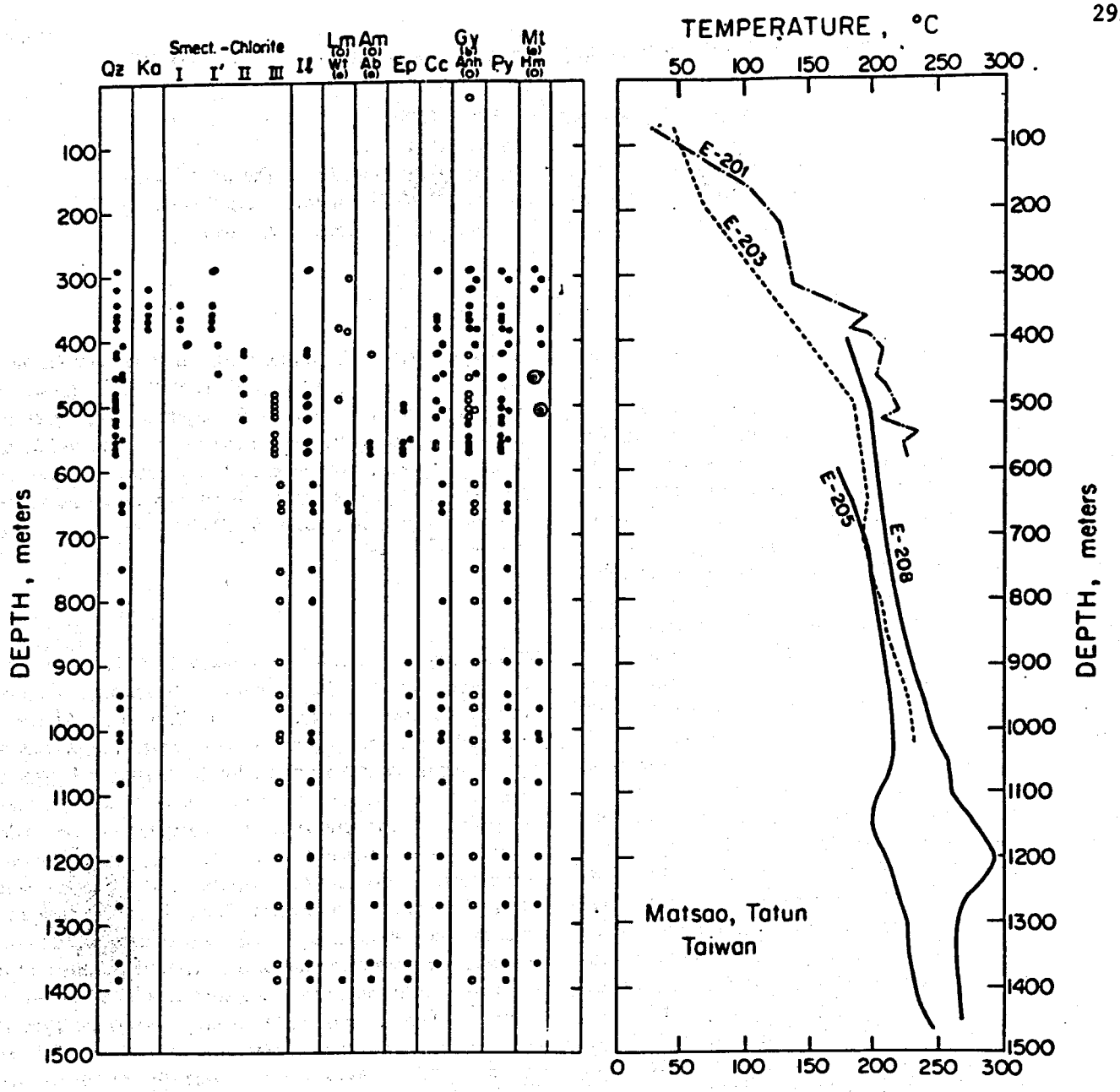

FIGURE 1. Variations of secondary minerals and temperatures with depths for exploratory drill holes E-201, 203, 205, and 208 from Matsao, Tatun Taiwan. Abbreviations for minerals: Qz-quartz, Ka-kaolinite, Il-illite, Lm-laumontite, Wt-wairakite, Am-analcime, Ab-albite, Ep-epidote, Cc-calcite, Gy-gypsum, Anh-anhydrite, Py-pyrite, Mt-magnetite, Hm-hematite.

The smectite-chlorite minerals of the altered andesitic rocks from the Tatun geothermal area and those from Onikobe and Hakone, Japan show systematic variations with depth and temperature. Detailed petrographic, X-ray diffraction (XRD), and differential thermal analysis (DTA) studies of the clay minerals reveal four distinct types, and their characteristic features are as follows. As shown in figure 1 together with the data from Hakone and Onikobe areas, Type I (alkaline montmorillonite) and Type I' (smectite) clay minerals are found commonly with mordenite and clinoptilolite, Type II smectite-chlorite with laumontite, and Type III with wairakite.

TABLE 1

XRD and DTA data on the four mineral associations, Tatun geothermal area

Type	Association	CuKα2θ(001)	CuKα2θEG(001)	DTA Endothermic T, C
I	alk. mont.	7.0	5.0	70,150,650
I'	smectite	6.0	5.0	70,150,650
II	chl.-smec.	3.0,6.0-6.2	3.0,5.6-5.9	70,150;550
III	chlorite	6.0-6.1	6.0-6.1	550

The smectite-chlorite minerals of the altered andesitic rocks from the Tatun geothermal area and those from Onikobe and Hakone, Japan show systematic variations with depth and temperature. Detailed petrographic, X-ray diffraction (XRD), and differential thermal analysis (DTA) studies of the clay minerals reveal four distinct types, and their characteristic features are as follows. As shown in figure 1 together with the data from Hakone and Onikobe areas, Type I (alkaline montmorillonite) and Type I' (smectite) clay minerals are found commonly with mordenite and clinoptilolite, Type II smectite-chlorite with laumontite, and Type III with wairakite.

The parageneses of secondary minerals in the Tatun geothermal area is consistent with the recorded temperature -depth relations as shown in figure 1. However, it should be noted that calcite is ubiquitous at depths below about 200 m, and its common occurrence as a replacement of plagioclase and pyroxene and as fissure fillings indicates that thermal waters at greater depth must be less acidic than those in the surface zone. The rare occurrence of Ca-zeolites and other calcium aluminum silicates, and abundance of calcite and anhydrite (and gypsum) suggest that the hydrothermal alteration in this area must have taken place at high activities of CO_2 and SO_2 and temperatures of 100 to 300°C.

This paper represents research accomplished during the tenure of the U.S.-Japan (NSF EAR 77-23172) and the U.S.-China (NSF EAR 77-23533) scientific cooperative projects. We thank our colleagues Y. Oki, F.W. Dickson, and W.E. Dibble for informative discussion and review.

References

Chen, C.H. (1975): Thermal waters in Taiwan, a preliminary study; #119 International Association of Hydrogeological Sciences, Proceedings Grenoble Symposium, pp. 79-88.

Oki, Y. and T. Hirano (1974): Hydrothermal system and seismic activity of Hakone volcano. The Utilization of Volcano Energy; Proceedings of U.S.-Japan Cooperative Science Seminar, Hilo, Hawaii, pp. 13-40.

Seki, Y., H. Onuki, K. Okumura, and I. Takashima (1969): Zeolite distribution in the Katayama geothermal area, Onikobe, Japan; Japanese Journal of Geology and Geography, V. XI, pp. 63-79.

Appendix A

References for the Tatun Geothermal Area, Taiwan

Chen, Chao-Hsia (1970) Geology and geothermal power potential of the Tatun volcanic region: U. N. symposium on the development and utilization of geothermal resources, Pisa, 1970, v.2, part 2, 1134-1143.

____ (1975) Thermal waters in Taiwan, a preliminary study: Publication no. 119 of the international association of hydrological sciences, Proc. of the Grenoble Symposium, Aug. 1975, 79-88.

____ and Wu, Y.J. (1971) Volcanic geology of the Tatun geothermal area, northern Taiwan: Proc. Geol. Soc. China, 14, 5-20.

Chen, Cheng-Hong (1975) Petrological and chemical study of volcanic rocks from Tatun volcano group: Proc. Geol. Soc. China, 18, 59-72.

____ (1977) Geochemistry and origin of Pleistocene volcanic rocks from northern Taiwan: Ph. D. Dissertation, the Institute of Geology, National Taiwan University.

____ (1978) Significance of ultrabasic inclusions in Tatun volcano group, northern Taiwan: Proc. Geol. Soc. China, 21, 80-91.

____ (1979) Igneous cordierite in andesite from Shamaoshan, Tatun volcano group: Proc. Geol. Soc. China, 22, 159-164.

Chen, P. Y. (1959) Clay deposits and their mineral composition in northwestern Taiwan: Proc. Geol. Soc. China, 2, 93-122.

____ (1961) Post-volcanic alteration of andesite lava and pyroclasts in Tatun volcano group, Taipei-hsien, Taiwan: Acta Geol. Taiwanica, 9, 19-38.

____ (1965) On the xenoliths of sandstone and shale in andesite from Chihsinshan, Tatun volcanic group, Taiwan: Proc. Geol. Soc. China, 8, 91-96.

____ (1969) Occurrence and genesis of kaolin minerals from Taiwan, Part I: kaolinite, halloysite ad allophane: Proc. Geol. Soc. China, 12, 30-48.

Fuh, T. M. (1968) Sedimentary xenoliths from andesite in the vicinity of Chutzushan, Taiwan: Acta Geol. Taiwanica: 12, 9-14.

Hsu, L. C., Yao, T. H. and Juan, V. C. (1963) Geologic map of the Tatun volcano group and its adjacent area, Taiwan (scale 1:25,000): National Taiwan University.

Hu, G. L. (1970) Mineralogical studies on hypersthene from the Tatun volcanoes, Taiwan: M.S. thesis, Inst. Geol., National Taiwan University, 17p.

Huang, C. K. (1954) Basaltic hornblende from the Tatun volcanoes, Taiwan: Acta Geol. Taiwanica, 6, 113-124.

____ and Hu, G. L. (1970) Hypersthene from the Tatun volcanoes, Taiwan: Acta Geol. Taiwanica, 14, 1-8.

Huang, T. G. (1974) Studies of silica minerals in hydrothermal alteration zone of Tatun volcano group: M.S. thesis, Inst. Geol. National Taiwan University, 79p.

Huang, W. Y. (1968) Studies of clay minerals in hydrothermal alteration zones of Chinkuashih, Chuifen and Yangminshan: M.S. thesis, Inst. Geol., National Taiwan University, 39p.

Juan, V. C., Hsu, L. C. and Yao, T. S. (1963) High-alumina basalt from northern Taiwan: Proc. Geol. Soc. China, 6, 67-71.

Lan, C. Y. Liou, J. G. and Seki, Y. (1980) Investigation of drillhole core samples from Tatun geothermal area, Taiwan. Proceedings, 3rd Internat. Sym. Water-Rock Interaction, Edmanton, Alberta, Canada p. 183-185.

Lin, N. S. (1958) Exploration of alunite in Chihsinshan region: Annual report 1957-1958, Mineral Survey Team, MOEA, 79-85 (in Chinese).

Mining Research and Service Organization (Taiwan, China) Rept. No. 85 (1968) Geothermal investigations in Taiwan by J. Healy, 15p.
____ 90 (1969) Geothermal investigations in Tatun volcanic region (1), 36p.
____ 102 (1970) Geothermal investigations in Tatun volcanic region (2), 86p.
____ 105 (1970) Assembled reports by foreign experts in geothermal investigation (1), 160p.
____ 105 (1970) Assembled reports by foreign experts in geothermal Investigations, No. 1, 160p.
a. McNitt,, J. R. (1970) Geothermal resources in Taiwan, p.19-28.
b. White, D. E. and Truesdell, A. H. (1970) Geothermal resources of Taiwan - an Evaluation of existing data, p.49-82.
c. Palmason, G. (1970) Geophysical exploration in the Tatun geothermal areas, northern Taiwan, p. 83-102.
d. Macdonald, W. J. P. (1970) Geophysical investigations for power in the Tatun volcanic area, Taiwan, p.103-116.
e. Keppelmeyer, O. (1970) Geothermal energy in Tatun area, Taiwan, p. 117-152.
f. Hayakawa, M. (1970) Seismic prospecting for power in the Matsao volcanic area, Taiwan, p. 153-160.
____ 111 (1971) Geothermal investigations in Tatun volcanic region (3), 48p.
____ 126 (1973) Geothermal investigations in Tatun volcanic region (4), 78p.
____ 127 (1973) Assembled reports by foreign experts in geothermal investigation (2), 173p.
MRSO Rept. No. 127 (1973) Assembled reports by foreign experts in geothermal investigation, No. 2, 173p.
a. Healy, J. (1973) Geothermal investigation in Taiwan p. 1-18.
b. Braithwaite, W. R. (1973) Geothermal power development in Taiwan-proposals for a corrosion test program, p.19-44.
c. Banwell, C. J. (1973) Report on the Tatun geothermal field, p.45-102.
d. Ellis, A. J. (1973) Extraction of Dr. A. J. Ellis's report p.103-105.
e. Kappelmeyer, O. (1973) Geophysical methods for investigation of the thickness of lava flows in the Tatun volcanic area, Taiwan, China, p.107-112.
f. Italian Mission to geothermal fields of Taiwan - Final Report, p.113-154.
MRSO Rept. No. 146, Exploration of geothermal resources in Taiwan, Rept. No. 1 (from Jan. 1973 to Dec. 1974), 70p.
____ Rept. No. 163, Exploration of geothermal resources in Taiwan, Rept. No. 2 (from Jan. 1975 to Dec. 1976) 150p.
____ Rept. No. 170, Exploration of geothermal resources in Taiwan, Rept. No. 3 (from Jan. to Dec. 1977) 150p.
Shieh, Y. N. Cherng, F. P. and Hoering, T. C. (1980) Oxygen and hydrogen isotope ratios of hot springs and geothermal waters in Taiwan. A preliminary study. Proc. 3rd Internat. Sym. Water-Rock Interaction, Edmanton, Alberta, Canada, p.186-187.
Tan, L. P. (1959) The sulfur-melnikovite deposits of the Szehuangtzeping area, Taipei-hsien, Taiwan: Proc. Geol. Soc. China, 2, 123-145.
____ (1972) Trace elements in the cryptocrystalline pyrite deposits of the Tatun volcanic area, Taiwan: Proc. Geol. Soc. China: 15, 119-122.

____ (1973) Copper content of biotites from the andesitic rocks in northern Taiwan: Acta Geol. Taiwanica, 16, 47-55.

Wang, Y. (1967) Studies on rock-forming minerals from Taiwan (3): Low Temperature cristobalite from altered andesites, Tatun volcanic region: Proc. Geol. Soc. China, 10, 125-129.

____ (1970) Variation of potash content in the Pleistocene andesites from Taiwan: Proc. Geol. Soc. China, 13, 41-50.

____ (1973a) Wall rock alteration of late Cenozoic mineral deposits in Taiwan: Geologic settings and field relations: Proc. Geol. Soc. China, 16, 145-160.

____ (1973b) Wall rock alteration of late Cenozoic mineral deposits in Taiwan: Mineralogical and physicochemical aspects: Acta Geol. Taiwanica, 16, 1-29.

Yen, T. P. (1950) Alunite deposits in the neighborhood of the Chihsinshan, Taipei (in Chinese): Taiwan Reconstruction Monthly, 1, 32-35.

____ (1958) Cenozoic volcanic activity in Taiwan: Taiwan Mining Industry, 10, 1-39.

____ (1970) Petrochemistry of the Pliocene to Pleistocene volcanic rocks of Taiwan: Proc. Geol. Soc. China, 13, 51-62.

____(1971) The Pleistocene tectonics, volcanism and ore deposits in Taiwan: Soc. Mining Geol. Japan, Spec. Issue 3, 60-64.

Appendix B

References for the Hakone (and its vicinity) Area, Japan

Awaya, T., Hirano, T., and Suzuki, T., 1974: Calcium carbonate deposit of Yugawara hot spring. Bull. Hot Spring Res. Inst., 5, pp. 67-80.

Fukutomi, T., 1937: On the hot springs of Atami, Izu peninsula. Bull. Earthq. Res. Inst. 15, pp. 113-133.

Geol. Surv. Japan, 1962: Chemical composition of volcanic rocks in Japan.

Hiraga, S., 1972: Earthquake swarms of geothermal fields in Japan. Jour. Japan Geoth. Ener. Assoc., 9, pp. 30-39.

Hiraga, S., Hirota, S., Kasai, M., and Suzuki, M., 1971: Seismometrical observation in Hakone volcano, 1970. Bull. Hot Spring Res. Inst., 2, pp. 1-20.

Hiraga, S., Ito, H., and Inaba, K., 1972: Seismometrical observation in Hakone volcano, 1971. Bull. Hot Spring Res. Inst., 3, pp. 1-24.

Hiraga, S., Ito, H., Hakamada, K., and Kozuma, N., 1973: Seismometrical observation in Hakone volcano, 1972. Bull. Hot Spring Res. Inst., 4, pp. 1-22.

Hiraga, S., Ito, H., Hakamada, K., Kozuma, N., and Kobayashi, T., 1974: Seismometrical observation in Hakone volcano, 1973. Bull. Hot Spring Res. Inst., 5, pp. 1-14.

Hirano, T., Oki, Y., and Tajima, Y., 1965: Mineral precipitates in sulfate waters in Owakidani, Hakone. Jour. Soc. Engineer. Mineral Springs Japan, 3, pp. 131-138.

Hirano, T., and Oki, Y., 1971: Geochemistry of groundwaters of Hakone caldera. Bull. Hot Spring Res. Inst., 2, pp. 89-108.

Hirano, T., Oki, Y. and Awaya, T., 1972: Geochemistry of hydrothermal system of the Yumoto-Tonosawa area, the eastern foot of Hakone volcano. Bull. Hot Spring Res. Inst., 3, pp. 109-130.

Kanroji, Y., and Tanaka, A., 1979: Thermal water of two type, chloride and sulfate, in Minami-Atami spa. Jour. Soc. Engineer. Mineral Springs Japan, 13, pp. 160-168.

Kimbara, K., and Yoshimura, T., 1973: Clay minerals and rock alteration of the Green Tuff. Memoir. Geol. Soc. Japan, 9, pp. 227-237.

Kitano, Y., Yoshioka, R., Okuda, S., and Okunishi, K., 1967: Geochemical study of ground waters in the Matsushiro area, Part I, Chemical composition of ground waters. Bull. Disaster Prev. Res. Inst., 17, pp. 47-71.

Kuno, H., 1950a: Petrology of Hakone Volcano and adjacent areas, Japan. Bull. Geol. Soc. Amer., 61, pp. 957-1020.

Kuno, H., 1950b: Geology of Hakone Volcano and adjacent areas, Part I. Jour. Fac. Sci., Univ. Tokyo, sec. 2, 7, pp. 351-402.

Kuno, H., 1951: Geology of Hakone Volcano and adjacent areas, Part II. Jour. Fac. Sci., Univ. Tokyo, sec. 2, 7, pp. 351-402.

Kuno, H., Oki, Y., Ogino, K. and Hirota, S., 1970: Structure of Hakone caldera as revealed by drilling. Bull. Volcanologique, 34, pp. 713-725.

Matsubaya, O., Sakai, H., Kusachi, I., and Satake, H., 1973: Hydrogen and oxygen isotopic ratios and major element chemistry of Japanese thermal water systems. Geochem. Jour., 7, pp. 123-151.

Matsuda, T., 1968: Crustal structure along N-S cross section of "Fossa Magna", Japan. Proceed. Symp. Fossa Magna, Tokai Univ., pp. 231-235.

Matsuo, S., Kusakabe, M., Niwano, M., Hirano, T., and Oki, Y., 1979: Water budget in the Hakone caldera using hydrogen and oxygen isotope ratios. Isotopes in Lake Studies, International Atomic Energy Agency, Vienna, pp. 131-144.

Minakami, T., 1960: Fundamental research for predicting volcanic eruptions, Part I. Bull. Earthq. Res. Inst., 38, pp. 497-544.

Minakami, T., Hiraga, S., Miyazaki, T., and Utibori, S., 1969: Fundamental research for predicting volcanic eruptions, Part II. Bull. Earthq. Res. Inst., 47, pp. 893-949.

Nakamura, H., Maeda, K., Abe, K., Yamada, T., and Kodai, K., 1969: Remarks on hydrothermal system in Atami Hot Spring area, central Japan. Bull. Geol. Surv. Japan, 20, pp. 367-394.

Oki, Y., and Hirano, T., 1970: Geothermal system of Hakone volcano. U.N. symposium on the development and utilization of geothermal resources, Pisa. Geothermics, Spec. Issue 2, 2, pp. 1157-1166.

Oki, Y., and Hirano, T., 1972: Geothermal activity and hot springs of Izu and Hakone district. Izu Peninsula, Tokai Univ. Press, Tokyo.

Oki, Y., and Hirano, T., 1974: Hydrothermal system and seismic activity of Hakone volcano. Utilization of volcanic energy, pp. 13-40.

Oki, Y., Hirano, T., and Suzuki, T., 1974: Hydrothermal metamorphism and vein minerals of the Yugawara geothermal area, Japan. Proceed. Internat. Symp. Water-Rock Interaction, Prague, pp. 209-222.

Oki, Y., Aramaki, S., Nakamura, K., and Hakamata, K., 1978: Volcanoes of Hakone, Izu and Oshima, Hakone Town.

Otuka, Y., 1943: Geologic consideration of the abnormal temperature distribution in the Hot Springs at Atami, Sizuoka Pref. Japan Bull. Earthq. Res. Inst., 21, pp. 414-433.

Otuka, Y., and Kuno, H., 1932: On two borings near Atami-mati, Izu peninsula, Bull. Earthq. Res. Inst., 10, 472-475.

Sakurai, K., 1953: Studies on zeoloites from Yugawara hot springs, Kanagawa Prefecture, Japan (I). Bull. National Sci. Museum, No. 32, pp. 83-98.

Sakurai, K., 1955: Studies on zeolites from Yugawara hot springs, Kanagawa Prefecture, Japan (II). Bull. National Sic. Museum, No. 34, pp. 1-10.

Sato, K., and Hayashi, A., 1952: Yugawaralite, a new zeolite. Sci. Rep. Yokohama National Univ., ser. II, No. 1, pp. 69-77.

Sato, K., 1961: On the types of Japanese volcanic thermal water. Japan Jour. Geol. Geogr., 32, 293 pp.

Sato, K., 1962: On the thermal springs and geology of Izu-Hakone district. Jour. Balneol. Soc. Japan, 13, 41 pp.

Suzuki, T., Hirano, T., Tajima, Y. and Oki, Y., 1971. Hot spring deposits of Hakone volcano. Bull. Hot Spring Res. Inst., 2, pp. 121-132.

Watanabe, S., Kusakabe, M., Hirano, T., and Oki, Y., 1977. Carbon and Oxygen isotopic composition of calcite in drill cores from the Yugawara geothermal system. Proceed. Geochem. Soc. Japan, 1977.

Yuhara, K., 1961: Hydrological study of Atami hot springs., Memoirs College Sci. Univ. Kyoto, ser. A, 26, pp. 283-311.

Yuhara, K., Kodai, K., Abe, K., Kotada, K., and Hosono, Y., 1966: Hydrothermal system of Owakudani-Gora zone, Hakone volcano. Rep. Cooperative Res. Disaster Prevention, No. 18, pp. 29-42.

Yuhara, K., Okubo, T., and Takeuchi, S., 1969: Mass and heat discharged from Owakudani and Sounzan geothermal areas, Hakone volcano. Bull. Geol. Surv. Japan, 20, pp. 83-100.

Appendix C*

List of Published Papers and Conference Reports Supported by DE-FC07-80ID-12148

Monographs:

Seki, Y., Liou, J. G., Oki, Y., Dickson, F. W., Sakai, H. and Hirano, T. (1980) The interactions between volcanogenic rocks and seawater-meteoric water mixture in the near coast undersea part of the Seikan Tunnel, Japan. Hydroscience and Geotechnology Lab., Saitama Univ., Memoir No. 1, 123 p.

Seki, Y., Liou, J. G., Guillemette, R. N., Sakai, H. Oki, Y., Hirano, T., and Onuki, H., (1983) Investigation of drill hole core samples from the Onikobe geothermal system, Japan. Hydroscience and Geotechnology Lab., Saitama Univ. Memoir No. 3, 206 p.

Guillemette, R. N., 1983. Geochemical and experimental investigations of andesite-water interactions to island-arc geothermal system. Ph.D. thesis, Stanford University, 319 p.

Scientific papers:

Zeng, Y., and Liou, J. G. (1982) Experimental investigation of yugawaralite-wairakite equilibrium. Amer. Mineral., v. 67, p. 937-943.

Liou, J. G., Kim, H. S. and Maruyama, S. (1983) Prehnite-epidote equilibria and their petrologic applications. Jour. Petrol., 24, p. 583-604.

Zeng, Y. and Liou, J. G. (in press) Investigations of hydrothermal reactions of CO_2-bearing solutions with basaltic glass at 300°C and 500 bars pressure. Scientific Sinica.

Liou, J.G., Seki, Y., Guillemette, R. and Sakai, H. (in press) Compositions and parageneses of secondary minerals in the Onikobe geothermal system, Japan. Chem. Geol.

Potter, J. M., Guillemette, R., and Liou, J. G. (in review) A new system for flow through expmerimental studies at elevated temperatures.

Liou, J. G., Pohl, D. C., Potter, J. M. and Gordon, P. (in review). Dickson-type hydrothermal apparatus and modifications. Sakai, H. ed. Water-Rock Interaction IV Special Publication.

Proceedings, 4th International Symposium on Water-Rock Interaction, Misasa, Japan, August 1983:

Brigham, R. H., and O'Neil, J. R. (1983) The genesis and movement of water in a two mica pluton: A stable isotope study: p. 63-66.

Donahoe, R. J. and J. G. Liou, 1983. An experimental study on the process of zeolite formation: p. 119-121.

Liou, J. G., Guillemette, R. and Seki, Y. (1983) Compositions and paragenesis of some hydrous Ca-Al silicates in the Onikobe geothermal system, Japan: p. 290-293.

Maruyama, S., Liou, J. G., and Cho, M. (1983) Expmerimental investigation of heulandite-laumontite equilibrium: p. 305-308.

Pohl, D. C., and Liou, J. G. (1983) Flow-through reaction of basalt glass and seawater at 300°C and 200°C, 250 bars pressure: p. 389-392.

Zeng, Y. and Liou, J. G. (1983) Expmerimental investigation of interactions between basaltic glass and Na-carbonate (+NaCl) solutions at 300°C and 500 bars: p. 561-564.

Other Conference Reports:

Lan, C. Y., Liou, J. G. and Seki, Y. (1980) Investigation of drill hole core samples from Tatun geothermal area, Taiwan. Proc. 3rd Internat. Symposium on Water-Rock Interaction, Edmonton, Canada 1980, p. 183-185.

Liou, J. G., and Seki, Y. (1980) Paragenesis of carbonate minerals from volcanogenic rocks interacted with seawater and meteoric water in the Seikeri Undersea Tunnel, Japan. Proc. 3rd Internat. Symposium on Water-Rock Interaction. Edmonton, p. 151-152.

Guillemette, R. N., Liou, J. G., and Dickson, F. W. (1980) The effect of glassy versus crystalline starting materials on andesite-water interactions. Proc. 3rd Internat. Symposium on Water-Rock Interactons, Edmonton, p. 168-169.

Guillemette, R. N. (1981) Progressive hydration and alteration of volcanic glass under hydrothermal conditions. Trans. Amer. Geophysics Union, v. 62, no. 45, p. 1077.

Kim, H. S., and Liou, J. G. (1981) Prehnite-epidote equilibria and their petrologic applications. Trans. Amer. Geophysics Union, v. 62, no. 11, p. 1066.

Zeng, Yishan, and Liou, J. G. (1981) Expmerimental determination of yugawaralite-wairakite equilibrium. Trans. Amer. Geophysics Union, v. 62, no. 11, p. 1066.

Liou, J.G., Kim, H.S. and Maruyama, S. (1983) Expmerimental determination of prehinte-epidote equilibria. Geol. Soc. Amer. Abst. with Program, v. 15, no. 6, p. 628.

Maruyama, S., Cho, M. and Liou, J. G. (1983) Expmerimental investigation of heulandite-laumontite equilibrium. Trans. Amer. Geophysics Union, v. 64, no. 8, p. 897.

Pohl, D. C., and Liou, J. G. (1983) Flow-through basalt glass-seawater reactions from 200°C to 300°C and 250 bars pressure. Trans. Amer. Geophysics Union, v. 64, no. 8, p. 888-889.

* Reprints for most of these publications are available from the Principal Investigator J. G. Liou, Stanford University.

☆U.S. GOVERNMENT PRINTING OFFICE:1984 -746 -081/ 2700 REGION NO. 4